Fabrication of Rib Waveguides and Optical Fibres in Chalcogenide Glasses

Zheng Gang Lian, BEng.

Thesis submitted to University of Nottingham

for the degree of Doctor of Philosophy

February 2011

Abstract

Chalcogenide glasses offer transmission from the far visible to the far - infrared (IR) wavelength range. They exhibit photosensitivity and have high linear and nonlinear refractive indices. There are many potential applications involving near- and mid- infrared light such as laser delivery, optical data storage and all-optical switching. Two types of optical waveguides based on chalcogenide glasses were developed in this project:

(1) The fabrication of planar optical waveguides in thin $As_{40}Se_{60}$ glass films was carried out via a hot embossing pressing technique. Previous work had shown it possible to fabricate optical waveguides in polymers using hot embossing techniques. Nevertheless using hot embossing to pattern waveguides in a thin chalcogenide glass film did not receive much success. In the present work, single-mode optical rib waveguides operating at telecommunication wavelengths were successfully patterned in a thermally evaporated $As_{40}Se_{60}$ glass thin film on a $Ge_{17}As_{18}Se_{65}$ chalcogenide glass substrate. This experimental line demonstrated a fast and economic way of producing planar waveguides in thin chalcogenide glass films.

(2) For the first time, a one-layer, solid micro-structured optical fibre (MOF) was successfully drawn from $As_{40}Se_{60}$ and $Ge_{10}As_{23.4}Se_{66.6}$ (atomic %) chalcogenide glasses for operation in the near- to mid-infrared. This experimental line showed a new and flexible route to micro-structuring of mid-infrared fibre for operation in the near- to mid-infrared, presenting an all-solid (i.e. glass-glass) alternative to air – glass micro-structuring. The principal advantage of the new approach is mechanical rigidity. A sufficiently large refractive index step between the component glasses exists to enable structures that rely on photonic bandgap effects for their operation to be realised in future work.

Underpinning the development of these optical waveguides, the refractive index dispersion of bulk chalcogenide glasses $As_{40}Se_{60}$, $Ge_{10}As_{23.4}Se_{66.6}$ and $Ge_{17}As_{18}Se_{65}$ was measured using ellipsometry from 0.3 μm to 2.3 μm wavelength in this project. Also, the refractive index of thin $As_{40}Se_{60}$ films was measured and compared with that of bulk $As_{40}Se_{60}$ samples. Finally a Se precursor purification process was developed to enhance the purity of the end-glasses.

Acknowledgements

I would like to express my respect to my supervisors, Prof. Angela Seddon, Prof. Trevor Benson and Dr. David Furniss, for their constant guidance and support in both theory and experimental work during the PhD.

I am thankful to the Interdisciplinary Doctorial Training Centre for Photonics and Electronics, University of Nottingham for financial support.

I thank the technicians in the Wolfson Centre for Materials Research, especially Nigel Neate for his help with Environmental Scanning Electron Microscopy; Tom Buss for the help with the use of Hydrofluoric acid and Mr. Keith Dinsdale for his help with changing nitrogen cylinders. I also thank Catrina Bryce (University of Glasgow, UK) for supplying the silicon moulds used in this work.

I would like to thank the lecturers and researchers in George Green Institute for Electromagnetics Research in the University of Nottingham, for their guidance in electromagnetic theory during the PhD.

Thanks to my parents and my family, for their encouragement and support during my PhD.

Glossary of Symbols and Abbreviations

Chemicals

Al	Aluminium
As	Arsenic
Bi	Bismuth
Er	Erbium
Ge	Germanium
H	Hydrogen
Hg	Mercury
O	Oxygen
S	Sulphur
Se	Selenium
Si	Silicon
Sn	Tin
Te	Tellurium

Techniques

CVD	Chemical Vapour Deposition
DSC	Differential Scanning Calorimetry
ESEM	Environment Scanning Electron Microscopy
FTIR	Fourier Transform Infrared Spectroscope
PVD	Physical Vapour Deposition
TMA	Thermomechanical Analysis
XRD	X-ray Diffraction

Properties and Miscellaneous

A_{fibre}	Cross-sectional area of fibre
$A_{preform}$	Cross-sectional area of preform
c	Velocity of light in free space
D	Dispersion
F	Force
FIB	Focused Ion Beam
GG	Glass-Glass
GGS	Glass-Glass-Semiconductor
GPS	Glass-Polymer-Semiconductor
ID	Internal diameter
IR	Infrared
k	Extinction coefficient
MOF	Microstructured Optical Fibre
n	Refractive index

OD	Outer diameter
P	Electric polarization vector
PAI	Polyamidoimide polymer
PBGF	Photonic band gap fibres
PMMA	polymethylmethacrylate
RF	Radio frequency
T	Time
Tg	Glass transition temperature
UofN	University of Nottingham
UofP	University of Pardubice
V	Volume
V_{fibre}	Volume of fibre
$V_{preform}$	Volume of preform
α	Thermal expansion coefficient
ε_0	Free space permittivity
η	Viscosity / poise
λ	Wavelength
χ	Susceptibility of a medium
ω	Angular velocity

List of Publications

The following journal and conference papers have resulted in whole or part from the work described in this thesis.

[1] A. B. Seddon, D. Furniss, Z. G. Lian, W. J. Pan and T. M. Benson, *Review: Tg - reversible glass door to fabrication of photonic devices and integrated circuits*, Proc. SPIE, 2010, vol. 7604, 76040CV, San Francisco, California, United State.

[2] Z.G. Lian, Q.Q. Li, D. Furniss, T.M. Benson and A.B. Seddon, *Solid microstructured chalcogenide glass optical fibres for the near- and mid-infrared spectral regions*, IEEE, Photonic Technology Letters, 2009, vol. 21, No. 24, p.1804-1806.

[3] A. B. Seddon, Z. G. Lian, W.J. Pan, D. Furniss and T. M. Benson, *Review: Tg: the glass door to photonic integrated devices and circuits*, in proceedings of 11th International Conference on Transparent Optical Networks (ICTON), 2009, We. A5.1, 1-4, Azores, Portugal.

[4] Z. G. Lian, W. Pan, D. Furniss, T. M. Benson, A. B. Seddon, T. Kohoutek, J. Orava, and Thomas Wagner, *Embossing of chalcogenide glasses: mono-mode rib optical waveguides in evaporated thin films*, Optics Letters, 2009, vol. 34, p. 1234 -1236.

[5] Z. G. Lian, D. Furniss, T. M. Benson, A.B. Seddon, *Chalcogenide Glasses: A disruptive technology platform for photonics*, European Action COST MP0702, 2009, Metz, France.

[6] T. M. Benson, Z. G. Lian, N. Prasad, D. Furniss, W.J. Pan, E. A. Romanova, T. Kohoutek, J. Orava, T. Wagner, S. Muraviov, A. Andrianov, G. Gelikonov, A. Konyukhov, A. B. Seddon, *Technologies for the fabrication of photonic devices based on chalcogenide glasses*, Proc. 4th International CAOL Conference, 2008, p. 12-14, Alushta, Crimea, Ukraine.

[7] Z.G. Lian, J. Wykes, P. D. Sewell, A. Vukovic, T.M. Benson, E. Bekker, L. Melnikov, *Modelling Microstructured Optical Fibres*, The 24th PIERS, Progress in Electromagnetics Research Symposium, 2008, p. 180, Cambridge, USA.

[8] Z.G. Lian, W. Pan, D. Furniss, T. M. Benson, A. B. Seddon, Poster: *New technology for the fabrication of photonic devices based on chalcogenide glasses*, International Symposium on Non Oxide glasses, XVI, 2008, Montpellier, France.

[9] Z.G. Lian, D. Furniss, T. Benson, A. Seddon, Poster: *New technologies for the fabrication of photonic devices based on chalcogenide glasses*, COST P11 Training School, 2007, Warsaw.

Contents

Chapter 1

Introduction

1.1Aim and objectives

Optical devices provide the technological backbone of fast telecommunication and signal processing systems. The optical devices include optical waveguides, optical fibres, amplifiers and lasers etc. Optical waveguides can be considered as the connecting wires in an optical circuits and optical fibre could be used as a method of conveying information. Many materials have been used for fabricating optical devices with different capabilities, e.g. silica glass, polymers and inorganic glasses etc [1]. Nowadays, silica based glasses have been used widely for telecommunications. The low transmission loss of silica based fibres can achieve 0.2 $dBkm^{-1}$ at 1.55 μm wavelength [2]. However, the longest wavelength that can be generated in silica fibres is below 2.5 μm due to material loss [3]. Therefore, alternative materials are required to work at longer wavelengths. Polymers are generally less cost, but its high attenuation makes it not suitable for longer distance transmission. Chalcogenide glasses belong to the inorganic glasses group and they are novel materials with promising properties. Low loss and photoinduced effects [1, 4-15] make these glasses suitable candidates for fabrication of devices such as gratings and waveguides. They have relatively high linear and non-linearity refractive indices which makes them good for supercontinuum generation and optical switching applications [4, 16]. One objective of present project is to study the physical and optical properties of some of chalcogenide glasses to find suitable compositions for fabricating optical devices: planar waveguides and Microstructured Optical Fibres (MOFs) or Holey Fibres (HFs).

There were several methods proposed to fabricate planar optical waveguides in chalcogenide glasses, such as direct laser writing [17, 18], ion implantation [17], photolithography [19], dry etching [20, 21] and hot embossing [1] etc. Chalcogenide glasses have low softening temperature which is suitable for the hot embossing fabrication method. The hot embossing technique was used previously in our group to

pattern both bulk chalcogenide glasses [1] and to press chalcogenide glass fibres onto a chalcogenide glass substrate in a 'one-step' fabrication process. The lowest loss was measured to be 2.2 dB/m [22]. It was considered as a fast and economic way to fabricate optical waveguides. In this project, another objective is to investigate the feasibility of fabricating rib waveguides directly in chalcogenide glass thin films. The target loss is below 1 dB/cm but it is preferred an order of magnitude lower. This requires the design and realisation of a suitable thin film and substrate pair followed by the development of appropriate processing conditions.

Optical fibres were one of the major technological successes of the 20th century [23, 24]. The MOFs in silica glass has gone through a remarkable development recently. MOF is able to guide light in a solid core on the same index guiding principle as the conventional fibre [24, 25]; also it can confine light in an air core [26] which is impossible for conventional fibres. The first chalcogenide glass MOF was fabricated by Monro *et al.* in 2000 [27] in gallium lanthanum sulphide (GLS) glass. But optical guidance was not shown in the report. Since then, several groups reported the fabrication of chalcogenide glass MOFs [5, 28, 29] using stack-and-draw process with different core sizes. A small core Ge-Sb-S MOF was fabricated using a stack and draw technique by Desevedavy *et al.* [28]. Single mode guiding behaviour was obtained at 1.55 μm. The Naval Research Laboratory (NRL) produced solid core sulphide based glasses MOFs and demonstrated supercontinuum generation [30]. One objective of this project is work towards the fabrication of air-core chalcogenide glasses MOFs using the stack-and-draw process for the application of power delivery.

The MOFs are sensitive to the cladding configuration, therefore a minor variation in the microstructure can cause noticeable deviation in properties such as dispersion [31, 32]. This property requires the air core MOFs with uniform cladding and consequently leads to a challenging fabrication process. This is because during MOF fibre drawing process, the microstructured profile changes due to the change of pressure inside of holes. As a result, it is difficult to fabricate kilometre-scale long air core MOF with identical and controllable cladding configurations [31]. However, it should be noted that, the MOF optical guiding properties are not restricted to single material fibre designs. A solid core-cladding MOF comprised of two materials could potentially solve this problem. The requirement is to have a high refractive index contrast between the material in the holes and cladding materials [31]. In practice, to

realise an all-solid MOF requires one to seek a suitable pair of solid materials whose thermal properties are compatible yet which have a substantially different refractive index [31]. This is maybe one of the main reasons that there is not many reports in the literature about all-solid MOF. Feng *et al.* [31] fabricated the first all-solid MOF in a borosilicate glass (n=1.75 at 1.55 μm wavelength) and potassium fluoride glass (n=1.53 at 1.55 μm wavelength) pair. The fibre had 3 layers cladding and the attenuation was reported to be 5 dB/m at 1.55 μm wavelength. According to Devyatykh *et.al*[33], the champion fibre losses for simple chalcogenide glass compositions such as As-S are a few hundred dB/km. This level of losses may be not suitable for power delivery applications, but will probably be acceptable for supercontinuum generation. In this project, one of the objectives is to fabricate a one layer cladding all-solid MOF in chalcogenide glasses; the optical loss aspired is below ~5 dB/m.

1.2 Layout of the thesis

The thesis is comprised of seven chapters and these chapters are grouped in two parts. The first part includes chapters 1 to 3. Chapter 1 is an introduction, Chapter 2 reviews the background knowledge relating to the project and Chapter 3 describes the experimental procedures of glass characterisation methods used throughout the project. In Chapter 3, only the generic procedure for each process is presented; in the results and discussion chapters (Chapters 4 to 6), full details of the procedures are described.

Part two of the thesis is composed of Chapters 4 to 7 which describe the work carried out towards achieving the aims of the project. The results obtained are discussed within each chapter. The mechanical and optical properties of bulk and thin film glasses are discussed in Chapter 4. In Chapter 5, the waveguides fabrication procedure and results of fabrication in chalcogenide glasses thin film are discussed. In Chapter 6, the procedures developed for producing air core and solid core MOFs are described. The steps developed in order to produce hollow core and solid core MOF are described in this chapter, including the rotational casting of chalcogenide glass tube, the extrusion of core/cladding preforms and fibre drawing. Chapter 7 is a summary of the critical conclusions reached in the project and some suggestions for future work.

Page 4 missing in original

Chapter 2

Background and Literature Review

The project comprised both the fabrications of planar optical rib waveguides and Microstructured Optical Fibre (MOFs) from chalcogenide glasses. This chapter describes the background knowledge relevant to the project. Section 2.1 introduces chalcogenide glass technology. Chalcogenide glass refractive index and dispersion will then be discussed in section 2.2. Sections 2.3 and 2.4 describe chalcogenide glass thin film deposition methods and the development of optical waveguides in these glasses, respectively. The development of MOFs is introduced in section 2.5, including: the MOF structural designs, fabrication methods and the progress in the fabrication of chalcogenide glass MOFs.

2.1 Glass science and technology

The definition of glass described by the Committee of the U.S. National Research Council in 1976 is quoted as: "Glass is an X-ray amorphous material which exhibits the glass transition, this being defined as that phenomenon in which a solid amorphous phase exhibits with changing temperature a more or less sudden change in the derivative thermodynamic properties, such as heat capacity and expansion coefficient, from crystal-like to liquid-like values" [34].

The formation of glass is best understood by examining how the volume of a given mass of substance changes with temperature at constant pressure. Figure 2.1 indicates a volume per unit mass / temperature diagram, which depicts the volume differences between a glass and a crystalline material as they are formed on cooling from the liquid state to the solid state [34]. In Figure 2.1, from point a to e, the volume of the liquid decreases as the temperature falls and this is due to the decreasing amplitude of atomic vibrations. At point b, structural changes can occur very rapidly (line b-c-d) as the melt solidifies at the equilibrium freezing point. Along

the line b-e-f, as the viscosity of the super-cooled melt decreases as temperature falls. The structure of the supercooled liquid changes increasingly slowly until the viscosity becomes so low that no more changes occur. The temperature range where the temperature/volume per unit mass line departs from the supercooled liquid line (b-e) and joins the glass state line (e-f) is known as the glass transition range, Tg. The change from supercooled liquid to glass does not take place suddenly; therefore, Tg is a temperature range [34]. Also, it should noted that all amorphous polymers, such as epoxy resins, exhibit a Tg [35].

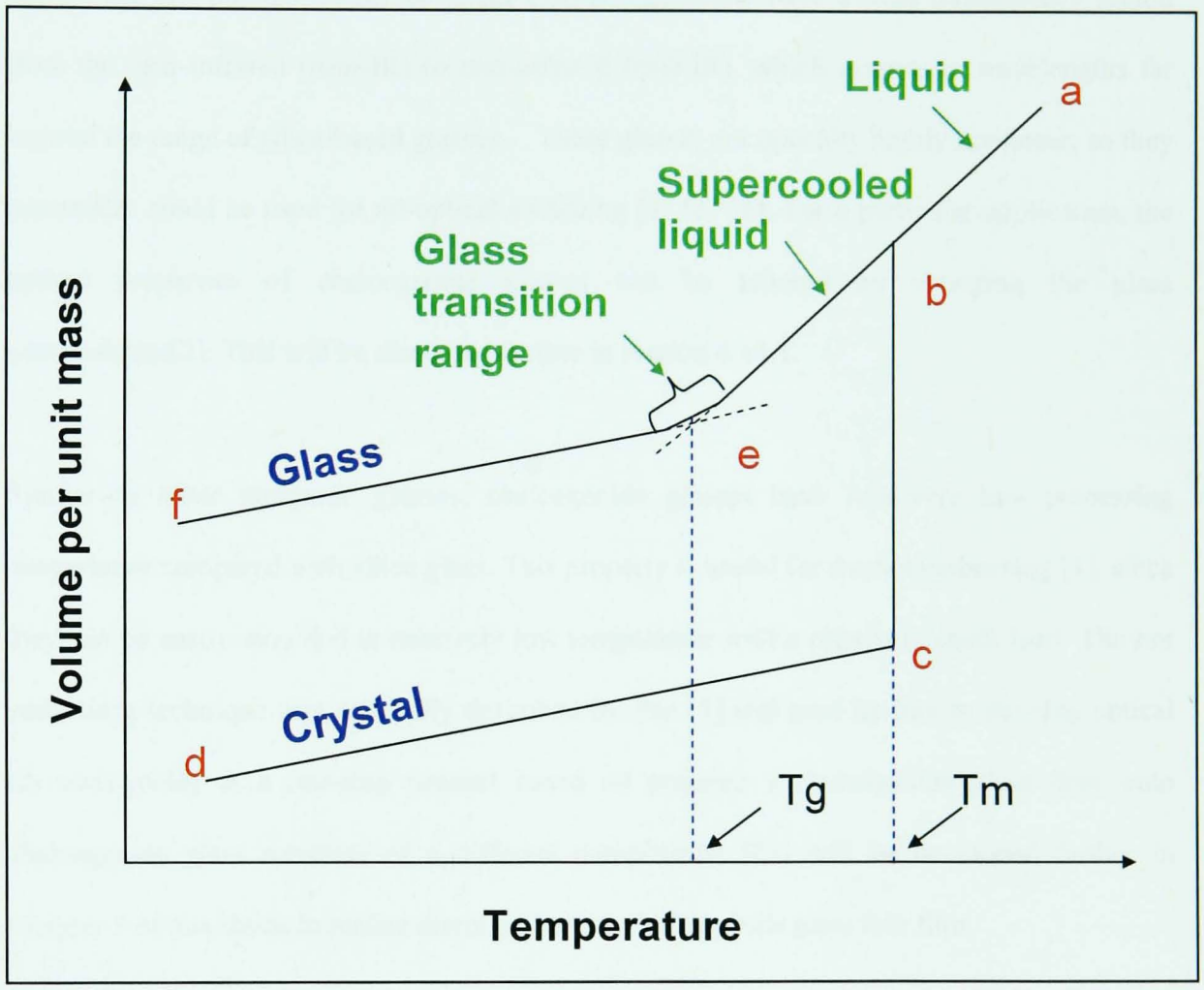

Figure 2.1: Schematic volume per unit mass / temperature diagram of the relationship between liquid and solid states; the glass transition temperature (Tg) range is shown, Tm is the melting point [34].

2.2 Optical properties of chalcogenide glasses

Glasses based on the chalcogen elements (S, Se and Te), i.e. those found in Group 16 in the Periodic Table but excluding oxides, are commonly termed chalcogenide [16]. These glasses are formed by the addition of other elements such as Ge, As, Sb and Ga etc. Like the conventional silicate glasses, chalcogenide glasses can be shaped and polished as lenses and for bulk optics; drawn into optical fibres; deposited as thin films and extruded. Chalcogenide glasses are low-phonon energy materials [16] and generally have a wide transparency region from the near-infrared (near-IR) to mid-infrared (mid-IR), which extends to wavelengths far beyond the range of silica-based glasses. These glasses are optically highly nonlinear, so they potentially could be used for all-optical switching [4, 16, 36]. For a particular application, the optical properties of chalcogenide glasses can be tailored by changing the glass compositions[2]. This will be discussed further in section 4.10.1.

Similar to other inorganic glasses, chalcogenide glasses have relatively low processing temperature compared with silica glass. This property is useful for the hot embossing [1], since they can be easily moulded at relatively low temperature with a relatively small load. The hot embossing technique was originally described by Pan [1] and used by him to develop optical rib waveguides in a one-step process based on pressing a chalcogenide glass fibre onto chalcogenide glass substrate of a different composition [22] will be developed further in Chapter 5 of this thesis to realise direct pattern on chalcogenide glass thin film.

Certain chalcogenide glasses compositions can be doped by rare-earth elements such as Er, Nd and Pr etc [4]. Hence, some optically active devices could be proposed using chalcogenide glasses. Table 2.1 lists some of the properties of chalcogenide glasses that are described in the literature. The information listed includes: glass transition temperature (Tg), refractive index and the optical transparency wavelength range. The optical transparency wavelength range is also called transparency window of material, it is bound by optical band gap at short wavelength and multi-phonon absorption at longer wavelength [2]. The glass compositions in Table 2.1 are ordered by the atomic % of each element.

Table 2.1 Summary of chalcogenide glass properties viz.: glass transmission temperature (Tg); refractive index (n) and glass transparency window (TW).

Glass composition / mol%	Tg /°C	n (λ / μm)	TW / μm	Reference
$As_{40}S_{60}$	215	2.45 (1.55)	-	Cardinal *et al.*, 1999 [6]; Harbold *et al.*, 2002 [37]
$As_{40}S_{60}$	-	2.43 (1.05)	-	Weber *et al.*, 1996 [38]
$As_{40}S_{60}$	208	2.45 (1.3)	0.6-10	Pope, 2006, [39]
$As_{45}S_{55}$	-	2.27 (1.50)	-	Petkov *et al.*, 1999 [10]
$As_{24}S_{38}Se_{38}$	121	2.5 (1.3)	0.8-12	Pope, 2006, [39]
$As_{24}S_{38}Se_{38}$	135	-	-	Cardinal *et al.*, 1999 [6]
$As_{40}S_{10}Se_{50}$	-	2.76 1.55)	-	Harbold *et al.*, 2002 [37]
$As_{40}S_{15}Se_{45}$	196	-	-	Cardinal *et al.*, 1999 [6]
$As_{40}S_{30}Se_{30}$	202	-	-	Cardinal *et al.*, 1999 [6]
$As_{40}S_{40}Se_{20}$	-	2.55 (1.55)	-	Harbold *et al.*, 2002 [37]
$As_{40}S_{45}Se_{15}$	207	-	-	Cardinal *et al.*, 1999 [6]
$As_{40}Se_{60}$	180	2.7 (1.3)	0.8-12	Lezal *et al.*, 2004 [40]
$As_{40}Se_{60}$	180	2.78 (1.5)	-	Lenz *et al.*, 2000 [41]
$As_{40}Se_{60}$	180	2.828 (1.3)	-	Pan, 2008 [1]
$As_{40}Se_{60}$	180	2.81 (1.55)	-	Harbold *et al.*, 2002 [37]
$As_{40}Se_{60}$	180	2.8014 (3)	-	Popescu *et al.*, 2000 [42]
$As_{40}Se_{60}$	180	2.784 (8)	-	Savage, 1985 [43]
$As_{40}Se_{60}$	191	2.81 (1.55)	-	Cardinal *et al.*, 1999 [6]; Harbold *et al.*, 2002 [37]
$As_{40}Se_{55}Cu_5$	-	2.93 (1.55)	-	Harbold *et al.*, 2002 [37]
$As_{40}Te_{60}$	-	-	1.5-15	Lezal *et al.*, 2004 [40]
$Ge_{33}S_{67}$	-	2.27 (1.50)	-	Petkov *et al.*, 1999 [10]
$Ge_{10}Se_{90}$	-	102 (1.5)	-	Smektala *et al.*, 2000 [7]
$Ge_{20}Se_{80}$	-	2.35 (1.3)	0.9-12	Lezal *et al.*, 2004 [40]
$Ge_{25}Se_{75}$	-	2.4 (1.5)	-	Lenz *et al.*, 2000 [41]
$Ge_{30}Se_{70}$	-	3.24 (1.5)	-	Smektala *et al.*, 2000

				[7]
$Ge_{20}As_{20}S_{60}$	-	2.112 (1.50)	-	Petkov, 1999 [10]
$Ge_{10}As_{10}Se_{80}$	128	-	-	Smektala *et al.*, 2000 [7]
$Ge_{15}As_{10}Se_{75}$	153	-	-	Smektala *et al.*, 2000 [7]
$Ge_{25}As_{10}Se_{65}$	305	-	-	He *et al.*, 1999 [44]
$Ge_{30}As_{10}Se_{60}$	280-340	-	8-12	Mecholsky Jun *et al.*, 1976 [45]
$Ge_{33}As_{12}Se_{55}$	-	2.53 (1.05)	-	Weber *et al.*, 1996 [38]
$Ge_{35}As_{12}Se_{50}$	380	-	-	He *et al.*, 1999 [44]
$Ge_{25}As_{15}Se_{60}$	-	2.22 (1.05)	-	Weber *et al.*, 1996 [38]
$Ge_{22}As_{20}Se_{58}$	292	-	-	He *et al.*, 1999 [44]
$Ge_{33}As_{12}Se_{55}$	362	-	-	He *et al.*, 1999 [44]
$Ge_{25}Se_{65}Te_{10}$	-	2.5 (1.5)	-	Lenz *et al.*, 2000 [41]
$Ge_{25}Se_{60}Sb_{12}$	-	2.61 (1.5)	-	Lenz *et al.*, 2000 [41]
$Ge_{28}Se_{60}Sb_{12}$	-	2.63 (1.05)	-	Weber *et al.*, 1996 [38]
$As_{25}S_{55}Te_{20}$	-	2.52 (1.55)	-	Harbold *et al.*, 2002 [37]
$65GaS_3$. $32La_2S_3$. $3La_2O_3$	-	2.41 (1.52)	-	Requejo-Isidro *et al.*, 2003 [46]
$68Ga_2S_3$. $32Na_2S$	-	2.14 (1.52)	-	Requejo-Isidro *et al.*, 2003 [46]
$70Ga_2S_3$. $15La_2O_3$.$15LaF_3$	-	2.26 (1.52)	-	Requejo-Isidro *et al.*, 2003 [46]
$70Ga_2S_3$. $30La_2O_3$	-	2.25 (1.52)	-	Requejo-Isidro *et al.*, 2003 [46]

Note: - information unavailable in the literature.

In this PhD project, $As_{40}Se_{60}$ was chosen as the core for both rib waveguides and Microstructured Optical Fibre (MOF). There are several advantages in choosing this composition. (1) This binary composition is well studied by many groups throughout the world and is considered as a relatively stable composition [2]. (2) Both As and Se precursors can be purified using a sublimation technique to form high purified glass. This offers opportunities to fabricate low loss planar waveguides and fibres. (3) Compared with other compositions in Table 2.1, the refractive index of $As_{40}Se_{60}$ is relatively high. Therefore, it is potentially good for nonlinear applications such as optical switches. (4) The optical and mechanical properties of $As_{40}Se_{60}$ may be tailored by adding other elements to change the composition. Therefore,

other suitable glass compositions which have close Tg, thermal expansion coefficient etc. can be developed by adding an extra element such as Ge into the $As_{40}Se_{60}$ composition. A more detailed discussion is presented in chapter 4.

2.2.1 Refractive index and zero dispersion

Refractive index is one of the fundamental optical properties of a material. The refractive data for varies over the optical frequency range of interest and this variation is termed dispersion. By controlling the refractive index of a medium the propagation of optical signals can be controlled. Table 2.1 depicts typical refractive index of a variety of chalcogenide glass compositions from the literature. The refractive index of $As_{40}Se_{60}$ was measured using the minimum deviation by Pan *et al.* [1] to be 2.828 at 1.3 μm wavelength; Sanghera *et al.* [37] reported the refractive index of $As_{40}Se_{60}$ to be 2.81 at 1.55 μm wavelength. Popescu *et al.* [42] reported the refractive index of $As_{40}Se_{60}$ over a large wavelength range from 3 μm to 12 μm to be 2.80 to 2.77; also Savage [43] reported the refractive index of $As_{40}Se_{60}$ at 8 μm, 10 μm and 12 μm. The refractive index of bulk $As_{40}Se_{60}$ as reported by all of these authors is plotted in Figure 2.2. This plot shows a general trend of the variation of refractive index against the wavelength.

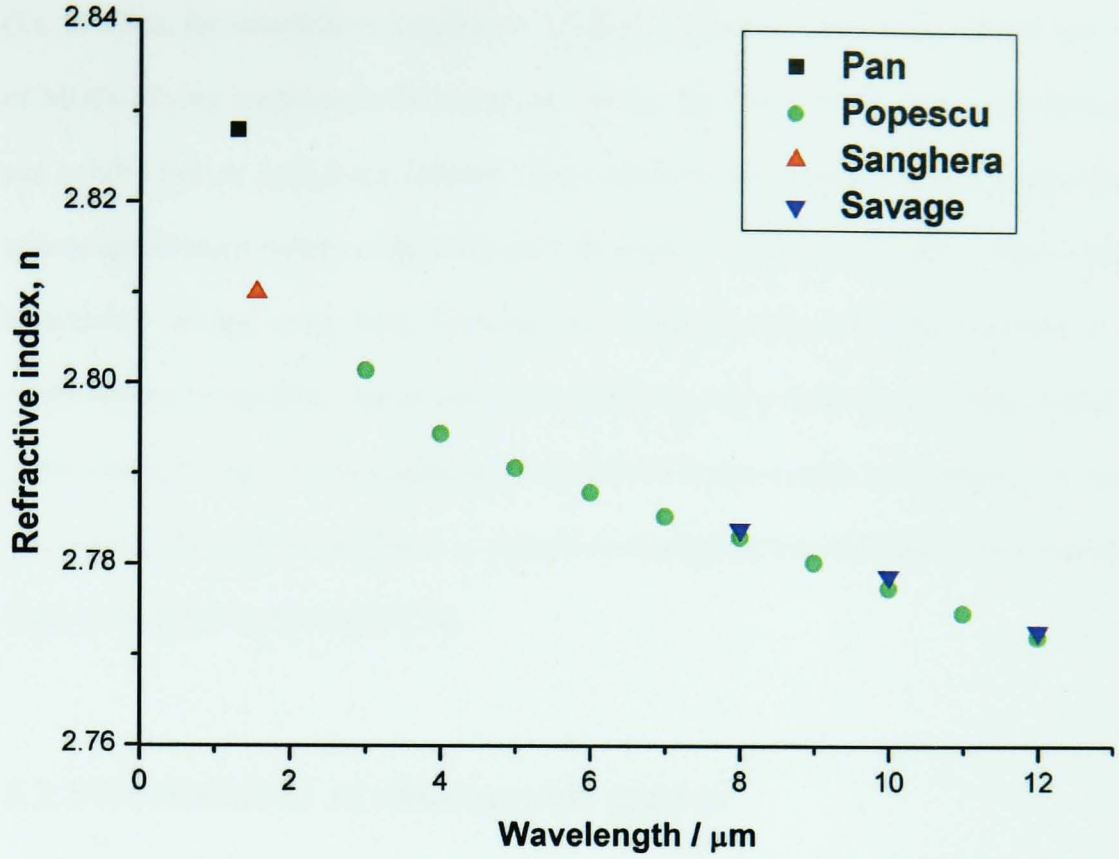

Figure 2.2: Bulk $As_{40}Se_{60}$ refractive index over the wavelength range of 1.3 μm to 12 μm, taken from the literature [1, 37, 42, 43].

When considering waveguide materials, dispersion, which is the variation in refractive index with wavelength, plays a pivotal role in dispersion-compensated waveguides. Overall waveguide dispersion is the combined effect of material dispersion and waveguide dispersion, in simplest terms describes how different wavelengths propagate in the waveguide. Silica glass dispersion was measured for bulk samples by Fleming *et al.* [47] and Kobayashi *et al.* [48]. The measurement was fitted to a Sellmeier dispersion relation. Also the dispersion of silica glass based optical fibre specimens were measured by Payne *et al.* [49] and Cohen *et al.* [50, 51].

The zero dispersion wavelength, e.g. for an optical fibre, is the wavelength where the group delay dispersion is zero. For a standard telecommunication fibre, this wavelength is ~ 1.3 μm, but by employing designs with modified waveguide dispersion it is possible to shift the zero dispersion wavelength to the 1.5 μm region where optical loss is also a minimum [52]. The dispersion is normal for shorter wavelengths (group velocity decreases with increasing optical frequency) and anomalous for wavelengths longer than the zero dispersion wavelength

(i.e. in silica, for wavelength longer than 1.3 μm). Photonic crystal fibres (which are a sub-set of MOFs relying on photonic band gaps to confine light) as well as some other fibre designs, can exhibit two or even three different zero dispersion wavelengths [26, 52]. Operation of a telecommunication system around the zero dispersion wavelengths greatly reduces dispersive broadening. At the same time, however, the signals become relatively sensitive to optical nonlinearities of the fibre, which give rise to effects such as four-wave mixing, which can be phase matched under these conditions. Therefore it is not always advantageous to operate in this regime; an improved approach is dispersion management in the form of successively using fibres with different dispersion [52].

2.2.2 Nonlinearity of chalcogenide glasses

In electromagnetism, the permittivity, ε, measures how much 'resistance' is encountered when forming an electric field in a medium, and it determined by the ability of a material to polarise in response to the field. The relative permittivity of a medium ε_r is related to susceptibility, χ, which measures how easily a dielectric polarises in response to an electric field. The relationship they have is: $\varepsilon_r = 1 + \chi$ [23]. In a vacuum, χ is 0, so ε_r is 1.

Before the 1960s, some basic mathematical equations or formulae manifested the linear nature of conventional optics [44]. In order to interpret the refraction, reflection, dispersion, scattering of light propagation in a medium, one important quantity should be considered, this is the electric polarisation induced in the medium. Electric displacement D is related to the polarisation density P as:

$$D = \varepsilon_0 E + P = \varepsilon_0 (1+\chi) E = \varepsilon_0 \varepsilon_r E \qquad 2\text{-}1$$

In the regime of conventional optics, the electric polarisation vector P is assumed to be linearly proportional to the electric field strength E of an applied optical wave:

$$P = D - \varepsilon_0 E = \varepsilon_0 \varepsilon_r E - \varepsilon_0 E = \varepsilon_0 \chi E \qquad 2\text{-}2$$

where ε_0 is the free space permittivity and χ is the susceptibility of a medium [44].

Shortly after the demonstration of the first laser device, i.e. the ruby laser, in 1960 [53], it was found that the simple linear assumptions were no longer adequate for circumstances in which an intense laser beam was incident on certain types of optical media. It was then realised that all of these new effects could be reasonably explained if the linear term on the right hand side of equation 2-1 was replaced by a power series:

$$P = \varepsilon_0[\chi^1 E + \chi^2 EE + \chi^3 EEE + \cdots] \qquad 2\text{-}3$$

where, χ^1, χ^2 and χ^3 are known as the first order, second order and third order susceptibilities [44]. These high order (nonlinear) properties give use to optical devices including all optical switching (AOS).

All optical switching (AOS) has exciting prospects for extremely fast signal processing and is considered as an important goal for high speed optical communication networks. There were many attempts to demonstrate AOS using silica but since the non-linearity of silica is small (n_2 = 2.8×10^{-16} cm^2/W) [4], either high power levels or long device lengths are required for switching applications. Compact and low threshold non-linear photonic circuits require non-linear materials with low loss and non-linearity at least several hundred times higher than silica [4]. Chalcogenide glasses are composed of heavy elements such as S, Se and Te, and possess a large value of optical nonlinearity materials (χ^3 materials) compared to silica glass [54]. Hence, chalcogenide glasses are considered to be good candidates for non-linear optics applications.

The third order nonlinear properties lead to the refractive index changes occurring on a time scale of ultra-short femtosecond laser pulses [4]. The non-linear refractive index n_2 is related to the third order susceptibility χ^3 as:

$$n_2 = 3\chi^3 / 4\varepsilon_0 n^2 c \qquad 2\text{-}4$$

where n is the linear refractive index and c is the velocity of light in vacuum. The suitability of

a nonlinear material for an application as a photonic switch is related to its ability to generate a relatively high nonlinear phase change in the propagation distance [4].

Multi-photon absorption is a nonlinear process that occurs at harmonics of the electronic band absorption frequency causing two or more photons to be absorbed at the same time [55]. The figure of merit (FOM) of two photon absorption (TPA) is defined as [55, 56]:

$$FOM = n_2 / \beta \times \lambda > 1 \qquad 2\text{-}5$$

where β is the TPA coefficient; λ is free space wavelength. A strong TPA of a material may accompany a large n_2, plays an important role in limiting the performance of all optical switching [57]. The value of FOM is required to be greater than 2, in order to ensure the transmission loss less than 20% [55]. Assuming the linear propagation losses are low, the suitable materials should have high n_2 to minimise the effect of TPA [55]. A comparison of the FOMs of some materials in the literature is useful. For the large optical band gap of bismuth oxide and silica, TPA is negligible at a wavelength of 1.5 μm [55], but they have relatively small n_2. The β of $As_{40}S_{60}$ is <0.1 at a wavelength of 1.5 μm [21], so the FOM is >10 [55]. For the Se-based chalcogenide glasses, the FOM of $As_{40}Se_{60}$, $Ge_{25}Se_{75}$, $Ge_{25}Se_{65}Te_{10}$ and $Ge_{28}Se_{60}Sb_{12}$ are 2, 1,3 and 2, respectively at 1.5 μm wavelength [41]. Chalcogenide glasses, in this case, have relatively large refractive index, high nonlinearity and moderate TPA, so they can be used for all optical switching applications [57].

The purpose of this project is to fabricate optical devices based on the chalcogenide glasses. Optical losses as the light propagates along the optical devices need to be considered. The sources of the optical losses include waveguide losses such as scattering imperfections in the core / cladding interfaces, surface roughness of the waveguide; impurity elements which absorb at the transmission wavelength or light scattering spots such as bubbles, crystalline inclusions, or phase-separation in the glass; also glasses exhibit intrinsic absorption loss, such as electronic absorption, multi-photon absorption and vibration absorption, and scattering loss, such as Rayleigh scattering [58].

2.2.3 Photosensitivity

Chalcogenide glasses many exhibit light-induced changes. These effects are of fundamental interest because of the information they yield on defects and metastable structural states in amorphous solids and because they are mostly unique to the amorphous states [58]. The photo-induced phenomena that occur in the chalcogenides may be classified according to whether they are primarily structural or physicochemical in nature and whether they are reversible or irreversible. The reversible photo-induced effects changes in local atomic structure and performs photodecomposition. The irreversible photo-induced effects include photocrystallisation, photopolymerisation, morphological changes and photovaporisation [58].

This optical property makes some waveguide fabrication methods possible such as laser writing [17, 59, 60]. Laser writing for producing waveguides within chalcogenide glasses will be discussed in section 2.4.2.

2.3 Chalcogenide glass thin films and thin film preparation methods

The attractive properties, e.g. high refractive index and high nonlinearity, of chalcogenide glasses (section 2.2) have indicated that they are good candidates for integrated optic devices. One requirement to use these materials in planar integrated optics is their availability as thin films. From the materials' aspect, a thin film is composed of one to several hundred atomic / ionic layers usually deposited on a solid substrate such as glass, ceramic or semiconductor. In an integrated optics context, it can be several microns thick.

There are several methods of fabricating chalcogenide thin films, i.e.: sputter coating [61, 62], thermal evaporation [49, 52, 53], spin coating [63-65], pulsed laser deposition [66, 67] and chemical vapour deposition [53, 59, 60]. Table 2.2 lists some reported thin chalcogenide glass films deposited using a variety of methods available in the literature [50-58]. A brief

description of each deposition technique is given and the advantages and disadvantages of each deposition techniques will be discussed.

Table 2.2: Thin chalcogenide film coating methods reported in the literature.

Coating method	Chalcogenide glass composition (mol %)	Reference
Sputter coating	$Ge_{33}As_{12}Se_{55}$, $Ge_{28}Sb_{12}Se_{60}$ and $Ge_{10}As_{40}Se_{25}S_{25}$	Balan *et al.*, 2004 [61], Ramachandra *et al.*, 1998 [62]
Thermal evaporation	$As_{40}S_{60}$ and As_xS_{100-x}	Fick *et al.*, 2002 [68]; Nagels *et al.*, 2003 [13]; Viens *et al.*, 1999 [49, 52, 53]
Spin coating	$As_{40}S_{60}$, $As_{50}S_{50}$, $As_{40}Se_{60}$, $As_{40}Te_{60}$, and $Ag_x(Ag_{33}S_{67})_{100-x}$.	Song *et al.*, 2001 [63]; Chem *et al.*, 1982 [64]; Kohoutek *et al.*, 2004 [65]
Chemical vapour deposition	As_xS_{100-x}, $Ge_{33}S_{67}$ and $Ge_{20}Se_{80}$	Nagels *et al.*, 2003 [13]; Huang *et al.*, 2004 [69]; Katsuyama, 1986 [70]
Pulsed laser deposition	$As_{40}S_{60}$ and $7Ga_{40}S_{60}.3La_{40}S_{60}$	Rode *et al.*, 2006 [66], Youden, 1993 [67]

Radio frequency sputtering coating [61, 62]

Several steps are involved in the deposition of chalcogenide glass thin films using a radio frequency (RF) sputter coating technique: (1) Prepare a target glass. Normally, the glass target is a bulk glass disc about 50 mm diameter and 10 mm thickness. (2) Prepare the substrate material, e.g. a piece of flat surface glass substrate. (3) RF frequency is 13.56 MHz. The operation chamber is normally evacuated to 10^{-4} Pa to avoid ambient contamination. (4) Ar+ ions are generated to sputter off the atoms from the target; (5) the sputtered atoms are transported and condensed on the surface of the substrate to form a thin film. The deposition rate reported was 0.25 μm/hour and the deposition condition was under an argon pressure of 5 Pa [61, 62].

One advantage of sputter coating is that high melting point materials can be deposited. Also, Sputtered films typically have a better adhesion on the substrate than evaporated films [61].

However, the stoichiometry of the deposited thin film may be slightly different from those of the target glass [61, 62].

Thermal evaporation [13, 17, 68]

The steps for depositing thin film using a thermal evaporation technique include: (1) Source material and substrate material preparation; (2) Placing the source material in a container connected a heating source; (3) Heating the source material and allowing the evaporated atoms to condense on a substrate in a vacuum atmosphere. Using a thermal evaporation technique, chalcogenide glasses $As_{40}S_{60}$ and As_xS_{100-x} thin films were reported to be able to deposited [13, 17, 68].

Compared with sputter coating technique, a thermal evaporation method can deposit at a higher speed. $As_{40}Se_{60}$ has a relatively low melting point and suitable for this technique. However, it has problems to deposit material with high melting point. In addition, for multi-component system, the non-congruent evaporation usually occurs leading to non-homogenous film [16]. The thermal evaporation technique is widely considered to produce inferior quality chalcogenide glass films [16].

Spin coating

Chalcogenide glasses can be dissolved in particular solvent, for example, Chern *et al.* [64] reported that $As_{20}S_{60}$, $As_{50}S_{50}$, $As_{40}Se_{60}$, $As_{40}Te_{60}$ and GeSe can be dissolved in high concentration in n-propylamine, n-butylamine, n-pentylamine and so on. In this process, (1) A few drops of the chalcogenide glass solution are pipette onto a substrate [1]. (2) The substrate is fixed to a rotational stage. (3) The rotational stage is spun to allow the chalcogenide glass solution to fully cover the substrate. (4) A post heat treatment is used to eliminate the solvent, e.g. n-propylamine, eventually leaving the chalcogenide glass film coated onto the substrate.

Spin coating is a relatively simple and low cost deposition technique. However, holes with diameters below 50 nm were observed in thin film of $As_{40}Se_{60}$ prepared in this way by Pan [1]. This observation indicated the quality of spin coat of film was not good.

Chemical vapour deposition

Chemical vapour deposition is widely used in the semiconductor industry to produce thin films. This technique is also used to produce the core of a conventional silica fibre preform. For chalcogenide glasses, Huang *et al.* [69] demonstrated that $Ge_{33}S_{67}$ can be deposited using chemical vapour deposition. The chemical reaction is described as follows: $GeCl_4$ was vaporised by means of bubbler and reacted with H_2S gas at temperature in the range of 450 – 600 °C,

$$GeCl_4 + 2H_2S \leftrightarrow GeS_2 + 4HCl.$$

This reaction takes place under atmospheric pressure in a horizontal quartz tube which is heated in a tube furnace.

Chemical vapour deposition produces good thin film quality [69] but several disadvantages also need to be considered: chemical vapour deposition is a complex process and requires high temperature. Also, toxic and corrosive gasses may be evolved.

Pulse laser deposition (PLD)

The experimental process of PLD involves several steps: (1) The source material, such as $As_{40}S_{60}$, is prepared and used as an ablation target, (2) The thin film deposition is carried out in a vacuum chamber (i.e. pressure $< 10^{-4}$ according to Youden [67]) and the target is ablated using a laser beam, such as a KrF excimer laser (operating at 248 nm wavelength and pulse duration of 20 ns) [67]. (3) A plume of ablated material is ejected perpendicular to the target surface and scanned in a vertical direction over the substrate surface. Rode *et al.* [66] reported

$As_{40}S_{60}$ chalcogenide films were successfully deposited using pulsed laser deposition (PLD). Also, Youden *et al.* [67] deposited Ga-La-S glass thin film using PLD. Ruan *et al.* [21] demonstrated that a low loss (0.25dB/cm) $As_{40}S_{60}$ rib waveguide was fabricated with the thin film that produce using PLD.

PLD is a relatively quick and simple technique for depositing thin films of a wide variety of materials [67]. However, it is difficult to produce uniform thin film over a relatively large area using PLD [71].

In general, all the preparation methods have advantages and disadvantages, to choose a proper method for experiments may depond on how good thin films the applications require, the time duration required for the fabrication process and also the safety issue. In this work, an $As_{40}Se_{60}$ thin film was deposited on a $Ge_{17}As_{18}Se_{65}$ substrate via thermal evaporation technique at the University of Pardubice.

2.4 Chalcogenide glass planar and strip waveguide fabrication methods

An optical waveguide is any structure which is able to direct the propagation of light energy in the form of an electromagnetic wave along a path. Optical waveguides provide the connections between functional optoelectronic components and behave as the building blocks of planar components such as couplers. In general, optical waveguides can be classified into three groups, planar slab waveguides, planar strip waveguides and fibre waveguides. Planar waveguides have their guiding structures on a surface of substrates; compare with fibre waveguides, they are easier to be integrated into optical device. In this project, rib waveguides were produced; they belong to the strip waveguide group. Optical fibre waveguides will be introduced in section 2.5.

The cross sectional view of a three layer slab waveguide is shown in Figure 2.3. Three layers of dielectric are considered in the structure: layer 1 which has refractive index n_1 locates in the middle and surrounded by layer 2 and layer 3 which have refractive index n_2 and n_3 respectively. Assume that $n_1 > n_2$ and $n_1 > n_3$, so total internal reflection can occur at each interface. The layer 1 (refractive index = n_1) is the guiding layer and layer 2 (n_2) and 3 (n_3) are cover layer and substrate layer.

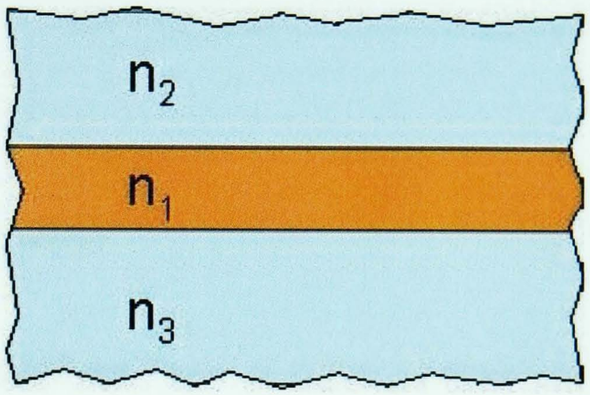

Figure 2.3: Schematic diagram of the cross section of a three layer slab waveguide. The refractive indices obey: $n_1 > n_2$ and $n_1 > n_3$.

The strip waveguides include several structures such as the raised waveguide, the embedded waveguide and the rib waveguide etc. as shown schematically in Figure 2.4. The orange colour area of each waveguide is the guiding region and the blue colour area of each waveguide is the substrate which normally has lower refractive index than the guiding region. An air cladding is assumed. The structures are also assumed to be invariant in the direction into the paper. They guide light in a 'pencil beam'.

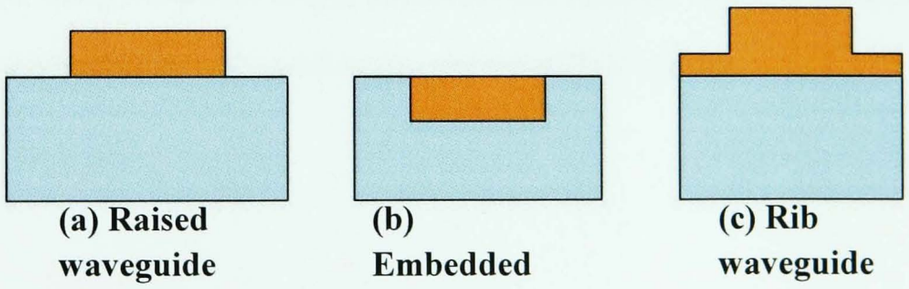

Figure 2.4: Schematic diagram of the cross section of (a) raised, (b) embedded and (c) rib strip waveguides. The orange colour area of each waveguide is the guiding region and the blue colour area of each waveguide is the substrate.

In this section, chalcogenide glass strip waveguide fabrication methods will be described. Some of the chalcogenide glass properties such as higher thermal expansion coefficient and lower glass transition temperature, compared with silica glass, affect the difficulties of fabricating these devices [21]. Some reports have described the successful fabrication of a chalcogenide waveguide; the methods include: photolithography and subsequently etching [21, 69]; laser beam writing [17, 72-75]; ion implantation [17] and femtosecond laser writing [60]. Sections 2.4.1 to 2.4.3 will describe some of these techniques and show their advantages and disadvantages.

2.4.1 Photolithography

Huang *et al.* [69] reported that a series of channel waveguides was patterned in a CVD deposited $Ge_{33}S_{67}$ thin glass film using Ar^+ ion beam etching. Waveguide structures of ~5 μm width and ~1.9 μm thick was deposited on CaF_2 and Schott N-PSK58 substrates. The reported waveguides loss was 2.1 ± 0.3 dB / cm at 632.8 nm using a He-Ne laser. A dry etching method to was used fabricate a $As_{40}S_{60}$ rib waveguide by Yuan *et al.* [21] and the waveguide is shown in Figure 2.5 (a) and (b). The substrates were a silicon wafer covered with a 2.4 μm thermal oxide layer; the thin films were prepared using ultra fast pulsed laser deposition. The width of the rib was 2 μm and the height was ~ 1.5 μm. An index contrast (Δn ~1) was reported and the rib waveguide exhibited a minimum propagation loss of 0.25 dB / cm at 1.55 μm wavelength over waveguide lengths between 12 mm and 50 mm. The dry etching system used to produce the rib waveguide was an Oxford Instruments RIE (Reactive Ion Etch)-100 ICP (Inductively Coupled Plasma) etcher; the etchant gas used was a CF_4/O_2 mixture.

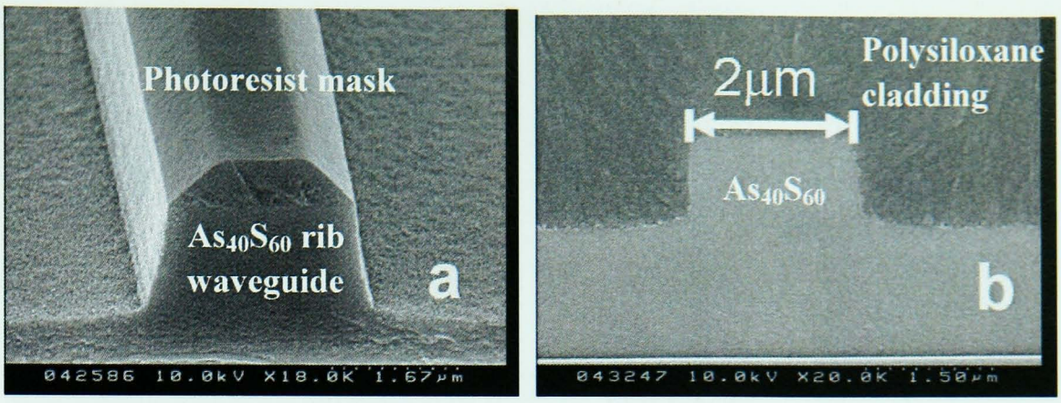

Figure 2.5: Scanning Electron Microscopy (SEM) micrographs showing the profile of an $As_{40}S_{60}$ rib waveguide fabricated using Inductively Coupled Plasma (ICP) etching by Yuan *et al.* [21]. (a) Top view of the $As_{40}S_{60}$ rib waveguide with photoresist mask and (b) Cross-sectional view of the $As_{40}S_{60}$ rib waveguide coated with a polysiloxane cladding (n= 1.53 @ 1.55 µm).

Chemical wet etching was also used to fabricate an $As_{24}S_{38}Se_{38}/As_{40}S_{60}$ chalcogenide ridge directional coupler by Viens *et al.* [17] as shown in Figure 2.6. The substrate was an oxidized silicon wafer, a further SiO_2 layer was deposited using thermal evaporation technique to provide a cladding between the substrate and the chalcogenide glass films. The higher refractive index $As_{24}S_{38}Se_{38}$ served as the core of the waveguide. However, compared with dry etching, undercutting of the mask layer always resulted in slanting sidewalls [21, 76]. The propagation loss reported was 1 dB/cm at 1300 nm for a single mode 5 µm × 1.25 µm waveguide.

Dale *et al.* [20] reported using a photolithographic method to produce metal dissolved diffractive structures in As-S glasses. A photolithographic technique was used to fabricate a surface relief grating in a bi-layer structure consisting of a 0.8 um $As_{30}S_{70}$ film by Zakery *et al.* [76].

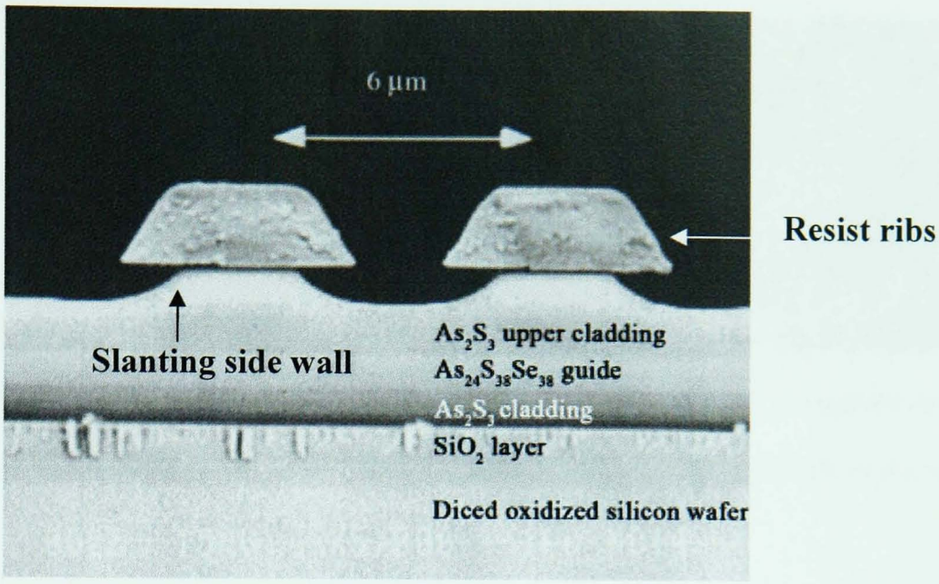

Figure 2.6: $As_{24}S_{38}Se_{38}/As_{40}S_{60}$ chalcogenide ridge directional coupler fabricated by Viens *et al.* [17] using chemical wet etching. The undercutting of the mask layer results in the slanting side wall.

2.4.2 Laser beam writing

Several reports have proposed the possibility of patterning using laser beam writing [17, 59, 72-75], where waveguides are produced using the photosensitivity of most amorphous chalcogenides to light of photon energy near their optical band edge [17]. The photostructural changes include structural e.g. photoexpansion [12] and optical e.g. photodarkening and refractive index change [9, 17] and have been shown to be wavelength and intensity dependent [77]. The advantage of laser writing is that it is non-contacting with the sample [59].

Zoubie *et al.* [59]created waveguides with penetration depth ≥ 1 mm over 10 mm in length and ~ 10 μm diameter in a thin $As_{40}S_{60}$ film using direct transverse writing employing an unamplified Ti: Sapphire laser see Figure 2.7. The operating wavelength of the femtosecond laser used was $\lambda = 845$ nm.

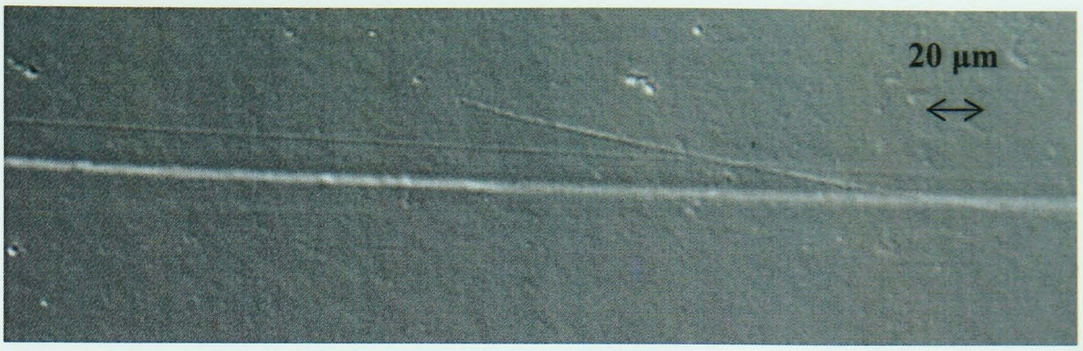

Figure 2.7: Fabricated $As_{40}S_{60}$ waveguide using unamplified Ti sapphire laser by Zoubie *et al.*[59]. The penetration depth was greater than 1 mm, the length of the waveguide was ~ 10 mm and the diameter was ~ 10 μm.

Efimov *et al.* [60] used a train of λ = 850 nm (Ti: sapphire laser) femtosecond pulses to produce a uniform channel within a bulk $As_{40}S_{60}$ glass. Waveguides of ~ 32 μm and ~ 9 μm diameter were produced as shown in the optical micrograph images illustrated in Figure 2.8 (a) and (b), respectively. The chalcogenide glass $As_{40}S_{60}$ is transparent to visible light; Figure 2.8 (c) shows the cross-sectional view of the ~32 μm diameter waveguide.

Viens *et al.* [17] fabricated waveguides using laser beam exposure at 514 nm wavelength in a thermally evaporated thin As-S-(Se) film. A 20 mm long $As_{40}S_{60}$ planar waveguide was achieved. Also, a vertical directional coupler was fabricated in two 2 μm thick $As_{24}S_{38}Se_{38}$, $As_{40}S_{60}$ layers which were used as the waveguide buffer and outer cladding, respectively, as shown in Figure 2.9. The light was first launched into the top channel of the waveguide; then it couples into the lower channel. The coupler was 12 mm in length, as indicated in Figure 2.9.

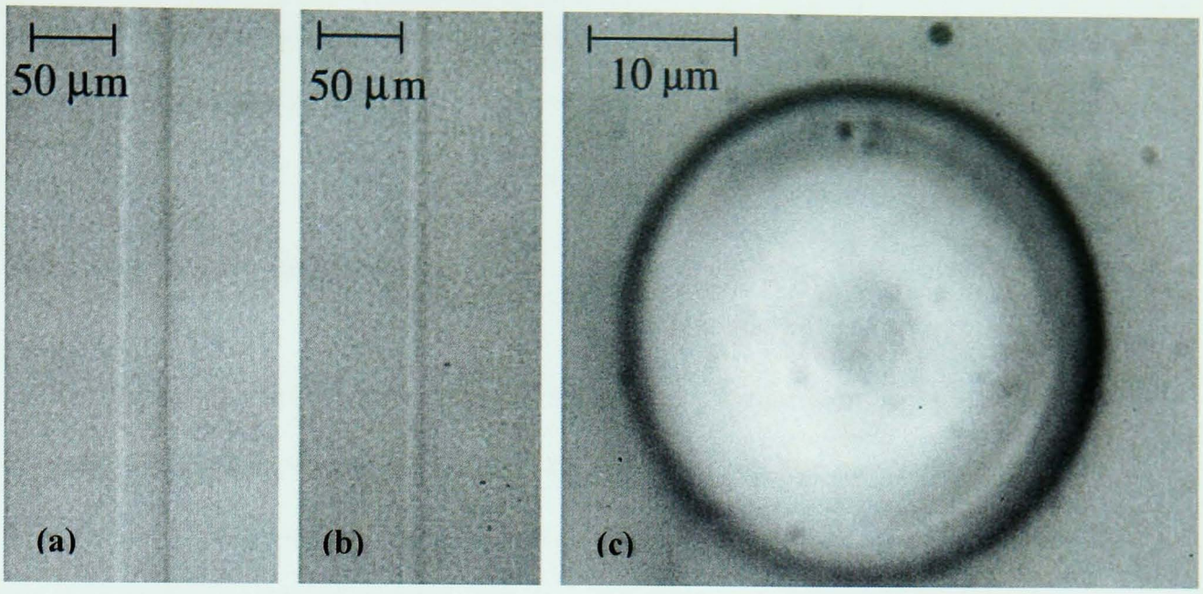

Figure 2.8: Optical micrographs of the $As_{40}S_{60}$ waveguide. A train of λ = 850 nm femtosecond pulses was used to produce the uniform channel. (a) Top view of one waveguide of ~ 32 µm diameter; (b) top view of one waveguides of ~ 9 µm diameter and (c) cross-sectional view of the ~32 µm diameter waveguide [60].

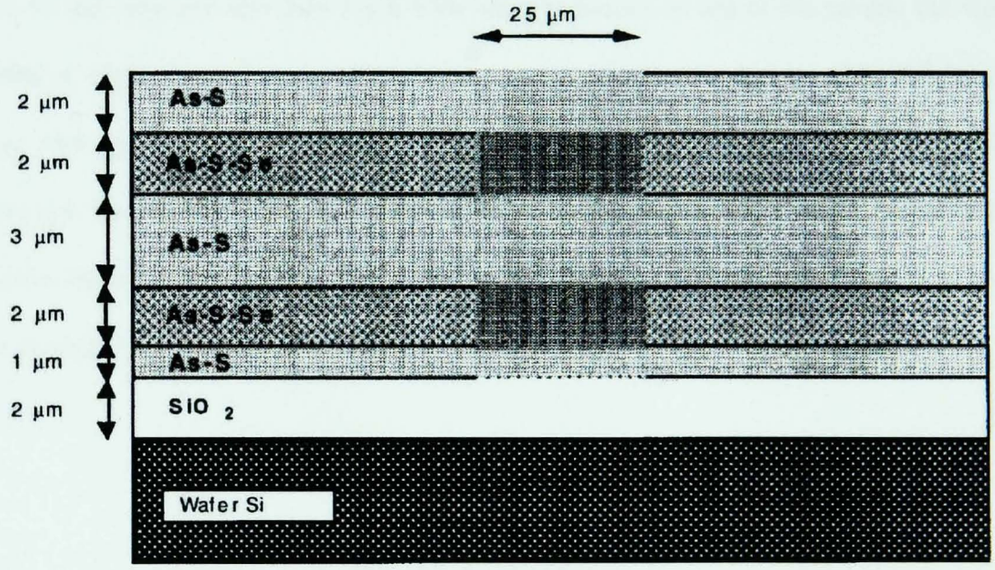

Figure 2.9: 12 mm long vertical directional coupler fabricated by Viens *et al.* [17] in two 2 µm thick $As_{24}S_{38}Se_{38}$ guiding layers. $As_{40}S_{60}$ layers were used as a waveguide buffer and as the outer cladding.

In most cases these changes, which were photo-induced, could be reversed after thermal treatment of 2 hours at 25 °C below the glass transition temperature and the waveguides were not visible using optical microscopy any more [8, 78]. These properties may make this method

unsuitable for producing photonic devices which are required to be stable over a long period under fluctuating conditions [21].

2.4.3 Ion implantation

The ion implantation technique is widely used for modifying the chemical, physical and optical properties of the surface layers of insulating materials [17, 79]. The main advantage of this technique is the possibility of controlling both the depth profile and the lateral distribution of the implanted ions [17]. But there are only rare reports on using ion implantation in chalcogenide glass [17].

Figure 2.10 depicts the fabrication process using ion implantation by Viens *et al.* [17]. A thin $As_{40}S_{60}$ film was thermally deposited onto a SiO_2 layer on a silicon wafer. A metallic mask with a 50 μm long and less than 5 μm wide slit was placed on top of the sample but without touching it. Helium ions were implanted at an energy of 113 keV, a dose of 2×10^{16} ion / cm^2 and an average current density of 1 $\mu A/cm^2$ to fabricate the waveguide [17]. A 1300 nm wavelength laser beam was guided through the waveguide channel confirming a positive refractive index change was obtained due to the helium implantation. The precise refractive index change obtained was not reported.

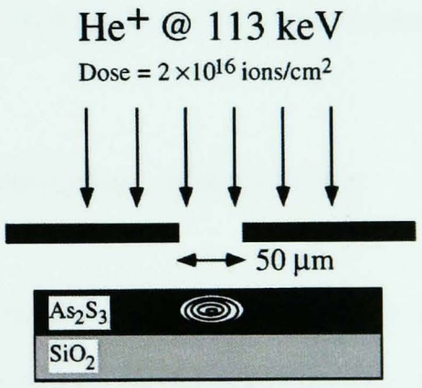

Figure 2.10: A schematic diagram of the fabrication of a buried channel waveguide using ion implantation. A 50 μm mask aperture produced a multimode $As_{40}S_{60}$ waveguide. [17].

2.4.4 One-step embossing

A one-step hot embossing fabrication method for optical rib waveguides was demonstrated by Pan [1]. This method is relatively simple and fast. A silicon mould was used to emboss $As_{40}Se_{60}$ fibre onto a flat $Ge_{17}As_{18}Se_{65}$ bulk glass to form a thin film and rib waveguide simultaneously [22]. Single mode optical guiding at wavelength of 1.55 μm was demonstrated using this fabrication method and the propagation loss was reported to be 3dB/cm. In this PhD work, the hot embossing method is employed to fabricate rib waveguide structures in $As_{40}Se_{60}$ thin films.

2.5 Microstructured Optical Fibres and their fabrication methods

The conventional core / cladding fibre has been used widely and behaves like a carrier for delivering light signals and delivered optical telecommunications [26]. The development of Microstructured Optical Fibres (MOFs) [25] realises a larger refractive index difference fibre by including air in the structured cladding. Also photonic band gap MOFs [24] realise that light could be trapped in lower refractive index cores (e.g. hollow core fibre) by creating a periodic wavelength-scale lattice of microscopic holes in the cladding glass [26]. Thus these fibres can carry more power and find use in optical sensing. This section summarises the development of MOFs, glasses of interest for MOFs, and MOF fabrication methods.

2.5.1 Conventional silica glass optical fibres

The use of an optical carrier for communication has been common for many years. A conventional optical fibre is a light conduit consisting of a cylinder of dielectric material surround by another dielectric material of lower refractive index. The light signal is transported through the inner medium of the fibre. In the 19^{th} century, the photophone (the device allowed for the transmission of sound on a beam of light) was proposed by Bell [80] after the development of the telephone, but due to lack of a suitable light source (no laser), the

development progressed slowly. The interest in optical communication awakened in the early 1960s after the invention of the laser [53, 81].

2.5.2 Microstructured Optical Fibres (MOFs)

In the early 1970s, micro-scale air holes were introduced into optical fibres for low loss data communication at Bell Laboratories by Kaiser *et al.* [81]. The fibre core was suspended in air within a robust solid jacket by the use of a thin glass membrane. The use of air as a cladding enabled the fabrication of a single mode fibre using a single material. In 1996, the first demonstration of optical guidance in a silica fibre with a complex holey cladding structure, as shown in Figure 2.11 (a) [25], catalysed interest in Microstructured Optical Fibres (MOFs). The structure of the MOF is a modified form of total internal reflection as the average refractive index in the solid core region is greater than that of the surrounding air-filled cladding region [82]. Photonic band gap fibres (PBFGs) were driven by the development of photonic crystals [83] and realised in 1999 by Cregan *et al.* [84]. It was proposed that via the introduction of a defect into the periodic transverse structure, light could localised by the defect for wavelengths within the photonic bandgap. Therefore, it is possible to guide light within an air core, which cannot be achieved by conventional fibres. Figure 2.11 (b) depicts the structure of a PBFG [84], the periodic structure has seven holes removed in the centre which act as a defect in the photonic bandgap.

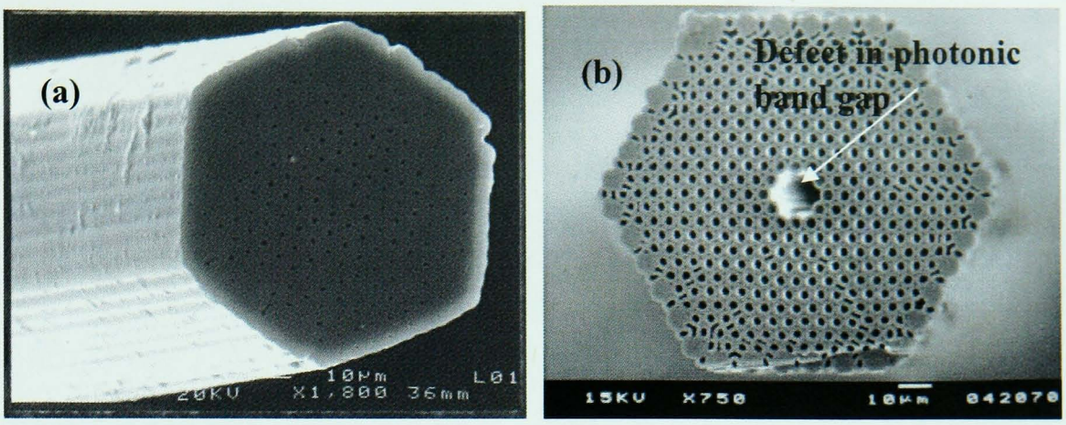

Figure 2.11: (a) First optical guidance in a silica glass fibre with a complex holey cladding structure by Knight *et al.* [25]. (b) Photonic Band Gap Fibre (PBGF) first produced by Cregan *et al.* [84]. Seven silica tubes were removed from the core to form the defect in the PBGF.

The Omni-directional fibre fabricated by the MIT, USA, photonics group [85-87] generated much attention. The mechanism of Omni-guiding fibre is using Bragg-reflection, hence this type of fibre is also called Bragg-reflection fibre [88]. As depicted in Figure 2.12 (a), the Omni-directional fibre has 10 bi-layers containing $As_{40}Se_{60}$ (refractive index ~ 2.75 at 10.6 μm wavelength) and a thermoplastic polymer with refractive index ~1.55 at 10.6 μm wavelength. This offers a perfect mirror to the inside of the tube which supplies total internal reflection. The hollow core was ~ 350 μm diameter. The thickness of the $Ae_{40}Se_{60}$ layer and polymer layer were 270 nm and 135 nm, respectively. The transmission loss of this fibre was reported to be less than 1 dB m^{-1} at a wavelength of 10.6 μm [85].

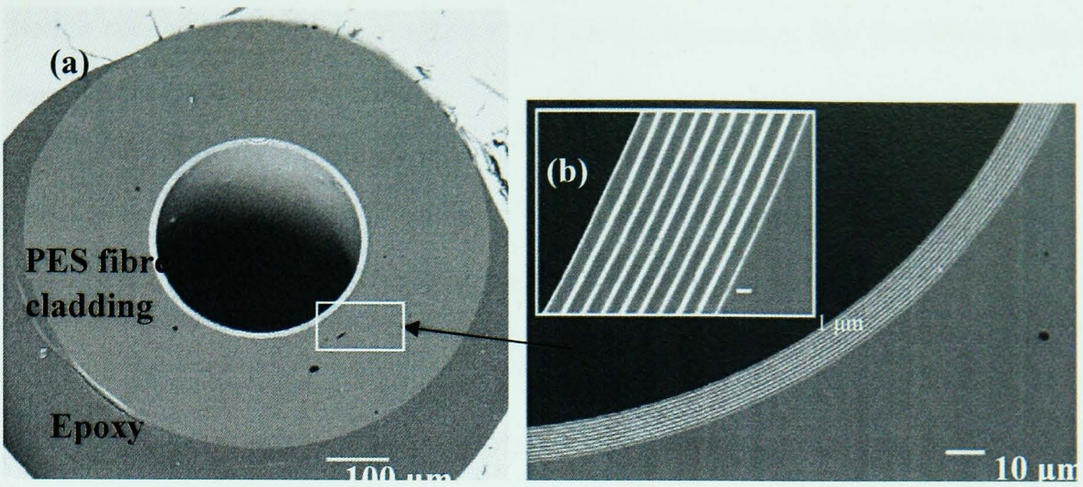

Figure 2.12: Omni-directional fibre fabricated by Temelkuran *et al.* [85]. The Omni-directional fibre shown has 10 bi-layers consisting of $As_{40}Se_{60}$ and thermoplastic polymer. The thickness of each $Ae_{40}Se_{60}$ layer was 270 nm and the thickness of each polymer layer was 135 nm. The hollow core was ~ 350 µm diameter.

2.5.3 Materials for MOFs

Potential materials for fabricating MOFs include silica, inorganic compound glasses and polymers. In this section, the advantages and disadvantages of these candidates will be described.

2.5.3.1 Silica glass

Silica glass is widely used to form the conventional optical fibre and holey fibre. It is routinely possible to fabricate fibres with losses less than 0.2 dB km^{-1} [82]. Index guiding MOFs and PBGFs can be made from pure un-doped silica glass. The applications for silica fibre include power delivery and fibre based nonlinear devices. Er^{3+} and Yb^{3+} doped silica fibres were fabricated [82] for amplifier applications.

The benefits of choosing silica glass for fabrication of MOFs are power handing capability [82] and relatively low cost. But the low intrinsic nonlinearity makes it not well suited for nonlinear devices. Also, the intrinsic absorption of silica increases for wavelengths larger than 2 µm.

Hollow core silica MOFs are not affected by material absorption as light is confined in the air core.

2.5.3.2 Inorganic compound glasses

Inorganic compound glasses refer to telluride, fluoride and chalcogenide glasses etc. A number of inorganic compound glasses transmit at wavelengths into the mid-infrared (mid-IR), which is far beyond the capability of silica glass. Glasses consisting of heavy metal oxides such as TeO_2, GeO_2, and those having low bond strength such as ZrF_4-BaF_2 and $As_{40}S_{60}$, exhibit a low phonon energy [82]. For low phonon energy glasses, the multi-phonon edge is shifted to longer wavelengths [89]. As will be discussed below, inorganic compound glasses exhibit high intrinsic optical nonlinearity which can be used to produce MOFs with extreme values of effective fibre nonlinearity[82].

Many reports demonstrate the successful fabrication of inorganic compound glasses fibres. In the University of Southampton, a single mode telluride glass holey fibre was made from an extruded preform by Feng *et al.* [90, 91]. The telluride holey fibre was produced via an extrusion technique and showed single mode guidance at 1.55 μm. A broad and flat supercontinuum from 0.9 to 2.5 μm with 6 mW output was obtained with a 9 cm length telluride fibre [91]. Richardson *et al.* fabricated 'wagon-wheels' shaped bismuth glass holey fibres [92]. The holey fibre had < 3 dB/m propagation loss and the nonlinearity was γ = 1100 $W^{-1}km^{-1}$ [92]. In the University of Adelaide, Monro *et al.* [93] fabricated many MOF structures, e.g. holey fibre and 'wagon-wheel' shapes [94], based on inorganic compound glasses such as fluoride glass, F2 (PbO-SiO_2) glass, bismuth glass and telluride glass [94, 95]. Using a two-step stack-and-draw technique, a chalcogenide glass $Ge_{15}Sb_{20}S_{65}$ MOF was produced by Desevedavy *et al.* [28]. An As-Se MOF has been reported for infrared wavelength region supercontinuum generation extending from 2.1 μm to 3.2 μm using a 2.5 μm pump laser by Shaw *et al.* [96].

2.5.3.3 Polymer

A variety of polymers has been used for fabricating MOFs, due to their low cost and ability to form transverse geometries not easily achievable in silica glass fibres [82]. Microstructured polymer optical fibre was first fabricated by Eijkelenborg *et al.* [97, 98]. It is also possible to allow dopants to be introduced in polymer microstructured fibres using atactic polymethylmethacrylate (PMMA) [97, 98].

2.5.4 Optical fibre and preform fabrication methods

This section describes fibre fabrication methods; the fabrication of MOFs normally employs a combination of several steps.

2.5.4.1 Conventional silica optical fibre fabrication methods

For conventional core / cladding silica optical fibres, the fabrication can divided into two main methods, (i) direct fibre drawing, e.g. double crucible processes [99-102] and (ii) fibre drawing from a fibre preform, e.g. rod-in-tube type processes [100, 103] or extrusion [104-106]. These are discussed in turn:

(i) Direct fibre drawing means fibre is drawn from a silica glass melt with no need for a solid preform. The method uses double crucible processes [95-98]. The double crucible technique employs two quartz tube crucibles as shown in Figure 2.13. One of the crucibles contains the core glass and is located inside of the other crucible which contains the cladding glass. Each crucible is connected to an individual gas source and pressure controller which supply pressures (P1 for core and P2 for cladding). Core and cladding materials are melted inside of the inner and outer crucibles; the temperature is then cooled down very quickly to the drawing temperature as the fibre drawing starts [76].

(ii) Production of a core / cladding preform for fabricating core / cladding fibre has been commonly used. Two methods to produce a preform will be described: (a) rod-in-tube type and (b) using the extrusion technique.

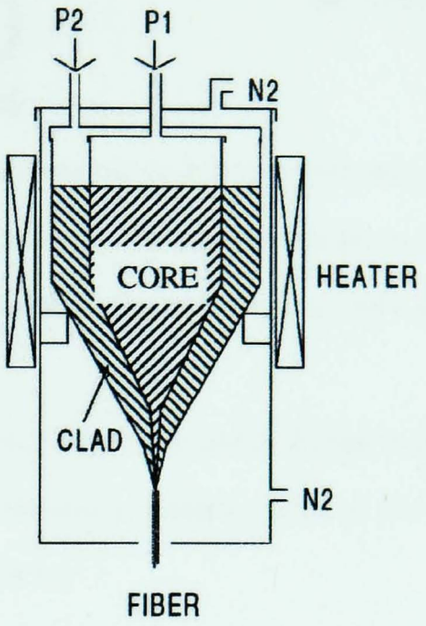

Figure 2.13: Double crucible processes. One of the crucibles contains the core glass and is located inside of the other crucible which contains the cladding glass. The crucibles are heated to a temperature above Tg; then the melt is drawn to fibre from the bottom of the crucible [99-102]. Both crucibles connect to an individual pressure controller, i.e. P1 and P2 control the inner pressure of core crucible and cladding crucible, respectively.

(a) The rod-in-tube technique has been a popular technique for producing single mode optical fibre. Heating glass preforms via rod-in-tube type processes [100, 103] is shown in Figure 2.14. A glass tube is prepared using core drilling, rotational casting methods [107] or via extrusion [108] to form the cladding of the preform of the fibre. Then a prepared glass rod is slotted into the tube to form the core of the preform. The assembled preform is then drawn down to fibre. Due to the need for more than one material in this technique, it may not suitable for all glass compositions due to the material thermal mismatch [76].

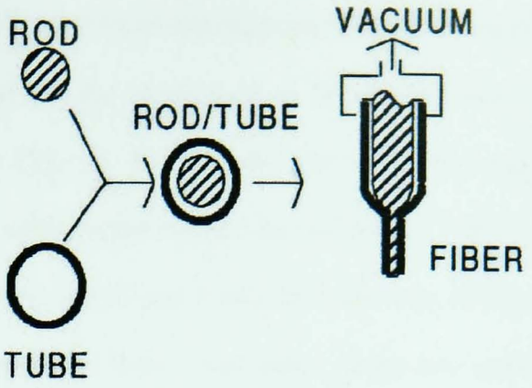

Figure 2.14: Schematic diagram of rod-in-tube type processes. A prepared core glass rod was slotted into a prepared tube and the assembled preform was then drawn into core / cladding fibre [100]. A vacuum is applied to contract the tube onto the rod.

(b) The extrusion technique was first demonstrated by Roeder in the 1970s [104, 105]. Roeder extruded multi-component oxide glasses, including silicates. The extrusion technique will be discussed in detail in section 2.5.4.2.

2.5.4.2 Conventional inorganic compound glasses optical fibre fabrication methods

The methods used to produce conventional core/clad optical fibre from inorganic compound glasses include the methods used for fabricating silica fibre, e.g. double crucible technique, rod-in-tube process and extrusion. However, depending on the glass properties, the temperature conditions used for these methods vary correspondingly.

An extrusion technique was used for producing both core / cladding and hollow fibre preforms [106]. Figure 2.15 shows a schematic diagram of the extrusion technique [106]. Two glass billets which become core and cladding of the fibre respectively are placed above an orifice die. The temperature is raised to melt the glass to a supercooled liquid then a high pressure is applied to push the supercooled liquid through the orifice of the die.

Extrusion has been widely used for producing many different inorganic glasses MOF preforms by many groups through out the world such as in the University of Southampton and the University of Adelaide [31, 82, 90, 93] etc. Our laboratory has pioneered extrusion of chalcogenide glass fibre optic preforms since the mid 1990s [108-112]. Ga-La-S glass rod was formed with a good surface finish and 5 mm diameter with 0.08% diameter variation [108, 111]. Also, the co-extrusion of high / low index plates into core/clad preform tubes was demonstrated [19, 107, 110].

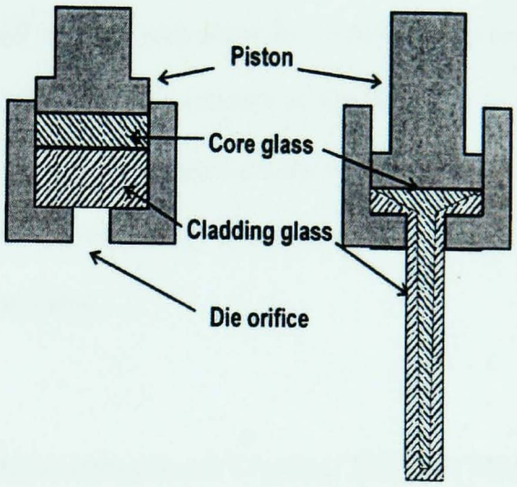

Figure 2.15: Schematic diagram of extrusion technique to produce a inorganic glass core / cladding preform [106].

The rotational casting tube method for fabricating optical fibre was introduced for heavy metal fluoride glasses material [113, 114] as depicted in Figure 2.16. A precise amount of the cladding melt was first melted in a platinum crucible then poured into a gold-plated mould (preheated at Tg). The mould was spun at several thousand rpm to form a tube cladding. The cladding size was controlled by the amount of cladding glass. The core glass was then cast into the tube. The cast preform was then annealed to prevent cracks.

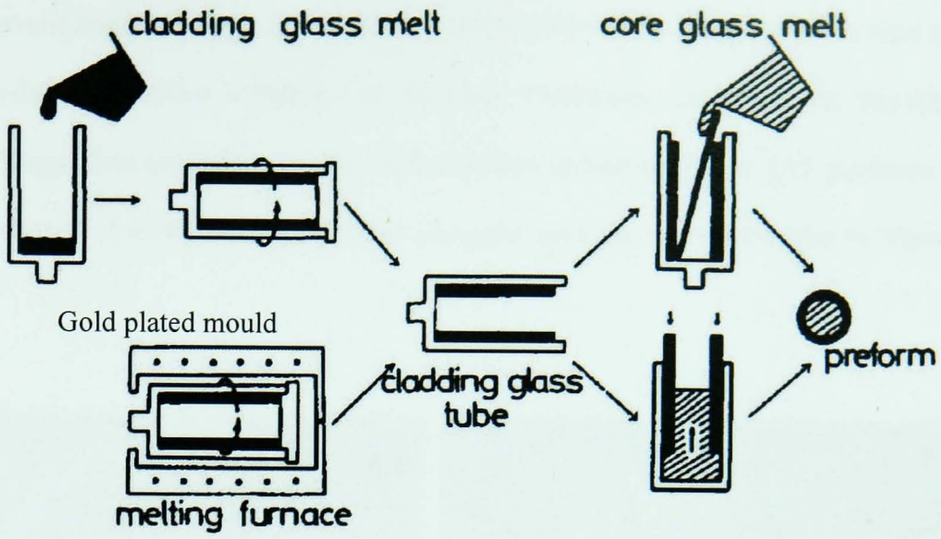

Figure 2.16: A rotational casting technique for fabricating heavy metal fluoride glass fibre optic preforms [113]. A precise amount of the cladding melt was first melted in a platinum crucible then poured into a gold-plated mould. The mould was spun at several thousand rpm to form a tube cladding. The core glass was then cast into the tube. The cast preform was then annealed.

2.5.4.3 Silica glass Microstructured Optical Fibres (MOFs): fabrication methods

There is no direct fibre drawing method available in the literature to date to fabricate either silica glass or inorganic glass Microstructured Optical Fibres (MOFs). Therefore, preforms need first to be created which contain the desired fibre structure to draw down to fibres. The silica glass photonic crystal fibres (PCFs) [24, 26] and the silica glass Bragg fibres [85] use a stack-and-draw technique.

In the 1970s, Bell Laboratories developed the capillary stacking technique [81], which then was used to produce silica MOFs [25]. Silica glass tubes which are commercially available 10 – 30 mm OD were fibre drawn down to a diameter of ~1 mm from a fibre tower, then stacked layer by layer in a closed packed normally hexagonal configuration as demonstrated in Figure 2.17 (a) to form a preform. The stacked preform was then drawn into fibre. For a solid core MOF, the centre tubes of the stacked preform were replaced by rods which behave as the core.

For photonic band gap fibre, the centre 1, 7 or 19 tubes of the stacked preform were removed to form defects as shown in Figure 2.11 (b) where 7 holes have been removed. The fabrication of the Bragg fibres could also use the stack-and-draw technique. Figure 2.17 (b) shows the first demonstration of an air silica Bragg fibre using the stack-and-draw technique by Vienne *et al.* [115].

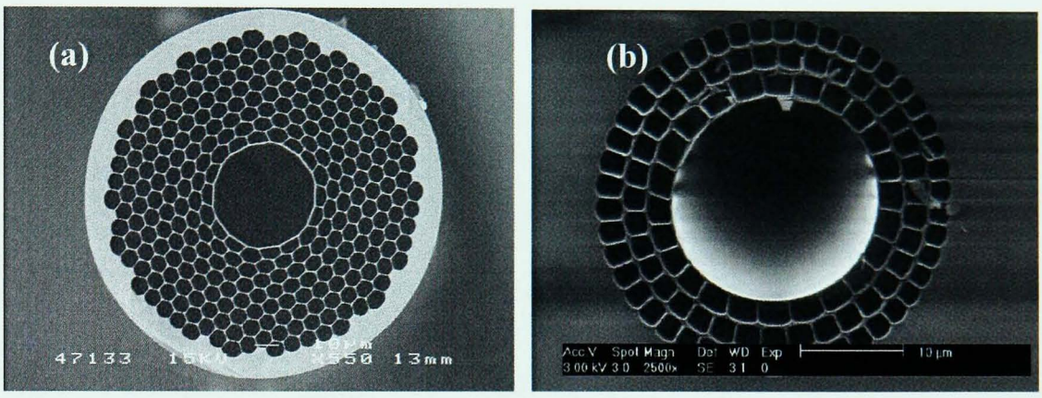

Figure 2.17: The capillary stacking technique was used to produce silica glass photonic band gap fibres and Bragg fibres. (a) Silica tube was drawn down to ~1 mm thick and stacked layer by layer in a closed packed normally hexagonal configuration. The silica tube in the core was removed to form a photonic band gap fibre [25]. (b) Bragg air – silica glass fibre fabricated using the stack-and-draw technique [115].

2.5.5 Chalcogenide glasses Microstructured Optical Fibres (MOFs): fabrication methods

The fabrication of MOF based on chalcogenide glasses is one of the aims of this PhD project. The fabrication methods reported in the literature include the stack-and-draw technique and the spiral rolling technique for Bragg fibres.

The first chalcogenide glasses Air / glass microstructuring of Ga-La-S-O glasses was reported by Monro *et al.* in the University of Southampton [27] as shown in Figure 2.18 (a). The fibre has an outer diameter of 100 μm and the core diameter of 10 μm. The holes in the cladding capillaries rang in diameter from 1.5 to 4.0 μm. Ga-Ge-Sb-S MOF was produced by Troles *et al.* [116] as illustrated in Figure 2.18 (b). Selenium based glass / air microstructured fibres have

been developed by Shaw *et al.* [117] and Désévédavy *et al.* [28] (Figure 2.19). Shaw *et al.* [117] fabricated air / chalcogenide ($As_{39}Se_{61}$) glass microstructured fibre which exhibited a supercontinuum in the mid-IR from 3.1 μm to 4.8 μm wavelength, a wavelength range that was reported not to be limited by the glass transmission edge. Similar air / glass microstructured fibre of chalcogenide glasses, developed since by Désévédavy *et al.* [28] and illustrated in Figure 2.19, had a lowest loss at 1.55 μm wavelength of 13 dB/m.

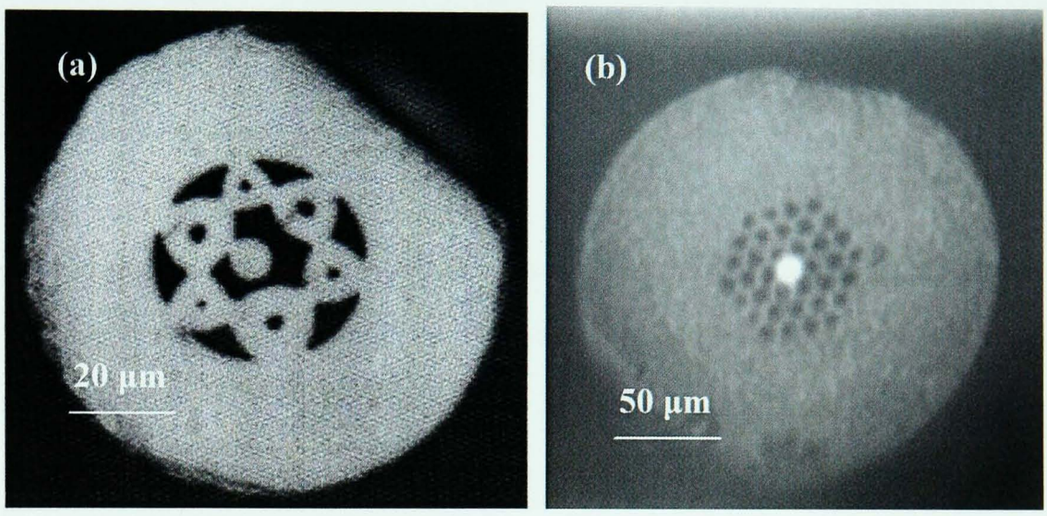

Figure 2.18: Chalcogenide glass optical fibres. (a) Air / glass microstructuring of Ga-La-S-O glasses was reported by Monro *et al.* [27]. The fibre has an outer diameter of 100 μm and the core diameter of 10 μm. The holes in the cladding capillaries rang in diameter from 1.5 to 4.0 μm. (b) Ga-Ge-Sb-S MOF was produced by Troles *et al.* [116]. Fibre diameter is 400 μm, pitch between holes is 28 μm and hole diameter/pitch ratio is 0.5.

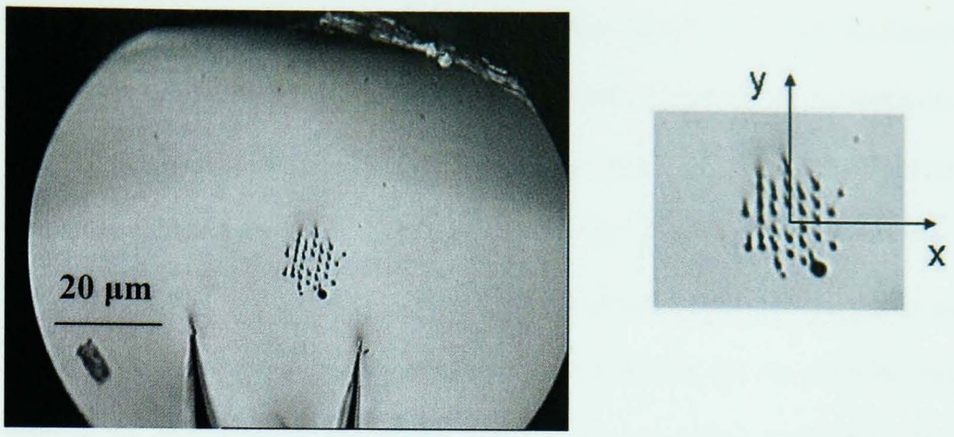

Figure 2.19: Small core chalcogenide glass MOFs was fabricated by Désévédavy *et al.* [28] from $Ge_{15}Sb_{20}Se_{65}$ glass. Diameter of the fibre is 80 μm, the pitch between holes is 2.5 μm and the hole diameter/pitch ratio is 0.34.

Notice that in the reported chalcogenide glasses MOFs, the hole sizes are not uniform in shape. This suggests that the strength of the chalcogenide glass is weak to realise holey fibres structures. According to Feng *et al.*[31], the pressure inside of holes of hollow MOFs changes during the fibre drawing process. Therefore, the surface tension of the glass increases which can reduce or close the holes in the microstructured profile. In order to prevent the collapse of the holey microstructure in MOFs, the upper part of the holes in the perform is normally sealed [31]. However, the sealed holes in the preform cause the internal pressure to build up gradually and means the microstructured profile cannot to be maintained in a kilometre-scale long MOF. Consequently, the non-uniform holey fibre profile may result a deviation of properties such as dispersion [31]. In this PhD work, several attempts were made to fabricate holey structure chalcogenide glass fibre, but the fabrication results confirmed the difficulties. Therefore, a straightforward solution is to introduce a second chalcogenide glass to replace the holes in the holey structured MOFs. The advantage of a two materials solid MOF is the easier fabrication process, because the microstructured profile can be maintained without applying internal pressure. However, a negative side is difficult to find suitable material pairs which have matched thermal properties and sufficient refractive index contrast.

Another method for fabricating chalcogenide glass fibres is spiral rolling. Chalcogenide glass – polymer Bragg fibre was produced by the researchers in a group in MIT [118] using this

method. Thermoplastic polymer having a refractive index of 1.55 at a wavelength of 10.6 μm, poly (ether sulphone) (PES), was used. Chalcogenide glasses having a softening point close to that of the polymer offer possible composite structures [119]. This method comprises 4 steps as shown in Figure 2.20 [118]. (1) the $As_{40}Se_{60}$ thin glass film was deposited onto the PES polymer [85] film using a thermal evaporation technique (section 2.3); (2) the coated film was rolled into a hollow multilayer cylinder on a SiO_2 former; (3) the cylinder was heated under vacuum for consolidation and (4) the SiO_2 former was etched (the etching chemical was not clearly reported) out to obtain the chalcogenide glass – polymer preform. The preform was then drawn into fibre. The omni-directional guide Bragg fibre is single mode and has low loss of 1.0 dB/m at wavelength of 10.6 μm. The bending loss is about 3.0 dB/m through a 1 cm radius knot.

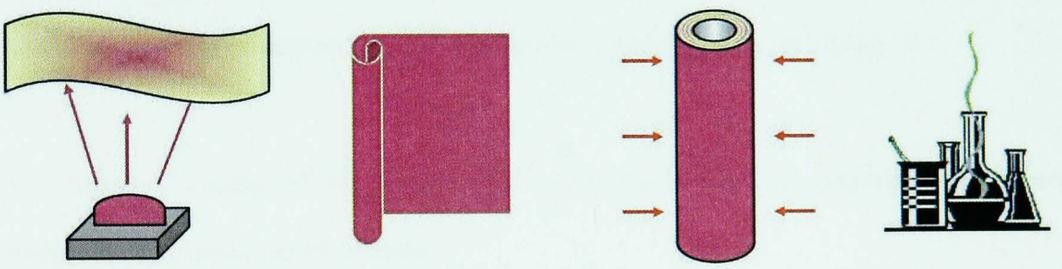

Step 1: Stoichiometric thermal evaporation of $As_{40}Se_{60}$ onto free-standing PES film

Step 2: Rolling of coated film into hollow multilayer cylinder on SiO_2 tube substrate

Step 3: Vacuum thermal consolidation

Step 4: Etching and removal of SiO_2

Figure 2.20: Four steps for fabrication of the Omni-directional fibre using a spiral rolling method. (1) the $As_{40}Se_{60}$ thin glass film was deposited onto a polymer film using thermal evaporation method; (2) the coated film was rolled into a hollow multilayer cylinder on SiO_2; (3) the cylinder was heated under vacuum and (4) removal of the SiO_2 former by etching [118].

2.6 Summary

The background of this PhD project has been reviewed in this chapter. Based on the objectives of this project, some relevant topics were particularly addressed. (1) Glass science was briefly introduced and several interesting properties of chalcogenide glass were also described, e.g. high refractive index, high nonlinearity and transparency in the infrared wavelength region. These properties make it a good candidate for optical devices and optical fibre at near - far infrared wavelengths. (2) Thin glass films and their preparation methods were discussed. The fabrication of planar and strip waveguides was then introduced. (3) Optical fibres include both conventional silica glass fibre and Microstructured Optical Fibres (MOFs) and their fabrication methods were reviewed. The field of MOFs is just at the beginning. With optical losses being reduced beyond those in conventional fibres and with understanding of the enormous potential offered by the new structures, MOFs will be widely employed in the future.

In Chapter 3, some of the experimental procedures used to prepare and characterise chalcogenide glasses are introduced.

Chapter 3

Experimental Procedures

This PhD project involves the design and fabrication of optical waveguides in strip rib and microstructured optical fibre (MOF) forms. A fundamental task is thus to study chalcogenide glass preparation and characterisation. This chapter describes the general experimental procedures of these tasks as listed in Table 3.1, more detailed descriptions will be given as appropriate in later chapters.

Table 3.1: Experimental procedures to be described in this chapter.

Glass melting	Ampoule preparation, batching, melting, quenching, annealing, cutting and polishing.
Batch & Purification	As and Se purification.
Glass characterisation	Differential Scanning Calorimetry, Fourier Transform Infrared Spectroscope, Scanning Electron Microscope, X-ray Diffraction, Thermomechanical Analysis and refractive index.
Fabrication of Rib waveguide	Hot embossing.
Fabrication of Micro-structured optical fibre	Fibre design, rotational casting, stacking and drawing.

3.1 Preparation of Chalcogenide Glass

This section provides the experimental process for melting chalcogenide glasses. Experimental procedures will be described in the following order: silica glass ampoule preparation, batching of components and chalcogenide glass melting, quenching and annealing.

3.1.1 Ampoule preparation

The ampoule (supplier: Multi-Lab Ltd.) used was made of silica glass (OH level < 1 ppm) with 10 mm inner diameter (ID), 16 mm outer diameter (OD), a length of 300 mm and one end was sealed.

Before the raw materials were batched into the ampoule, it was cleaned thoroughly and baked out. The first stage of ampoule cleaning was to rinse the ampoule three times with distilled water and leave it in a drying oven which was held isothermally at 70°C. The second stage was to bake the ampoule under ambient air at 1000°C under a dust cover for at least 6 hours to remove any carbon based deposition (dust or some other organic debris) from the inside surface The third stage was to repeat the second stage time schedule but under vacuum conditions (8.0×10^{-7} mBar; 8.0×10^{-5} Pa, pressure was measured at the vacuum pump) in an effort to remove physisorbed and chemisorbed water (Figure 3.1). Details of the ampoule air and vacuum baking are detailed in Table 3.2.

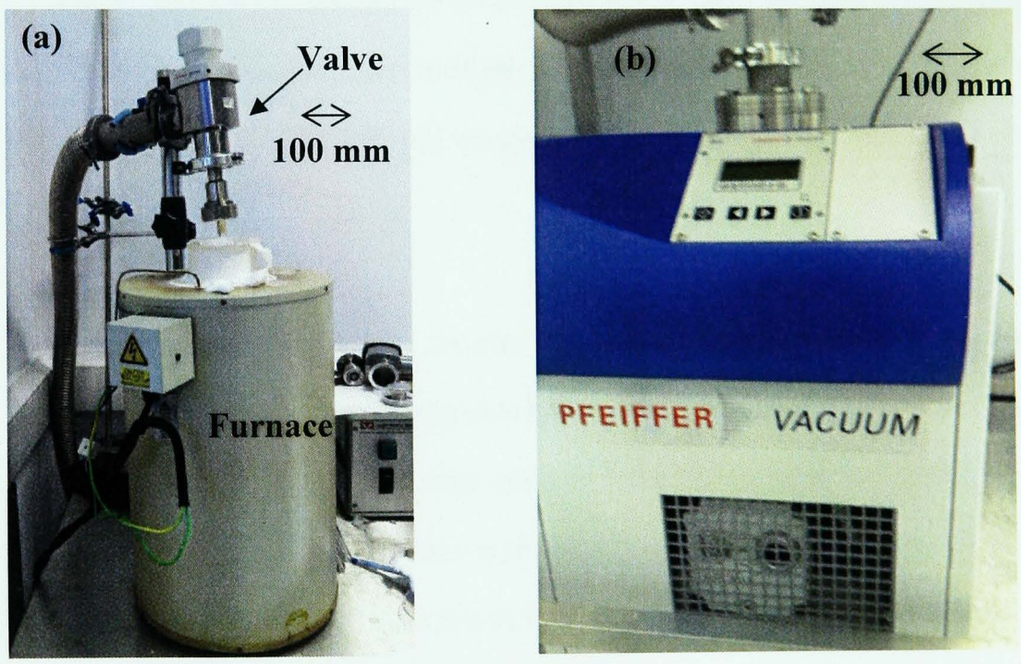

Figure 3.1: Vacuum bake of an ampoule. (a) Ampoule was attached to vacuum pump by a valve. (b) Pfeiffer vacuum pump.

Table 3.2: Procedure for silica glass ampoule air baking and vacuum baking.

Steps	Procedure for air and vacuum baking
1	70°C→200°C @rate of 200°C/h
2	200°C→1000°C @rate of 200°C/h
3	Dwell 6 h
4	1000°C→70°C @rate of 200°C/h

3.1.2 Batch chemicals

The main batch chemicals used throughout the project were arsenic (Source: Furukawa Ltd. manufacture specified purity: 99.9999%), selenium (Source: Cerac Ltd. manufacture specified purity: 99.999%) and germanium (Source: Cerac Ltd. manufacture specified purity: 99.999%). The chemicals were kept inside the containers in which they were supplied, which were usually plastic bottles, in an MBraun 150B-G glovebox. The glovebox contained a recirculating nitrogen atmosphere (O_2 - free, supplier: BOC) with less than 0.1 ppm moisture (H_2O) and less than 0.1 ppm oxygen (O_2) to prevent the surface of the raw materials from hydrolysis and oxidation. The chalcogenide glass types normally produced and used in this word described in this thesis were $As_{40}Se_{60}$, $Ge_{17}As_{18}Se_{65}$ and $Ge_{10}As_{23.4}Se_{66.6}$, as batched, and the diameter of the samples was 10 mm.

A balance (Sartorious, model BP211S accurate to $\pm$ 0.1 mg) was used to weigh the batch chemicals. Each component was measured individually in a plastic boat (100 ml, anti-static, supplier: Fisher) and poured into a prepared ampoule. Then the ampoule was closed with a Saunders valve. The other end of the valve was attached to vacuum pump (VRC 200-7.0 rotary pump and Edwards B30207240 diffusion pump) to achieve a pressure of approximately 8×10^{5} mBar for 30 minutes. The ampoule was sealed using an oxy-propane torch (supplier: BOC) as shown in Figure 3.2 (a).

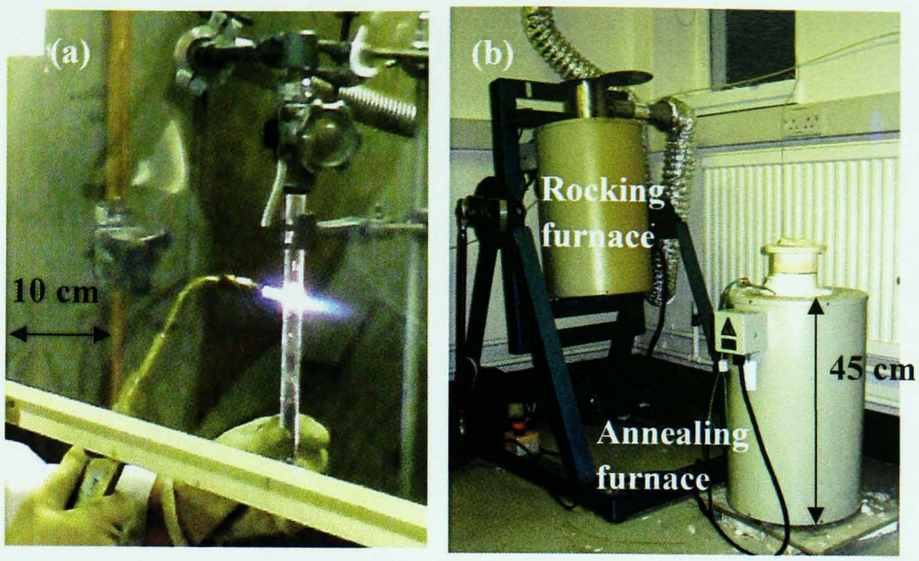

Figure 3.2: (a) Sealing of the silica glass ampoule, containing the chalcogenide glass batch, with an oxy-propane torch. (b) Images of in-house modified rocking furnace and the annealing furnace; length of each furnace is approximately 500 mm.

3.1.3 Melting, quenching and annealing

The sealed silica glass ampoule containing the batch was wrapped in a thermal blanket (supplier: Superwood^{TM} 607^{TM} Blanket) from the top of the ampoule to the top of the batch (Figure 3.3). Then the ampoule was secured by steel wire (Kanthal) and placed vertically in the middle of a resistance tube melting furnace (Instron, TF105/4.5/1ZF, tube ID 86 mm) (see Figure 3.2 (b)). The rocking furnace had been modified in-house and had a rocking angle 30° ± 5° above and below the horizontal axis. The rocking furnace was rocked from when the melting procedure started. The rocking duration of the furnace was controlled by a Eurotherm controller to be a full period between 1 and 5 min. Depending on the composition of the chalcogenide glass to be melted, the rocking furnace was scheduled to ramp to a temperature above the glass liquidus temperature. After holding at this temperature for 12 hours, the furnace was cooled down to a temperature above the liquidus. Then the furnace rocking was stopped and the furnace was held vertically with the rounded end of the ampoule at the bottom for 20 minutes before quench.

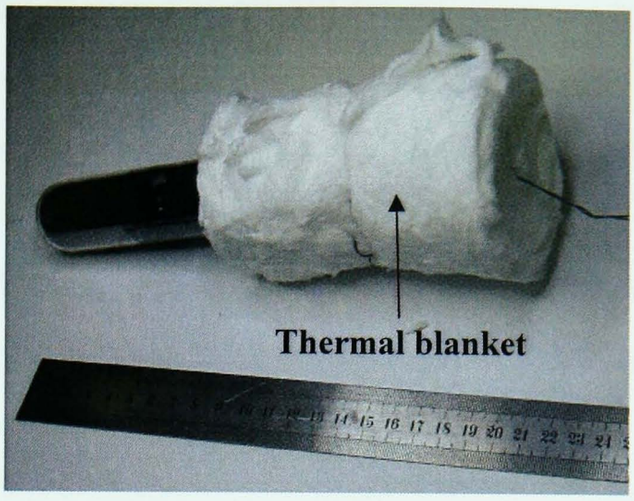

Figure 3.3: Thermal blanket (supplier: Superwood TM 607TM Blanket) was used for preventing the high temperature chalcogenide liquid vapour condensing at the top of the ampoule during quenching.

The As-Se glass is more stable glass former than Ge-As-Se [2]; therefore it could be quenched in air. As the Ge-As-Se glasses required a faster quench, they were quenched in (almost) boiling water until solid [2] or in a liquid metal (Sn and Bi alloy, liquid metal pot supplied by Seba developments Ltd) pot. A skin of the liquid alloy adhered to the outside of the ampoule and solidified during the glass annealing when using liquid metal quenching. During air quenching of the glass melt, the ampoule was taken out from the melting furnace using a pair of tongs and held steady by hand in ambient air. The time duration for air quenching depends on the quantity of batched chemicals and the temperature of the ampoule just before quenching. During water quenching, the ampoule was taken out from the melting furnace and immersed into (almost) boiling water contained in a 2 L (2 dm^3) beaker until the chalcogenide liquid was solidified. A thermal blanket (supplier: Superwood TM 607TM Blanket) was used for preventing the high temperature chalcogenide liquid vapour condensing at the top of the ampoule during quenching.

Annealing of the quenched melt was carried out immediately after quenching. The ampoule with the quenched glass melt inside was placed into the annealing furnace (Figure 3.2 (b)) which was pre-heated to the glass transition temperature (Tg) (see section 3.3.1, for a description of the technique by which Tg was determined using a Differential Scanning

Calorimetry (DSC)). The ampoule was held at this temperature for 1 hour and then the furnace and ampoule were cooled gradually according to the schedule. Table 3.3 lists the schedule of melting, quenching and annealing of the three chalcogenide glasses studied in this project.

Table 3.3: Melting, quenching and annealing procedure of the three chalcogenide glasses (batch compositions in at %): $As_{40}Se_{60}$, $Ge_{17}As_{18}Se_{65}$ and $Ge_{10}As_{23.4}Se_{66.6}$.

Steps	$As_{40}Se_{60}$	$Ge_{17}As_{18}Se_{65}$	$Ge_{10}As_{23.4}Se_{66.6}$
Melting			
1. Fast ramp	RT to 200°C @ 200°C/h	RT to 250°C @ 300°C/h	RT to 250°C @ 300°C/h
2. Slow ramp	200°C to 800°C @ 40°C/h	250°C to 930°C @ 40°C/h	250°C to 930°C @ 40°C/h
3. Dwell	800°C for 12h	930°C for 12h	930°C for 12h
4. Ramp	800°C to 650°C @ 40°C/h	930°C to 800°C @ 60°C/h	930°C to 800°C @ 60°C/h
5. Quenching	650°C to anneal temperature	800°C to anneal temperature	800°C to anneal temperature
Quenching			
Quenching	Air	(Almost) boiling water + 30 sec air	(Almost) boiling water; liquid metal
Annealing			
1. Dwell	180°C for 1h	240°C for 1h	180°C for 1 h
2. Slow ramp	180°C to 140°C @ 5°C/h	240°C to 190°C @ 5°C/h	180°C to 140°C @ 5°C/h
3. Fast ramp	140°C to RT @ 20°C/h	190°C to RT @ 15°C/h	140°C to RT @ 20°C/h

Notes: RT = Room temperature, h = hour.

3.1.4 Cutting, grinding and polishing

The bulk chalcogenide glass samples were normally cut to shapes such as discs for experimental use. The sample cutting was done using an Isomet Low Speed Saw with a Beuhler diamond wafering blade (diameter 40 mm, thickness 0.35 mm). Grinding and polishing chalcogenide glasses may be divided into six steps as listed in Table 3.4. (1) The sample (e.g. disc or prism) was mounted onto a brass jig (home made) using wax glue (supplier:

Buehler, Coventry, UK) then fitted into a plastic holder. (2) and (3) The chalcogenide glass sample was ground on a silicate float glass plate using silicon carbide powder (400 grit and 1000 grit progressively. supplier: Buehler, Coventry) with silicone based polishing oil (supplier: Buehler, Coventry) as the lubricant medium. (4), (5) and (6), The sample was polished using a Metaserv 2000 polishing wheel with progressively finer Metaserv diamond paste (6 μm, 3 μm, 1 μm). In between changing the polishing media, the glass sample was thoroughly washed with acetone (Fisher Chemicals, Certified grade) and dried using a blue towel (supplier: Tork, Advanced, blue).

Table 3.4: Chalcogenide glass grinding and polishing procedure.

Step	Method
1	Mount samples onto a brass jig using wax glue.
2	Grind on a float silicate glass plate using 400 grit SiC powder with silicone based polishing oil as the lubricant medium. Rinse and dry.
3	Repeat step 2 and used a 1000 grit SiC powder. Rinse and dry.
4	Polishing was carried out using a Metaserv 2000 polishing wheel with 6 μm diamond paste. Rinse and dry.
5	Repeat step 4 and using 3 μm diamond paste. Rinse and dry.
6	Repeat step 5 and using 1 μm diamond paste. Rinse and dry.

3.2 Precursor purification

Purifying the raw elements by vaporising the impurities is based on the principle where the pure batch element, such as As, has a lower vapour pressure at the selected temperatures than the associated impurity oxide, such as As_2O_3. Table 3.5 summarises the vapour pressure for arsenic, selenium and tellurium and their representative oxides where the vapour pressure is 200 mm Hg for SeO_2 and 49.2 mm Hg for As_2O_3, respectively, at 300°C and 0.005 Hg for TeO_2 at 630°C [43].

Table 3.5: Vapour pressures of Se / SeO_2, As / As_2O_3 and Te / TeO_2 [43].

Temperature / ℃	Vapour pressure / mm Hg					
	Se	SeO_2	As	As_2O_3	Te	TeO_2
300	0.24	200	0.12	49.2	-	-
630	-	-	-	-	10	0.005

Arsenic and selenium were suitable for vaporising purification treatment due to the lower vapour pressure of the elemental components, compared with the vapour pressure of their respective oxide impurity; the surface oxide was therefore removed from some of the raw components by baking out prior to glass melting as shall be now detailed in sections 3.2.1 and 3.2.2.

3.2.1 As purification

In order to produce a lower oxide chalcogenide glass, the arsenic elemental precursor had to be purified before being mixed with the other batch materials. Normally, for each purification, 7 g - 8 g (measured accurately) As was batched in a purified (section 3.1.1) silica glass ampoule (ID 10/ OD 16 mm) inside the MBraun MB 150B-G glovebox and closed with the Saunders valve. As described in section 3.1.3, the valve was attached to the vacuum pump ((VRC 200-7.0 rotary pump and Edwards B30207240 diffusion pump) to achieve a vacuum (8×10^{-3} Pa) and held inside a vertical resistance tube furnace (27 mm ID).

Table 3.6 represents the As purification procedure and the observations during purification. The furnace was firstly ramped from room temperature to 200°C at a rate of 200°C/h. Then, the temperature was ramped from 200°C to 250°C at rate of 100°C. Thirdly, the temperature was held at 250°C for one hour. Fourthly, the temperature was ramped from 250°C to 300°C at a rate of 100°C/h and held at 300°C until dark depositions were viewed on the inside surface of the ampoule. Finally, the purification was finished and the furnace was allowed to cool down to ambient (see Table 3.6) with the purification tube in situ, by switching it off.

The ampoule containing purified arsenic was detached from the pump with the valve closed and taken into the MBraun glovebox. The purified As was weighed and the average mass loss was usually approximately 0.01-0.02 g from a 7g - 8 g batch. Then the empty silica glass ampoule was stored in the MBraun glove-box. Each ampoule could be re-used for two more As purifications before it was disposed of.

Table 3.6: The As chemical was batched inside of a silica glass ampoule. The As purification schedule is listed along with observations made during the process of purification.

Stage	Schedule	Observation
1	RT → 200°C @ 200°C/h	-
2	200°C → 250°C @ 100°C/h	-
3	Hold at 250°C for 1h	-
4	250°C → 300°C @ 100°C/h	Slightly grey colour deposition appeared on the inner surface of ampoule.
5	Hold at 300°C for 1h	Large amount of grey colour deposition appeared. Black/silver depositions (As) appeared.
6	300°C → 170°C @ 100°C/h	-
7	Remove from the furnace when the temperature is at RT	- As chunks which appear shiny.

Note: RT = Room Temperature.

3.2.2 Se purification

Previous work in our laboratory had concluded that the selenium raw material did not produce better quality chalcogenide glass after being purified [2]. However, repetition of this work during the present project has demonstrated the opposite. FTIR results showed that the selenium after purification produced a smaller Se-H vibrational absorption band at 4.8 μm wavelength but a larger Si-O band at 9.0 μm wavelength for $As_{40}Se_{60}$ compared with $As_{40}Se_{60}$ made with the un-purified selenium. Therefore, for any applications at wavelengths around 4.8 μm, it was concluded from the work carried out here, that it was preferable to use purified Se.

Se purification was prepared in four steps. (i) In the MBraun Glovebox, a standard ampoule (10/14 mm ID/OD, rinsed and baked, section 3.1.1) was weighed. (ii) Se chemicals were weighed and placed inside the ampoule. (iii) As shown in Figure 3.5 (a) and (b), a small tube (8 mm OD, provider: Multi-Lab Ltd.) was fitted with a rubber ring (imperial nitrile O-ring, supplier: RS) on the top of the ampoule for collecting the Se-O during purification. (iv) The ampoule and tube were held by the Saunders valve inside to a vertical resistance tube furnace (27mm ID) under a drawing vacuum of 8×10^{-3} Pa. Figure 3.5 (c) represents a red or orange deposition appeared and the Se melted. The purification process and observations made are further detailed in Table 3.7. (1) The temperature of the furnace was ramped from room temperature to 200°C at a rate of 200°C/h. (2) The temperature was ramped from 200°C to 250°C at rate of 100°C. A small amount of grey colour deposition appeared on the inner surface. (3) The temperature was held at 250°C for one hour. A red or orange deposition appeared and the Se melted. (4) and (5) When the deposition became thicker, and the Se inside the furnace liquified, the furnace was switched off. The Se became solid after purification, and the Se-O deposition was collected on the tube. The ampoule containing the purified Se (still under $\sim8\times10^{-3}$ Pa vacuum) was moved to the glove box.

The ampoule containing the purified Se (Figure 3.5 (d)) was weighed and this weight was subtracted from the sum of the pre-process weights of the batched Se and the ampoule to give a precise weight loss. The lost weight was due to the Se-O deposited onto the inner surface of the silica tube. Subsequent preparation of glasses was then carried out using the solidified Se.

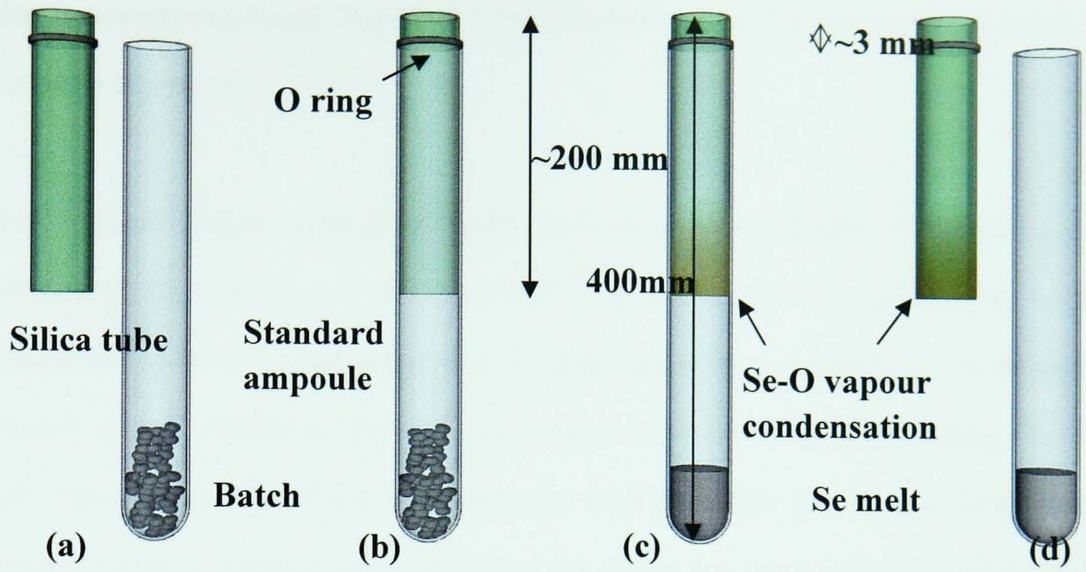

Figure 3.5: Se purification process. (a) Se chemicals were batched inside a standard ampoule (10/14 mm ID/OD); (b) a small tube (10 mm OD) with a rubber ring was fitted inside the top of the standard ampoule; (c) the ampoule and tube were attached to a vacuum and the purification procedure of Table 3.7 followed and (d) Se became solid after purification, and SeO_2 deposition was viewed on the tube.

Table 3.7: Se purification schedule and the observations.

Stage	Schedule	Observation
1	25°C → 200°C @ 200°C/h	-
2	200°C → 250°C @ 100°C/h	Grey colour deposition appeared on the inner surface.
3	Hold at 250°C for 1h	- Red/orange deposition appeared and Se boiled at temp 212°C.
4	250°C → 150°C @ 100°C/h	- Se liquified.
5	Remove furnace at 150°C	-Se solidified, glassy.

Moleculers absorb specific frequencies that are characteristic of their structure, so a comparison of the absorption spectrum purified and non-purified Se chalcogenide glass, e.g. $As_{40}Se_{60}$, will provide useful information. Two $As_{40}Se_{60}$ samples were prepared using purified Se (ZGLCF027) and non-purified Se (ZGLCF009). The two $As_{40}Se_{60}$ samples were sliced into 2.0 mm discs with both surfaces polished to a 1 μm finish. The absorbance of the two samples

was measured using Fourier Transform Infrared Spectroscopy (FTIR, see section 3.3.6) and are shown in Figure 3.6.

For the un-purified Se sample (ZGLCF009), the Se-H stretching vibration [120] shows a clear absorbance peak at 4.6 μm wavelength[121-125]. However, in the purified Se sample (ZGLCF027), the Se-H absorbance peak has disappeared. Also in Figure 3.6, an absorption band at 2.9 μm is observed in both samples. This is identified with an O-H stretching vibration [2]. This absorbance peak could be eliminated using distillation [2]. There is an absorption band at 3.4 μm wavelength in both samples. This can be associated with a C-H band and this may due to the polishing fluid residual on the sample surface [126]. It should be possible to eliminate this C-H band by rinsing the sample thoroughly. The absorption peak at 6.2 μm is associated with an H-O-H bending vibration. It is possible to remove the oxygen-based impurity by applying a magnesium distillation [2]. Also, this water contained absorbance peak may possible associated with the measurement environment (moisture in air).

An additional absorption attributed to Si-O stretching bond is observed at a wavelength of ~9 μm. The reason for this may associated with the fact that the Se material contacted with the silica ampoule for a longer time at a relatively high temperature. Therefore, the Se purification may not be of benefit for the applications at wavelengths around 9.0 μm. Indeed if the Si-O absorption observed is due to particulate SiO_2 in the chalcogenide glass then it may be responsible for extra optical loss by extrinsic scattering.

In applications that require the chalcogenide glass to be doped with rare earth ions, the high purity of the base chalcogenide materials is essential to get successful doping with a high dissolution rate [126]. Therefore, Se purification may also in the future be accompanied by a distillation method [2] to obtain a ultra-high pure material before doping.

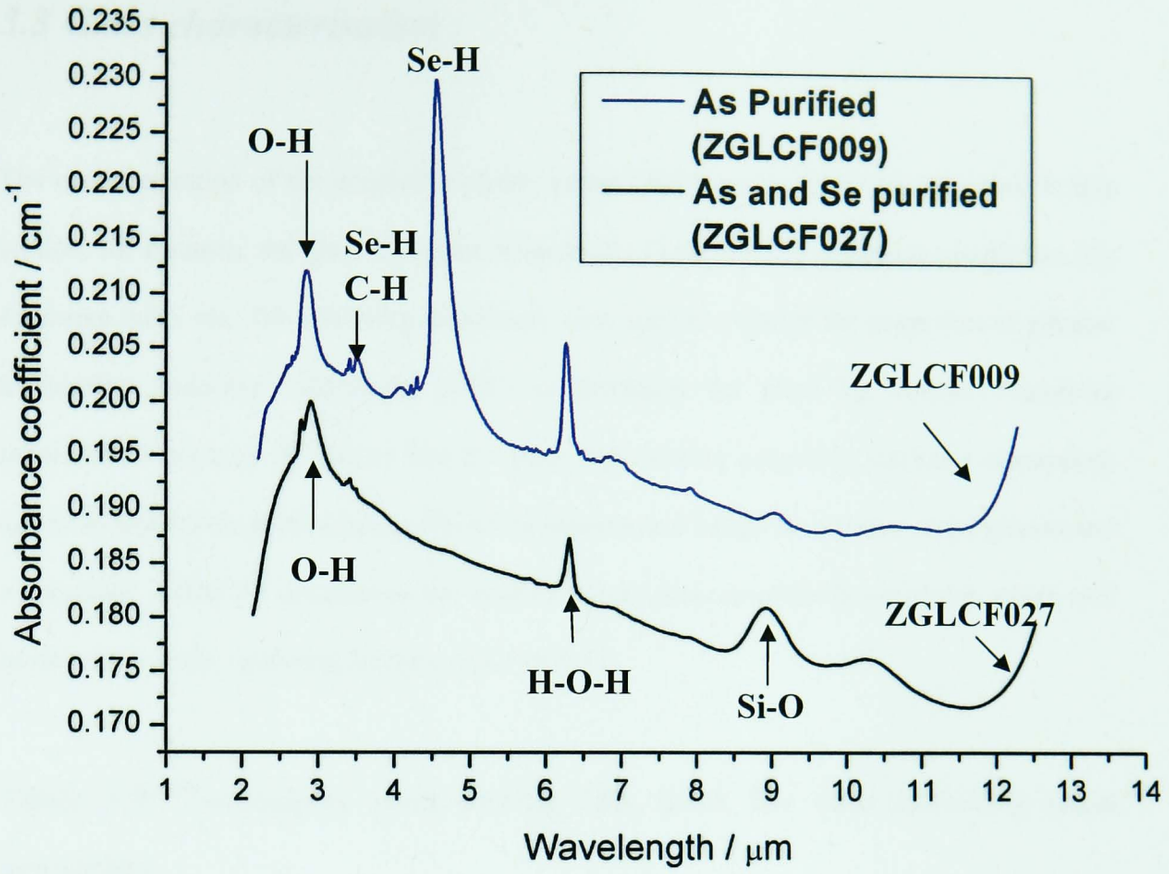

Figure 3.6: Blue line shows the absorption spectrum of the bulk $As_{40}Se_{60}$ glass ZGLCF009 melted with as-received Se; note the Se-H fundamental stretching bond is shown at wavelengths of 4.6 μm. Black line shows the absorption spectrum of the bulk $As_{40}Se_{60}$ glass ZGLCF027 when Se was purified before glass melting. The Se-H absorption band is reduced, but an additional absorption attributed to Si-O is observed at wavelength of ~9 μm. Before each measurement, the FTIR was purged with Ar for 10 minutes.

Se purification was not one of the original objectives of this project. However, since the Se-H absorption band at 4.6 μm wavelength was dramatically reduced after the purification process, and this process was fast and not harmful for glass melting, it is recommended that Se purification should be routinely used. Se purification was not involved for the glass meltings using boule ampoules, because the shape of the boule ampoule was not suitable for this purification method.

3.3 Glass characterisation

The characterisation of the properties of the melted chalcogenide glasses is described in this section, for instance, the glass transition temperature (Tg), thermal expansion coefficient (α), refractive index etc. The following techniques were used to examine the properties of glasses: Differential Scanning Calorimetry (DSC) to determine the glass Tg; Fourier Transform Infrared Spectroscopy (FTIR) to find the glass transmission properties (includes absorption) and Scanning Electron Microscopy (SEM) to observe and image the surface of the glasses and waveguides. Table 3.8 summarises the techniques and purpose of the investigation which will be described in the following sections: 3.3.1 to 3.3.6.

Table 3.8: Techniques used during this work for characterising glass properties.

Section	Techniques	Purpose of Investigation
3.3.1	Differential Scanning Calorimetry (DSC)	Tg.
3.3.2	X-ray Diffraction (XRD)	The amorphous nature of glass.
3.3.3/3.3.4	Thermal Mechanical Analyser (TMA)	Viscometry and thermal expansion coefficient (α).
3.3.5	Scanning Electron Microscopy (SEM), Environmental mode Scanning Electron Microscopy (ESEM)	Observe and image the surface of the glasses and waveguides.
3.3.6	Fourier Transform Infrared Spectroscope (FTIR)	The glass transmission properties.

3.3.1 Glass transformation temperature measurement

Differential Scanning Calorimetry (DSC) was used for measuring glass transition temperature (Tg). Sections 3.3.1.1 to 3.3.1.4 describe the experimental method of DSC.

3.3.1.1 Theory of operation

Differential Scanning Calorimetry (DSC) was carried out on the Perkin Elmer DSC7 which allowed determination of the glass Tg. In the DSC measurement, the basic principle is that, when the sample undergoes a physical transformation, more or less heat is required to flow to it than to a reference to maintain both the sample and reference at the same temperature.

Two hermetically sealed and thermally matched (i.e. same composition, mass, shape, (including wall thickness) and therefore, the same heat capacity and thermal diffusivity) aluminium crucible pans (supplier: Perkin Elmer) were introduced to the measurement chamber. As Figure 3.7 indicates, the crucible pan on the left contained the chalcogenide glass specimen and the other crucible pan was empty as a reference. The two crucible pans were heated from underneath and thermocouples were located under the pans. Baseline runs (where both pans are empty) were carried out before measurement and subtracted from the traces to remove the effect of any artefacts unrelated to the specimen.

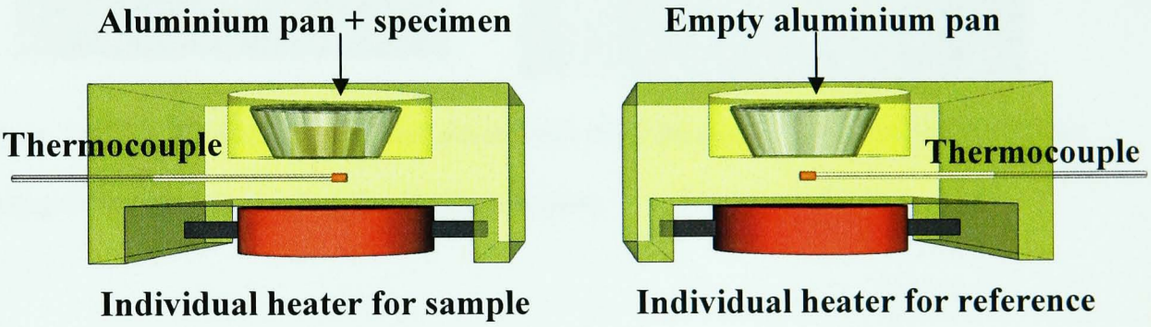

Figure 3.7: Two hermetically sealed and thermally matched aluminium pans. The pan on the right contains the chalcogenide glass specimen and the pan on the right is empty as a reference. The two pans were heated from underneath.

3.3.1.2 Sample preparation

As noted above, one empty crucible pan was used as reference and the other crucible pan contained the chalcogenide glass sample. The typical mass of a chalcogenide glass sample measured was 15 mg and this was placed inside the aluminium pan and covered by an aluminium lid (see Figure 3.8 (a)). Then it was sealed with the Perkin Elmer cold-weld sealing device (Figure 3.8 (b)). The Al crucible pan, and lid, containing the sample were placed in a sample holder of the Perkin Elmer sealing device when the handle was lifted up, then force was applied by hand on the handle to press and seal the edge of the lid and pan together.

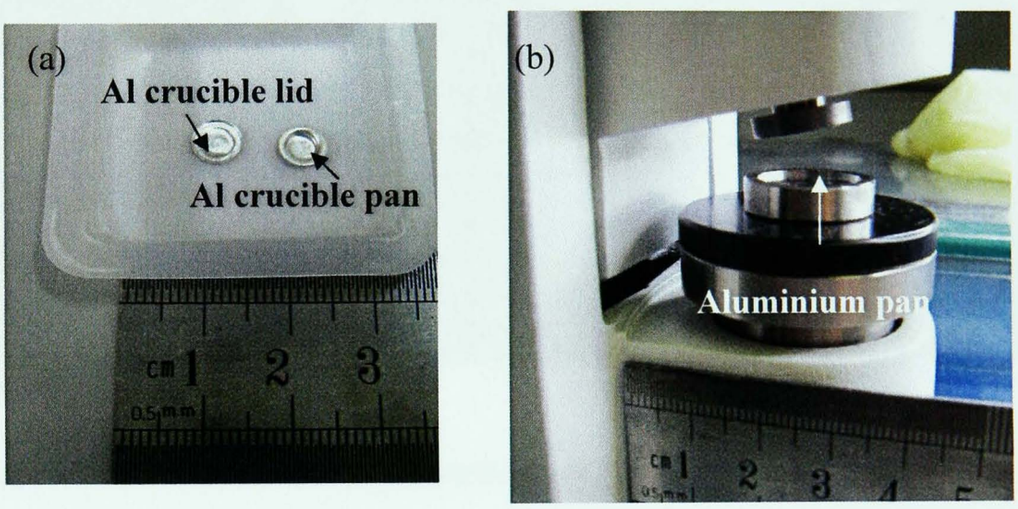

Figure 3.8: (a) Aluminium pan and cover indicating dimensions and (b) Perkin Elmer sealing device used for sealing the aluminium pans.

3.3.1.3 Equipment setup and measurement

The Perkin Elmer DSC7 equipment is shown in Figure 3.9 (a). The sample crucible pan was placed on the left sample holder and the reference crucible pan was placed on the right of the sample holder as shown in Figure 3.9 (b). Individual heaters and thermocouples for both sample and reference were located below the sample holders.

A computer controlled and measured the electrical power output in order to maintain the same temperature in the sample and reference compartments throughout the analysis. The

temperature was first held at 40°C for one minute and then ramped upwards (to 50°C above Tg) at a rate of 10°C/min. The temperature of the sample changes significantly relative to that of the reference at temperature around Tg as shown in Figure 3.10. To maintain the same temperature in both compartments, excess energy is transferred to heat the sample during the process [127]. If a glass crystallises, then heat is given out and the sample becomes hotter than the reference, therefore the sample was cooled to maintain the temperature identical to the reference. The temperature ramp was continued up to temperatures 50°C above the (onset of) Tg.

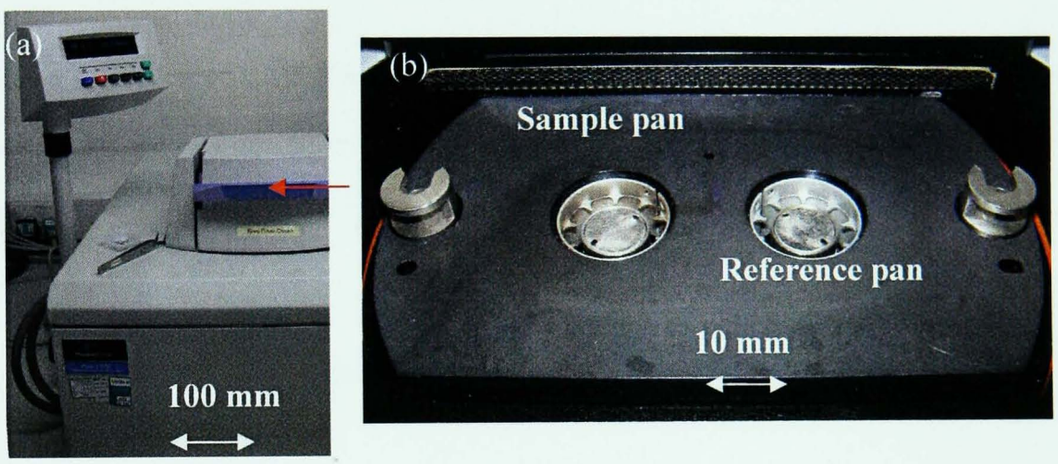

Figure 3.9: (a) Perkin Elmer DSC7 equipment and (b) close view of the sample holder for sample and reference pans. The sample Al crucible pan was located on the left and the reference Al crucible pan was located on the right, as viewed from the front of the equipment.

3.3.1.4 Treatment of results and errors

The software provided by Perkin Elmer shows the enthalpy flow differences. A typical DSC result is shown schematically in Figure 3.10. The intersection of the tangential lines shown was taken as indicating the onset Tg.

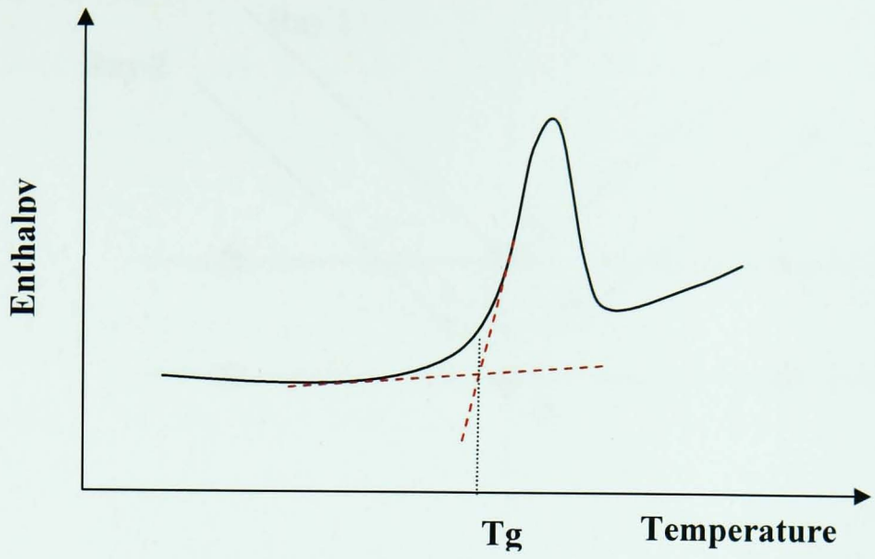

Figure 3.10: A schematic of a typical DSC result. The x axis is the temperature and the y axis shows the enthalpy flow. The intersection point of the red tangential lines shown was taken as the onset Tg.

3.3.2 Material amorphous nature analysis

In this PhD project, XRD was mainly used to analyse the amorphous nature of as-prepared chalcogenide glasses.

3.3.2.1 Theory of operation

In general, the principle of XRD operation follows Bragg's Law [128] which is illustrated in Figure 3.11. The Bragg constructive interference assumes that the phases of the two parallel rays shown in Figure 3.11 are coincident (an integral multiple of 2π) and that the incident angle equals the reflecting angle. Ray 1 is diffracted at atom C and the second beam continues to the next layer where it is scattered by atom D. Ray 2 has then travelled the extra distance AD + DB if the two rays continue to travel parallel. The distance between the two layers is d and the incident angle is θ. Thus the Bragg condition Equation 3-1 is derived.

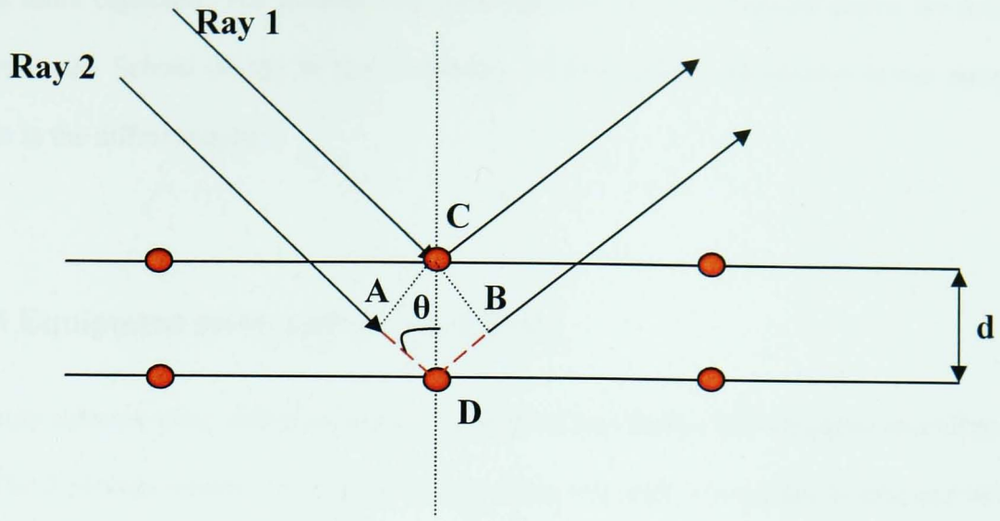

Figure 3.11: Deriving Bragg's Law using reflection geometry and applying trigonometry. The lower beam must travel the extra distance (shown in red) to continue travelling parallel and adjacent to the top beam [128].

$$AD + BD = d\sin(\theta)\,;\ \frac{2\pi}{\lambda}\cdot(d\sin(\theta)) = 2n\pi$$

$$n\lambda = \sin(\theta)\times d \qquad 3\text{-}1$$

where n is an integer. Bragg's law indicates that when rays are incident on a crystalline material, the reflected rays from the atom are constructive at certain angels of incidence and peaks which can be reflected to the particular crystal lattice separation through equation 3-1 would be shown on an X-ray diffraction pattern. However, amorphous materials would not show any sharp peaks as they do not have any crystalline structure. Typically, the XRD pattern of an amorphous material gives broad peaks, the first peak which is known as first sharp diffraction peak (FSDP) [129] and could be used to analyse the structure of amorphous solid (For more detailed discussion see section 4.10.2).

3.3.2.2 Sample preparation

XRD was carried out on chalcogenide glass powder which was ground from the bulk samples (typically 3 g bulk sample) using an agate mortar and pestle (supplier: Fisher Scientific Ltd.)

inside a fume cupboard. The powder was then mounted on an aluminium sticky tab (made in-house in the School of M3 in the University of Nottingham) and placed in the sample chamber in the diffractometer.

3.3.2.3 Equipment setup and measurement

Diffraction patterns were collected using a Siemens Krystalloflex 810 diffractometer (Figure 3.12). The 0.154 nm wavelength copper X-ray source was used. The sample holder and beam detector stage could be rotated while the emitting beam stage was fixed. The sample, together with the holder, was rotated at 0.01°/s from 2.5° to 40° (θ) and the beam detector stage rotated at 0.02°/s from 5° to 80° (2θ).

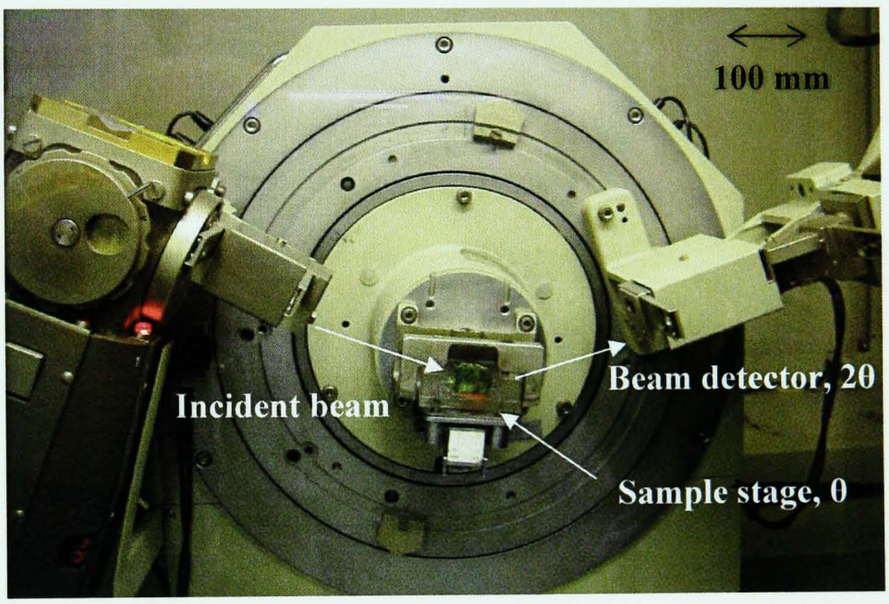

Figure 3.12: Siemens Krystalloflex 810 diffractometer. The sample holder and beam detector stage could be rotated while the emitting beam stage was fixed.

3.3.2.4 Treatment of results

The resulting data were recorded by the 'Diffrac plus XRD commander' software supplied by Bruker – AXS GmBh 2000. The data could then be exported to MS Excel.

3.3.3 Viscometry measurement

Knowledge of the chalcogenide glass viscosity is important for later work in making rib waveguides using hot embossing; drawing fibres and extrusion. Viscosity is a measure of the resistance of a fluid which is being deformed by shear stress. A shear stress is defined as a stress which is applied parallel or tangential to a face of a material. Fluids have resistance to shear stress (τ) [130]. For instance water is 'thin', and it has a smaller viscosity, i.e. a low resistance to shear stress compared to liquid oil which is 'thick', i.e. it has a larger viscosity and a larger resistance to shear stress. Viscosity measurement was carried out using Thermomechanical Analysis (Perkin Elmer TMA7) equipment as shown in Figure 3.13 (a).

3.3.3.1 Sample preparation and equipment setup

The standard melt of chalcogenide glass rod (10 / 14 mm ID/OD) was too large for the TMA equipment. Therefore, the standard chalcogenide glass rod was crushed in an agate mortar and pestle in the MBraun Glovebox. Then the chalcogenide glass piece was batched in a silica glass ampoule (250 mm length, 4 mm /7 mm ID/OD, rinse and baked) and sealed under vacuum. The glass was re-melted, quenched and annealed using the procedures described in section 3.1.3. Then the re-melted chalcogenide glass rod (~50 mm length, 4 mm diameter) was mounted on a silica glass piece using wax. Parallel and flat top and bottom faces of several chalcogenide glass rods (~8 mm length) could be obtained by two perpendicular cuts. The cuts were carried out using an Isomet Low Speed Saw with a Beuhler diamond wafering blade (section 3.1.4) inside a fume cupboard. The chalcogenide glass rod was gently placed vertically under the silica pushrod of the TMA (Figure 3.13 (b)). The resistance furnace was then slid up to cover the operation area.

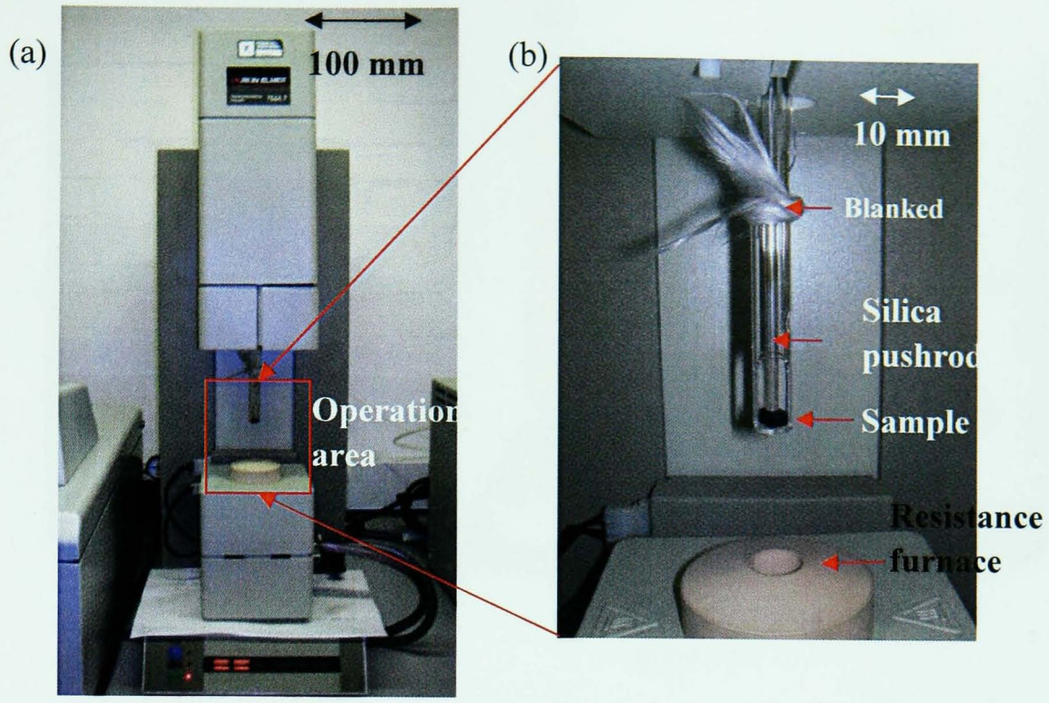

Figure 3.13: (a) Thermo-Mechanical Analyser (Perkin Elmer TMA7) equipment and (b) illustrates a closer view of the working area. The silica pushrod applied load on the sample during the controlled temperature rise.

3.3.3.2 Viscosity measurement process

Figure 3.14 shows a schematic diagram of the measurement process. The TMA furnace was purged with helium (zero grade, supplier: BOC). The applied force was set to be 200 mN and the temperature ramp rate was 10°C/min from room temperature to the target temperature (~Tg+50°C) [131]. The viscosity was calculated through the following equation [132]:

$$\eta = \frac{2\pi F h^5(t)}{3V[dh(t)/dt][2\pi h^3(t)+V]} \qquad 3\text{-}3$$

where, η is the viscosity in poise (1 poise = 0.1 Pas), F is the applied force is dynes (1 dynes = 10^{-2} mN), h(t) is the sample thickness at the time t in cm, dh(t) is the compression rate at the time t in cm/s and V is the sample volume in cm^3.

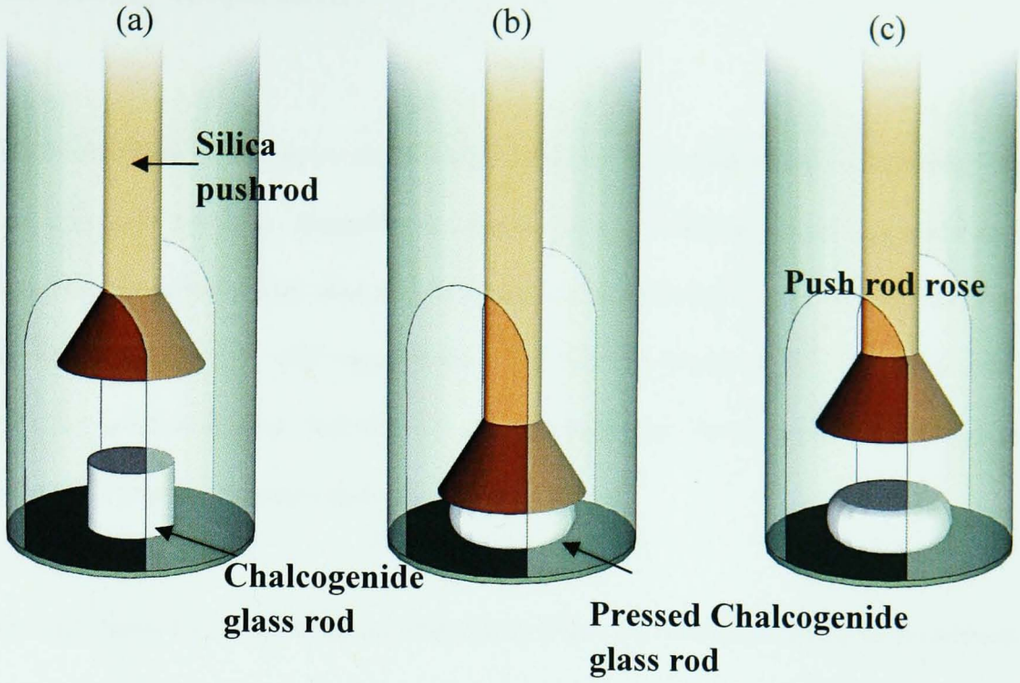

Figure 3.14: Schematic diagram of the process of the viscosity measurement. (a) Chalcogenide glass rod (4 mm diameter, 8 mm length) is loaded inside of the working area; (b) load is applied on the chalcogenide glass rod by the silica pushrod as the temperature is raised from room temperature to ~Tg+50 °C. The shape of the chalcogenide glass sample is then changed and (c) the measurement finished.

3.3.4 Thermal expansion coefficient (α) measurement

Most glasses, like most other solids, expand on heating and shrink on cooling [34]. The thermal expansion coefficient (α) is an important parameter during cooling after processing such as hot embossing of rib waveguides (section 3.4) and producing core-clad optical fibres as they require two different glass compositions. An α mismatch of two different glasses could cause cracking of the glasses during a change in temperature below Tg where stress relaxation can no longer occur. Knowledge of the chalcogenide glass thermal expansion coefficient is important in making waveguide using hot embossing; draw multi-material fibres and extrusion. The measurement was carried out also using Thermomechanical Analysis (TMA).

3.3.4.1 Theory of operation

The molecular basis for α may be explained as follows. As the temperature is increased, more thermal energy is available; therefore the atomic bonds vibrate at greater amplitude at the characteristic frequency. The thermal expansion arises because of the shift in the mean equilibrium bond length with temperature. The Condon-Morse [133] potential energy diagram for an atomic bond describes the mean equilibrium bond length with temperature which helps to explain thermal expansion of solid materials.

Figure 3.15 shows the Condon-Morse diagram in which the potential energy of the system is plotted against atomic separation (r). In the case of the ionic bond, there is a long range electromagnetic attraction which becomes repulsive at short range.

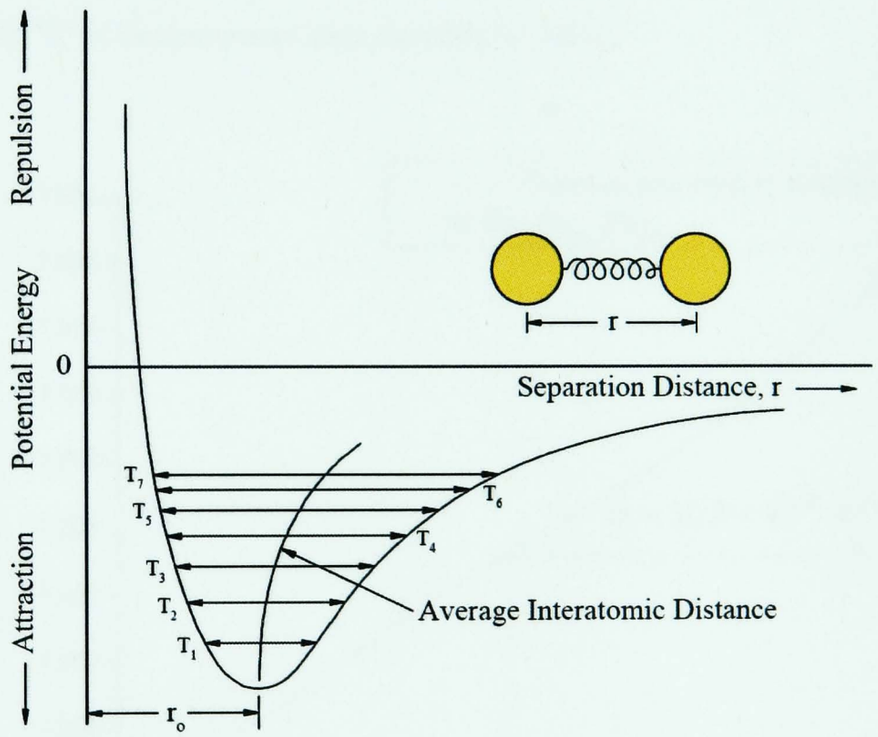

Figure 3.15: Condon-Morse potential energy diagram [133] in which the potential energy of the system is plotted against atomic separation (r).

Linear thermal expansion coefficient (α) can be calculated using equation 3-4:

$$\frac{L_{final} - L_{initial}}{L_{initiial}} = \alpha \Delta T \qquad 3 - 4$$

where L_{final} and $L_{initial}$ are the length of the sample at two corresponding temperatures and ΔT is the temperature difference.

3.3.4.2 Sample preparation, equipment setup and measurement

A measurement was carried out in the Thermomechanical Analyser (TMA) (Figure 3.13). The sample preparation and measuring process were similar to those already described for viscosity measurement (section 3.3.3). The TMA furnace was purged with helium (zero grade supplier: BOC). The applied force was set to be 80 mN and the temperature ramp rate was 10℃/min from room temperature to the target temperature (normally Tg+50℃). A $Ge_{10}As_{23.4}Se_{66.6}$ cylinder was cut from sample ZGLCF034_b rod. The height of the cylinder was 7.05 mm and the diameter was 4.00 mm. Figure 3.16 shows α of the $Ge_{10}As_{23.4}Se_{66.6}$ which was 21.5 (± 0.5) $\times 10^{-6}$ °C^{-1} in the temperature range from 80°C to 140°C.

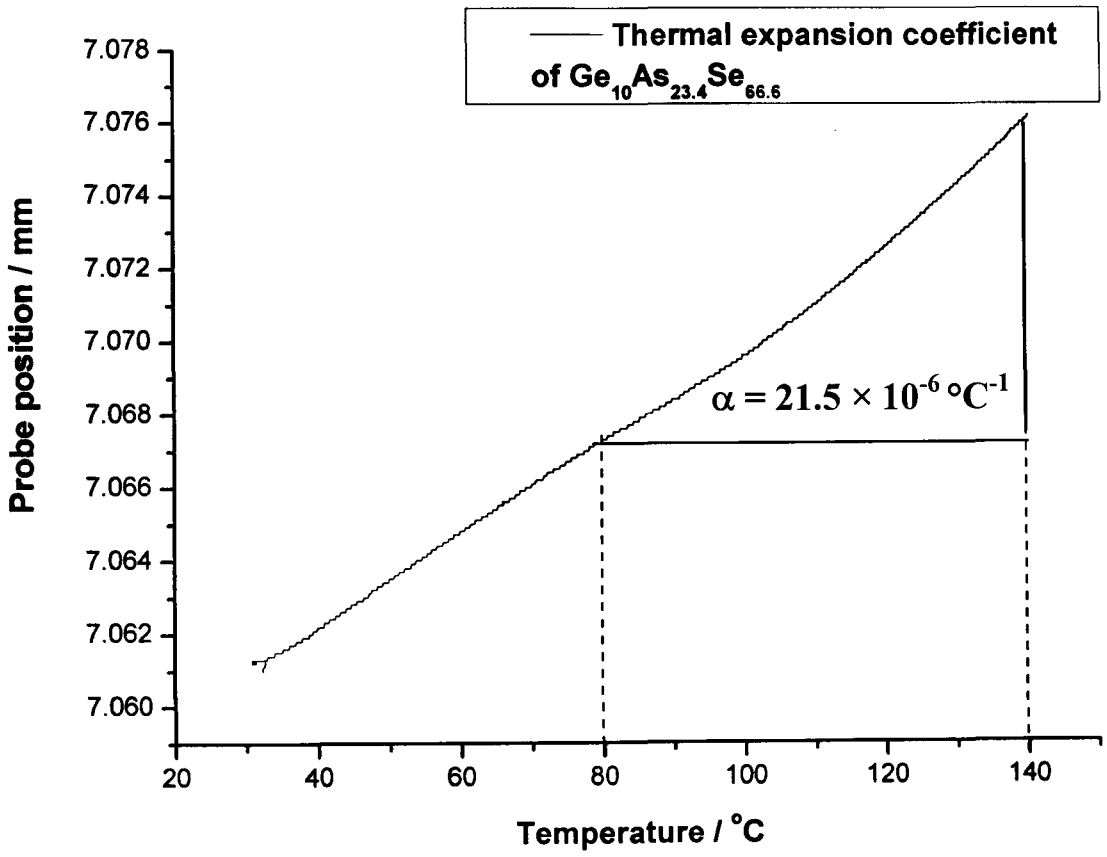

Figure 3.16: Thermal expansion of $Ge_{10}As_{23.4}Se_{66.6}$ (sample ZGLCF034_b). It was found that in the temperature range from 80°C to 140°C: α was 21.5 (± 0.5) $\times 10^{-6}$ °C^{-1}.

3.3.5 Scanning Electron Microscopy (SEM) and Environmental Scanning Electron Microscopy (ESEM)

Scanning Electron Microscopy (SEM) allows images to be viewed at a much higher resolution (up to 2 nm) than the optical microscope. A schematic diagram of the operation of an SEM is shown in Figure 3.17. An electron gun emits a beam of high energy electrons from the top downwards through a series of lenses (condensing lens and object lens) to the sample. At the bottom of the chamber, scanning coils control the focused beam row by row across the specimen. As the primary electron beam hits each spot on the specimen, secondary electrons are released from the sample surface. The secondary electrons are detected and amplified before being sent to the PC monitor. The final image of the specimen surface is built up from the number of electrons emitted from each spot on the sample.

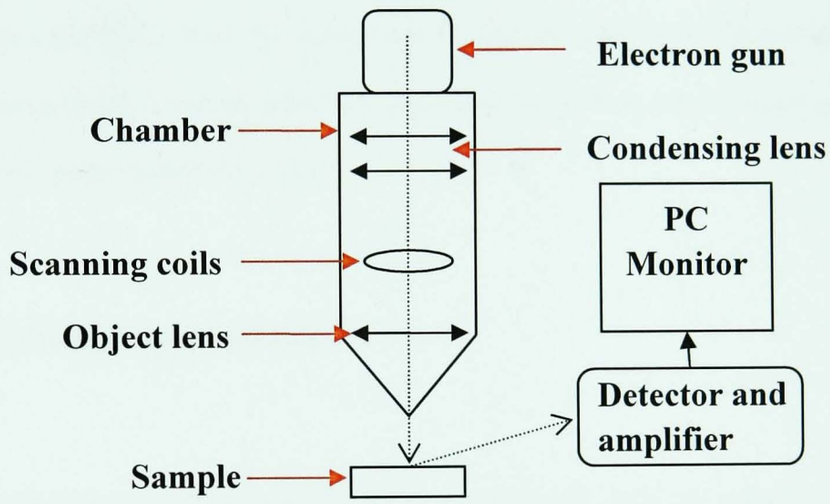

Figure 3.17: Schematic diagram of the operation of an SEM. After the sample is placed under the electron beam, the chamber was purged with nitrogen gas. The beam travels downward through a series of lenses (condensing lens and object lens) to focus the electrons to a very fine spot and hit the sample. The scanning coils control the beam spot on the specimen row by row. The reflected beam from the sample is then received by the detector and the signal is amplified.

A SEM is operated under high vacuum. Chalcogenide glasses are semi-conductors, but they do not conduct sufficiently well to avoid electron charging at high vacuum. In order to view

chalcogenide glass samples using SEM, a gold or carbon coating is required to conduct electricity and prevent the build up of charge which leads the distortion of images. The environmental mode Scanning Electron Microscopy (ESEM) can be operated under a gas atmosphere to prevent sample charging. Therefore, one advantage of using this approach is that the samples could be observed without a prior coating procedure.

Scanning Electron Microscopy (SEM) and Environmental Scanning Electron Microscopy (ESEM) were routinely used for observing the surface quality of bulk chalcogenide glasses, chalcogenide glass rib waveguides and optical fibres produced using chalcogenide glasses. ESEM is especially useful in the current work, because it may image a sample without destroying its usefulness by having it coated to make it conductive. SEM and ESEM are also used for chemical analysis; this technique is called Energy dispersive X-ray spectroscopy (EDX). Since the current work is more focused on the fabrication of devices, this chemical analysis is not the main task, and therefore EDX is not discussed in detail here. The interested reader is referred to [134].

3.3.5.2 Sample preparation

All samples must be of an appropriate size to fit in the specimen chamber and are generally mounted rigidly on an aluminum specimen stub (Figure 3.18 (a)), e.g. glass samples from which rib waveguides were embossed were 10 mm diameter discs. Two kinds of stubs were used for viewing the sample surfaces and sample cross-sections, respectively. In Figure 3.18 (a), stub (i) was used for viewing sample surface. Samples were mounted on a sticky carbon pad on the surface of stub (i). Sample cross-sections could be viewed using stub (ii). The sample was plugged in the gap as shown in Figure 3.18 (a) stub (ii) and secured by two screws.

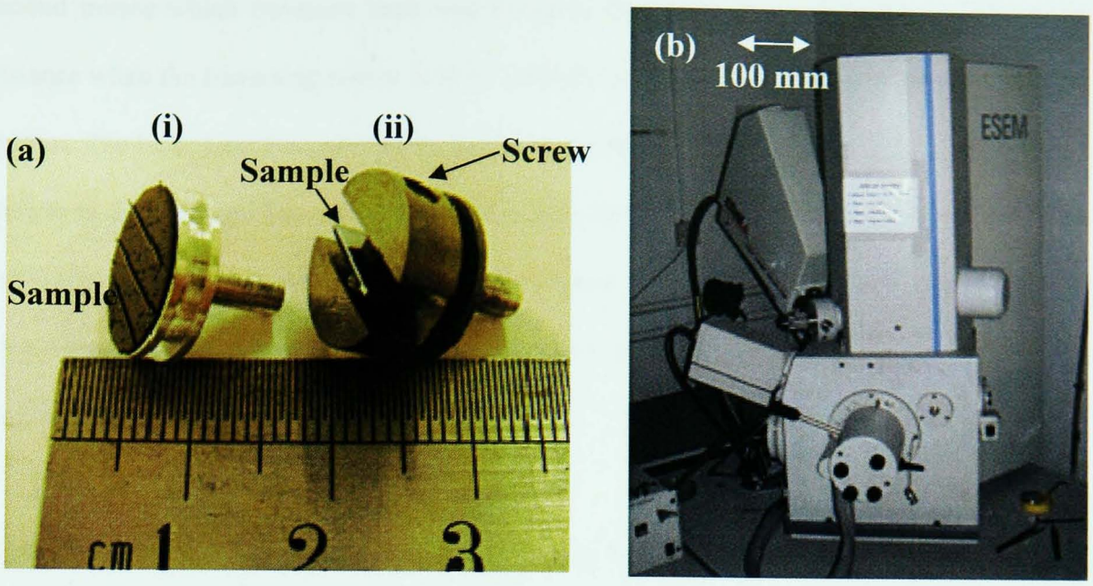

Figure 3.18: (a) ESEM specimen stubs. Stub (i) had a sticky carbon pad on the top which was used for mounting the samples. The sample cross-section could be viewed using stub (ii): the sample was plugged in the gap and secured by the two screws and (b) ESEM equipment: EDAX, CDU™ LEAP™ detector, model: New XL-30 139-2.5.

3.3.5.3 Equipment setup and measurement

The sample holders were fitted under the electron beam in the ESEM chamber. A photograph of the ESEM equipment used is shown in Figure 3.18 (b) (EDAX, CDU™ LEAP™ detector, model: New XL-30 139-2.5). The ESEM imaging was carried out in-house with the kind help of Dr. Nigel Neate (technician in the School of M3 in the University of Nottingham).

3.3.6 Material transmission properties

Fourier Transform Infrared Spectroscopy (FTIR) is used to determine the optical transparency of a glass in bulk or fibre form. This section describes the FTIR measurement.

The Michelson interferometer is at the heart of the fundamental operation of an FTIR spectrometer (Figure 3.19). A light beam is emitted from a source and split into two by a beam splitter; one of the beams is reflected off a stationary mirror, the other beam is reflected off a

second mirror which traverses back and forward. The two beams of light travel the same distance when the traversing mirror is at its central position and are reflected back to the beam splitter. The beams are recombined by the beam splitter and the new light passed through the sample to the detector. The wavelength of the light passing through the sample is derived from the complex spectrum caused by the constructive and destructive interference of the split then reconverged beams. A Fourier transform is applied to this complex spectrum, i.e. interferogram, to give the sample spectrum.

It was imperative that the test sample for FTIR was flat, with parallel entry and exit surfaces presented orthogonally to the FTIR beam [1, 2]. The sample surfaces were therefore ground and polished flat to a ≤ 1 μm finish using the techniques presented in section 3.1.4.

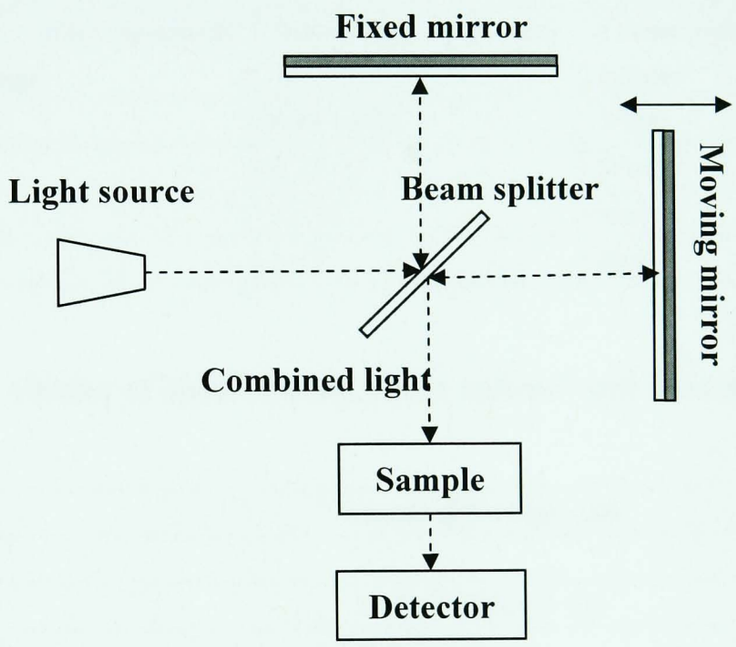

Figure 3.19: A schematic diagram of the internal working of a FTIR spectrometer. The beam splitter separates the incoming light beam into two beams. The fixed mirror reflects one beam from the beam splitter back to the splitter; similarly the moving mirror reflects the beam back to the splitter. The combined interference signal passes through the sample to the detector.

3.3.6.1 Equipment setup and measurement

FTIR analyses were carried out using Bruker IFS 66/S equipment. The absorption or transmission data collected gave a measurement of the amount of surface reflection loss and absorption and scattering occurring in the bulk of the glass and on the glass surface.

Depending on the wavelength range to be measured, the light source, beam splitter and detector were chosen accordingly. The wavelength ranges covered by each source are given in Table 3.9 and by each beam splitter and detector in Table 3.10.

Table 3.9: List of range of electromagnetic wave and the corresponding beam splitter, (supplied by Bruker for the IFS 66/S spectrometer).

Region of electromagnetic wavelength range	Wavelength range / μm	Colour code of the beam splitter
Visible	0.35 – 0.75	White
Near-Infrared	0.75 – 2	Brown
Mid-Infrared	2 – 15	Red
Far-Infrared	> 15	Red

Table 3.10: Choice of light source, beam splitter and detector (supplier: Bruker).

Items	Wavelength range / μm
Light source	
Tungsten	Visible/ NIR 0.4 - 1.5
SiC/Globar	MIR 2 – 15
Beam Splitter	
CaF_2	Visible / NIR 0.4 - 1.5
KBr	MIR 2 - 15
Detector	
DTGS	MIR 2 - 25
InGaAs	NIR 0.75 - 1.7/1.8
Si	Visible 0.4 - 2

The polished chalcogenide glass sample was placed and secured using plasticine© on a steel sample holder which was rectangular with an aperture in the centre (supplier: Bruker OPTIK).

Three circular apertures, 1 mm, 3 mm and 5 mm in diameter were used depending on the sample size. The sample holder was then slotted into the FTIR compartment and the lid replaced. The FTIR was purged with dry air (Parker Filtration, FT-IT purge gas generator, 75-52-12VDC) to remove the vibrational absorption bands at ≈ 4.0 μm and at ≈ 6.3 μm due to CO_2, H_2O, respectively in the ambient atmosphere.

3.3.6.2 Treatment of results and errors

The resulting FTIR spectra were divided by the path-length which was the optical thickness in centimetres of the glass pieces, to determine the absorption coefficients (cm^{-1}) of the various absorption bands. Figure 3.20 shows a schematic FTIR spectrum. One absorption band is schematically indicated in the spectrum, points a and b show the top and the bottom of the band respectively. The absorption coefficient per cm is calculated by (a-b) /cm^{-1}. However, because the thickness, the refractive index and the launching angle of each sample may not identical; the Fresnel reflection may need to be counted in further experiments. Mr Zhuoqi Tang (PhD student in the University of Nottingham) has been investigating the affects of the Fresnel reflection on the FTIR results.

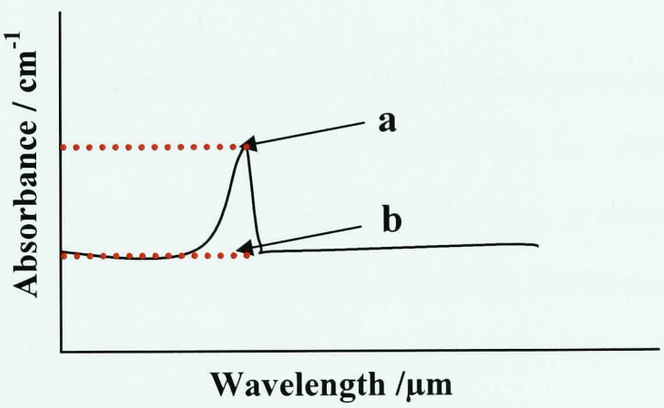

Figure 3.20: An example of an FTIR spectrum. One absorption band is indicated schematically in the spectrum; points a and b show the top and the bottom of the band respectively. The absorption coefficient is calculated by (a-b) /cm^{-1}.

3.3.7 Refractive index measurement

The refractive index measurement is perhaps the most fundamental in the process of characterising glass in terms of its optical properties. The difference in the refractive index of two or more materials over the optical frequency range of interest serves as a basis for propagating optical signals in all types of optical waveguide. In this PhD project, the refractive index measurements were done using ellipsometry by J. Orava (in the group of Prof. Tomas Wagner) in the University of Pardubice and by the minimum deviation method by D. Orchard in QinetiQ, UK.

Ellipsometry

Ellipsometry was used for measuring both bulk and thin film samples. Chalcogenide glasses discs with 10 mm diameter and 2 mm thickness were prepared by the author of the University of Nottingham. One surface of the discs was polished to a 1 μm finish. Chalcogenide thin film samples with ~ 4 μm thickness were deposited by thermal evaporation on to some of these discs in the University of Pardubice.

The refractive index was evaluated from experimental Ψ (related to amplitude) and phase shift Δ data measured using a VASE® J. A. Woollam Co., Inc. ellipsometer, with an automatic rotating-analyzer, in the spectral range from 0.3-2.3 μm, at angles of incidence 60°, 65° and 70°. Spectra were measured at 20 nm wavelength steps. The ellipsometer was equipped with an AutoRetarder®, which allowed the measurement of the ellipsometric parameter Δ at a 360° interval. The experimental ellipsometry data were evaluated using the Tauc-Lorentz dispersion formula [135] in the entire spectral region and Cauchy dispersion model [136] in the spectral region below the bandgap [135]. According to Wagner *et al.* [137] the Tauc-Lorentz formula ensures the Kramers-Kronig consistency of the real and imaginary parts of the optical functions,

$$N = n + ik \qquad 3\text{-}5$$

where n, the real part of the refractive index, measures the reduction of the velocity of light through a medium and k (the imaginary part) is the extinction coefficient which indicates the amount of absorption loss when an electromagnetic wave propagates through the medium. Both n and k depend on the frequency (wavelength).

The dielectric constant is the square of the refractive index:

$$\varepsilon = \varepsilon_1 + \quad i\,\varepsilon_2 = N^2 = (n+ik)^2 \qquad 3\text{-}6$$

so the conversion between refractive index and dielectric constant is:

$$\varepsilon_1 = n^2 - k^2 \qquad 3\text{-}7$$

$$\varepsilon_2 = 2nk \qquad 3\text{-}8$$

$$n = ,^{1/2} \qquad 3\text{-}9$$

$$k = \{[(\varepsilon_1^2 + \varepsilon_2^2)^{1/2} - \varepsilon_1]/2\}^{1/2} \qquad 3\text{-}10\ [138]$$

When modelling the ellipsometric results a correction for surface roughness of the thin film was introduced by Wagner *et al.* [137] using the Bruggeman effective medium approximation of a porous layer on top of the $As_{40}Se_{60}$ thin film, i.e. the surface porous layer was supposed to consist of the same bulk material as that of the thin film but with a void density of 50 volume % [138, 139]. An oxide layer was not included in the fit. The dispersion measurements were made at room temperature, i.e., 23 °C.

The Cauchy equation [136] was used to model the real part of the refractive index. The Urbach equation [138, 140] was used to model the extinction coefficient k.

$$k(\lambda) = C_1 \exp^{C_2(E-E_b)} \qquad 3\text{-}11\ [138, 140]$$

where E is photon energy, $E = 1240 / \lambda$ if the photon energy E is given in electron volts and λ is in nm. $E_b = 1240 / \lambda_0$ where the parameter λ_0 has an arbitrary value, but is often set as the lowest measured wavelength. C_1 is the extinction coefficient amplitude and C_2 the exponent factor.

Minimum deviation measurement

The minimum deviation measurement of the refractive index of the bulk chalcogenide sample was kindly carried out by Dr. David Orchard in QinetiQ, UK. Chalcogenide prism samples with 20° apex angle (accurately measured) were produced at the University of Nottingham from as prepared $As_{40}Se_{60}$ glass rod using the procedure described by Pan [1] .

As Figure 3.21 shows, the prism was mounted on a calibrated rotation stage and adjusted to ensure both faces were parallel to the axis of rotation. The laser beam passed through a beam splitter and was normal to the axis of rotation. The minimum deviation angle was measured using retro-reflection from the mirror when rotating the prism. The prism angle (19.39 ± 0.08°) was measured using retro-reflection from the prism faces and the condition of the retro-reflection was identified from observing the laser beam with the camera. The measurements and results obtained at a wavelength of 10.6 μm will be described in detail in section 4.7.1.

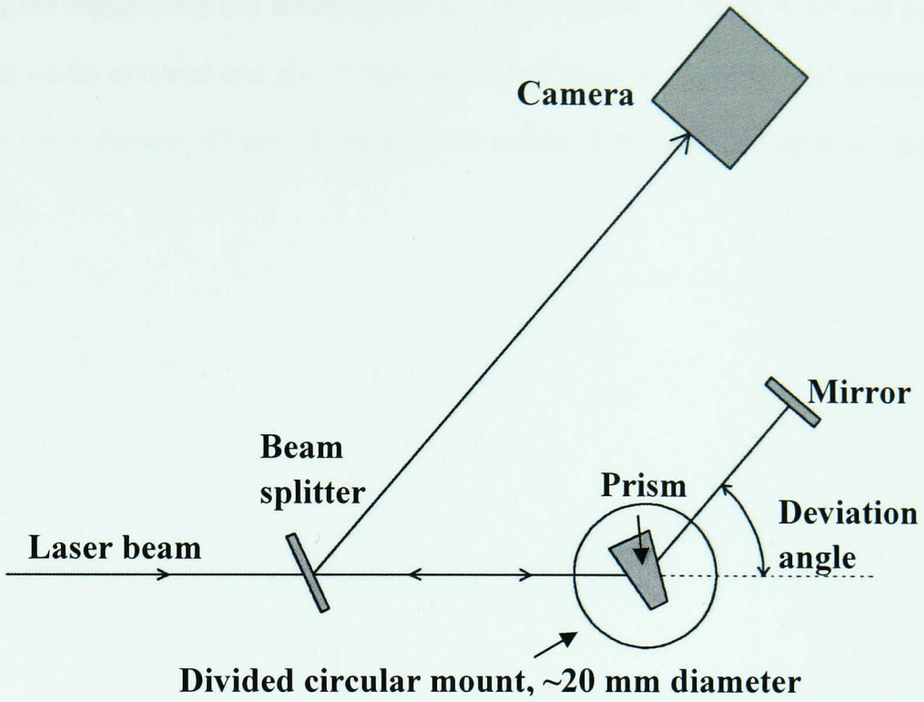

Figure 3.21: Experimental setup for measurement of refractive index by the minimum deviation method. The prism was located on a calibrated rotation stage. The laser beam passed through a beam splitter and was normal to the axis of rotation. The minimum deviation angle was measured using retro-reflection from the mirror. The prism angle was measured using retro-reflection from the prism faces and the condition of the retro-reflection was identified from observing the laser beam with the camera.

3.4 Summary

The general experimental procedures for material characterisations carried out in this project were introduced in this chapter. They are the procedure of the chalcogenide glass melting, quenching, annealing and polishing; the schedule of chemical precursor purification; the methods for glass characterisation, i.e. Differential Scanning Calorimetry (DSC) for examining the glass Tg, X-ray Diffraction (XRD) for checking the amorphous nature of glass, Thermomechanical Analysis (TMA) for measuring the thermal expansion coefficient (α) and viscosity of glass, Environment Scanning Electron Microscopy (ESEM) for viewing and imaging the sample at micro-scale and Fourier Transform Infrared Spectroscopy (FTIR) for

finding the transparency and absorption peak of certain glasses. Chapter 4 to 6 will present and discuss results obtained and give further detailed of some key experimental procedures. The first of these chapters (Chapter 4) presents the results of the characterisation of chalcogenide glasses.

Chapter 4

Characterisation of Chalcogenide Glasses

The fabrication of optical waveguides in the forms of strip planar rib optical waveguides and Microstructure Optical Fibres (MOFs) based on chalcogenide glasses is the objective of this PhD project. This chapter presents measurements of the properties of certain chalcogenide glasses and identifies suitable glass compositions for realising the above objective.

In order to investigate suitable glass compositions for fabrication waveguides, the properties will be studied are classified into two areas, i.e. non-optical properties and optical properties. The non-optical properties include glass amorphous nature, glass transition temperature (Tg), glass thermal expansion coefficient (α) and viscometry (η/T). The glass optical properties considered here including optical loss, introduced via glass impurities, and the glass refractive index. A suitable glass composition could be decided after considering all the properties.

A Se precursor purification process developed will be introduced; this potentially enhances the purity of Se containing glasses and thus lower the impurity related optical losses. This chapter will also present and discuss the experimental results of obtained for refractive index of bulk $As_{40}Se_{60}$ $Ge_{17}As_{18}Se_{65}$ and $Ge_{10}As_{23.4}Se_{66.6}$ and $As_{40}Se_{60}$ thin film samples.

4.1 Glass melting

Standard glass melting schedules for melting $As_{40}Se_{60}$, $Ge_{17}As_{18}Se_{65}$ and $Ge_{10}As_{23.4}Se_{66.6}$ compositions and samples were used taken from Rowe [2]. The melting and annealing procedures are described in detail in Table 3.3 in section 3.1.3.

Figure 4.1 (a) depicts a typical as – annealed $Ge_{17}As_{18}Se_{65}$ (ZGLCF002) glass rod; the surface was smooth and glossy. A contraction cone was observed at one end of the sample. The chalcogenide glass rod was then sliced into several ~2 mm thickness discs and one surface of each disc was polished to a 1 μm finish as shown in Figure 4.1 (b). The $Ge_{17}As_{18}Se_{65}$ polished discs could be used as the substrates of rib optical waveguides.

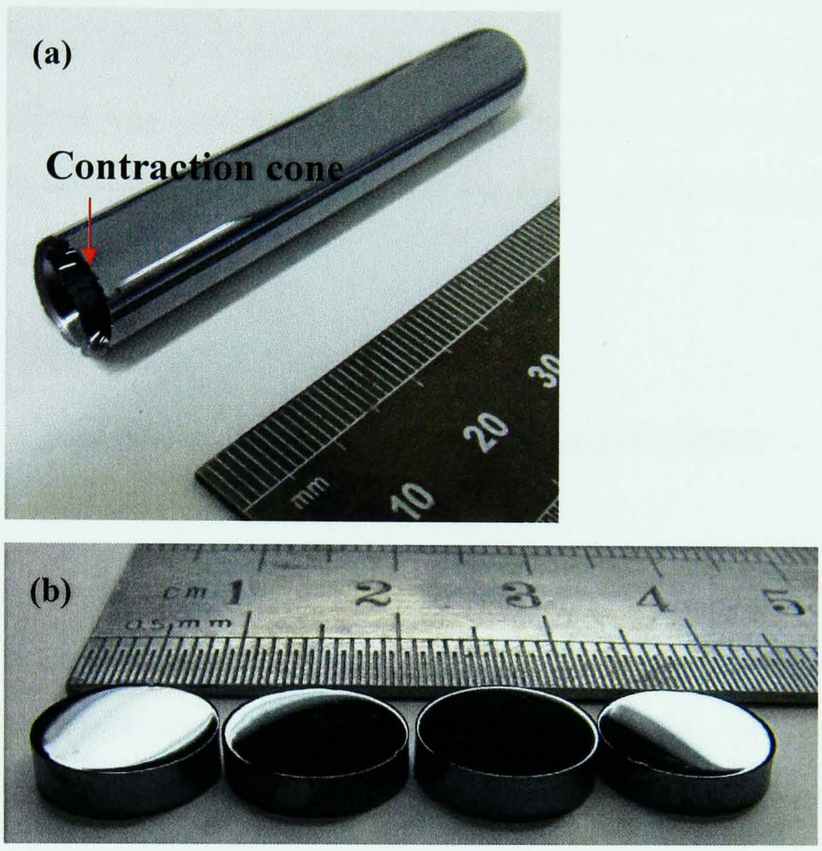

Figure 4.1: (a) $Ge_{17}As_{18}Se_{65}$ (ZGLCF002) as annealed glass rod, 10 mm diameter and ~ 55 mm length. (b) Several chalcogenide glass discs sliced from the ZGLCF002 sample rod; the top surfaces were polished to a 1 μm finish.

Figure 4.2 (a) depicts 95 g of $Ge_{10}As_{23.4}Se_{66.6}$ (ZGLCF034) and 97 g of $As_{40}Se_{60}$ (ZGLCF031) glasses each melted then annealed inside a 29 mm / 33 mm ID/OD ampoule following the manner of Table 3.3 in section 3.1.3. The glasses, which were melted in ampoules, were prepared as billets for core/clad extrusion. Figure 4.2 (b) shows that after annealing, the two billets were cut to 15 mm height and the surfaces, which would later mate inside the extruder, were ground then polished to a 1 μm finish.

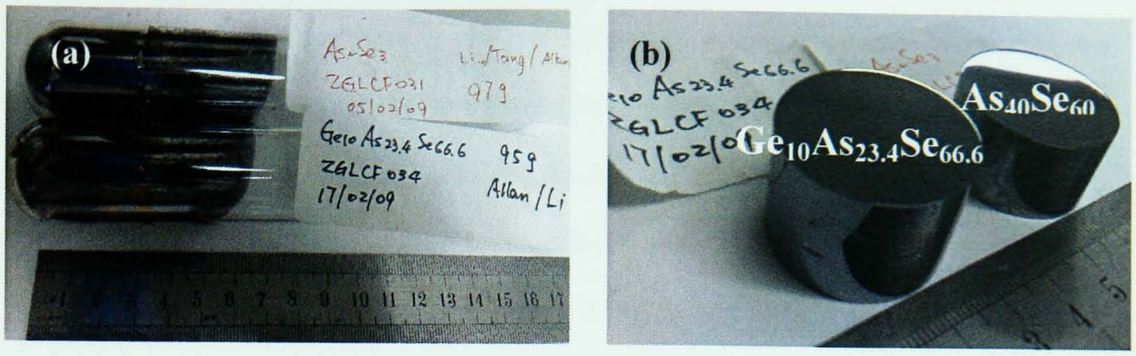

Figure 4.2: (a) 95 g of $Ge_{10}As_{23.4}Se_{66.6}$ (ZGLCF034) and 97 g of $As_{40}Se_{60}$ (ZGLCF031) glasses were each melted then annealed inside a 29 mm / 33 mm ID/OD ampoule. (b) These two glass rods were cut to 15 mm height and one surface polished to a 1 µm finish for later extrusion.

4.2 Material amorphous nature measurement

In this project, X-Ray Diffractometry (XRD) measurements were mainly performed for the purpose of conforming the chalcogenide glass amorphous nature. XRD was carried out, using a Siemens Krystalloflex 810 diffractometer, on each glass composition that was used and developed throughout this work. Powder was produced from chalcogenide glass samples $As_{40}Se_{60}$ (ZGLCF007), $Ge_{17}As_{18}Se_{65}$ (ZGLCF002) and $Ge_{10}As_{23.4}Se_{66.6}$ (ZGLCF034) for the measurement. The XRD patterns of the $As_{40}Se_{60}$, $Ge_{17}As_{18}Se_{65}$ and $Ge_{10}As_{23.4}Se_{66.6}$ are plotted in Figure 4.3. During the glass melting procedure, a crystalline solid may result if an inappropriate annealing process took place (see glass science in section 2.1). The basic difference between the XRD pattern of a crystalline solid and that of an amorphous solid is the absence of sharp peaks for the glassy material due to the absence of long-range order in glasses [141]. The halo-like XRD patterns of $As_{40}Se_{60}$, $Ge_{17}As_{18}Se_{65}$ and $Ge_{10}As_{23.4}Se_{66.6}$ were shown in Figure 4.3. These broad peaks indicate that there is a certain irregular arrangement of molecules and a lack of molecular orientation [142] and no long-term periodicity as occurs in crystals. Therefore, the amorphous nature of the materials is confirmed. Furthermore, this confirms that the glass melting procedures adopted are well-founded for melting amorphous chalcogenide glasses.

The First Sharp Diffraction Peak (FSDP) of the pattern is potentially able to estimate the underlying atomic structure. In Figure 4.3, the first sharp diffraction peak (FSDP) of the XRD patterns of $As_{40}Se_{60}$, $Ge_{10}As_{23.4}Se_{66.6}$ and $Ge_{17}As_{18}Se_{65}$ are at angles 2θ around 17.8°, 16.0 ° and 15.5° respectively. The 2θ is the angle between the incident X-ray beam and the detector. The position of the FSDP of $As_{40}Se_{60}$ is similar to that reported by Kavetskyy [143]. According to Kavetskyy *et al.* [144] the percentage of As contained in the glass affects the position of the FSDP, which suggests that the percentage of As may influence the atomic structure.

The FSDP of an XRD pattern is potentially able to provide an estimate the material structure. In a disordered networking forming system, such as an amorphous solid, two atomic structure schemes are invoked by the origin of FSDP. (1) FSDP represents crystalline-like layers, its position being related to the interlayer separation [145]; (2) The basic structure is described as cluster-voids, leading to a correlation distance typical of intermediate range order [146]. However, Massobiro *et al.* [145] proposed that both the layered structure and cluster-void correlation interpretations are inadequate to account for the appearance of the FSDP.

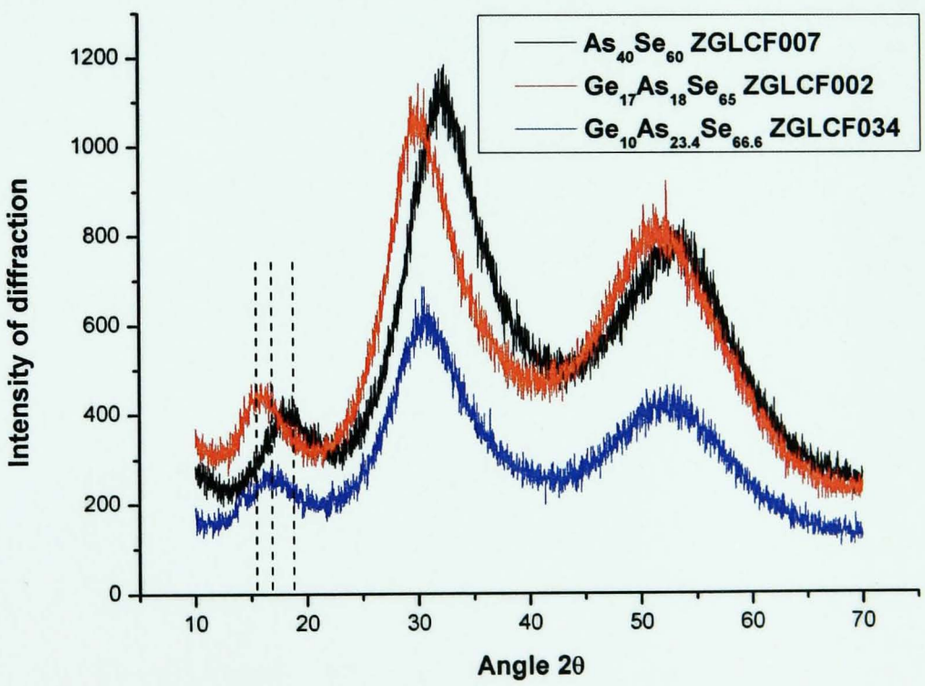

Figure 4.3: The XRD pattern of $As_{40}Se_{60}$ (ZGLCF007), $Ge_{17}As_{18}Se_{65}$ (ZGLCF002) and $Ge_{10}As_{23.4}Se_{66.6}$ (ZGLCF034). The pattern shows no sharp peaks due to crystal phases. Hence the amorphous nature of the glass was confirmed.

4.3 Glass transition temperature (Tg) measurement

The extrapolated onset Tg was measured using a Perkin Elmer Pyris 1 Differential Scanning Calorimeter (DSC), by heating the as-annealed glass at rate of 10°C min^{-1} from room temperature to a temperature higher than Tg. For each measurement using DSC, only small piece of sample is required, typically around 18 mg. Figure 4.4 illustrates the DSC results of 18.2 mg $As_{40}Se_{60}$ (ZGLCF007), 21.0 mg $Ge_{17}As_{18}Se_{65}$ (ZGLCF002) and 19.0 mg $Ge_{10}As_{23.4}Se_{66.6}$ (ZGLCF034), respectively. The change from supercooled liquid to glass is not taking place suddenly, therefore the temperature range is more accurately describe by the extrapolated Tg. Typically, the crossing point of the tangential to the DSC curve is taken as Tg (Figure 4.4). According to DSC analysis, the Tg of $As_{40}Se_{60}$ is 180 ± 5 °C, that of $Ge_{17}As_{18}Se_{65}$ is 235 ± 5 °C and that of $Ge_{10}As_{23.4}Se_{66.6}$ is180 ± 5°C.

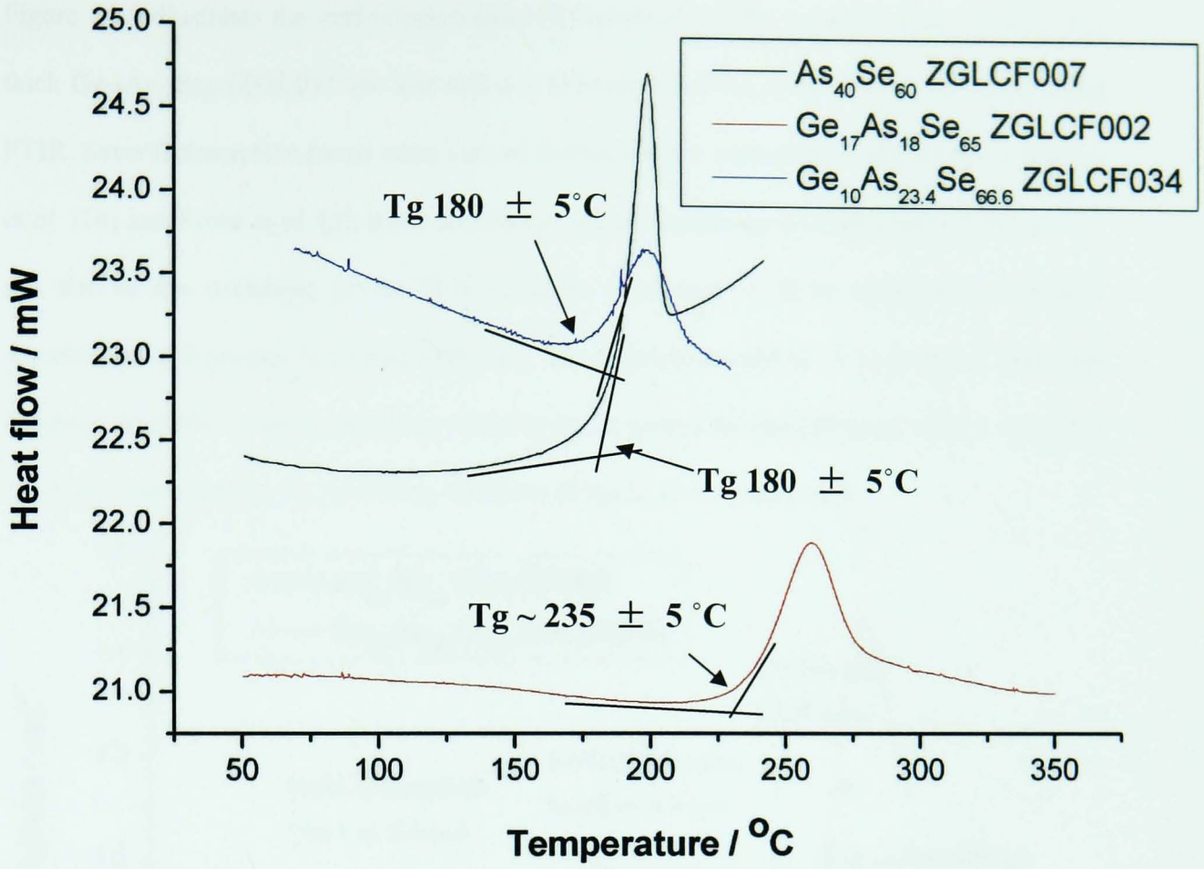

Figure 4.4: Differential Scanning Calorimetry (DSC) results of $As_{40}Se_{60}$ (ZGLCF007) and $Ge_{17}As_{18}Se_{65}$ (ZGLCF002) and $Ge_{10}As_{23.4}Se_{66.6}$ (ZGLCF034). The tangential crossing point of the extrapolated onset and steep decline was taken as the glass Tg. The Tg of $As_{40}Se_{60}$ was 180 ± 5 °C; that of $Ge_{17}As_{18}Se_{65}$ was 235 ± 5 °C and that of $Ge_{10}As_{23.4}Se_{66.6}$ was 180 ± 5 °C.

4.4 Transparent window and absorption coefficient measurement

Chalcogenide glasses have a transmission range from a wavelength of ~800 nm through the mid-infrared region depending mainly on the mole percentage of selenium and tellurium added in the chalcogenide glass [16]. Fourier Transform Infrared Spectroscopy (FTIR) was used to observe the glass transmission window and absorbance bands. The impurities such as OH^-, H^- and oxides in the chalcogenide glass absorb light which would influence chalcogenide glass transmission window [16]. Some purification processes (section 4.9.2) were required prior to the sealing to minimise the impurities contained in the chalcogenide glass after melting.

Figure 54.5 illustrates the mid-infrared (mid-IR) spectrum results collected from a 3.221 mm thick $Ge_{17}As_{18}Se_{65}$ (ZGLCF004) disc and a 2.110 mm thick $As_{40}Se_{60}$ (ZGLCF026) disc using FTIR. Several absorption bands were viewed in Figures 4.5. According to the study by Seddon *et al.* [16] and Rowe *et al.* [2], those absorbance bands include an -OH absorption band at ~2.7 μm due to the stretching of the O-H vibration bond and an H-Se absorption band at a wavelength ~4.6 μm due to a bond stretching. The absorption band at ~6.3 μm is due to H-O-H bending vibration. A Ge-O stretching vibration bond causes the absorption at ~8 μm. The peak at ~9 μm is assigned to the stretching vibration of the Si-O-Si bond [147].

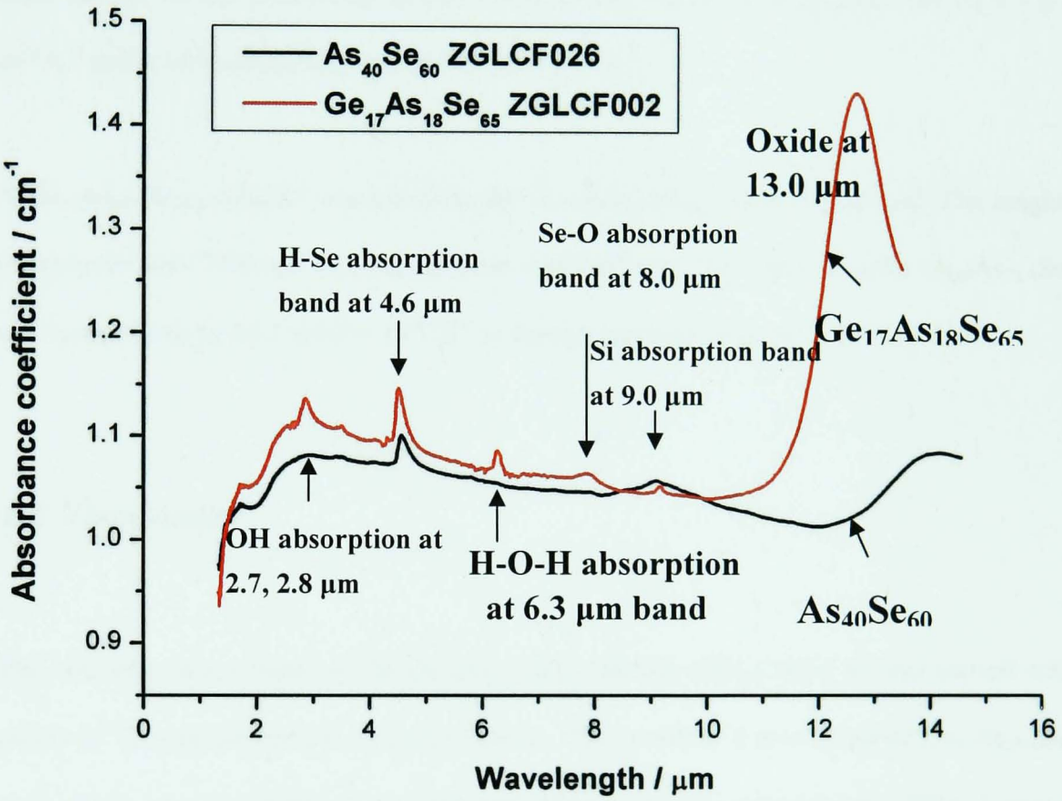

Figure 4.5: FTIR absorption spectrum of $As_{40}Se_{60}$ (ZGLCF026, thickness: 2.110 mm) and $Ge_{17}As_{18}Se_{65}$ (ZGLCF002, thickness: 3.221 mm) sample. The wavelengths at maximum impurity absorption over the band are: OH^- absorption band at 2.7 μm, H-Se band at wavelength 4.6 μm, H-O-H band at 6.3 μm, Ge-O absorption band at 8 μm and Si-O-Si absorption band at 9 μm.

Both As and Se precursors were purified to eliminate the oxidisation, but Ge used was as-purchased. Therefore, the Ge would tend to bring in oxide contamination if its surfaces were already oxidised. Therefore, $Ge_{17}As_{18}Se_{65}$ was believed to have more oxidisation contamination than $As_{40}Se_{60}$ as shown in Figure 4.5.

4.5 Thermal expansion coefficient

The thermal expansion coefficient (α) of each glass was measured using chalcogenide glass cylinders having 4.00±0.05 mm diameter and 7.00±0.05 mm height using a thermomechanical analyser (TMA) (Perkin Elmer TMA7), as described in section 3.3.4. It was found that in the temperature range from 80°C to 140°C: α of $As_{40}Se_{60}$ was 20.6 ± 0.5 × 10^{-6} K^{-1} and α of $Ge_{17}As_{18}Se_{65}$ was 20.5 ± 0.5 × 10^{-6} K^{-1}. The results of α of the two glass compositions were close enough for hot embossing, as also confirmed by Pan [1]. α of $As_{40}Se_{60}$ was 20.0 ± 0.5 × 10^{-6} K^{-1} and α of $Ge_{17}As_{18}Se_{65}$ was 20.2 ± 0.5 × 10^{-6} K^{-1}.

A $Ge_{10}As_{23.4}Se_{66.6}$ cylinder was cut from the $Ge_{10}As_{23.4}Se_{66.6}$ ZGLCF034_b rod. The height of the cylinder was 7.05 mm and the diameter was 4.00 mm. The value of α for $Ge_{10}As_{23.4}Se_{66.6}$ was measured to be 21.5 ± 0.5 × 10^{-6} °K^{-1} in the temperature range from 80°C to 140°C.

4.6 Viscometry

The viscosity measurement of the $Ge_{10}As_{23.4}Se_{66.6}$ sample (ZGLCF034_b) was carried out by means of Thermomechanical Analysis (TMA). The remelted 4 mm diameter $Ge_{10}As_{23.4}Se_{66.6}$ rod was cut into several discs of 1.5 to3 mm thicknesses and analysed using TMA. Figure 4.6 depicts the plots of $\log_{10}$ viscosity versus temperature for $Ge_{10}As_{23.4}Se_{66.6}$ sample (ZGLCF034_b). The initial dimension was 1.5775 mm height × 4.2975 mm diameter. The load used was 250 mN. The temperature range of measurement was from 230°C to ~ 315°C. The viscosity of $Ge_{10}As_{23.4}Se_{66}$ was $10^{7.8}$ Pas at 230°C, with increasing temperature, the viscosity decreased. The viscosities of $As_{40}Se_{60}$ (CF079) and $Ge_{17}As_{18}Se_{65}$ (CF109) was measured by Dr. Pan [1] and are plotted together with the data for ZGLCF034_b in Figure 4.6.

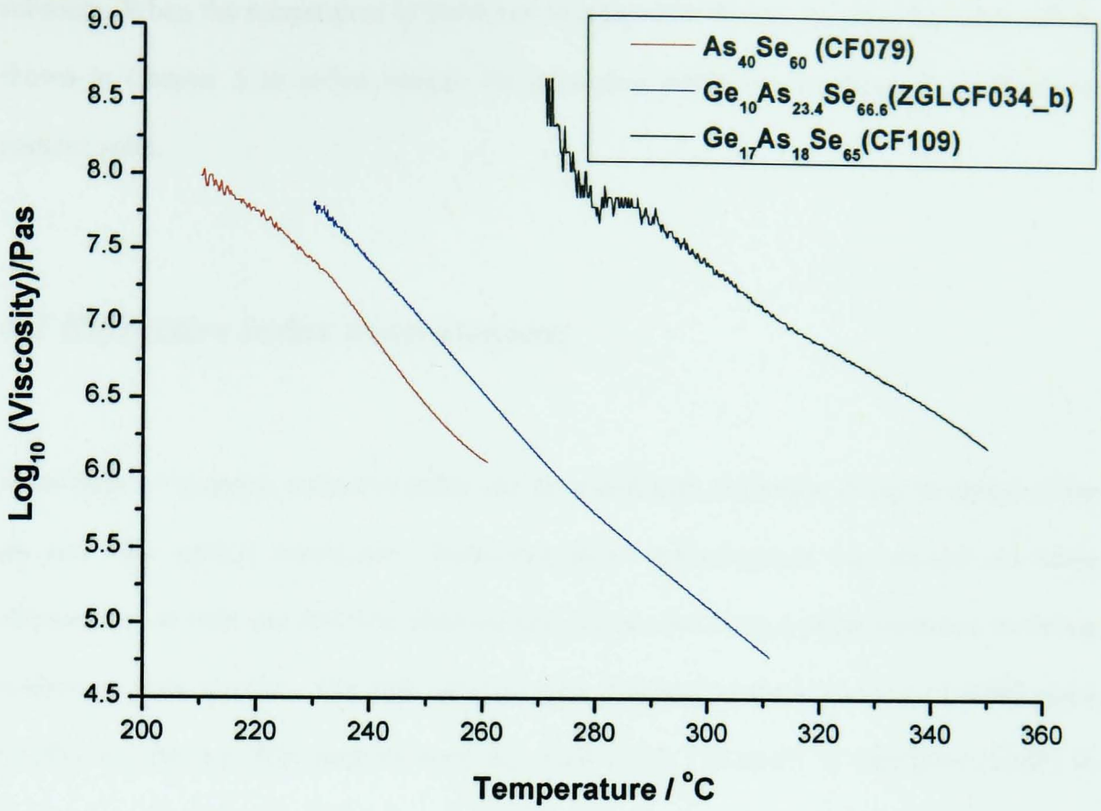

Figure 4.6: Log_{10} viscosity of $As_{40}Se_{60}$ (CF079), $Ge_{10}As_{23.4}Se_{66.6}$ (ZGLCF034_b) and $Ge_{17}As_{18}Se_{65}$ (CF109) plotted against temperature determined by means of TMA. For $Ge_{10}As_{23.4}Se_{66.6}$, the initial sample dimensions were 1.5775 mm height × 4.2975 mm diameter; the load used was 250 mN. For comparison purposes, the viscosity/temperature curves of $As_{40}Se_{60}$ (CF079) and $Ge_{17}As_{18}Se_{65}$ (CF109) measured by W.J. Pan [1] are also plotted here.

It can be observed from Figure 4.6 that chalcogenide glasses have a low viscosity at relatively low temperature; this property will be exploited in the hot embossing fabrication technique for rib waveguides described in detail in Chapter 5. Also, chalcogenide glasses show a steep viscosity against temperature behaviour, which means the viscosity changes significantly over a small temperature region. Consequently when fibre drawing (as described in section 3.7), the temperature must be controlled accurately. This requirement increases the difficulty of fibre fabrication. The viscosity of $Ge_{17}As_{18}Se_{65}$ was about 3 orders of magnitude larger than the viscosity of $As_{40}Se_{60}$ at a given temperature. This property of the materials is good for the hot embossing method used to fabricate rib waveguides. $As_{40}Se_{60}$ will be chosen as the thin film (guiding layer) which is later patterned to form the rib waveguide and $Ge_{17}As_{18}Se_{65}$ as the

substrate. When the temperature is increased to about 230 °C, the $As_{40}Se_{60}$ thin film will be shown in Chapter 5 to soften enough for patterning whilst the substrate glass effectively remains solid.

4.7 Refractive index measurement

Knowledge of material, refractive index and its wavelength dispersion is key to design of the rib and fibre optical waveguides. Refractive index measurements was carried out using ellipsometry on bulk and thin film chalcogenide glasses and using a prism minimum deviation method on bulk samples. The bulk samples were prepared in the University of Nottingham (UofN) and the thin film samples were deposited in the University of Pardubice (UofP) on substrates prepared in the UofN. The measurements were carried out at the UofP and the prism minimum deviation measurement at QinetiQ, UK. The record of the glasses that were measured is shown in Table 4.1. The columns of the table show: the samples composition; melting codes; measurement institutes; polishing condition; thin film sample and flat-embossed condition which will be described in section 4.8. The preparation procedure of chalcogenide glass prisms was explained in detail in the previous work of Pan [1]; a brief description is provided in section 4.7.1 for completeness of this thesis.

Table 4.1: Record of $As_{40}Se_{60}$, $Ge_{17}As_{18}Se_{65}$ and $Ge_{10}As_{23.4}Se_{66.6}$ samples' melting code and treatment (polishing, flat-embossing and coating) before ellipsometry measurement during this PhD project.

Sample composition	Bulk glass melt code	Made at UofN/ UofP?	Bulk glass cut / polished	$As_{40}Se_{60}$ thermal evaporation	Flat-embossed
$As_{40}Se_{60}$	ZGLCF007	UofN	√	N/A	√
$As_{40}Se_{60}$	ZGLCF009	UofN	√	N/A	×
$As_{40}Se_{60}$	ZGLCF027	UofN	√ (prism)	N/A	×
$As_{40}Se_{60}$	UofNas2se3(i)	UofN	√	N/A	×
$As_{40}Se_{60}$	UofNas2se3(ii)	UofN	√	N/A	×
$As_{40}Se_{60}$	UofPas2se3(i)	UofP	√	N/A	×
$As_{40}Se_{60}$	UofPas2se3(ii)	UofP	√	N/A	×
$Ge_{17}As_{18}Se_{65}$	ZGLCF010	UofN	√	√ (ID: GG 20080223)	√ (ID: GG 20080223_f)
$Ge_{17}As_{18}Se_{65}$	UofNGAS(i)	UofN	√	N/A	√
$Ge_{17}As_{18}Se_{65}$	UofNGAS(ii)	UofN	√	N/A	√
$Ge_{17}As_{18}Se_{65}$	UofNGAS(iii)	UofN	√	N/A	√
$Ge_{17}As_{18}Se_{65}$	UofNGAS(iv)	UofN	√	N/A	√
$Ge_{10}As_{23.4}Se_{66.6}$	ZGLCF038	UofN	√	N/A	√

Note: UofN is University of Nottingham; UofP is University of Pardubice.

4.7.1 Bulk chalcogenide glasses

Using ellipsometry

The ellipsometry measurement was carried out in the University of Pardubice. The measured refractive index of the three bulk samples $As_{40}Se_{60}$ (ZGLCF009 (i)), $Ge_{10}As_{23.4}Se_{66.6}$ (ZGLCF010(i)) and $Ge_{10}As_{23.4}Se_{66.6}$ (ZGLCF038 (i)) are plotted in Figure 4.7. The plot labelled with black solid squares represents the refractive index of $As_{40}Se_{60}$, that with blue triangles the refractive index of $Ge_{10}As_{23.4}Se_{66.6}$ (ZGLCF038 (i)) and that with red points the

refractive index of $Ge_{17}As_{18}Se_{65}$ (ZGLCF010 (i)) across the wavelength range from 0.3 μm to 2.3 μm. The corresponding extinction coefficients are represented with matched colour, hollow symbols.

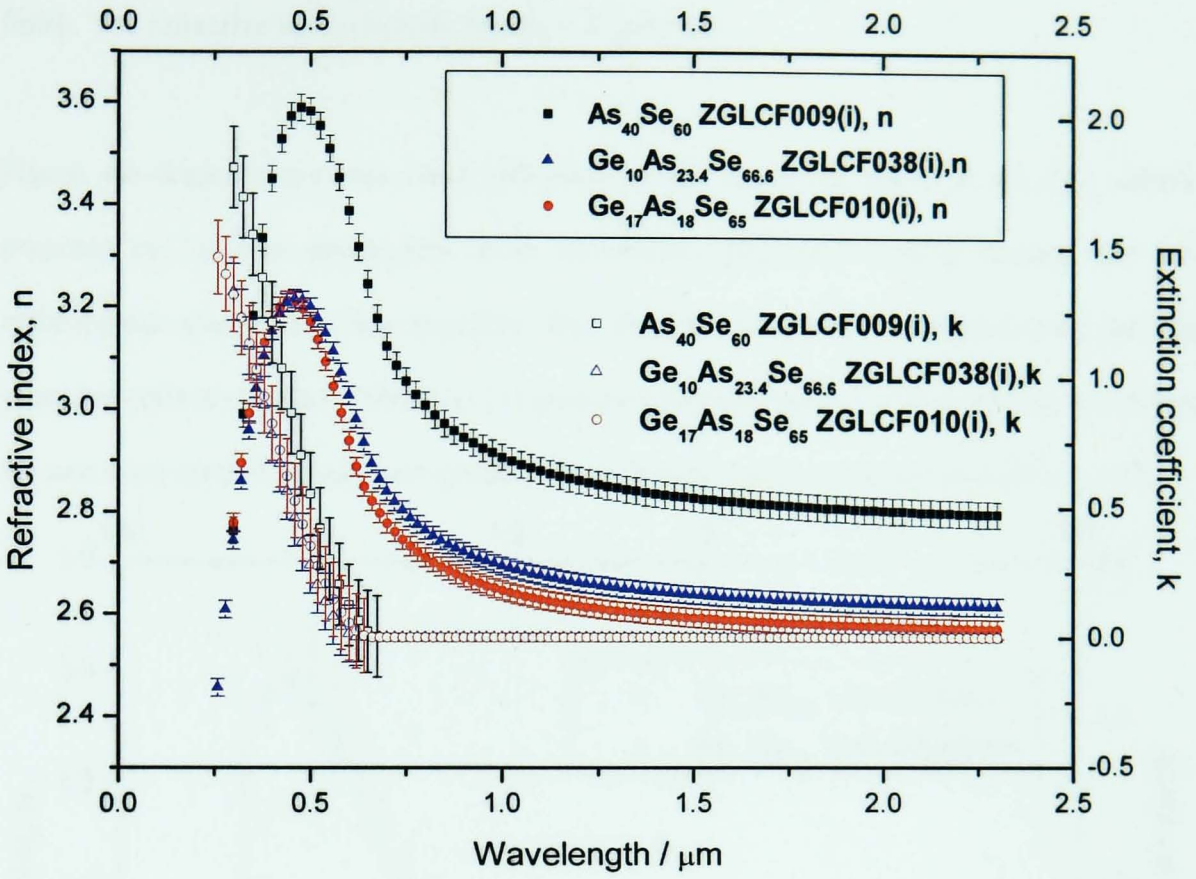

Figure 4.7: Ellipsometry measurement of refractive index dispersion of three chalcogenide glass samples. Red solid circles plot represent the refractive index of $As_{40}Se_{60}$ (ZGLCF009 (i)), blue solid squares represent $Ge_{10}As_{23.4}Se_{66.6}$ (ZGLCF038 (i)) and green solid triangles show the refractive index of $Ge_{17}As_{18}Se_{65}$ (ZGLCF010 (i)) across the wavelength range from 300 nm to 2300 nm. The hollow symbols represent the corresponding extinction coefficients (Appendix C).

Collaboration between the two laboratories gave opportunity to compare the optical properties of $As_{40}Se_{60}$ bulk glass melted by the two institutions, i.e. the University of Nottingham, UK and the University of Pardubice, Czech Republic. Several factors could influence the optical properties of the glass samples, such as the preparation process and raw material suppliers.

One bulk glass sample each was prepared by the University of Nottingham (UofN) (ID: UofNAs2Se3_01) and the University of Pardubice (UofP) (ID: UofPAs2Se3_01), respectively. The samples prepared in the UofN consistently followed the glass melting procedure describe

in section 3.1.3. Two glass discs each with ~ 10 mm diameter and ~2 mm thickness were cut from each of the $As_{40}Se_{60}$ rods, i.e. from UofNas2se3_01 and UofPas2se3_01. Please note that none of these samples was flat-embossed. One surface of each sample was polished to a 1 μm finish. The refractive index data are shown in Figure 4.8.

Figure 4.8 depicts there was clear difference of the refractive index of $As_{40}Se_{60}$ samples prepared by the two universities. Both universities employed rocking furnace and melt chalcogenide glasses in silica ampoules. But there are several preparation factors that may cause the refractive index difference: (1) precursor material purities; (2) quenching conditions; (3) annealing furnace temperature profile. These factors will be discussed in section 4.10.3.

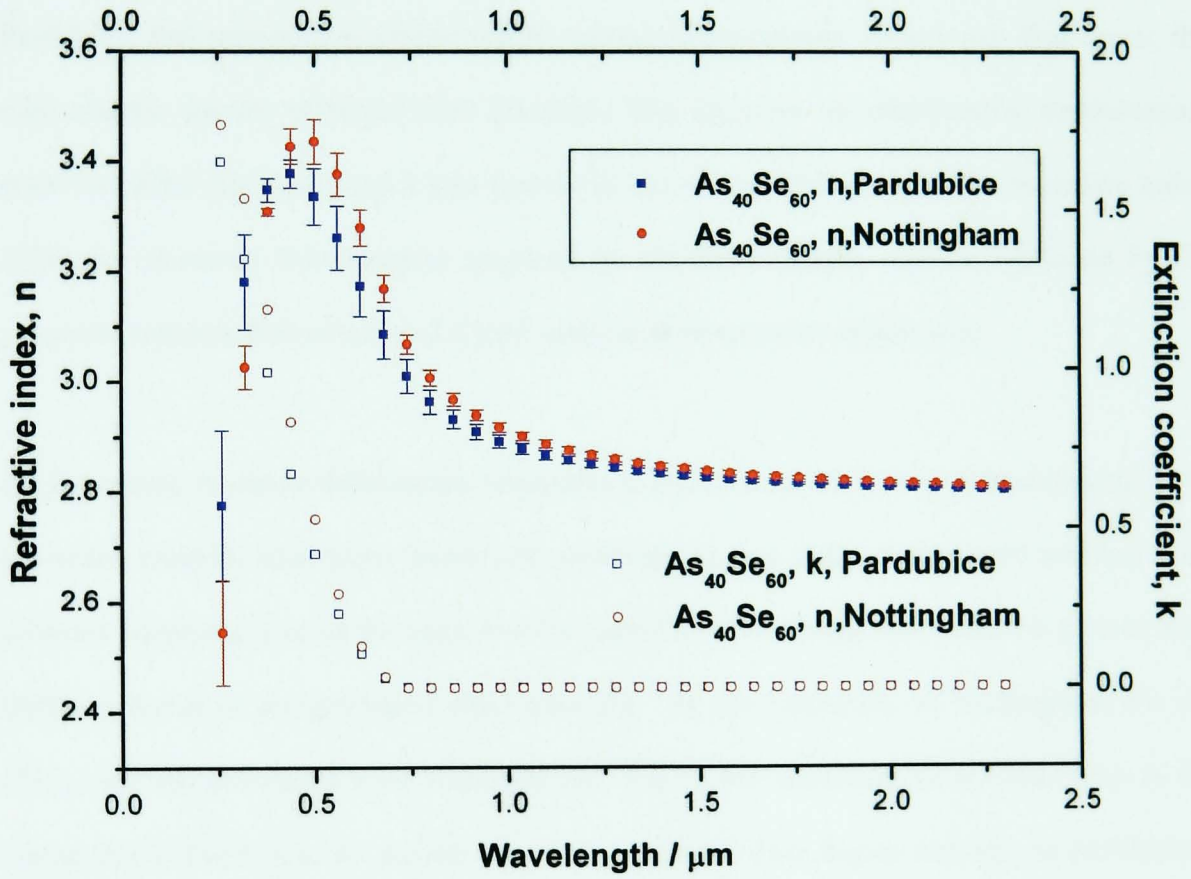

Figure 4.8: Refractive index of $As_{40}Se_{60}$ glass samples. The red dot is the refractive index of $As_{40}Se_{60}$ prepared in UofN (UofNAs2Se3_01) and the blue squares represent refractive index of $As_{40}Se_{60}$ prepared in UofP (UofPAs2Se3_01). Measurement wavelengths are between 0.3 μm and 2.3 μm. The hollow symbols represent the corresponding extinction coefficient.

Discussion of refractive index variation

Ellipsometry was used to measure the refractive index of chalcogenide bulk and thin film samples. Comparing the measurement results of the $As_{40}Se_{60}$ glasses that were prepared by the two institutions, it can be seen that they are not identical, especially at wavelengths lower than 800 nm. As shown in Figure 4.8, $As_{40}Se_{60}$ sample (ID: UofNAs2Se3_01) had a slightly higher refractive index than the sample that was prepared by the University of Pardubice (ID: UofPAs2Se3_01). These samples had been polished to 1 μm finish, so they had similar surface condition. The reason for this variation was initially thought to be attributable to the measurement error. However, it was confirmed by the operator, J. Orava in the University of Pardubice, that repeating the ellipsometry measurements on any sample e.g. five times, the ellipsometric spectra obtained were identical. This suggests the ellipsometry measurement error was relatively small and it was ignored in the current PhD project. The refractive index difference observed from samples prepared by the two institutes may be explained by (1) precursor resource differences and (2) the quenching temperature differences.

(1) Precursor resource differences. Impurities in the material are known to lead potentially to unwanted material absorption bands and scattering. It was noted that arsenic sourced from different suppliers, quoting the same level of purity for their chemicals, resulted in glasses with different levels of oxygen-based absorption [2]. In the University of Nottingham, the As (7n5) used was purchased from Furukawa Ltd. The Se was purchased from Cerac (5n). In the University of Pardubice, As and Se were both purchased from Sigma Aldrich. As purification is able to reduce the oxygen-based impurity bands and this has been studied by Rowe [2], so the As precursor was purified using sublimation method before batching by both universities. In the University of Nottingham, Se precursor was also purified when desired as discussed in section 4.9.

(2) The quenching temperatures are different. The quenching temperature, defined as that temperature to which the glass melt is quenched, is an important parameter in the glass making process. A too high quenching temperature (higher than Tg) could lead to crystallisation and if

the quenching temperature is too low (lower than Tg), this may cause permanent stress in the glass [2]. The Tg of $As_{40}Se_{60}$ was measured to be 180 ± 5 °C (section 4.3) and this temperature was used as quenching temperature in the University of Nottingham. Analysis by means of XRD showed that there was no sign of crystallisation in the glass (section 4.2). In the University of Pardubice however, the quenching temperature used was 0.9 × Tg which was ~162°C. The main purpose for using a lower quenching temperature than Tg was to minimise the chance of crystallisation. This quenching temperature could potentially generate stress in glass.

The two universities used different quenching temperatures which is likely to introduce optical property variation for the same glass composition. In order to test the influence of the quenching conditions on properties such as refractive index, more $As_{40}Se_{60}$ glasses should be melted in both universities based on the same temperature condition e.g. at 180°C.

The batching accuracy may associate with the refractive index variation from batch to batch. The accuracy of the weighing of the raw materials is considered as the most important factor to keep the composition stoichiometry correct. In the UofN, the weight of each of raw material is calculated according to the atomic mass of the element and the mole percentage in the glass composition using the 'Batch' software written by Dr. D. Furniss. The weight is measured using a balance (accurate to ± 0.0001 mg) in a glove box as described in section 3.1.2. Due to low moisture (<0.1 ppm) conditions in the glove box, static electricity may build up and might cause the measurement to become inaccurate. The recommendation for future experiments is that during each measurement the balance reading to be allowed to stabilise for at least 5 minutes. Also, large weight melting (>20 g) is affected less by the batching accuracy.

Ampoule sealing may cause material loss. Based on the ampoule sealing process, a silica ampoule requires a very high temperature (> 1200°C) flame to seal. So during the sealing process, the high temperature can potentially cause some of the chalcogenide material to vaporise which could consequently lead to a stoichiometry change. The recommendation for future experiment is to minimise the sealing duration.

It is worth checking the refractive index differences from sample to sample from the same ingot. **Several $Ge_{17}As_{18}Se_{65}$ discs from one batch were tested for verifying the refractive index variation caused by different annealing temperature.** Four discs having thickness 2 mm ± 0.1 mm were cut from one $Ge_{17}As_{18}Se_{65}$ ingot (UofNGAS 01(i) - (iv)). One surface of each disc was polished to 1 μm finish and the other surface was kept rough. These samples were not flat-embossed but left 'as-polished'. The refractive index and extinction coefficient values are shown in Figure 4.9. At 0.5 μm wavelength for example, the refractive index of these samples was 3.1765, 3.1528, 3.1442 and 3.1673, respectively. The refractive indexes of these samples at wavelengths beyond 0.5 μm almost overlap. This implies that the temperature differences in the annealing furnace may not affect the optical properties dramatically. The refractive index at wavelengths between 1.3 μm and 1.7 μm was zoomed in and shown in Figure 4.10. At 1.5 μm wavelength, the refractive index of these samples was 2.5622, 2.5642, 2.5619 and 2.5604, respectively (see Appendix E). The refractive index difference between these samples at this wavelength is thus approximately 0.004. This difference demonstrated the optical properties of bulk sample could be affected by the temperature difference in annealing furnace. However, in the current project, this variation of the refractive index was allowed for in the optical device design. Much larger refractive index differences, due to material composition changes, were used to design rib and fibre waveguides. In the current project, the refractive index difference for the glasses used to fabricate strip rib waveguides and Microstructured Optical Fibres is about 0.23 at a wavelength of 1.5 μm. $As_{40}Se_{60}$ and $Ge_{10}As_{23.4}S_{e66.6}$ compositions used in this project were prepared in the similar way as described in section 3.1, therefore, about 0.004 refractive index variation for different samples in the same batch is expected.

From an application point of view, most of the optical applications use the transparent region; therefore, the measured refractive index of $As_{40}Se_{60}$ is relatively reliable and accurate. However, concerning the measurement temperature, pressure and sample surface roughness, and more measurements should be taken to confirm the influences of the measurement conditions. The ellipsometry measurement of bulk and thin film chalcogenide glass samples is

continuing by a PhD student, Nabil Abdel Moneim, Novel Photonic Glasses Research Group, University of Nottingham.

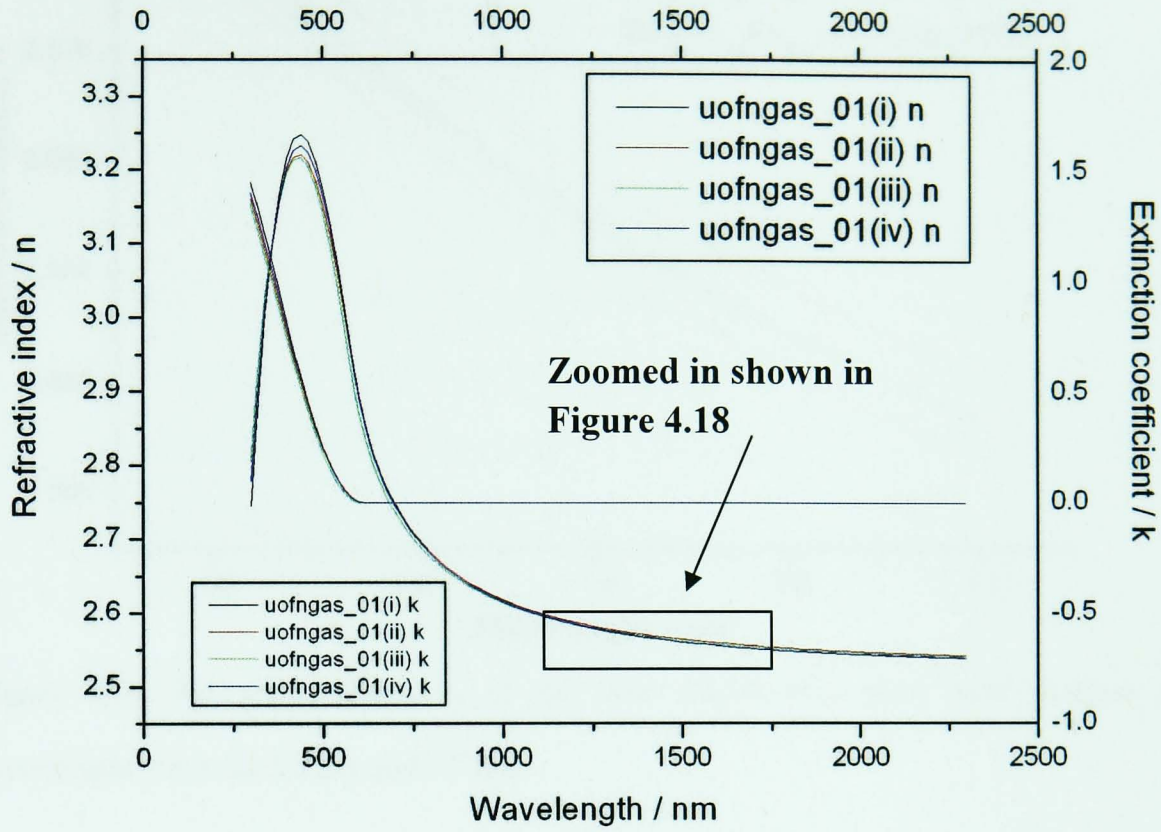

Figure 4.9: Refractive index of four $Ge_{17}As_{18}Se_{65}$ glass bulk samples (UofN GAS 01 (i)-(iv), prepared in the University of Nottingham) measured using ellipsometry at wavelength between 300 nm and 2300 nm. The refractive index at wavelengths between 1.3 μm and 1.7 μm is shown more detail in Figure 4.10 (Appendix D).

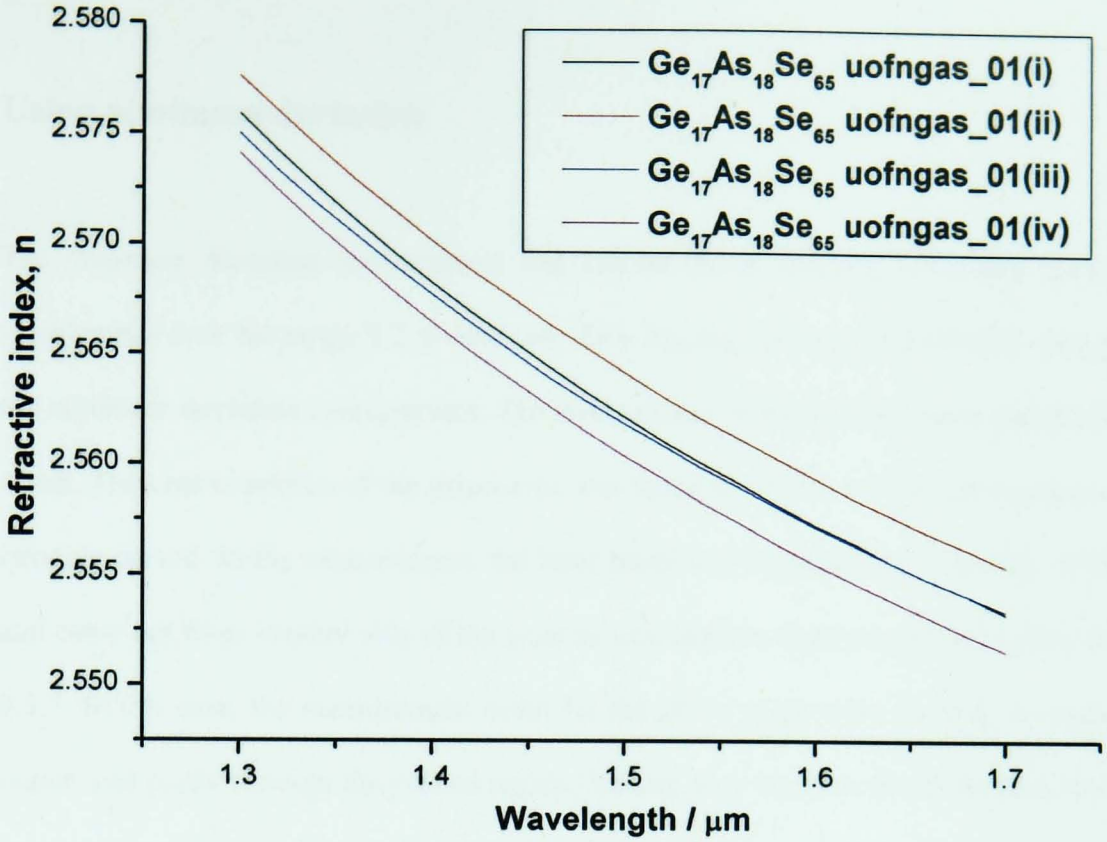

Figure 4.10: Refractive index, n, of the four $Ge_{17}As_{18}Se_{65}$ glass bulk samples at wavelengths between 1.3 μm and 1.7 μm.

(4) Temperature profile of annealing furnace.

The 0.004 refractive index variation of the different samples in a same batch may due to the temperature gradient in an annealing furnace. Rowe reported that there was a temperature gradient in the annealing furnace used for the sample preparation at UofN [2]. The temperature gradient is reproduced being up to 1.1°C/mm over the area where the chalcogenide boule is placed for annealing [2]. The same ingot therefore experiences different temperatures in the furnaces. Eventually, two pieces of discs from the same ingot may have slightly different heat history, consequently, optical properties such as refractive index show different values as observed in Figure 4.10.

The observation that the refractive index measured for samples from the same batch, were not identical could be explained by the fact that the samples used for ellipsometry were obtained from different parts of the ingot. The temperature gradient of the annealing furnace was also observed by J. Orava at UofP. Therefore, the samples produced by J. Orava at UofP were also expected to have similar refractive index variations.

Using minimum deviation

The minimum deviation measurement was carried out at QinetiQ, UK using specific laser wavelengths over the range 9.2 to 10.6 μm. Two $As_{40}Se_{60}$ prisms (ZGLCF027) were prepared for minimum deviation measurement. The two surfaces of both prisms were polished to 1 μm finish. The central portion of the prism area was found to be flat, but the surrounding region is strongly curved. In the measurement, the laser beam was launched from one side of the prism and came out from another side of the prim as described in experimental procedure in section 3.3.7. In this case, the measurement beam for the prism angle went partially through the flat region and partly through the curved region, leading to a variation in the measurement of the prism angle of 19.39° ± 0.08°. The measurements were made at ambient laboratory temperature (21 °C).

The best estimate of refractive index at 10.6 μm (this wavelength is associated with CO_2) wavelength was 2.774 ± 0.015. The refractive indices measured at the discrete wavelengths are shown in Figure 4.11 [148].

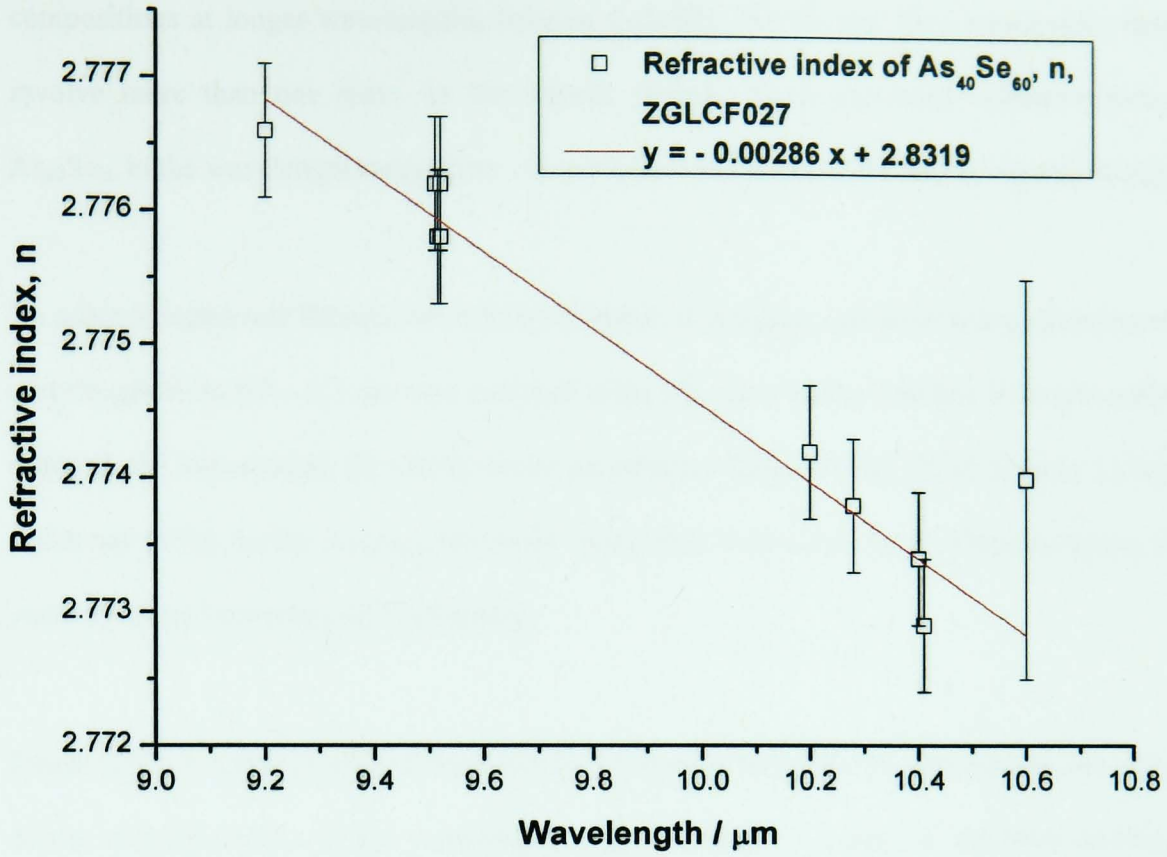

Figure 4.11: The refractive index of bulk $As_{40}Se_{60}$ (sample ID: ZGLCF027) measured at QinetiQ using minimum deviation method between wavelengths of 9.2 μm and 10.6 μm.

4.7.2 Numerical fittings of bulk chalcogenide glass

The ellipsometry and the minimum deviation methods measure the refractive index at wavelengths from 0.3 -2.3 μm and 9.2 – 10.6 μm. However, the refractive indices at wavelengths from 2.3 to 9.2 μm were not measured because of the lack of a laser source. Numerical fitting was used for predicting the refractive index over wavelengths from 2.3 to 9.2 μm. Also, the numerical fittings can be used to obtain the material dispersion across the near- and mid- infrared spectral regions. The dispersion (D) of a material is calculated using the dispersion equation 4-6 [149]:

$$D = -\frac{\lambda}{c}\frac{d^2 n}{d\lambda^2} \qquad 4\text{-}6$$

and is normally given in units of ps nm^{-1} km^{-1}. Symbols have their usual meanings (see glossary).The numerical fittings are shown only for $As_{40}Se_{60}$ in the current project, since data in the 9.2-10.6 μm wavelength range is only available for this composition. The suggestion for future work is to investigate the numerical fittings for the refractive index of other glass

compositions at longer wavelengths, because typically, the rib and fibre waveguides designs involve more than one glass. In the current project, the extrapolated refractive index of $As_{40}Se_{60}$ in the wavelength range from 2.3 to 9.2 μm was not used for any waveguide design.

To achieve numerical fittings, the refractive index of $As_{40}Se_{60}$ measured using ellipsometry at wavelength from 0.7 – 2.3 μm was analysed using the curve fitting function in Origin software (OriginLab Corporation). Physically based parametric fittings, Drude [150], Cauchy [136] and Sellmeier [151], to the $As_{40}Se_{60}$ refractive index data were done by H. Dantanarayana (PhD student) in the University of Nottingham.

Drude [150], Cauchy [136] and Sellmeier [151] models were used to approximate the real part of the refractive index in the wavelength range 0.7 μm to 2.3 μm, i.e. far from resonances, based on the Helmholtz formula for the complex index of refraction [152, 153]. In other words, the models were utilised in the regions where the imaginary part of the refractive index was very low. When using the Sellmeier equation, where the number of terms used depends upon the number of absorption bands in the material, the literature indicated that three terms is deemed necessary and sufficient for the numerical fitting of the refractive index of most materials [153, 154]. In practice, a two term fit proved sufficient [155] here as shown in Table 4.2 and Figure 4.12.

The Tauc-Lorentz dispersion formula [135] as mentioned by Wagner *et al.* in the University of Pardubice was used to analyse the entire measured near bandgap region. Jellison *et al.* [156] reported that a parameterisation of the optical functions of amorphous semiconductors was provided by the imaginary part of the dielectric function ϵ_2. According to Jellison *et al.* [156], multiplying the Tauc joint density of states by the ϵ_2 from a Lorentz oscillator model gives the imaginary part of the dielectric function ϵ_2. The real part of the dielectric function ϵ_1 was calculated from ϵ_2 using Kramers-Kronig integration [156]. The parameters of Tauc-Lorentz dispersion formula fit to n and k data for amorphous materials [156].

Table 4.2 shows the equations of Drude, Cauchy and Sellmeier and their parameters for $As_{40}Se_{60}$ (ZGLCF009). The three numerical fits of $As_{40}Se_{60}$ refractive index was depicted in Figure 4.12. Also, in Figure 4.12, the ellipsometry experimental data (ZGLCF009) is reproduced to compare the numerical fittings. The numerically fitted data are extrapolated to longer wavelength (~10.6 μm) to meet the minimum deviation experimental data.

Table 4.2: Drude [150], Cauchy [136] and Sellmeier [151] equations and their parameters for $As_{40}Se_{60}$ (ZGLCF009).

	Equation	Parameters
Drude	$n^2-1=\frac{A\lambda_0{}^2\lambda^2}{\lambda^2-\lambda_0{}^2}$	A=64.518553; λ_0=0.321738
Cauchy	$n^2=A+\frac{B}{\lambda^2}+\frac{C}{\lambda^4}$	A=7.694352; B=0.609262; C=0.150999
Sellmeier	$n^2-1=\sum_i \frac{A_i\lambda^2}{\lambda^2-a_i{}^2}$	A1=3.053333; a1=0.000000; A2=3.638903; a2=0.415945

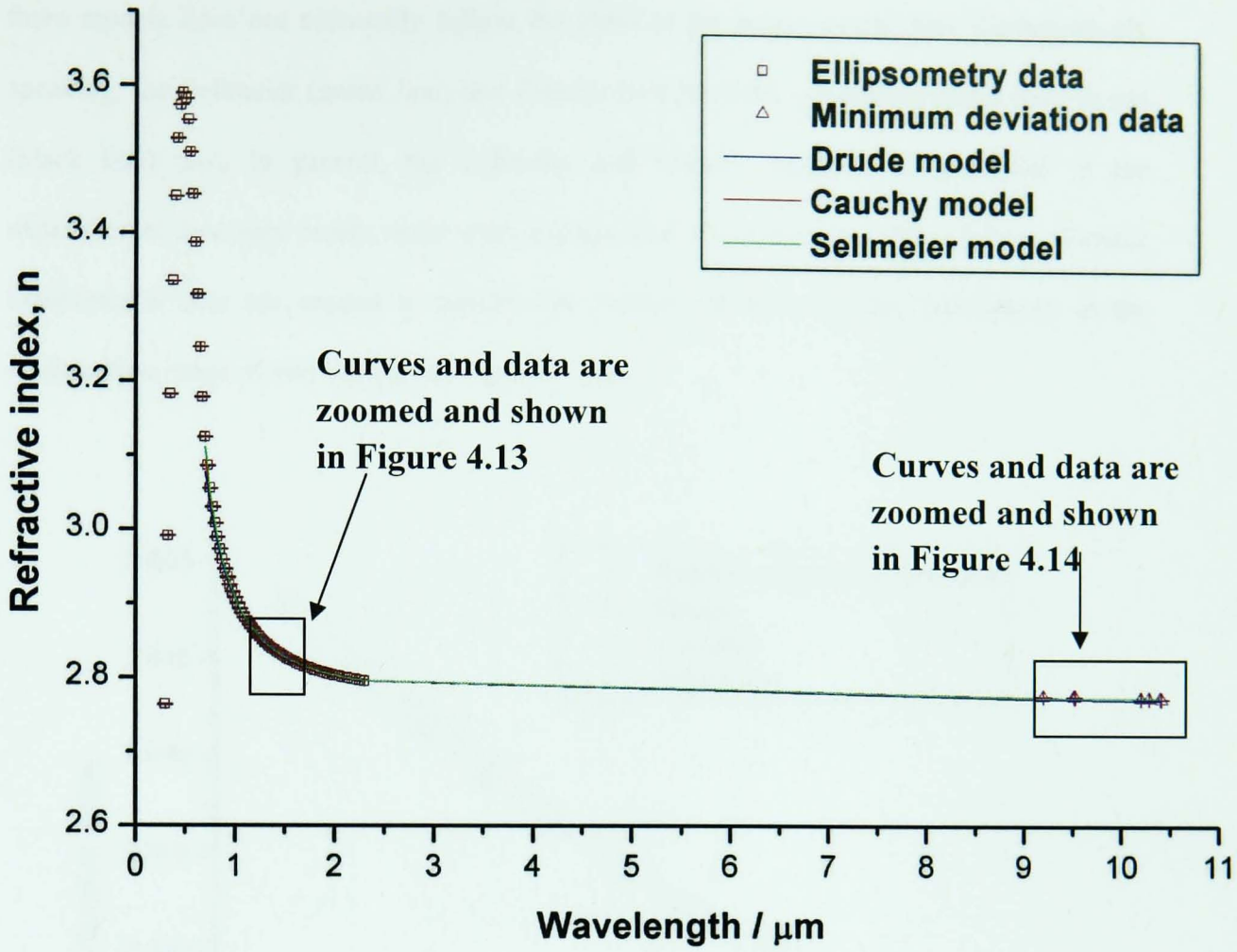

Figure 4.12: Refractive index of $As_{40}Se_{60}$ (ZGLCF009 and ZGLCF027) as a function of wavelength. Sellmeier [151], Cauchy [136] and Drude [150] plots fit the experimentally determined refractive index over the wavelength range 0.7 μm to 2.3 μm and are extrapolated to longer wavelength. The circles represent the experimental data of ellipsometry and the triangles represent the experimental prism (minimum deviation) data. A 2 term Sellmeier equation provides the best fit to both prism and ellipsometry data. (Data at wavelength from 1.3 to 1.6 μm will be shown in Figure 4.13).

In Figure 4.12, all the three equations seem to fit the experiemtnal data well. For closer comparison, Figures 4.13 and 4.14 zoomed the plot at both short wavelength (1.3 – 1.6 μm) and longer wavelength (9.2 -10.6 μm) ranges, respectively. In Figure 4.13, Sellmeier (green solid line) and Cauchy (red dash line) plots are almost identical (e.g. 0.0001 difference at wavelength 1.55μm). The Sellmeier and Cauchy equation are ploted within the experimental data error bar (e.g. ± 0.001), but the Drude (black solid line) plot is about 0.0001 above the experimental data (e.g. at wavelength of 1.55μm). Therefore, Sellmeier and Cauchy plots fit the experimental results better. In Figure 4.14, at longer wavelengths, extrapolation of all the

three models does not accurately follow the trend of the experimental data. Comparatively speaking, the Sellmeier (green line) and Cauchy (red line) fits extrapolate better than Drude (black line) plot. In general, the Sellmeier and Cauchy equations in particular fit the experimental data very nicely, even when extrapolated to wavelengths above 9.0 μm. Further experimental data are needed to confirm the validity of these fits for applications in the intermediate range of wavelengths (2.3 μm – 9 μm).

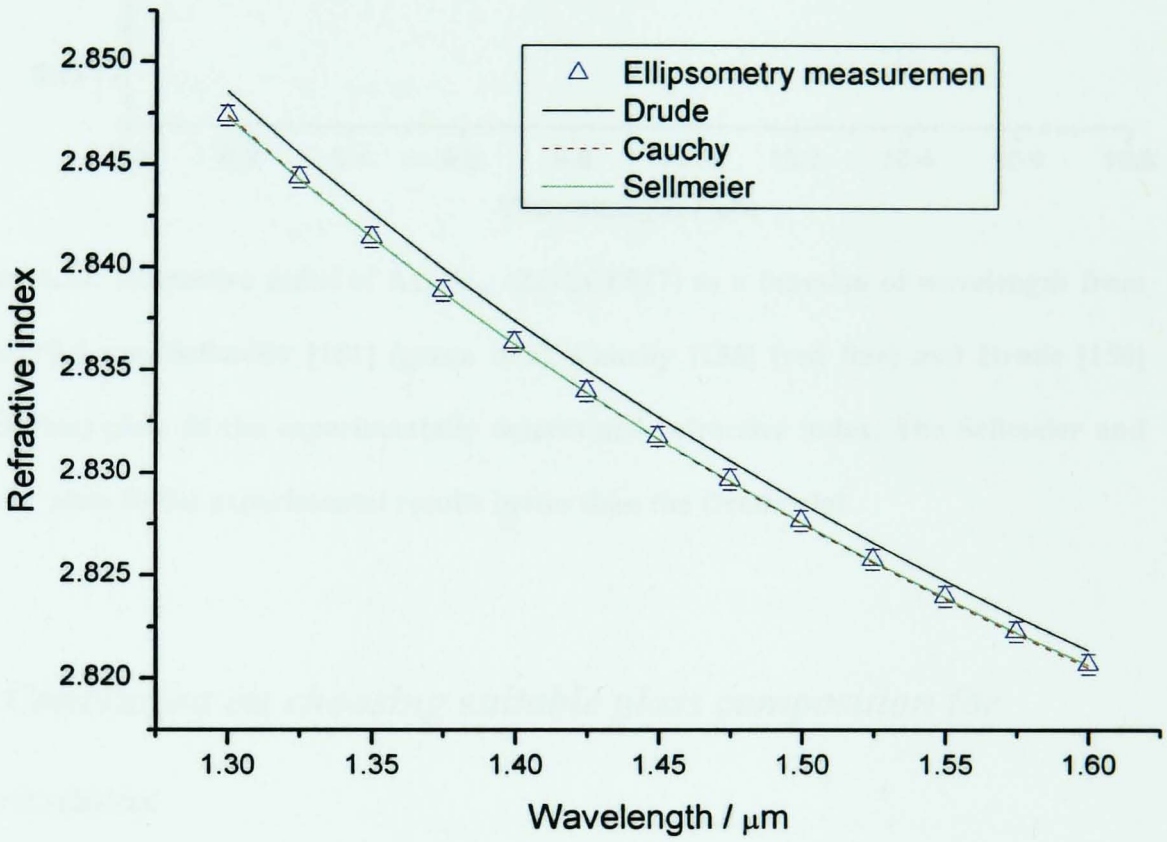

Figure 4.13: Refractive index of $As_{40}Se_{60}$ (ZGLCF009) as a function of wavelength from 1.3 to 1.6 μm. Sellmeier [151] (green solid line), Cauchy [136] (red dash line, overlap with Sellmeier plot) and Drude [150] (black solid line) plots fit the experimentally determined refractive index. The 2 terms Sellmeier and Cauchy equations are almost overlap and fit the experimental results better than the Drude plot.

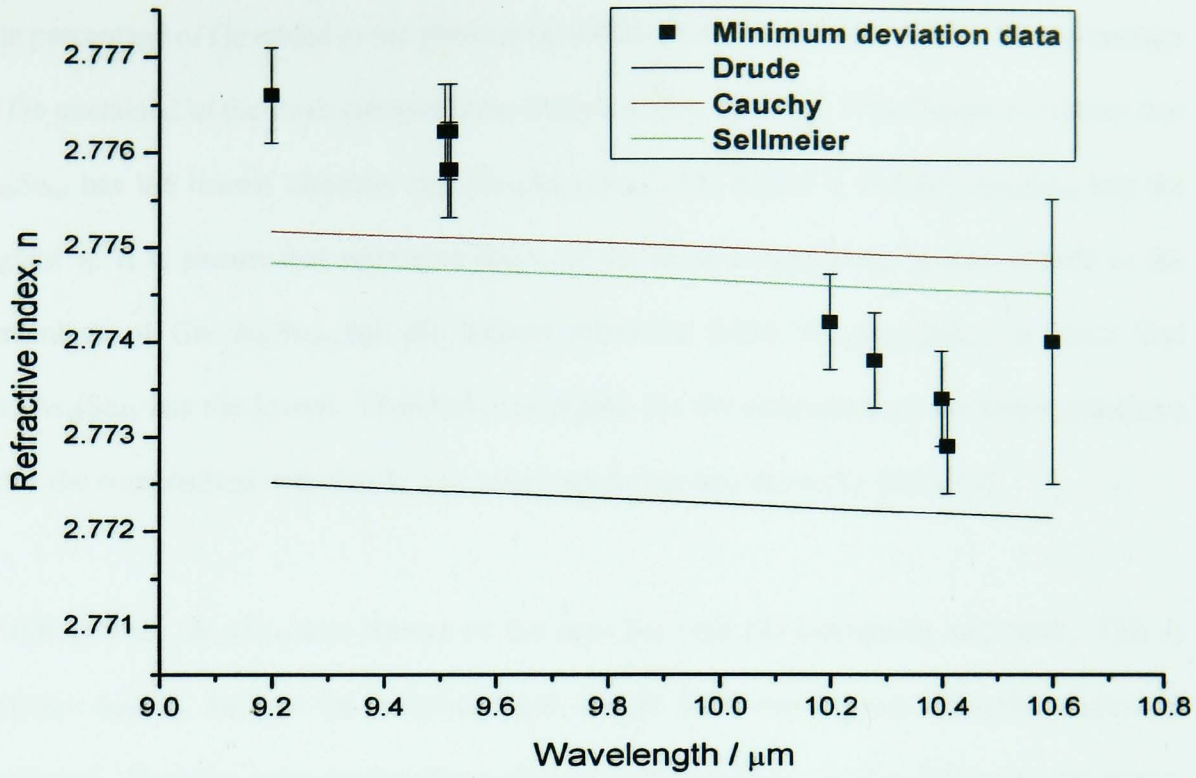

Figure 4.14: Refractive index of $As_{40}Se_{60}$ (ZGLCF027) as a function of wavelength from 9.2 to 10.4 μm. Sellmeier [151] (green line), Cauchy [136] (red line) and Drude [150] (black line) plots fit the experimentally determined refractive index. The Sellmeier and Cauchy plots fit the experimental results better than the Drude plot.

4.8 Conclusion on choosing suitable glass composition for fabrications

Chalcogenide glasses can be tailored (within reason) to meet the requirements of an application in terms of the optical and non-optical properties [2]. By altering the composition it is possible to match two or more glasses optically and thermally. One of the objectives of this PhD project was to find suitable chalcogenide glass core/cladding pairs used for waveguides and MOF fabrication in terms of the refractive index, thermal expansion coefficient and viscosity. Three chalcogenide glass compositions were studied in this chapter: $As_{40}Se_{60}$, $Ge_{10}As_{23.4}Se_{66.6}$ and $Ge_{17}As_{18}Se_{65}$, in terms of their refractive index, viscosity, thermal expansion coefficient and glass forming.

The percentage of Ge added to the glass composition alters the glass properties. The percentage of Ge contained in the three compositions studied is 0%, 10% and 17%. Figure 4.7 shows that $A_{40}Se_{60}$ has the lowest viscosity (η), $Ge_{10}As_{23.4}Se_{66.6}$ has higher η and $Ge_{17}As_{18}Se_{65}$ has the highest η. It is shown that refractive index of the three compositions is also related to the percentage of Ge. $A_{40}Se_{60}$ has the highest refractive index, $Ge_{10}As_{23.4}Se_{66.6}$ is lower and $Ge_{17}As_{18}Se_{65}$ has the lowest. Therefore, the higher the Ge concentration, the lower refractive index the composition will obtain. The same conclusion was drawn by Rowe [2].

In this project, $As_{40}Se_{60}$ was chosen as the core for both rib waveguide and MOF. This is because $A_{40}Se_{60}$ has no Ge contained and should have the highest refractive index, as confirmed. Then the other compositions chosen as the cladding involve different percentages of Ge for different applications. Also, the binary $As_{40}Se_{60}$ composition is very stable as confirmed by Rowe [2] and thus relatively more simple to preparation. The close vapour pressure of arsenic and selenium means that this composition can be thermally evaporated.

In rib waveguides fabrication: $Ge_{17}As_{18}Se_{65}$ was chosen for the substrate of glass on glass rib waveguides because it has a close thermal expansion coefficient (α) match to $As_{40}Se_{60}$. α of $As_{40}Se_{60}$ is $20.6 \pm 0.5 \times 10^{-6} K^{-1}$ and α of $Ge_{17}As_{18}Se_{65}$ was $21.5 \pm 0.5 \times 10^{-6} K^{-1}$. The close α prevents the $As_{40}Se_{60}$ thin film from cracking during embossing. The Tg of $Ge_{17}As_{18}Se_{65}$ is about 55°C higher than that of $As_{40}Se_{60}$ which will make sure the $Ge_{17}As_{18}Se_{65}$ is not deformed (viscosity curves were shown in Figure 4.7) during the embossing of an $As_{40}Se_{60}$ film deposited on it. The measured refractive index (n) difference between $As_{40}Se_{60}$ and $Ge_{17}As_{18}Se_{65}$ proves suitable for the realisation of rib waveguides that exhibit mono-mode guiding, for TE and TM like polarisations, at wavelengths around 1.55 μm [1]. This will be confirmed by numerical simulation and by experimental work in Chapter 5.

In optical fibre fabrication: For air core MOF fabrication, the stability of $A_{40}Se_{60}$ also makes it a good potential candidate for use in the fabrication of optical fibres. Ultra pure $As_{40}Se_{60}$ fibres, As purified but without Se purification, were successfully drawn with variable diameter by Rowe [2]. This indicated that a good drawing temperature and drawing rate could be

achieved using this composition. Therefore, $As_{40}Se_{60}$ will be used for investigations into air core MOF fabrication.

For solid core Microstructured Optical Fibre, the desired composition pair for the core and the cladding should have the same Tg, but slightly different viscosity at drawing temperature. This can be achieved by choosing $As_{40}Se_{60}$ as the central core, and $Ge_{10}As_{23.4}Se_{66.6}$ as cladding. One reason is the transition temperatures (Tg) of both core and cladding compositions are the same. There is an empirical rule that relates Tg and glass liquidus temperature (Tm): Tg/Tm = 2/3 [157]. A close Tg ensures that both core and cladding are able to liquify together. A large processing temperature difference between the core and cladding may cause the drawing to be unsuccessful. For example, if the core of the fibre has a lower Tg than the cladding, the core may deform before the cladding during fibre drawing. Consequently, this will distort the fibre structure. Another reason is that the viscosity of $Ge_{10}As_{23.4}Se_{66.6}$ is slightly higher than $As_{40}Se_{60}$, as plotted in Figure 4.7. In this project, the cladding of a solid core MOF is formed by a central core and several core/cladding ($Ge_{10}As_{23.4}Se_{66.6}$/ $As_{40}Se_{60}$) canes. This viscosity property means that at the drawing temperature, the $Ge_{10}As_{23.4}Se_{66.6}$ liquid is thicker than $As_{40}Se_{60}$ liquid. Therefore, the shape of the $Ge_{10}As_{23.4}Se_{66.6}$ cladding is maintained (stable) while the $As_{40}Se_{60}$ core can flow to fill the gaps of the cladding of the preform. The refractive index difference between $As_{40}Se_{60}$ and $Ge_{10}As_{23.4}Se_{66.6}$ is ~0.2 at 1.55 μm wavelength. The refractive index difference is sufficient for light guiding, as simulation will conform in Chapter 6.

4.9 Refractive index of thermally evaporated $As_{40}Se_{60}$ thin films before and after pressing and compared to that of bulk $As_{40}Se_{60}$

The hot embossing technique was used in the current PhD project to fabricate rib waveguides in the surface of a thin glass film. This section investigates the change of the refractive index of the thin film after embossing.

4.9.1 Experiments and results

Definition of flat embossing and hot embossing. To investigate the change of refractive index of the $As_{40}Se_{60}$ thin film on embossing, a thermally evaporated $As_{40}Se_{60}$ thin film was prepared at the UofP. Then the thin film was flat-embossed using a flat mould. In the current project, the term hot embossing and flat-embossing are the same process but hot embossing used a patterned mould for fabricating waveguides whereas flat-embossing used a flat mould for flattening thin film surfaces. The samples prepared for this composition are (1) $As_{40}Se_{60}$ thin film and (2) flat – embossed $As_{40}Se_{60}$ thin film.

(1) $As_{40}Se_{60}$ thin film.

For preparing $As_{40}Se_{60}$ thin glass films on $Ge_{17}As_{18}Se_{65}$ glass substrates, circular discs having a thickness 2 ± 0.1 mm and a diameter of 10 ± 0.1 mm were sliced from the prepared $Ge_{17}As_{18}Se_{65}$ glass rod (ZGLCF010) and one surface was polished to a 1 μm finish. The circular discs where after polishing, pressed slightly (i.e. flat-embossed) to ensure a surface flat. A 4344 ± 6 nm thin $As_{40}Se_{60}$ film (ID: GG20080223; target was prepared by Orava in UofP, target ID: uofptarget_01) was deposited on the flat-embossed $Ge_{17}As_{18}Se_{65}$ (ZGLCF010) discs using the thermal evaporation method.

(2) Flat – embossed $As_{40}Se_{60}$ thin film.

The flat-embossing process was carried out using the in-house built pressing rig (see section 3.4.2). The $As_{40}Se_{60}$ sample was place in the pressing rig and embossed using a flat Si wafer under 10^{-5} Pa. The embossing schedule is shown in Table 4.3: (1) Temperature was increased from room temperature (RT) to 245 °C. (2) The load was applied gradually until 100 N. (3) A 100 N load was applied for 15 minutes. (4) The load was released suddenly. After flat-embossing, the $As_{40}Se_{60}$ thin film (ID: GG20080223_f) was annealed at 180°C for 1 hour and the temperature gradually decreased to room temperature at a rate of 20°C / h.

Table 4.3: Flat-embossing schedule for pressing $As_{40}Se_{60}$ bulk sample (ZGLCF007) conditions and descriptions.

Step	Procedure	Descriptive
1	Room temperature(RT)→ 245°C in 60 min	Sample temperature raised above the Tg of the $As_{40}Se_{60}$.
2	Dwell at 245°C for 5 min	
3	Apply force: 0N→100 N in 10 min	Application of load.
4	100 N 15 min	
5	Release the force suddenly	
6	245°C →180°C 60 min	Post-flat-embossing anneal.
7	Dwell 60min	
8	180°C → RT @ 20°C /60min	

It was noticed that before thermal evaporation, the circular $Ge_{17}As_{18}Se_{65}$ discs were flat-embossed slightly to ensure they had a flat a surface. Due to the nature of the polishing technique, the disc could become slightly rounded at the edges. This rounding should be prevented, because the curved surface may lead to a non-uniform thin film thickness after evaporation. Therefore, in the current project, after polishing, the bulk discs were pressed slightly in the hot embossing rig to avoid round edges. The pressing process was similar to that of hot embossing process but with a shorter duration, typically, 3 minutes pressing. A proper annealing is required after each pressing as listed in Table 4.3.

Ellipsometry measurement

Ellipsometry was used to find the refractive index of the two samples: non-flat-embossed $As_{40}Se_{60}$ thin film (GG20080223) and flat-embossed $As_{40}Se_{60}$ thin film (GG20080223_f). Figure 4.15 shows the measurement results: the red points represent the refractive index of flat-embossed $As_{40}Se_{60}$ thin film (GG20080223_f) and the black squares represent the refractive index of the non-flat embossed $As_{40}Se_{60}$ thin film (GG20080223). The refractive index of the flat-embossed $As_{40}Se_{60}$ (GG20080223_f) was 2.8187 ± 0.002 at 1.55 μm and the non-flat-embossed $As_{40}Se_{60}$ (GG20080223) thin film was 2.7092 ± 0.003 at 1.55 μm. The flat-embossing process produced a refractive index difference (0.1095 ± 0.005) at 1.55 μm between the two $As_{40}Se_{60}$ films. The refractive index of the flat embossed thin film is closer to that of the bulk samples which was shown in Figure 4.7, sample ID ZGLCF009. This result

suggested the heat treatment of the flat embossing slightly modifies the optical properties of the thin chalcogenide film. The reasons for this will now be discussed.

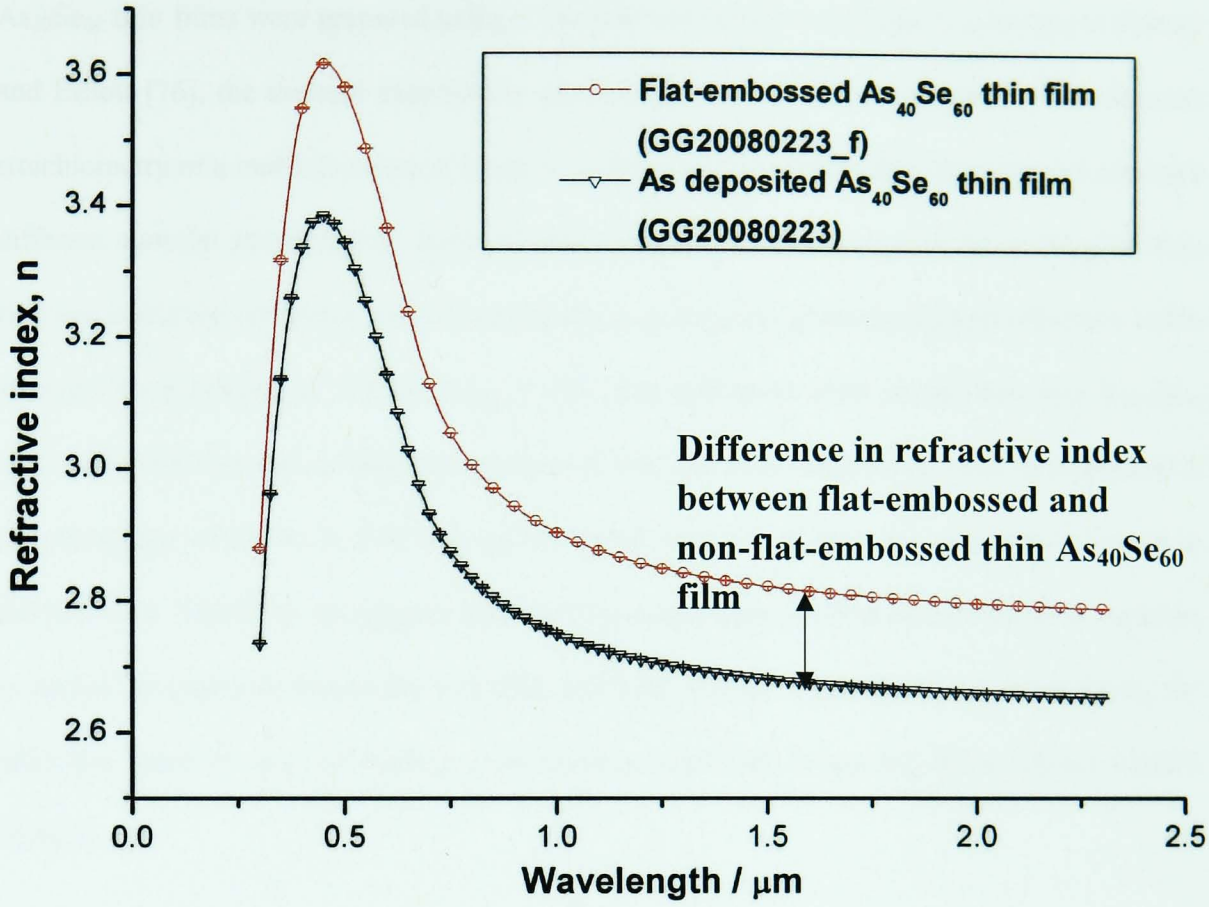

Figure 4.15: Ellipsometry measurement of refractive index dispersion for Non-flat-embossed (GG20080223) and flat-embossed (red triangles) $As_{40}Se_{60}$ thin film. Please see Appendix B for refractive index numerical data. The refractive index of the flat-embossed $As_{40}Se_{60}$ (GG20080223_f) was 2.8187 ± 0.002 at 1.55 μm and the non-flat-embossed $As_{40}Se_{60}$ (GG20080223) thin film was 2.7092 ± 0.003 at 1.55 μm.

4.9.2 Discussion on refractive index variation of bulk, thin film, flat-embossed thin film samples

According to the measurement results of the refractive index of bulk, thin film and flat-embossed thin film samples of $As_{40}Se_{60}$, it was found that $As_{40}Se_{60}$ show different refractive index in different forms, i.e. bulk and thin film. Also, the same $As_{40}Se_{60}$ thin film after flat-embossing raised its refractive index. The phenomenon may because of the preparation methods and thermal history.

The preparation methods of $As_{40}Se_{60}$ in the forms of bulk and thin film are: the bulk samples were prepared using the conventional glass melting which was described in Section 3.1 and the $As_{40}Se_{60}$ thin films were prepared using a thermal evaporation technique. According to Zakery and Elliott [76], the thermal evaporation method appears not able to be transfer the accurate stoichiometry of a multi-component target to a film. For this reason, thin film samples can have different material stoichiometry from the bulk samples. The percentage of As in the glass thin film can affect the refractive index dramatically, e.g. $As_{35}Se_{65}$ gives the highest refractive index amongst compositions of the As_xSe_{100-x} [158]. The refractive index of the thin film $As_{40}Se_{60}$ had ~ 0.1 refractive index difference compared with the bulk samples; this can be explained if the percentage of the As and Se was not accurately transferred from the evaporation source to the thin film. Therefore, it suggests that thermal evaporation method can introduce a variation in optical properties between the thin film and bulk. Further experiments of investigating the refractive index of series of As_xSe_{100-x} are recommended here to quantify these refractive index changes.

Wu *et al.* [159] studied polymer films on silicon samples and suggested that the density of the thin film material at and near its surface is lower than that of the bulk value. For this reason, in a chalcogenide glass thin film, the density of the thin film may also differ from the density of bulk glasses. Therefore, the thin film and bulk samples of $As_{40}Se_{60}$ are likely to have different density and consequently a variation of the refractive index occurs. A heat treatment may be able to change samples' optical properties. This was confirmed by the refractive index measurement results obtained from the embossed and non-embossed thin films. The results were shown in Figure 4.15. There was a near 0.1 refractive index difference between the embossed and non-embossed $As_{40}Se_{60}$ thin film sample. The flat-embossing process gave a heat treatment of the thin film and a load applied during this process compressed the heated thin film. The reason of heat treatment changes the optical properties could be explained by the embossing process increasing the density of the thin film towards that obtained for the bulk glass. In addition, the underlying atomic structure of the thin film may change due to heat treatment. The FSDPs of XRD patterns are potentially able to analyse the atomic structure of glass samples. The flat-embossed and bulk $As_{40}Se_{60}$ samples were analysed using XRD as

shown in Figure 4.16. The FSDPs are different which suggests that the bulk and flat-embossed thin film have different atomic structure. In Figure 4.16, the XRD pattern for the bulk sample is reproduced from Figure 4.3. Unfortunately, the XRD of the non-embossed thin film was not measured. Further experiments for analysing the FSDP of bulk and thin film chalcogenide glasses should be continued.

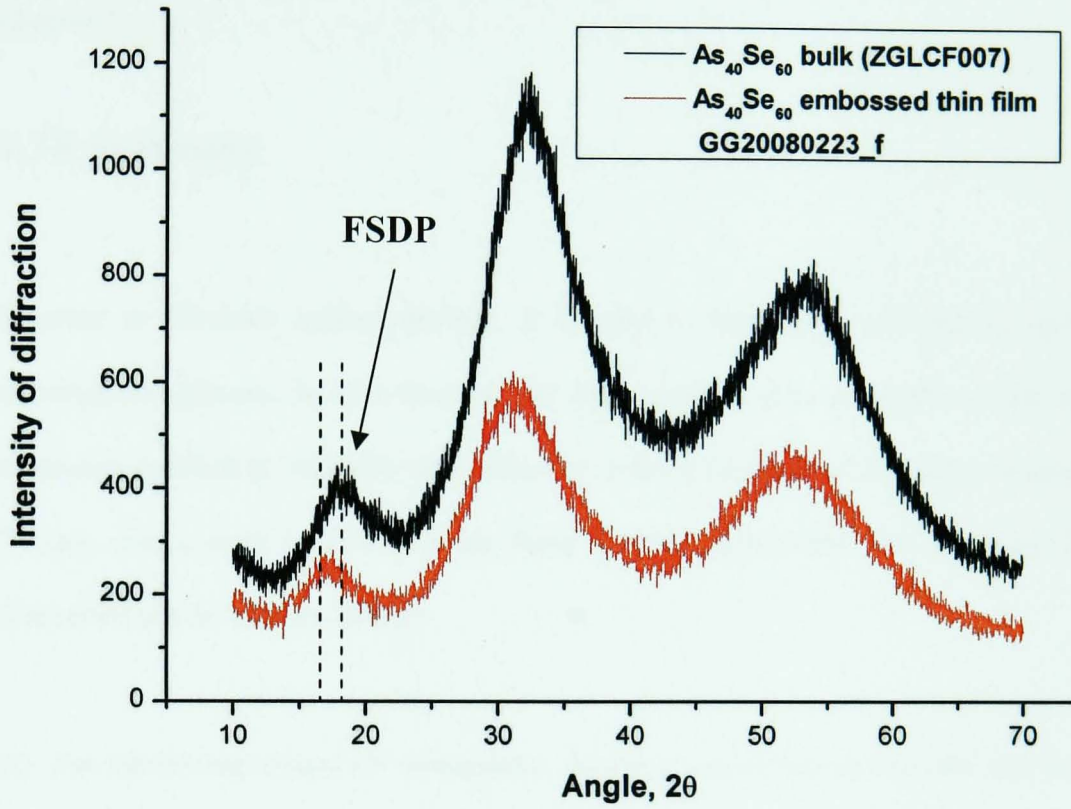

Figure 4.16: The XRD pattern of $As_{40}Se_{60}$ (ZGLCF007) and flat embossed $As_{40}Se_{60}$ thin film (GG20080223_f). The broad peaks confirm the amorphous nature of these samples. The FSDP of the bulk and thin film forms of the same composition are located at different positions. This indicates the underlying atomic structures of the bulk and flat-embossed thin film may differ.

In the ellipsometry measurement, the surface oxidisation was not considered. Therefore, the refractive index differences can be also due to the surface oxidisation of the samples during storage. Chalcogenide glasses after melting were normally stored in desiccators which prevented the ingress of a humid atmosphere. However, it is believed that a superficial oxidation layer did appear since oxygen is not prevented by desiccators. Lucas *et al.* [160] have observed the growth of oxidation on the surface of $Te_2As_3Se_5$ fibre, at room temperature under one atmosphere of air (1.013×10^5 Pa). The oxidation of the $Te_2As_3Se_5$ fibre appeared quickly

after only one week in contact with ambient air [160]. An oxidisation at a rate of about 2 nm per year was roughly estimated [160]. Therefore, the refractive index difference between the flat-embossed and non-flat-embossed sample may be caused by an oxidisation layer.

More ellipsometry measurements are required to confirm all the optical property changes. A sequence of further experiments will be mentioned in suggestions for future work presented in Chapter 7.

4.10 Summary

In order to fabricate optical devices, it is vital to investigate and decide upon suitable chalcogenide glasses. In this chapter, the chalcogenide glass properties, such as: thermal expansion coefficient, viscosity and refractive index dispersion of $As_{40}Se_{60}$, $Ge_{17}As_{18}Se_{65}$ and $Ge_{10}As_{23.4}Se_{66.6}$ were analysed. From these material properties, the materials for further fabrication are decided as follows:

(1) For fabricating optical rib waveguides, $As_{40}Se_{60}$ was chosen as the core and $Ge_{17}As_{18}Se_{65}$ was used as the substrate. These compositions were chosen due to the Δn of the two glasses which was ~ 0.3 at 1.55 μm wavelength and the ΔTg of the two glasses was purposely chosen to differ by 60°C.

(2) For the fabrication of MOFs, $As_{40}Se_{60}$ was used as the core and $Ge_{10}As_{23.4}Se_{66.6}$ was chosen to be the cladding. These compositions were chosen due to the relatively large Δn of the two glasses (~ 0.2 at 1.55 μm wavelength), whilst the Tg of the glasses was purposely the same and the thermal expansion coefficients (α) were only slightly different.

This refractive index study of the bulk and thin film sample was very useful for understanding the optical properties of the chalcogenide glasses used in this work. For the strip ribs and Microstructured Optical Fibres fabricated in the present project, the results to be presented in Chapter 5 and 6 will show that the achieved accuracy of the refractive index is sufficient to meet project objectives. However, the refractive indices measured were not consistant from

sample to sample. Further experiments should continue to investigate the reasons for the inconsistency. The evaporated thin $As_{40}Se_{60}$ films appear to have slightly lower refractive indices compared with that of the bulk material. Possible reasons found are a) the preparation method introduces thin films having different stoichiometry from bulk samples; b) the thin film and bulk glasses have different densities and c) the surface oxidisation. The subsequent heat treatment, e.g. flat-embossing, may increase the refractive index of the thin film prepared using thermal evaporation technique and towards the bulk value.

The Se purification process was introduced and the effect on the absorption spectrum of $As_{40}Se_{60}$ was analysed using FTIR. This purification process is recommended for the future glass melting, because the Se-H absorption peak at a wavelength of 4.6 μm is reduced. However, for those applications that will use the wavelengths at around 9.0 μm, Se purification process is not recommended, because the absorption peak of Si-C at this wavelength increases.

Chapter 5

Fabrication of Chalcogenide Rib Waveguides by Embossing Thin Glass Films

The hot embossing technique, also called nano-imprinting, was first proposed by Chou *et al.* in 1995 [161, 162]. Later, this technique was employed to fabricate a series of functional optical devices based on polymers [163-166]. One of the objectives in this PhD project is to investigate the feasibility of fabricating rib waveguides in chalcogenide thin films by further development of the hot embossing technique described by Pan [1]. Chapter 4 reports that $As_{40}Se_{60}$ (atomic %) was chosen as the guiding material (core of an optical waveguide) and $Ge_{17}As_{18}Se_{65}$ was chosen as the substrate (optical cladding) material of the desired waveguides. This chapter describes the design, fabrication and testing of rib waveguides fabricated via hot embossing technique.

5.1 Hot embossing preparation and experimental procedures

The dimensions of 'large cross-section'single mode strip rib waveguides in GeSi-Si and Si-on-SiO_2 was predicted by Soref *et al.*[167]. It is mentioned the rib width/height ratio is critical in designing rib waveguides. In the previous study, a rib waveguide structure in chalcogenide glasses was designed by Pan [1]. And in this project, a single mode guiding of a rib waveguide was confirmed for each polarisation using simulation software. The simulations were undertaken using the software called 'Phil's FD solver' that was designed and developed by Prof. Sewell in the George Green Institute for Electromagnetics Research at the University of Nottingham. Figure 5.1 depicts the single mode (transverse electric mode, TE mode) optical guiding of the designed rib waveguide using 'Phil's FD solver'. The waveguide had a 4 μm thick $As_{40}Se_{60}$ thin film, the width of the rib was 5.5 μm and the height was 2 μm. The substrate was $Ge_{17}As_{18}Se_{65}$. The refractive index of the $As_{40}Se_{60}$ and $Ge_{17}As_{18}Se_{65}$ were taken

as 2.824 and 2.590 at the operating wavelength of 1.55 μm as mentioned in section 4.7.1. The software was based on the finite difference and beam propagation methods; the finite difference grid size was 0.1 μm. The operation wavelength was 1.55 μm.

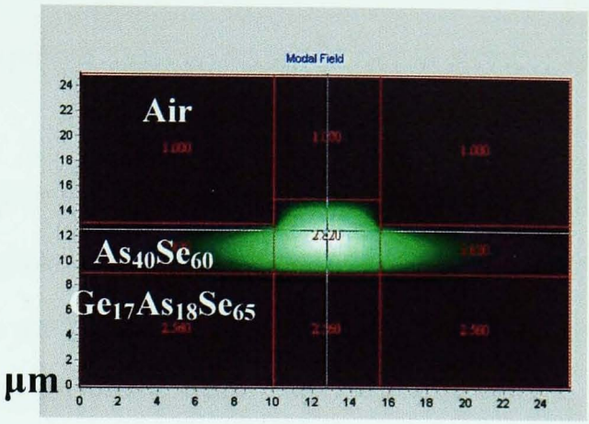

Figure 5.1: Single mode guiding for this $As_{40}Se_{60}$ on $Ge_{17}As_{18}Se_{65}$ waveguide using 'Phil's FD solver'. TE mode intensity distribution calculated using the finite difference method.

Based on the rib waveguide structure, chalcogenide glass rib waveguides will be formed using the hot embossing technique [1]. The hot embossing of chalcogenide glasses is based on the observation that the viscosity of the super-cooled melt (amorphous materials at a temperature above their transition temperatures and between melting temperatures) decreases with a rise in temperature above the glass transition temperature (Tg), which is itself a function of the glass composition. Then the low viscosity materials can be shaped by applying mould and load. Our previous studies have revealed that it is possible to use hot embossing both to pattern bulk chalcogenide glasses [168] and to press chalcogenide glass fibres onto another chalcogenide glass substrate in a 'one-step' process to form a rib waveguide [22, 169]. Also, Pan [1] attempted to pattern rib waveguide directly onto chalcogenide glass thin film, but did not receive any successful. The current work continues the research which will modify the materials and fabrication procedures to produce rib waveguides in thin film samples.

The chalcogenide super-cooled melt that forms above the Tg can be moulded by pressing it into a patterned mould. The mould is relatively rigid at the processing temperature. Cooling below Tg freezes-in the required pattern [43, 170]. Figure 5.2 schematically describes the steps in the hot embossing working process.

a) The thin chalcogenide glass film was deposited, e.g. thermally evaporated, onto a chalcogenide glass substrate. The sample was placed with the thin glass film uppermost and faces contacting a patterned surface of a mould which will be described in section 5.1.2. Two types of samples were pressed in this work which will be described in section 5.1.1.

b) Table 5.1 shows a general example of the embossing procedure for a glass on glass sample. Step (1), the temperature of the pressing area was raised to meet a required pressing temperature (typically 60°C > Tg); Step (2), 5 minutes dwell at the desired temperature was allowed for the temperature to be stabilised. Step (3), a load applied to the sample and mould assembly and Step (4) keep the load applied for about 15 minutes.

c) Step (5), the load was released after the embossing finished. Step (6), the glass was annealed to 'freeze-in' the required shape. The pressed sample was then cooled from the temperature, e.g. Tg + 60°C, down to Tg in 60 minutes. Step (7) held at Tg for 60 minutes and Step (8) ramped to room temperature at a rate of 20°C/60 minutes.

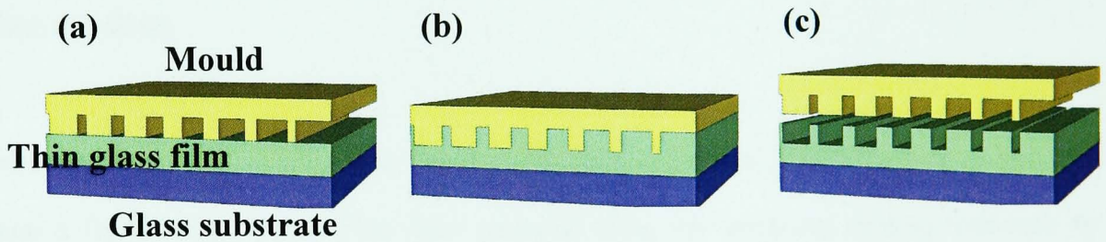

Figure 5.2: Schematic diagram of hot embossing process. A finely patterned mould was used to create rib waveguides in the upper part of thin glass films. (a) The thin glass film and glass substrate sample is placed with the thin glass film uppermost and faces contacting a patterned surface of the mould. (b) The temperature is raised to a required pressing temperature (Tg + 60°C) and the load applied to the sample and mould assembly. (c) The load was released and the glass was annealed at Tg for one hour to "freeze-in" (section 2.1) the required shape [169] before cooling to room temperature at a rate of 20°C /hour.

Table 5.1: Working conditions used for fine embossing and the working process. Steps 1 and 2 describe the temperature rise; step 3, 4 and 5 describe how the load was applied. Steps 6 and 7 show the annealing process and step 8, the final cool back to room temperature (RT).

Step	Procedure	Descriptive
(1)	Room temperature (RT)→ 60°C>Tg in 60 min	Sample temperature rose to a temperature 60°C above the Tg of the thin glass film.
(2)	Dwell at 60°C>Tg for 5 min	
(3)	Apply force: 0 N→120 N in 5 min	Application of load.
(4)	120 N for 15 min	
(5)	Release the force	
(6)	60°C>Tg →Tg for 60 min	Post-embossing anneal.
(7)	Dwell 60 min	
(8)	Tg°C → RT @ 20°C /60min	

5.1.1 Sample preparation

In this project, tests were undertaken to press rib waveguides into two types of film via the hot embossing. Figure 5.3 (a) and (b) shows schematic diagrams of these types of chalcogenide glass thin films:

(a) A nominal 2 μm $As_{40}Se_{60}$ thin film deposited onto a nominal 2 μm $Ge_{17}As_{18}Se_{65}$ thin film onto a GaAs wafer. These films were prepared using the sputtering coating technique by QinetiQ, UK. (Sample ID: GGS, glass-glass-semiconductor). The sputtering coating process is described in detail in [1]. The $Ge_{17}As_{18}Se_{65}$ (CT036t) and $As_{40}Se_{60}$ (CF087) targets for the sputtering were prepared at the University of Nottingham.

(b) A nominal 4 μm $As_{40}Se_{60}$ thin film thermally evaporated at the University of Pardubice onto a 2 mm thick $Ge_{17}As_{18}Se_{65}$ substrate. The $Ge_{17}As_{18}Se_{65}$ substrate was prepared as part of this project at the University of Nottingham and was supplied to the University of Pardubice for coating. (Sample ID: GG, glass-glass).

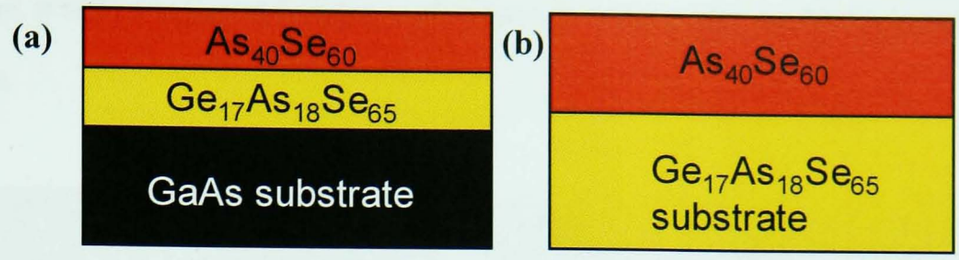

Figure 5.3: Schematic cross-sectional view of two types of chalcogenide glass thin film used in this project. (a) 2 μm $As_{40}Se_{60}$ thin film on 2 μm $Ge_{17}As_{18}Se_{65}$ thin film on GaAs wafer; (b) 4 μm $As_{40}Se_{60}$ thin film on $Ge_{17}As_{18}Se_{65}$ substrate.

5.1.2 Mould for embossing

A silicon mould is chosen to use as the hard mould [1]. The silicon wafer mould was kindly supplied by Professor Catrina Bryce at the University of Glasgow, UK. It was a 4 inch silicon wafer. The silicon wafer mould was prepared using reactive etching to form a series of channels in the mould surface. Each channel had a nominal depth of 2 μm. The channel widths increased from 1 to 10 μm, in steps of 0.5 μm. The length of each channel was 100 mm. The silicon wafer was cleaved to small segment for use, and each of the small mould normally had length between 15 mm to 30 mm. Figure 5.4 illustrates a typical silicon mould, (a) shows channel widths increasing from 3 μm to 7 μm in steps of 0.5 μm with a 50 μm centre-to-centre separation and (b) shows that the channels had nominal depth of 2 μm. The actual depth measured was 1.9 ± 0.1μm.

The nature of using hot embossing to produce rib waveguides is to duplicate the geometry of the mould in the thin film. Therefore, the quality of the mould was the key to producing high quality rib waveguides. As shown in Figure 5.4 (b), a side view of a channel in the mould showed that there were plenty of lines on the sidewall of the channel. These lines were part of the mould due to fabrication. The shape of the surface with these lines will be transferred to the sidewall of rib waveguides. Consequently, the scattering loss of the rib waveguides will increase [171]. The production of a high quality mould is the key for the embossing fabrication.

Therefore, it will be suggested in future work to produce better quality moulds for embossing purposes.

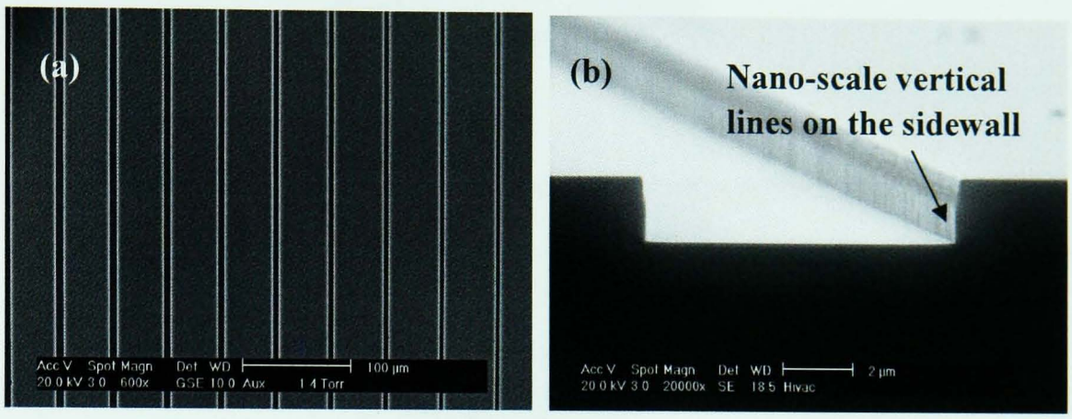

Figure 5.4: SEM image of part of the silicon mould. (a) Channel widths increasing from 3 µm to 7 µm in steps of 0.5 µm; (b) the channel had depth of 1.9 ± 0.1µm [1, 172].

5.1.3 Hot embossing equipment setup

In this project, pressing of thin chalcogenide glass films was carried out in an in-house designed and build embossing equipment for producing rib waveguides. The equipment was designed and built by Dr. D. Furniss of the Novel Photonic Glasses Research Group, University of Nottingham. Figure 5.5 shows a schematic diagram of the hot embossing equipment. Glass samples, i.e. chalcogenide thin films, were placed in between two flat and parallel aluminium plates. The position of the top plate was fixed and the lower plate was used to apply force by raising or lowering it. The temperature of the top and lower plates was controllable within ± 1°C up to 350°C [1]. The working vacuum condition (< 10^{-3} Pa, Edwards high vacuum unit BS5000-11 and PFEIFER, TCP 300) was used to avoid any gas becoming trapped in the surface of the thin film during pressing. Table 5.2 summaries the hot embossing experiments carry out in the current project using the embossing rig.

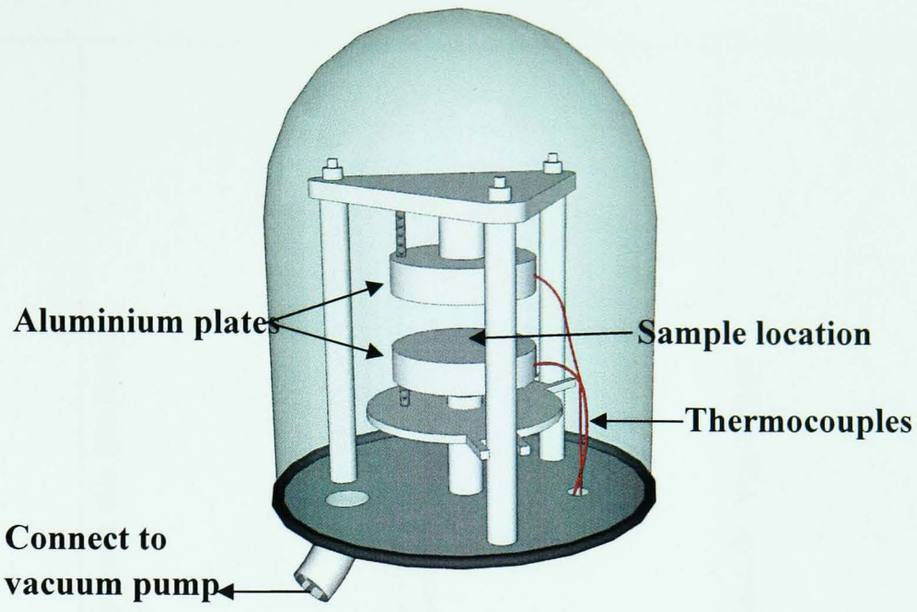

Figure 5.5: Schematic diagram of the working cell of the in-house designed and built hot embossing equipment. Samples were placed in-between the aluminium plates. Thermocouples were connected to each of the two aluminium plates; the temperature of the plates was controllable up to 350°C [1]. The working cell was connected to an Edwards high vacuum unit (BS5000-11).

Table 5.2: Record of pressing experiments in date order carried out on the in-house press rig, the sample structure is shown in Figure 5.7 and the mould used is shown in Figure 5.9.

Pressing No.	Date	Supplier	Thin film Sample ID	Pressing and annealing procedure	Results
1	20070928	QQ	GGS20070928	Room temperature→ 240°C in 60min; Dwell at 240°C for 60min; then apply load. Apply force: 0 N→120 N in 15 min; at 120 N for 15 min then release load; Load: 120 N → 0 N in 5 min; then decrease temperature from 240°C →180°C 60min; Dwell 60min; 180°C → RT @ 20°C / 60min	Not fully pressed, thin film broken
2	20070930	QQ	GGS20070930	Room temperature→ 240°C in 60min; Dwell at 240°C for 60min; then apply load. Load: 0 N→120 N in 10 min; at 120 N for 20 min; then release load. Load: 120 N → 0 N in 5 min; then decrease temperature from 240°C →180°C 60min; Dwell 60min; 180°C → RT @ 20°C / 60min	Fully pressed, thin film broken
3	20071002	QQ	GGS20071002	Room temperature→ 245°C in 60min; Dwell at 245°C for 60min; then apply load. Load: 0 N→120 N in 15 min; at 120 N for 15 min; then release load. Load: 120 N → 0 N in 5 min; then decrease temperature from 240°C →180°C 60min; Dwell	Fully pressed, thin film cracked

				60min; 180°C → RT @ 20°C / 60min	
4	20071026	QQ	GGS20071026	Room temperature→ 240°C in 60min; Dwell at 240°C for 60min; then apply load. Load: 0 N→100 N in 15 min; at 100 N for 15 min; then release load. Load: 120 N → 0 N in 5 min; then decrease temperature from 240°C →180°C 60min; Dwell 60min; 180°C → RT @ 20°C / 60min	Fully patterned but some areas shallow. Thin film cracked.
5	20071116	QQ	GGS20071116	Room temperature→ 245°C in 60min; Dwell at 245°C for 60min; then apply load. Load: 0 N→120 N in 15 min; at 120 N for 20 min then release load. Load: 120 N → 0 N in 5 min; then decrease temperature from 240°C →185°C 60min Dwell 60min; 185°C → RT @ 20°C / 60min	Small sample (5×10mm) fully pressed. No mode found
6	20080109	UofP	GG20080109	Room temperature→ 245°C in 60min; Dwell at 245°C for 10 min; then apply load. Load: 0N→120 N in 5 min; at 120 N for 15 min; Then release the force suddenly; then decrease the temperature from 245°C →180°C 60min Dwell 60min; 180°C → RT @ 20°C /60min	Fully pressed, single modes guiding found at rib widths of 5 μm, 5.5 μm and 6 μm.
7	20080111	UofP	GG20080111	Room temperature→ 245°C in 60min; Dwell at 245°C for 5 min; then apply load. Load: 0N→120 N in 5 min; at 120 N for 10 min.	Fully pressed, single mode guiding found at rib width of 5 μm, 5.5 μm and 6μm.

				Then release the force suddenly. Then decrease temperature from 245°C →180°C 60min; Dwell 60min; 180°C → RT @ 20°C /60min	
8	20080223	UofP	GG20080223	Room temperature→ 245°C in 60min; Dwell at 245°C for 10 min; then apply load. Load: 0N→120 N in 5 min; at 120 N for 10 min Then release the force suddenly; Then decrease temperature from 245°C →180°C 60min; Dwell 1 hr; 180°C → RT @ 20°C /60min	Coupler, fully pressed, some discontinuities
9	20080314	UofP	GG20080314	Room temperature→ 245°C in 60min; Dwell at 245°C for 5 min; then apply load. Load: 0N→120 N in 5 min; at 120 N for 15 min Then release the force suddenly; Then decrease temperature from 245°C →180°C 60min; Dwell 60min; 180°C → RT @ 20°C /60min	Coupler, fully pressed, some discontinuities
10	20080410	UofP	GG20080410	Room temperature→ 245°C in 60min; dwell at 245°C for 5 min; then apply load. Load: 0N→120 N in 5 min; at 120 N for 15 min Then release the force suddenly. Then decrease temperature from 245°C →180°C 60min; dwell 60min; 180°C → RT @ 20°C /60min	Coupler, some discontinue

11	20080722	UofP	GG20080722	Room temperature→ 245°C in 60min; dwell at 245°C for 5 min; then apply load. Load: 0N→120 N in 5 min; at 120 N for 15 min. Then release the force suddenly. Then decrease temperature from 245°C →180°C 60min; Dwell 60min; 180°C → RT @ 20°C /60min	Fully pressed, single mode guiding found at rib width of 4.5 μm, 5 μm and 5.5 μm. Used for testing the width mis-match between the of rib waveguides and channels in the mould

N.B.: U of P is the University of Pardubice; QQ = QinetiQ, UK; GPS = Glass – Polymer – Semiconductor; GGS = Glass – Glass – Semiconductor; GG = Glass – Glass; min=minutes

5.1.4 Discussion: the pressing conditions and results

Table 5.2 lists the hot embossing procedures undertaken in this project leading to the development of a successful technique for the fabrication of rib waveguides. The pressing conditions included several factors: temperature, load and pressing duration. These factors interact with each other and need to be manipulated correctly. Note that if the temperature of pressing was too low, the viscosity of the $As_{40}Se_{60}$ thin film was not low enough to be shaped. A too high pressing temperature, however, may lead sample and mould stick together after pressing. The duration for the embossing temperature to reach the desired temperature was one hour for a typical embossing process. This duration could be altered but it was better to make the duration longer, because a temperature overshoot would occur if the desired temperature was reached too quickly. The pressing temperature was maintained and the thin film sample held isothermally after it reached the desired temperature for the purpose of temperature stabilising. The load should be applied gradually, because it was found that a sudden load led to the thin film cracking. In contrast, after embossing, the load should be released suddenly. It was found that a sudden release minimises the chances of the thin film cracking. Two types of samples, i.e. glass on glass on semiconductor (GGS) and glass on glass (GG), were tested. It was found that the GGS samples always suffered thin film cracking and shallow pattern problems, but in GG samples these problems were overcome and rib waveguides successfully produced. In this section, the most successful results from each type of samples were selected for discussion the experimental approach.

5.1.4.1 Glass-glass-semiconductor (GGS), for Run 4 of Table 5.2

Pressing number 4 of Table 5.2 refers to GGS samples (a 2 μm $As_{40}Se_{60}$ thin film onto a 2 μm $Ge_{17}As_{18}Se_{65}$ thin film on to GaAs semiconductor) that were cleaved into several rectangular pieces (~20 mm × ~15 mm) for embossing. Take thin film sample GGS20071026 as an example. The sample was cut to a ~ 20 mm × 10 mm rectangular piece. Then the rectangular sample was placed on top of a silicon mould with the $As_{40}Se_{60}$ film contacted to the pattern in the silicon mould in the middle of the two aluminium plates. Silicone spray (supplier: Force® UK, X61700) was used on the surfaces of the upper

and bottom aluminium plates in the vacuum pressing rig to offer better thermal conduction between the aluminium plate surface and silicon mould surface.

As Figure 5.6 (a) shows, some regions of the thin film (GGS20071026) rib waveguides had been patterned. There are some defects on the rib waveguides and surface of the thin film. Those defects on the rib waveguides may be attributed to some organic debris trapped in the channels of moulds, then transferred to the ribs. The defects on the surface of the thin film may be also organic debris or segments from the cracked area. A dust free processing condition is hugely beneficial for fabricating better quality rib waveguides. Any dust trapped in the mould or on the surface of the thin film would spoil the rib waveguide. Therefore, hot embossing experiments should take place in a clean room environment to minimise any dust contamination.

The thin $As_{40}Se_{60}$ glass film cracked across the rib waveguides as shown in Figure 5.6 (b). The origin of the cracks came from the edge of the thin film. This might be due to the thermal expansion coefficient (α) of the underlying GaAs ($6.4 \times 10^{-6} K^{-1}$ [173]) being different from the α of these two glasses ($As_{40}Se_{60}$ = $20.0 \pm 0.5 \times 10^{-6} K^{-1}$ and $Ge_{17}As_{18}Se_{65} = 20.0 \pm 0.5 \times 10^{-6} K^{-1}$). Also, some parts on the thin film were not well patterned, which are shown as 'shallow area'. The shallow area made the ribs discontinuous and did not replicate the pattern on the mould. This was due to the non-uniform thickness of the sample itself, the mould and the surfaces of the two aluminium plate being not sufficient flat [1]. Similarly shallow areas can be observed on the samples, e.g. GGS20070928, GGS20071002, which were not shown.

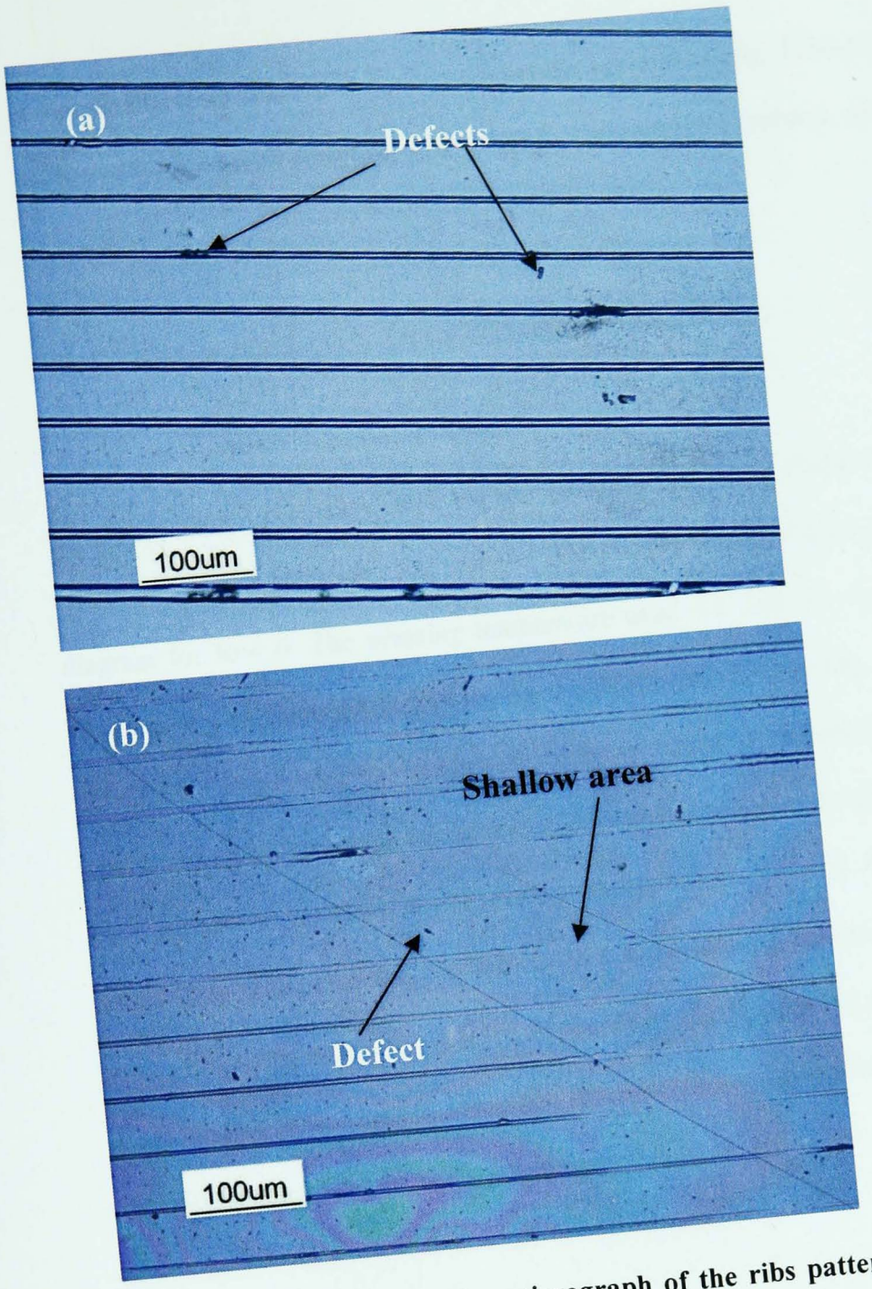

Figure 5.6: Optical reflection micrograph of the ribs patterned on a thin film sample with 2 µm $As_{40}Se_{60}$ on 2 µm $Ge_{17}As_{18}Se_{65}$ on a GaAs semiconductor (ID: GGS20071026). The pressing schedule is Run 4 shown in Table 5.2. (a) Defects can be observed on the rib waveguides and in the surface of the thin film. (b) The thin glass film cracked across the rib waveguides and some regions were only pressed shallowly.

In general, the set of experiments performed demonstrated that glass on glass on semiconductor (GGS) is not suitable for rib waveguide fabrication via hot embossing. Two main reasons are (1) the thermal expansion coefficient difference between glass and semiconductor is big and (2) the non-uniform thickness of the sample, the mould and the surface of the plates cause shallow areas in the thin film patterning. One possible solution to overcome this problem is to make a substrate which could

automatically level itself to the plates during the hot embossing. Thicker substrates which soften during the hot embossing (GG samples) were found to overcome this problem, as will now be discussed.

5.1.4.2 Glass-glass (GG samples), run 6, Table 5.2

The experimental procedure used as run 6 in Table 5.2 shows of the most successful result in producing rib waveguides in glass-on-glass samples (ID: GG20080109). Figure 5.7 shows the load and temperature diagram for Run 6. The pressing temperature used, i.e. 245 °C, was 10°C higher than the Tg of the $Ge_{17}As_{18}Se_{65}$ substrate (ZGLCF010, Tg = 235°C) and consequently ~ 65°C higher than Tg of $As_{40}Se_{60}$ (ZGLCF007, Tg = 180°C). The use of a pressing temperature slightly higher than the Tg of the substrate was found to be beneficial because a slightly softened substrate executes the function of self-levelling, enabling rib waveguides to be evenly patterned on the thin film surface [172]. An even higher temperature may cause the substrate to be distorted during embossing. After 15 minutes pressing at 120 N, the force was released suddenly. It was found if the pressing duration was too long, the samples are likely to stick to the moulds. Then the temperature was decreased from 245°C to Tg of $As_{40}Se_{60}$ (180°C) over 60 minutes (i.e. 65°C/60 minutes) and held at 180°C for 60 minutes. Then the temperature was decreased to room temperature at 20°C / 60 minutes.

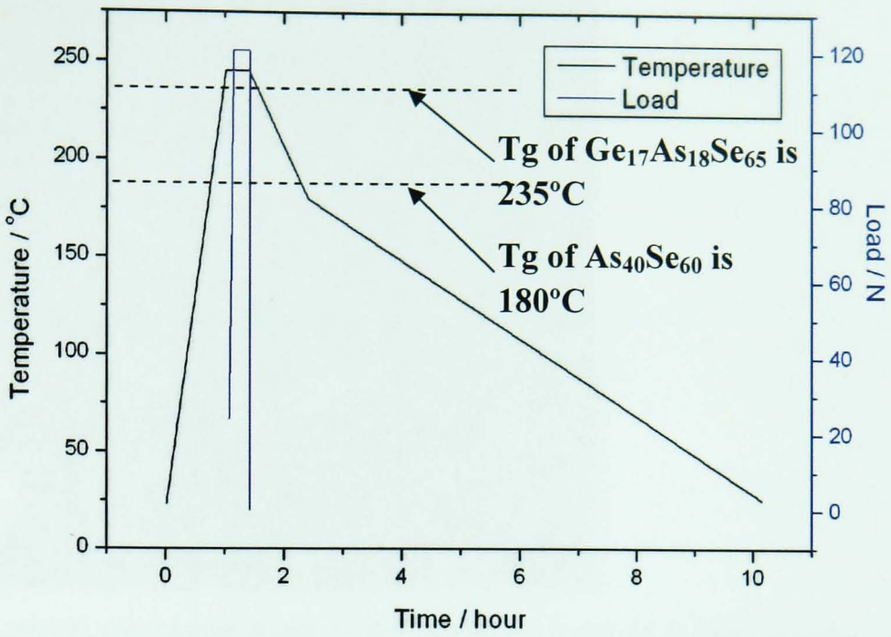

Figure 5.7: Load and temperature used in hot embossing pressing for $As_{40}Se_{60}$ – $Ge_{17}As_{18}Se_{65}$ sample (GG20080109). The procedure is summarised as Run 6 in Table 5.2.

Figure 5.8 shows an optical microscope image of the embossing result of sample $As_{40}Se_{60}$ – $Ge_{17}As_{18}Se_{65}$ (GG20080109). The rib waveguide patterns in the mould were transferred to the $As_{40}Se_{60}$ thin film and no cracks were observed on the surface. However, there were obvious surface bubbles on the thin film. This is due to the fact that the embossing temperature (235°C) is higher than Tg of $As_{40}Se_{60}$ (180°C). Figure 5.8 shows that none of the surface bubbles appeared on the rib waveguide. This suggests that a high embossing temperature does not affect the quality of the rib waveguides. Further investigations using an ESEM will be described in the next section (section 5.2).

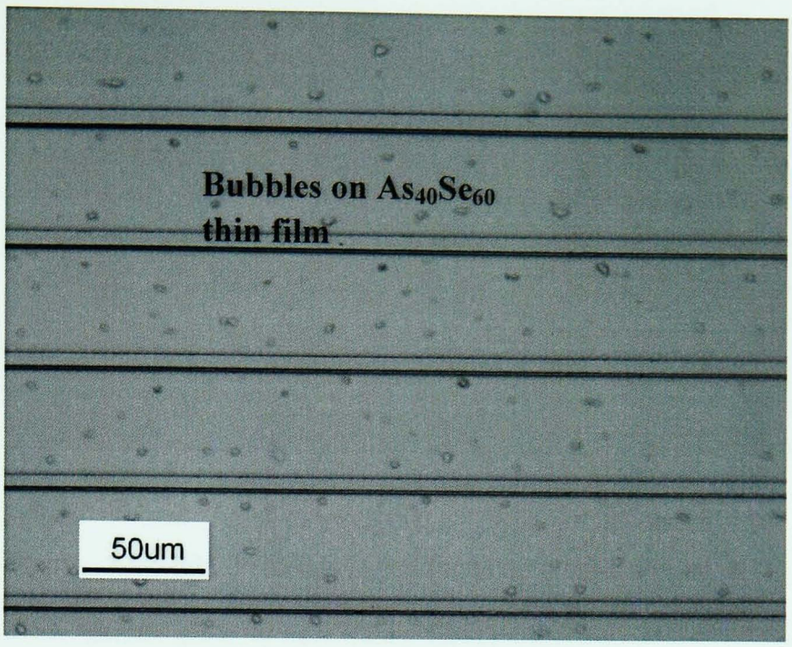

Figure 5.8: an optical microscope image of the embossing result of sample $As_{40}Se_{60}$ – $Ge_{17}As_{18}Se_{65}$ (GG20080109). Rib waveguide patterns were fully created and no cracks on the surface. Surface bubbles were observed, but none of them on the surface of the rib waveguides.

5.2 ESEM imaging and sample cleaving of glass-on-glass rib waveguides (GG samples)

An Environmental Scanning Electron Microscope (ESEM) was employed to view the surface quality of patterned rib waveguides. Figure 5.9 (a) shows a channel in the mould and the corresponding rib in (b). There were some defects on the surface and side wall of the rib waveguide in (b), similar features were found in the bottom and side walls of the channel in the mould in (a). These defects are part of the moulds and introduced during the fabrication. The sidewall roughness may cause extra optical loss of the rib waveguides produced using these moulds [171]. This investigation showed that hot embossing technique is able to transfer small scale patterns from the mould to the sample. However, this also suggested that the mould quality, such as surface quality, should be good enough to ensure the fabrication of high quality waveguides.

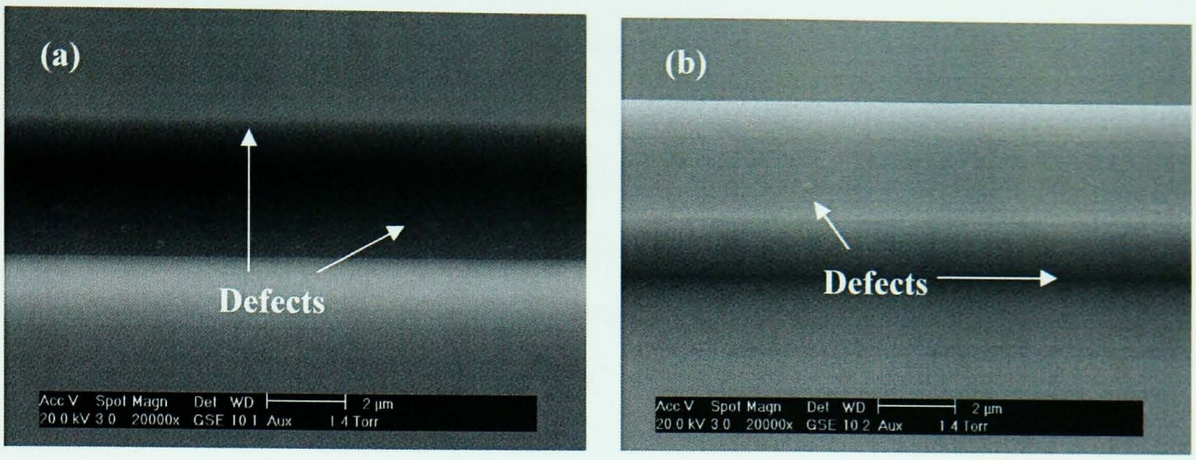

Figure 5.9: ESEM images of channels in the silicon mould and ribs in the surface of the chalcogenide glass sample (GG20080109, see Run 6, Table 5.2). (a) Top view (with slight angle) of one channel of nominal width of 5.0 ± 0.1 µm. (b) Top view of the corresponding embossed chalcogenide glass rib waveguide; the width is 4.8 ± 0.1 µm.

The width of the rib waveguide is 4.8 ± 0.1 µm as shown in Figure 5.9 (b) and the corresponding channel in the mould has width of 5.0 ± 0.1 µm. The slight mismatch of the dimension of the rib and channel is because silicon and $As_{40}Se_{60}$ have different thermal expansion coefficients i.e. α of silicon $2.3 \times 10^{-6}K^{-1}$ [1] and α of $As_{40}Se_{60}$ $20 \times 10^{-6}K^{-1}$. During the embossing process, the shape of the channels in the mould transferred to $As_{40}Se_{60}$ thin film. After the embossing, the temperature was decreased from the process temperature to room temperature. It was initially believed that this larger expansion coefficient the $As_{40}Se_{60}$ would shrink more than the silicon mould. This is sufficient to explain the slight mismatch of the dimensions of the rib waveguides formed and channels in the silicon mould.

The sample GG20080722 (Run 11, Table 5.2) was used for comparing the differences of width between the ribs and the channels in the mould. The mould used is shown in Figure 5.4. 18 rib waveguides were obtained on the GG20080722 thin film sample after hot embossing. The rib waveguides and the corresponding mould were viewed using ESEM.

The channels in the mould were slightly trapezoidal in shape, the measured width of both rib waveguides and channels were chosen as their middle-line length. In Figure 5.10, the x-axis shows the width of embossed rib from the first (nominally 2 µm) to the 18^{th} (nominally 9.5 µm) and the y-axis show the

corresponding channels in the mould in black square symbols. The width of rib and channels were measured through ESEM images. The width difference between the rib waveguides and the corresponding channels in the mould is shown as blue square symbols. A measurement, error may occur if the ESEM image was artificially distorted or the sample was not precisely orthogonal to the electron beam [126]. Two anomalous points of width difference in Figure 5.10 are highlighted with a red circle. These may be because of defects in the samples or incorrect measurement.

In Figure 5.10, it may be observed that as the width of the rib waveguide increases, the width difference become larger. The nominal 5.0 μm width waveguide was the same width as that of this channel in the mould. The width of rib waveguide was larger than the width of the channels in the mould for rib waveguides less than 5 μm wide. Moreover, the width of rib waveguides was smaller than the width of the channels in the mould for rib waveguides width larger than 5.5 μm. The same phenomenon was observed by Pan [1]. The study of width mis-match between ribs and corresponding channels suggests that in the future, for more precise optical components fabrications using the hot embossing method, the actual width of the channels in moulds need to be re-designed in order to produce the desired components structure.

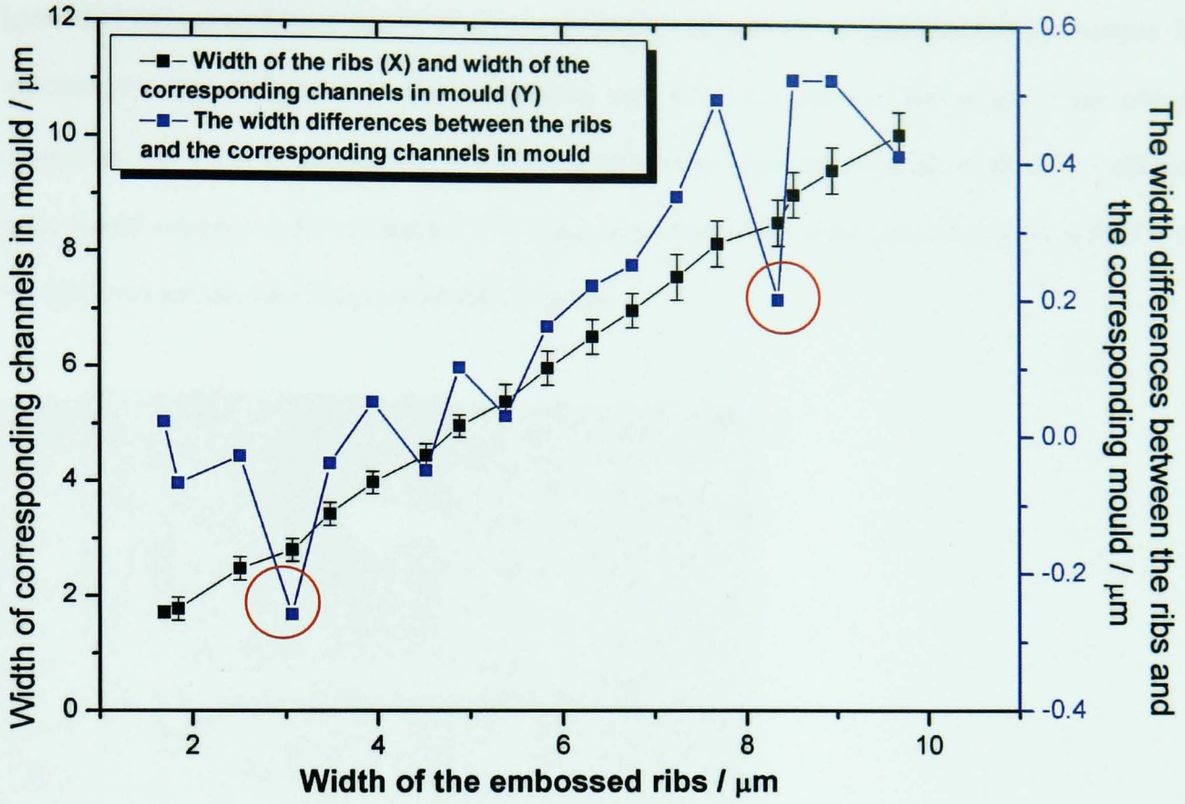

Figure 5.10: Rib waveguide width and the width of the corresponding channels in the mould and their difference. 18 rib waveguides were studied on the hot embossing pressed $As_{40}Se_{60}$ – $Ge_{17}As_{18}Se_{65}$ thin film sample (GG20080722, Run 18 in Table 5.1). The corresponding channels in the mould were measured using ESEM. The x-axis shows the width of the ribs and the y-axes show (1) the width of the corresponding channels in mould μm and (2) the width difference between rib and channels.

In order to couple light in to and out of the rib waveguides formed in the glass-on-glass samples, the waveguide samples need to be cleaved. The opposite ends of the rib waveguides needed to be cleaved. To achieve cleaving, the rib waveguide sample was mounted onto a silicate glass microscope slide (supplier: Sail Brand Ltd. 25.4 × 76.2 × 1.2 mm) by means of wax (Buehler, Coventry, UK) and fixed onto a saw cutting machine (see section 3.1.4). The cutting speed and time were carefully controlled so that the diamond blade (Buehler Isomet low speed saw and diamond wafering blade, thickness = 0.35 mm) did not cut through the sample, but left a channel underneath the chalcogenide glass substrate. Then a thin copper blade was placed into that channel and gently twisted by hand to break the sample into two parts. As the thickness of the part being broken was small (~ 0.5 mm) and the force was relatively uniform, the rib tended to break together with substrate thus giving a flat end-face cross-section.

Figure 5.11 shows an ESEM image of the cross section of two rib waveguides formed (sample ID: GG20080109). The height of the rib waveguides was 1.9 ± 0.1 μm and the width of the two rib waveguides was 7.7 ± 0.2 μm and 8.2 ± 0.2 μm, respectively. The corresponding widths of the channels on the mould were 8.2 ± 0.2 μm and 8.5 ± 0.2 μm, respectively. The centre-to-centre space is 50.1 ± 0.5 μm. (b) shows a magnified image of the left rib in (a).

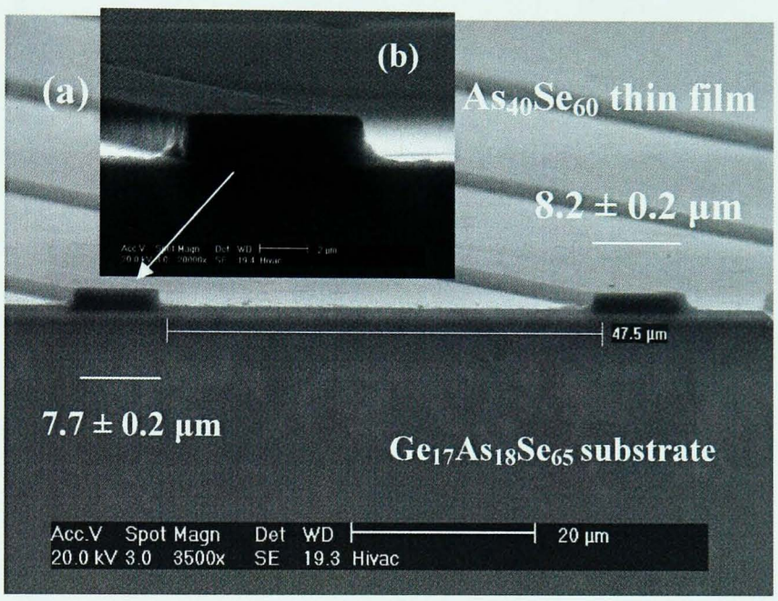

Figure 5.11: ESEM image of the cross-section of rib waveguides patterned in a glass on glass sample (GG20080109). The height of the rib waveguides was 1.9 ± 0.1 μm and the width of the two rib waveguides was 7.7 ± 0.2 μm and 8.2 ± 0.2 μm, respectively. The corresponding widths of the channels were 8.2 ± 0.2 μm and 8.5 ± 0.2 μm, respectively. The centre-to-centre distance of neighbouring waveguides was 50.1 ± 0.5 μm, to be compared with the nominal 50 μm centre-to-centre waveguide separation of the mould. (b) shows a magnified image of the left rib in (a).

Figure 5.12 shows compositional electron mapping of a rib waveguide in hot embossed thin film sample (GG20080109, Run 6, Table 5.2) by means of backscattered electrons and electron dispersive spectroscopy (EDS) in a series of ESEMs: (a) shows a typical rib waveguide in the hot embossed $As_{40}Se_{60}$ – $Ge_{17}As_{18}Se_{65}$ sample (GG20080109); (b) germanium mapping; (c) arsenic mapping; and (d) selenium mapping. EDS is an analytical technique that uses X-rays emitted from the specimen when bombarded by the SEM electron beam to identify the elemental composition of the specimen. The bright spots in the image represent the presence of that element. The elemental mapping provides evidence that the thin film

was As-Se and the substrate was Ge-As-Se, as expected. The shape of the rib is also clearly visible in the element map.

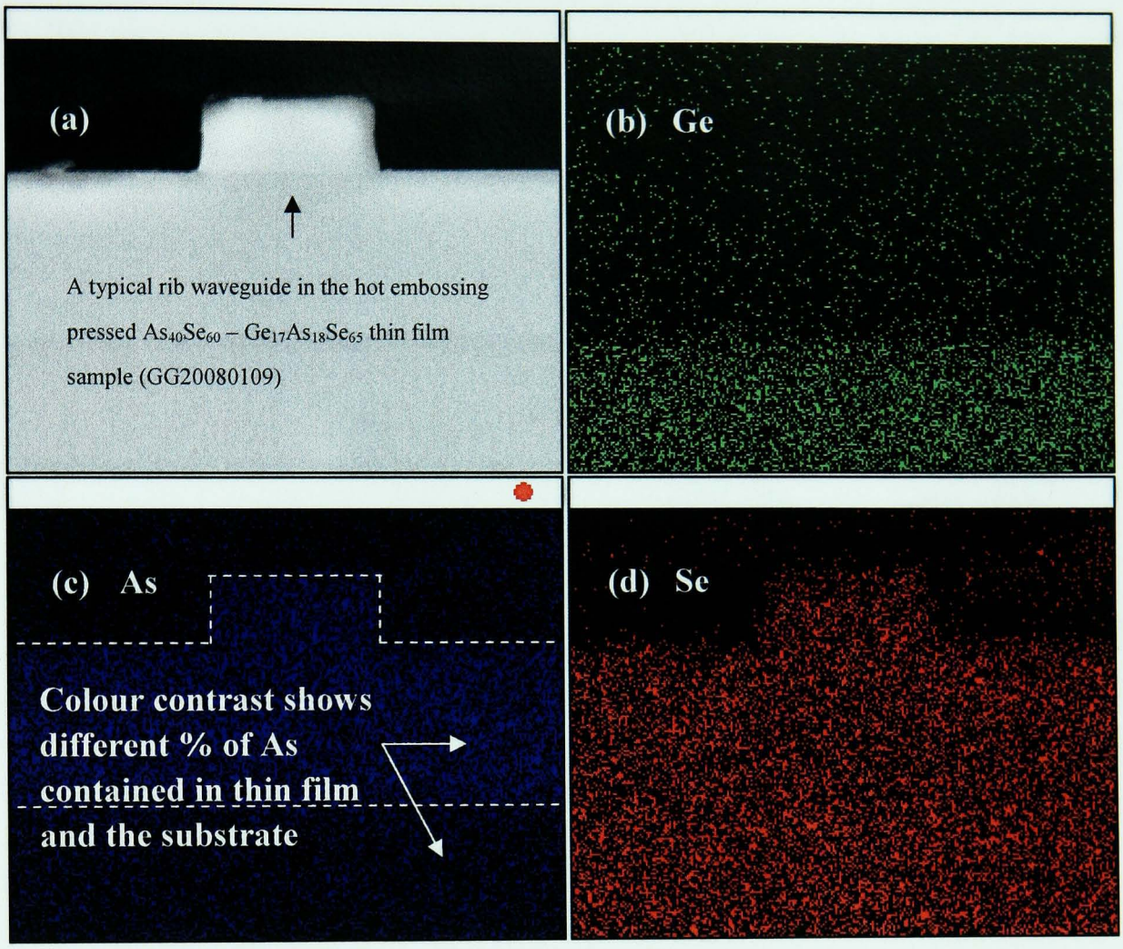

Figure 5.12: Compositional electron mapping of As, Ge and Se of a rib waveguide in hot embossed pressed $As_{40}Se_{60}$ – $Ge_{17}As_{18}Se_{65}$ thin film sample (GG20080109, see Run 18, Table 5.1). (a) a typical rib waveguide a typical rib waveguide in the hot embossed $As_{40}Se_{60}$ – $Ge_{17}As_{18}Se_{65}$ sample; (b) Ge elemental mapping: Ge only occurs in the spots arranged in the substrate; (c) As elemental mapping: As content inside the thin film is higher than in the substrate and (d) the Se content shows up as apparently uniform across the thin film and the substrate. The expected atomic % of Se in thin film and the substrate is between 60 at% and 65 at %.

5.3 Waveguide guiding assessment of glass-on-glass samples

Groups of rib waveguides having width from ~2.0 μm to ~8.5 μm in the hot embossing press were cleaved to a length of 5 ± 0.2 mm. The optical waveguiding characteristics of the $As_{40}Se_{60}$ – $Ge_{17}As_{18}Se_{65}$ rib

waveguides were evaluated using the experimental setup shown in Figure 5.13. A tapered silica glass optical fibre was used to end-fire couple a tunable laser beam (Agilent, model 81980A, range of wavelength is from 1.375 to 1.575μm) into one end of the cleaved waveguide sample. The polarisation of the light was controlled using a polariser. The transmitted light from the waveguide was collected from the opposite end-face of the waveguide using an X 40 microscope objective and focused onto an infrared sensitive camera (Siemens XQ1112). A television monitor and computer were connected to the infrared camera as a direct image output [172].

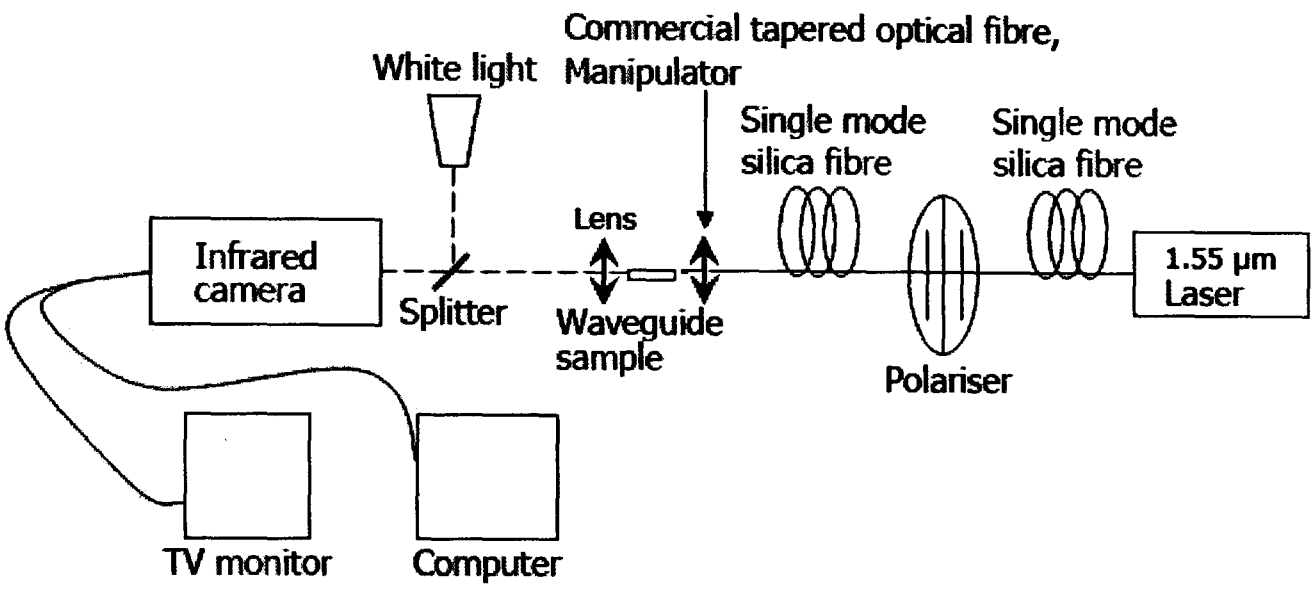

Figure 5.13: Optical bench set-up for waveguiding assessment.

The GG20080111 sample (Run 7 in Table 5.2) was used as an example for the optical guiding assessment because it showed clearest guiding across all ribs. Figure 5.14 (a), (b), (c) and (d) show the optical guiding for nominal rib width from 5 μm, 5.5 μm, 6 μm and 6.5 μm, respectively. The ribs having nominal widths of 5, 5.5 and 6 μm exhibited mono-mode propagation for the quasi-TE polarisation at 1.55 μm wavelength. Waveguides in this range were expected to be single mode by simulation. The rib having a nominal width of 6.5 μm exhibited 2 peaks multimode as shown in Figure 5.14 (d). The shape of the near-field intensity profile of a quasi-TE mode for the waveguide of nominal width 5.5 μm at 1.55 μm wavelengths was also close to the shape of the simulated mode profile (Figure 5.1). A horizontal line scan trace (Figure 5.15 (b)) through the highest intensity of light as shown in Figure 5.15 (a) confirms that the image is typical of a single mode waveguide.

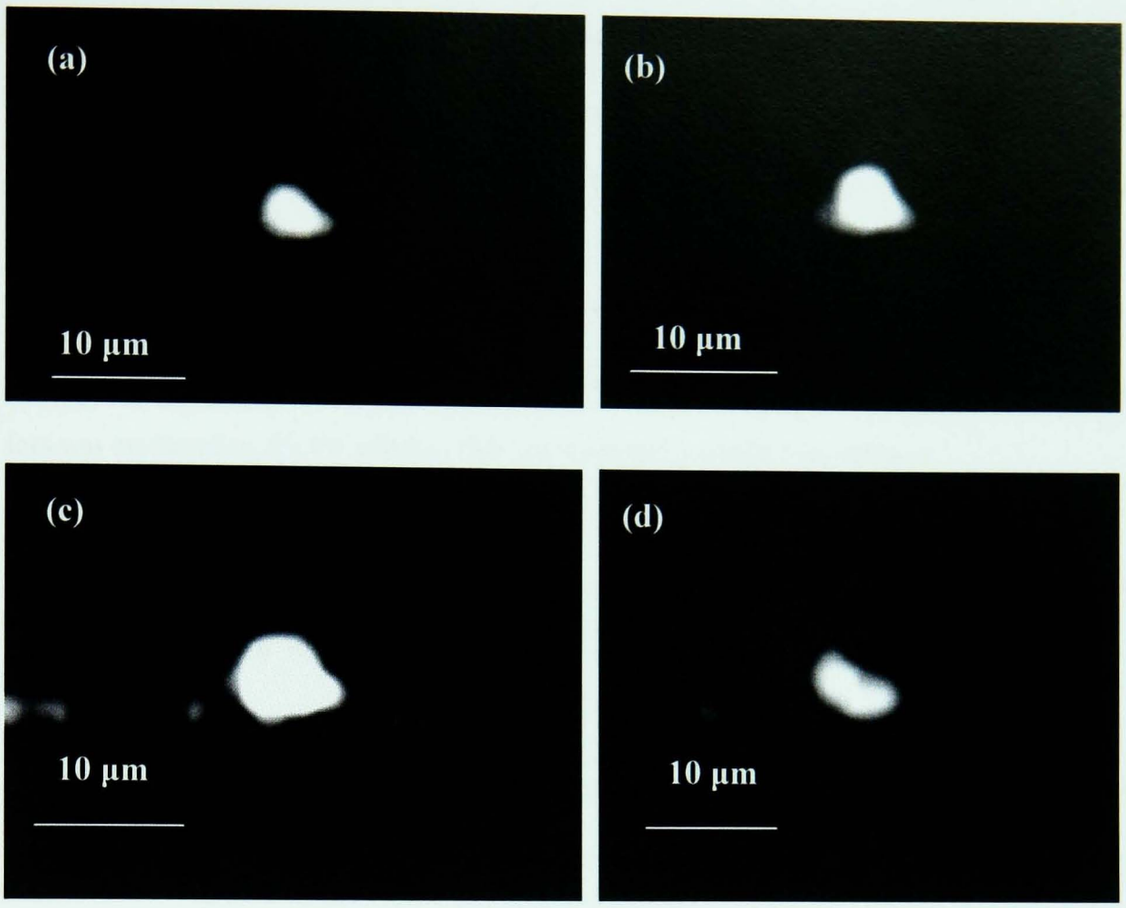

Figure 5.14: Near-field intensity profile observed at 1.55 μm wavelength for a nominal (a) 5.0 μm wide rib waveguide, (b) 5.5 μm wide rib waveguide, (c) 6.0 μm wide rib waveguide and (d) 5.0 μm wide rib waveguide captured by the infrared camera.

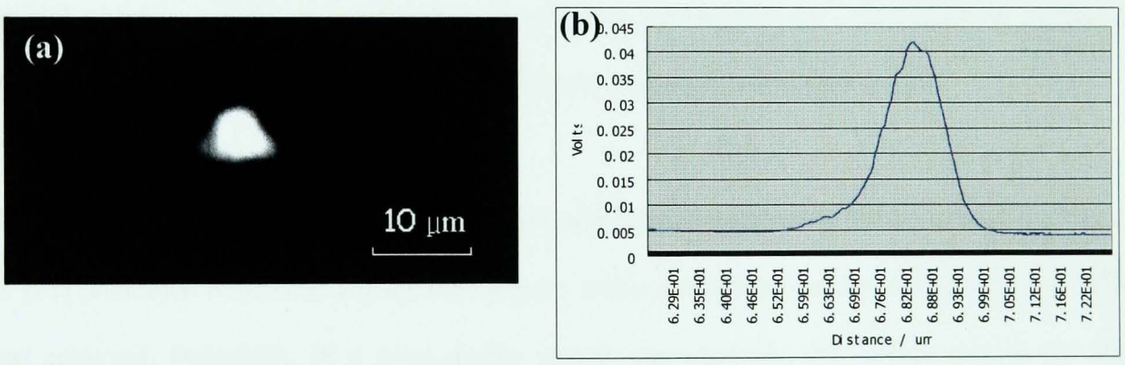

Figure 5.15: (a) Near-field intensity profile observed at 1.55 μm wavelength for a nominal 5.5 μm wide rib waveguide (reproduced from Figure 5.14 (b)) from the hot embossing pressed $As_{40}Se_{60}$ – $Ge_{17}As_{18}Se_{65}$ thin film sample (GG20080111, see Run 7, Table 5.2) captured by the infrared camera and (b) line scan trace confirming that the image was typical of a single mode waveguide (camera line sweep speed was 21.18 μm/μs).

The optical loss of the rib waveguide with nominal width 5.5 μm was measured by sweeping the wavelength of the tuneable laser from 1500 nm to 1550 nm and measuring the maximum and minimum intensities of the resulting Fabry-Perot resonances using a photodiode [174]. This ratio was found to be 0.73 for the quasi-single TE mode in a sample 5 mm long (of channel width of nominal 5.5 μm and nominal depth 2 μm). Assuming an endface reflectivity equal to the Fresnel value (0.219) (confirmed for the present large size ribs by Sewell using a reflective beam propagation method [175]) the maximum loss was evaluated as 2.9 ± 0.1dB/cm. The TM mode had a similar loss value.

One of the objectives of this project is to emboss rib waveguides with optical loss around 1 dB/cm. This target of the low loss was not achieved. The excess opical loss is believed to be attributable to the waveguides sidewall roughness which may be of the order 50 nm [1]. Barwicz and Haus reported an estimation method for rectangular waveguide scattering loss using its surface roughness; an optical loss figures was plotted against surface roughness and waveguide dimensions [176]. Based on this, the scattering loss of the embossed rib waveguides due to sidewall roughness was estimated at least 1 dB/cm. The loss value measured is also likely to be an over-estimation since the technique evaluates the 'round-trip' loss. The rib waveguide cleaving quality was not perfect. It would affect the optical coupling insertion loss and also lead to an overestimate of the waveguide loss found using the Fabry-Perot method. Optical polishing of the cleaved surface is one way to improve the cross-sectional surface quality. However, this will dramatically increase the cost and complexity of the fabrication.

Current propagation losses in laser written waveguides are 0.4 dB/cm by Viens *et al.* [17]. Also, Ruan *et al.* [21] fabricated $As_{40}S_{60}$ rib waveguide via a dry etching technique and a waveguide loss of 0.25 dB/cm was achieved. Potentially, if a good quality mould was available, the optical loss of rib waveguide fabricated using the hot embossed technique should be close to the values achieved by laser writing and dry etching. Further experiments to improve the waveguides losses will be suggested in Chapter 7.

5.4 Summary

The hot embossing technique is desirable for patterning at a relatively lower temperature; it offers high resolution and fast throughput patterning. One objective of this PhD project is to fabricate strip rib waveguides in chalcogenide glass thin films using a hot embossing technique.

In order to achieve this successful fabrication, glass-on-glass-on-semiconductor (GGS) ($As_{40}Se_{60}$ onto $Ge_{17}As_{18}Se_{65}$ onto GaAs) samples were firstly attempted, however, there were several problems such as: in thin film cracking and discontinuities. These problems were solved by using glass-on-glass (GG) samples. Those hot embossed GG samples showed complete rib waveguide patterns and none of the thin films cracked under all embossing conditions. Single mode rib waveguides were successfully fabricated on $As_{40}Se_{60}$-$Ge_{17}As_{18}Se_{65}$ samples. The optical loss of the GG rib waveguides made was relatively high (2.9 dB/cm), but some recommendations have been proposed for further improvement and this is discussed further in Chapter 7.

Chapter 6

The Fabrication of Microstructured Optical Fibres

One of the objectives of this PhD project was to investigate the feasibility of fabricating single material hollow core Microstructured Optical Fibres (MOFs) based on chalcogenide glass. Chapter 4 reports some of the properties of certain chalcogenide glasses that are potentially suitable for MOF fabrication. $As_{40}Se_{60}$ was chosen as a candidate material for producing hollow core MOF because of its relatively simple (binary) composition which aids preparation and because it has been widely studies to be a stable composition as described in section 2.2. The first section of this chapter reports the fabrication processes developed towards the demonstration of the air core MOFs in $As_{40}Se_{60}$ shown schematically in Figure 6.1 (a). The experimental steps included rotational casting tube, cane stacking and fibre drawing and are described in section 6.1.

Single material hollow core MOF was not successfully fabricated in this project. However an alternative, two glass composition, i.e. $As_{40}Se_{60}$ and $Ge_{10}As_{23.4}Se_{66.6}$, all solid MOF (solid core and solid cladding) was fabricated. A schematic diagram of a two material solid MOF is shown in Figure 6.1 (b). The fabrication procedures are described in section 6.2.

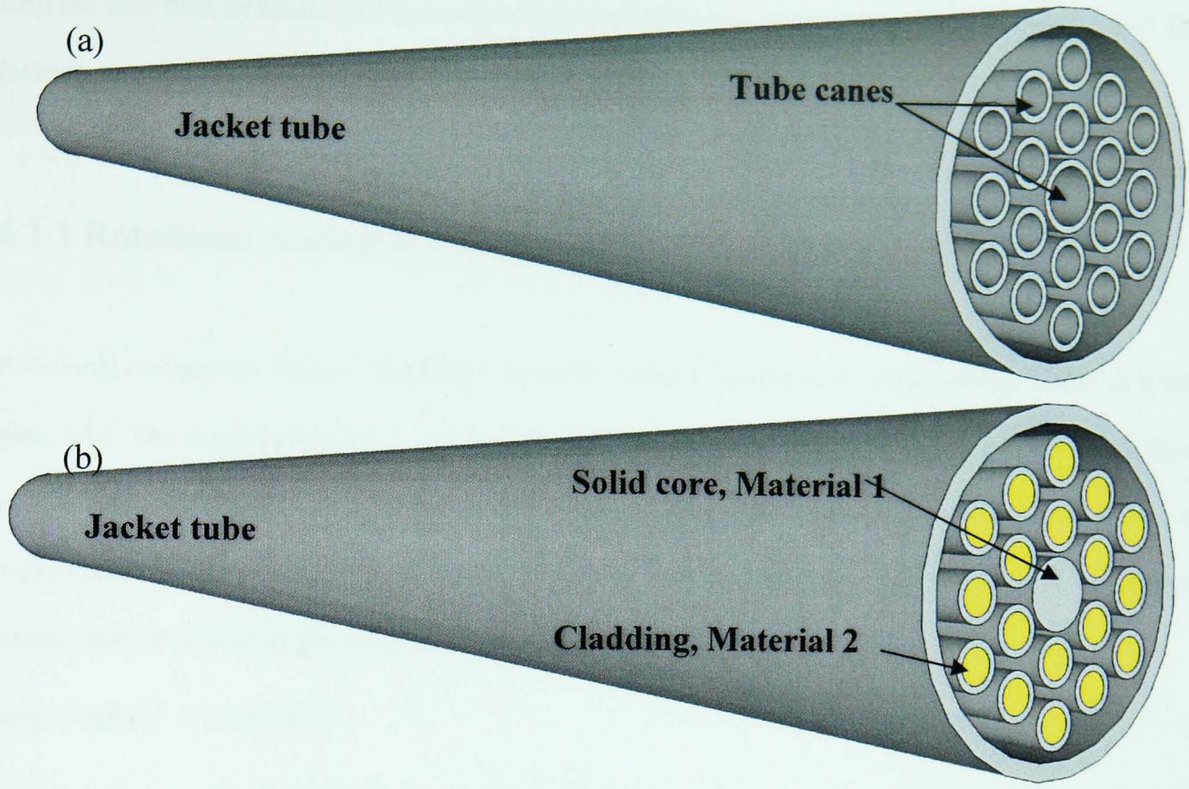

Figure 6.1: Schematic diagrams of (a) single material hollow core MOF preform. Several tube canes stacked inside of a jacket tube. The diameter and wall thickness of tube canes vary depending on the target application. (b) Two materials 'all solid' MOF preform. Several solid canes stacked inside of an outer jacket tube. The materials for solid core/cladding MOFs require having a sufficient large refractive index (n) difference between materials 1 and 2.

6.1 Single glass composition hollow core MOF

In this section, the fabrication processes of single material ($As_{40}Se_{60}$) Microstructured Optical Fibres (MOF) will be described. To achieve the desired goal, first step is to prepare a MOF preform, will subsequently be pulled down to an MOF. The hollow core MOF combines of two components: a 'jacket' tube and several tube canes stacked inside this tube (rod-in-tube technique as described in section 2.5.4.1. There are many methods to produce chalcogenide glass tube, such as extrusion technique; core drill and rotational casting etc. In the current project, the tubes were fabricated via a rotational casting technique. Rotational casting is considered as a faster process compared with the extrusion technique. This is because extrusion combines many steps for one task: die design, die fabrication, billet preparation and extrusion [2, 90]. So it is a time consuming and a relatively high cost technique. Also, when compared

with the core drill technique [177], rotational casting is faster if long samples need to be prepared. Both jacket tube and canes were fabricated via rotation casting technique.

6.1.1 Rotational casting of $As_{40}Se_{60}$ tubes

Rotational casting tube utilises centrifugal forces to produce chalcogenide glass castings inside of a silica glass tube. The chalcogenide glass – forming liquids exhibit a low enough viscosity above the liquidus to enable rotational casting to be carried out to make tubes. The quenching process then allows the super-cooled liquid to 'freeze' in the shape of a tube. The least angular velocity required for rotational casting was calculated by the circular motion equations.

$$mg = mR\omega^2 = mR(2\pi f)^2 \qquad 6 - 1$$

where m is the mass of chalcogenide material; g is the gravitational constant ~ 9.8 ms^{-2}; R is the inside radius of the ampoule; ω is the angular velocity and f is the rotational frequency. The angular motion of the equipment provides the centrifugal force to overcome gravitational acceleration.

6.1.1.1 Equipment setup and experimental procedures

The rotational casting technique involves several steps including: material preparation, ampoule re-seal, rotational casting and sample annealing. In this section, these steps will be described in detail.

(1) Raw materials in the correct batch ratio for making the desired chalcogenide glass composition (e.g. purified As and Se) were batched inside of a standard ampoule (10/14 mm ID/OD; HF etched to eliminate possible defects in the inner surface of the silica ampoule and increase the mechanical strength of the silica ampoule [2]; air and vacuum baked using the procedure described in section 3.1. Figure 6.2 (a) depicts that the ampoule was sealed under vacuum (8×10^{-3} mbar) as described in section 3.1.2 and Figure 6.2 (b) shows that the batched chalcogenide glasses were melted as described in section 3.1.3.

(2) The ampoule sealing point was found to be critical for the subsequent rotational casting of the chalcogenide glass tubes, because the resulting wall thickness of the rotationally cast chalcogenide tube

depends on the ratio of the batched material to the total internal volume of the ampoule. The more material batched, the thicker the tube wall would be.

Typically, to reduce jacket tube, a batch of more than 20 g of $As_{40}Se_{60}$ in a standard ampoule was required. The wall thickness of the jacket tube depended on the ratio of the volume of the as-melted $As_{40}Se_{60}$ to the volume of the empty space inside of the sealed ampoule. The emptier space then the thinner the wall thickness of the jacket tube. Equation 6-1 shows the calculation of dimensions of the tube. The mass of the $As_{40}Se_{60}$ before and after rotational casting was identical. Therefore the density ρ of $As_{40}Se_{60}$ remains constant,

$$\pi R^2 \times l_o \times \rho = \pi (R^2 - r^2) \times l_n \times \rho \qquad 6\text{-}2$$

where l_o is the original length of $As_{40}Se_{60}$ rod in the ampoule after melting, l_n is the new $As_{40}Se_{60}$ tube length. R is the inner radius of the ampoule and r is the target inner radius of the $As_{40}Se_{60}$ tube. Normally, the jacket tube had a relatively thicker wall thickness and small orifice (~5/10 mm ID/OD). Therefore, in order to produce a jacket tube, the ampoule which contained the $As_{40}Se_{60}$ required resealing to minimise the volume of empty space as shown in Figure 6.2 (c).

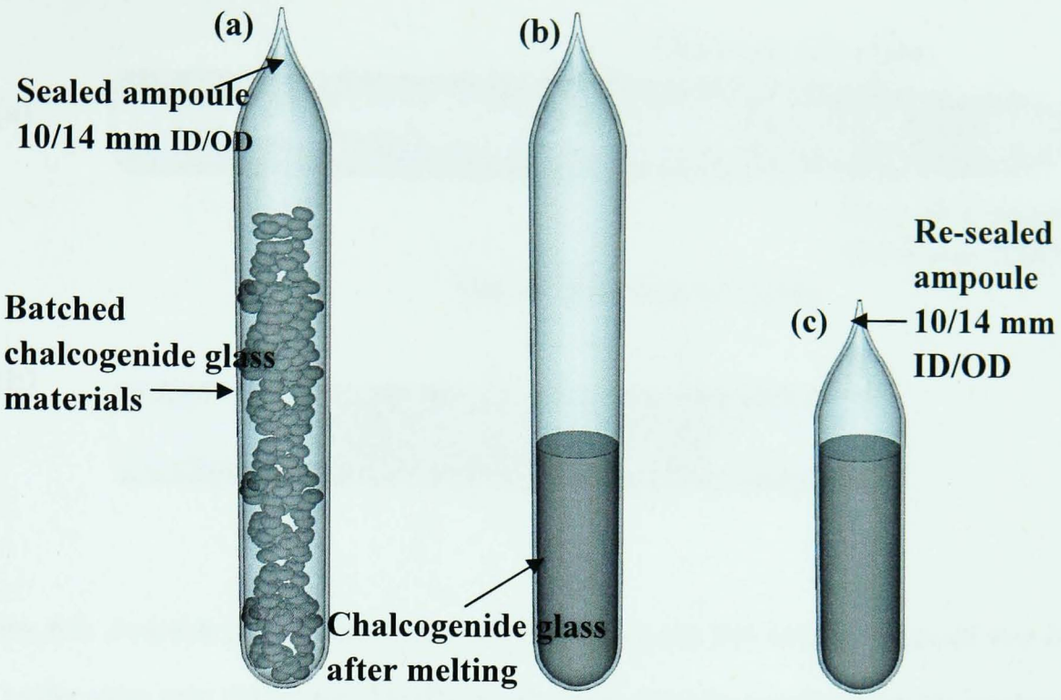

Figure 6.2: Ampoules and batched materials for rotational casting. (a) Chalcogenide precursor material batched inside of a standard ampoule (10/14 mm ID/OD) and sealed under vacuum (8×10^{-3} Pa); (b) after melting the chalcogenide glass was annealed *in situ*; (c) the ampoule was then resealed at a lower point along the ampoule to give a shorter ampoule ready for rotational casting.

(3) As Figure 6.3 (a) shows, the resealed ampoule (in Figure 6.2 (c)) was then slotted into a buffer silica tube (14/18 mm ID/OD). The buffer tube was used because during the process of rotational casting of chalcogenide glass tube, the high temperature (> 650°C for $As_{40}Se_{60}$) ampoule with liquid chalcogenide materials had to be moved from the furnace to the rotational casting rig (Figure 6.4). During handling of the ampoule, iron tongs, which were at room temperature, were required to contact the ampoule; therefore, this contacting point might have caused the inside material to cool and became solid. The resealed ampoule was supported by two copper (melting temperature ~1370°C) clamps. At room temperature, the resealed ampoule and the buffer tube were then placed into a rocking furnace to remelt the chalcogenide glass.

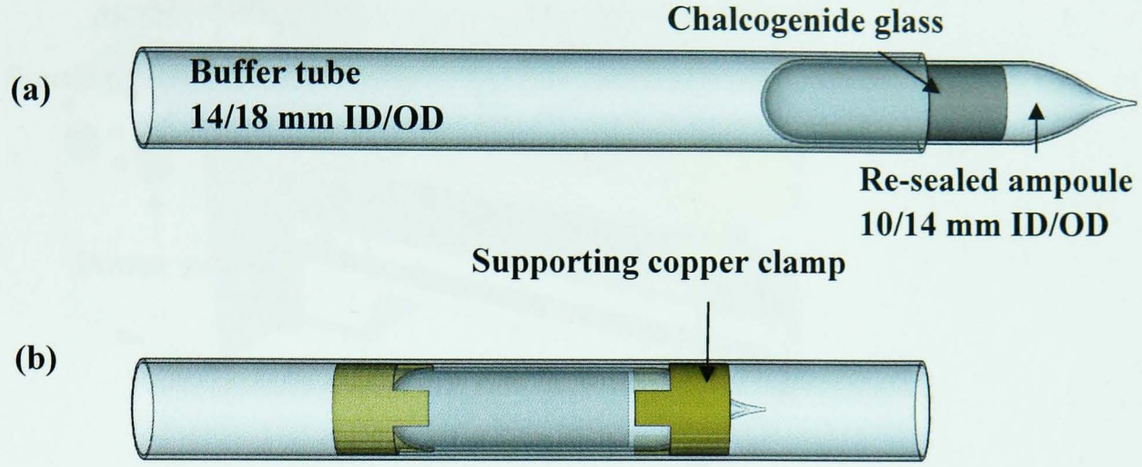

Figure 6.3: Ampoule preparation for rotational casting. (a) The resealed ampoule was slotted into the buffer silica tube (14/18 mm ID/OD). (b) The assembly: the resealed ampoule was located in the centre of the buffer tube and supported by two copper clamps. This assembly was then placed in the rocking furnace to remelt the chalcogenide glass ready for the rotational casting.

(4) Figure 6.4 shows schematically the rotational casting of a chalcogenide glass tube which was carried out by D. Furniss in the in-house modified and built rotational casting equipment (Metalworker variable speed lathe). After the melting of the chalcogenide glass, the resealed ampoule and the buffer tube with the copper clamps were moved and placed in the rotational casting equipment. Moving of the assembly needed to be achieved quickly to avoid the supercooled liquid solidifying and was normally performed in less than 5 second. Therefore two people were required for this task, the assembly was moved by one person and the other person controlled the rotational casting equipment and timing. In this project, the task was done by the current author and D. Furniss.

The rotational casting equipment was able to produce up to 2000 rpm angular velocity. According to equation 6-1 the speed chosen for the rotational casting depended on the quantity of the batched material. A typical time schedule of the rotational casting of $As_{40}Se_{60}$ is described in Table 6.1.

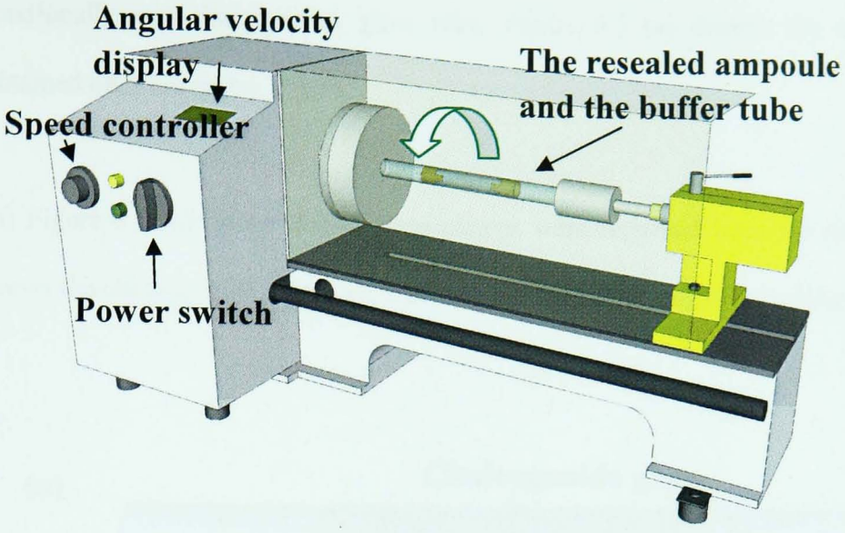

Figure 6.4: Rotational casting equipment. After melting, the resealed ampoule and the buffer tube were placed in the centre of the rotational casting equipment. The curved arrow shows the rotation direction in order to from the chalcogenide glass tube.

Table 6.1: Time / temperature schedule and observations during of the rotational casting procedure of making an $As_{40}Se_{60}$ tube.

Steps	Schedule	Observations
	Melting	
1	Room temperature (RT) → 200°C @ 200°C/60 min	Chalcogenide glass melting was carried out in rocking furnace (see section 3.1.3).
2	200°C → 800°C @ 40°C/60min	
3	800°C for 12hours	
4	800°C to 650°C @ 40°C/60min	
5	650°C until rotational casting	
	Rotational casting	
6	Place the resealed ampoule and buffer tube in the rotational casting equipment	The chalcogenide material inside of the resealed ampoule was liquid.
7	Adjust the angular velocity to 1000 rpm for 2 min	The chalcogenide material inside of the reseal ampoule solidified.
	Annealing	
8	Place the resealed ampoule and buffer tube in the annealing furnace	Chalcogenide glass annealing was carried out in annealing furnace (see section 3.1.3).
9	185°C→140 @ 5°C/60min	
10	140°C→ RT @ 20°C/60min	

(5) After the rotational casting of the chalcogenide glass tube, the resealed ampoule with the buffer tube and copper clamps were placed as a still intact assembly in the annealing furnace to anneal the

rotationally cast chalcogenide glass tube. Figure 6.5 (a) depicts the rotationally cast tube that was obtained after annealing *in situ*.

(6) Figure 6.5 (b) shows that the two clamps were removed from the resealed ampoule. Figure 6.5 (c) shows the chalcogenide glass tube that was obtained after carefully cutting the resealed ampoule.

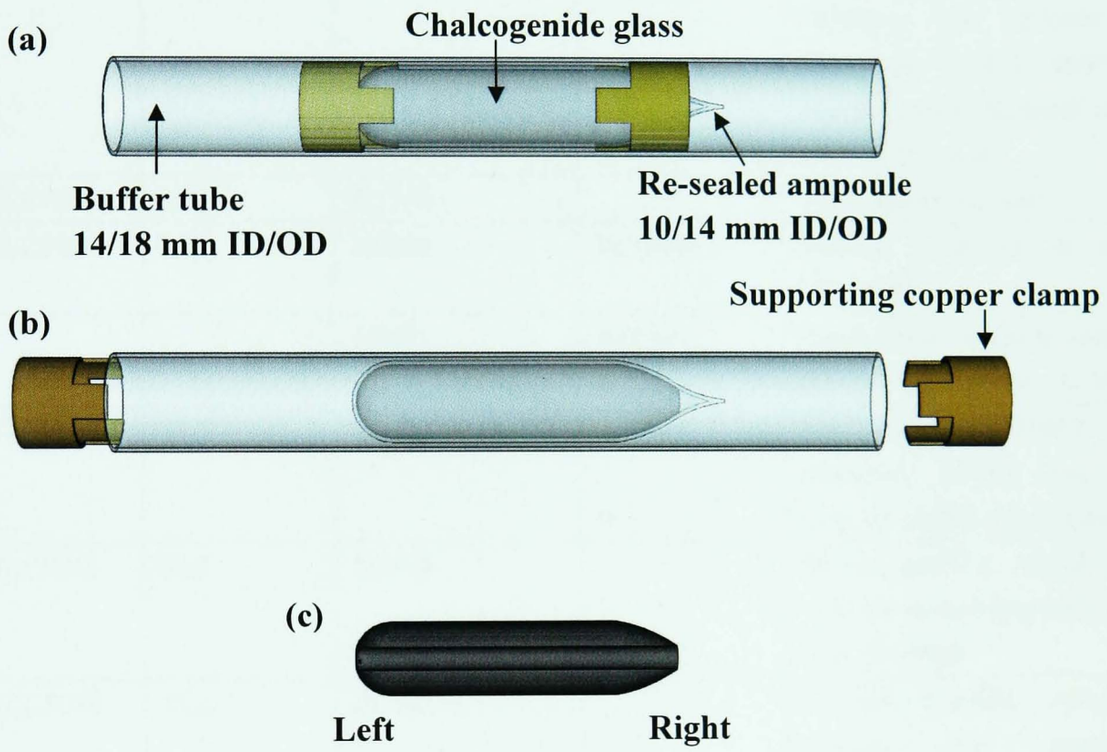

Figure 6.5: Chalcogenide glass tube recovery. (a) After annealing the resealed ampoule and the annealed chalcogenide glass tube were still locked by clamps inside the buffer tube. The whole assembly was place inside the annealing furnace. (b) The two clamps were removed and the resealed ampoule containing the annealed chalcogenide glass tube was obtained. (c) The resealed ampoule was then cut open to obtain the chalcogenide glass tube.

Table 6.2 records the glass batches and rotational casting undertake in the current project. The melting identities of each $As_{40}Se_{60}$ melt are listed in the first column and the weight of each batch are listed in the second column. The rotationally casted tubes can be used as jacket tubes or canes which will be described in next section (section 6.1.2). In table 6.2, the number of hollow fibre drawing (HFD) is listed in the fourth column. The last column shows the preform information.

Table 6.2: $As_{40}Se_{60}$ glass melting, rotational casting of preform tubes and cane-drawing records for air / glass MOF fabrication.

Melting ID	Weight / g	Rotational casting number	Cane-draw ID	Notes
ZGLCF017	10.5	RC001		Tube sample was cut for imaging.
ZGLCF018	12.0	RC002	HFD001 and HFD002	Stacked inside RC003 for MOF001.
ZGLCF019	33	RC003	HFD003	Sample cut for imaging. Clad: HFD001; core HFD002 & outer tube RC003. MOF001 was not produced, small tubes stuck on the wall.
ZGLCF020	24.8	RC004		Tube broken into half.
ZGLCF024	25.0	RC005	HFD004	Stacked in RC006 to form MOF002.
		RC006	HFD005	Small fibres tended to stick to the wall. Stacked into RC007.
ZGLCF028	23.3	RC007	HFD006	Air / glass MOF003 was produced; hollow core not seen, air cladding not uniform.
ZGLCF035	30.0	RC008	-	Se not purified; casted tube used for assembling solid core fibre MOF004.
ZGLCF036	34.6	RC009	-	Se not purified. Ampoule cracked after rotational casting.
ZGLCF041	31.0	RC010	-	Se purified. Jacket tube cracked during fibre drawing.

Note: ID = identification; RC = Rotational Casting and HFD = Hollow Fibre Drawing; SFD = Solid-core Fibre Drawing

6.1.2 Production of $As_{40}Se_{60}$ jacket tube and canes

Examples of the results of rotational casted $As_{40}Se_{60}$ tubes include (1) jacket tubes and (2) canes will be described in this section.

(1) $As_{40}Se_{60}$ jacket tubes. The required inner diameter (ID) and outer diameter (OD) of the jacket tube depend on the geometry of the MOF, i.e. core dimension and the layer numbers. 33.0 g $As_{40}Se_{60}$ was

melted inside a 10 mm / 14 mm ID/OD ampoule, air quenched *in situ* (ZGLCF019) and annealed at 180°C. The resealed ampoule was then re-heated to remelt the chalcogenide glass as listed in Table 6.1. Instead of the normal quenching, the ampoule was loaded into the rotational casting rig, secured and rotated at 1200 rpm for two minutes (a typical quenching duration for $As_{40}Se_{60}$ [2]). The melt had solidified to form a tube (RC003, RC means rotational casting). The ampoule was then placed inside the annealing furnace and the tube annealed. The size of RC003 was 115.0 mm length and 5 / 10 mm ID / OD as shown in Figure 6.6 (a) and (b).

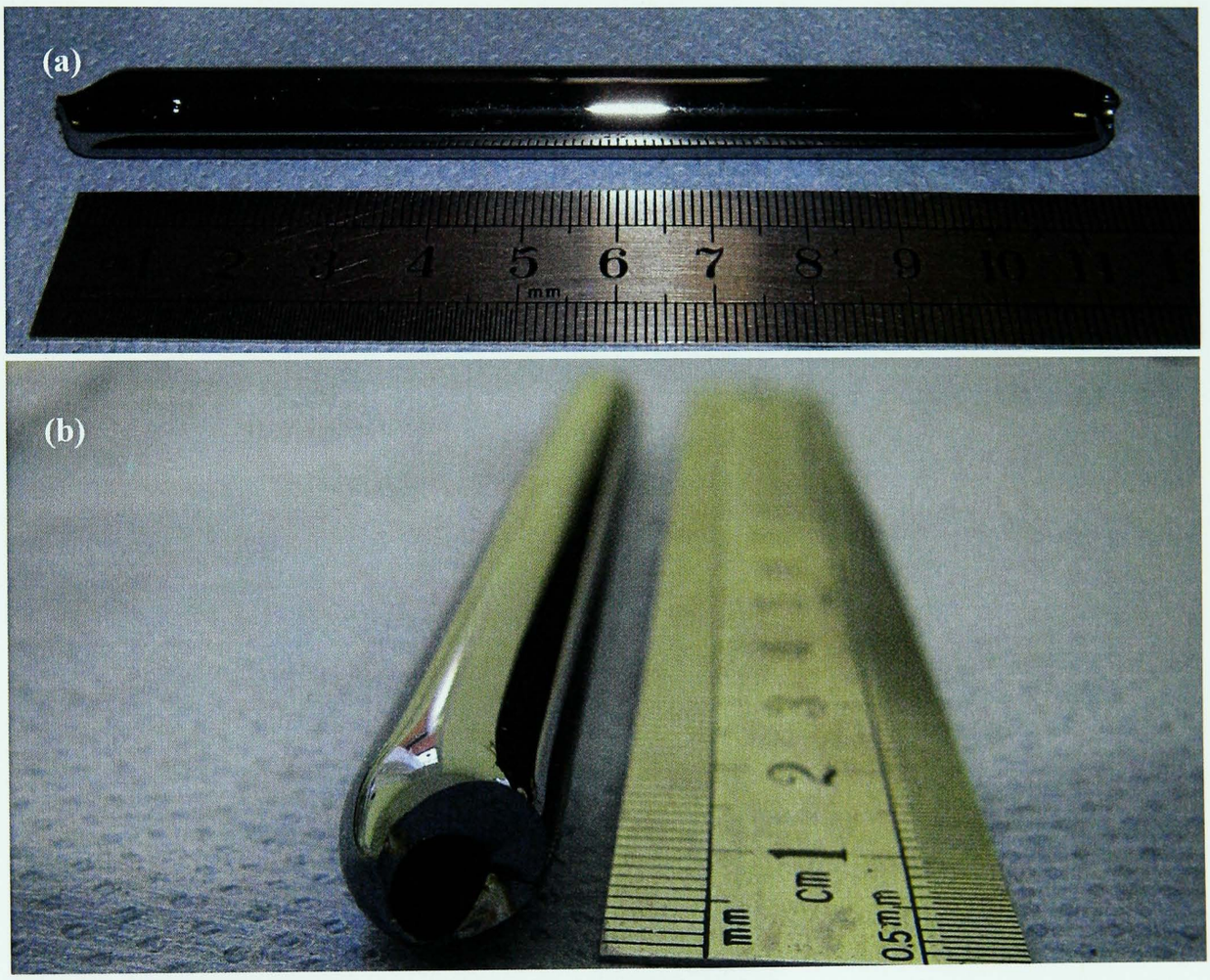

Figure 6.6: RC003 rotational casted jacket tube. (a) The size of RC003 was 115.0 mm length and (b) 5 / 10 mm ID / OD. One glass piece was chipped off during ampoule opening, so the end of the RC003 was not round in shape.

(2) Thin wall $As_{40}Se_{60}$ tube for caning. The first step for producing tube canes was to make thin wall $As_{40}Se_{60}$ tube via the rotational cast technique. A typical thin wall tube required a batch of 10 g to 15 g $As_{40}Se_{60}$. Similar to the preparation of the jacket tube, after melting the ampoule was place in the

rotational cast rig. (i), 10.5 g of As and Se in the ratio $As_{40}Se_{60}$ (ZGLCF017) was batched inside a 10 mm / 14 mm ID/OD ampoule. (ii), the batch $As_{40}Se_{60}$ was melted, rotationally cast as a tube then the tube was annealed in an annealing furnace. The annealing schedule is described in Table 6.1. (iii), after annealing, the $As_{40}Se_{60}$ tube (RC001) was obtained. (iv), the ampoule was carefully broken and the $As_{40}Se_{60}$ tube was removed from the ampoule. The side view of the $As_{40}Se_{60}$ tube (RC001) after it had been taken out of the ampoule is shown in Figure 6.7 (a). The cross-sectional view of the $As_{40}Se_{60}$ tube is shown in Figure 6.7 (b). The RC001 $As_{40}Se_{60}$ tube had an OD = ~10 mm, ID = ~8 mm and a length of 135 mm. The prepared tubes now draw down prior to form canes for later stacking. The cane drawing process will be described in section 6.1.3.

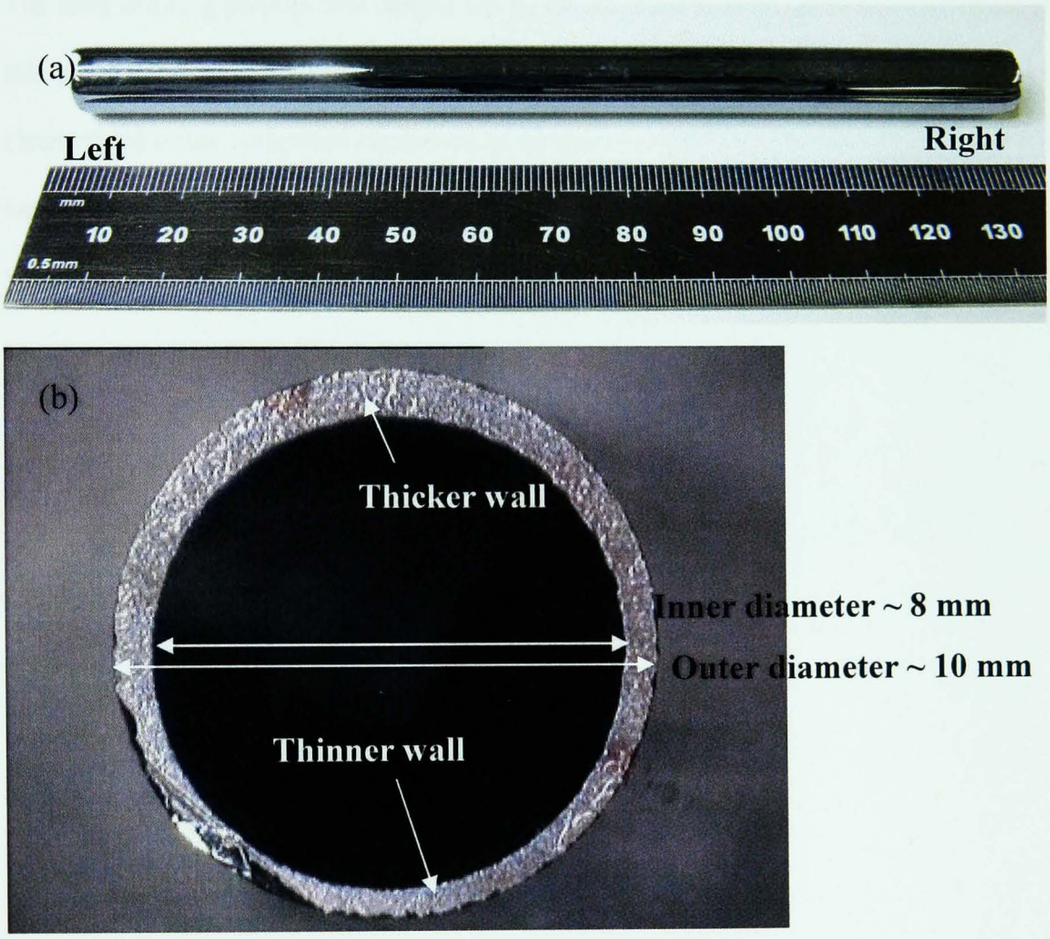

Figure 6.7: Photograph of an as-cast chalcogenide glass tube (RC001). (a) The length of the chalcogenide glass tube is ~135 mm. (b) left side cross-sectional view of the tube; the wall has OD = ~ 10 mm and ID = ~ 8 mm. The wall of tube were not uniform.

6.1.3 Cane drawing and fibre-drawing

Both cane drawing and fibre drawing were carried out using the in-house modified Heathway fibre tower. But as the canes are much thicker than fibres, they were pulled by hand by D. Furniss in this project. This section describes the fibre tower and the cane drawing of the rotationally cast tubes. Table 6.2 shows that $As_{40}Se_{60}$ tube canes HFD003, HFD005 and HFD006 were stacked into rotationally cast jacket tubes RC003, RC006 and RC007 and then fibre-drawn down to produce air / glass samples MOF001, MOF002 and MOF003. This section also describes the fibre drawing of these MOFs.

The fibre drawing process was carried out by Dr. D. Furniss in the University of Nottingham throughout this project. Figure 6.8 shows the fibre tower which was situated in a clean environment (class 10,000 clean room) under controlled conditions of temperature (20 °C). The fibre tower is ~3.0 metres high and has a solid feeding rod, a sample supporter, a preform furnace, a diameter reading sensor, a tensioning wheel and a polystyrene drum.

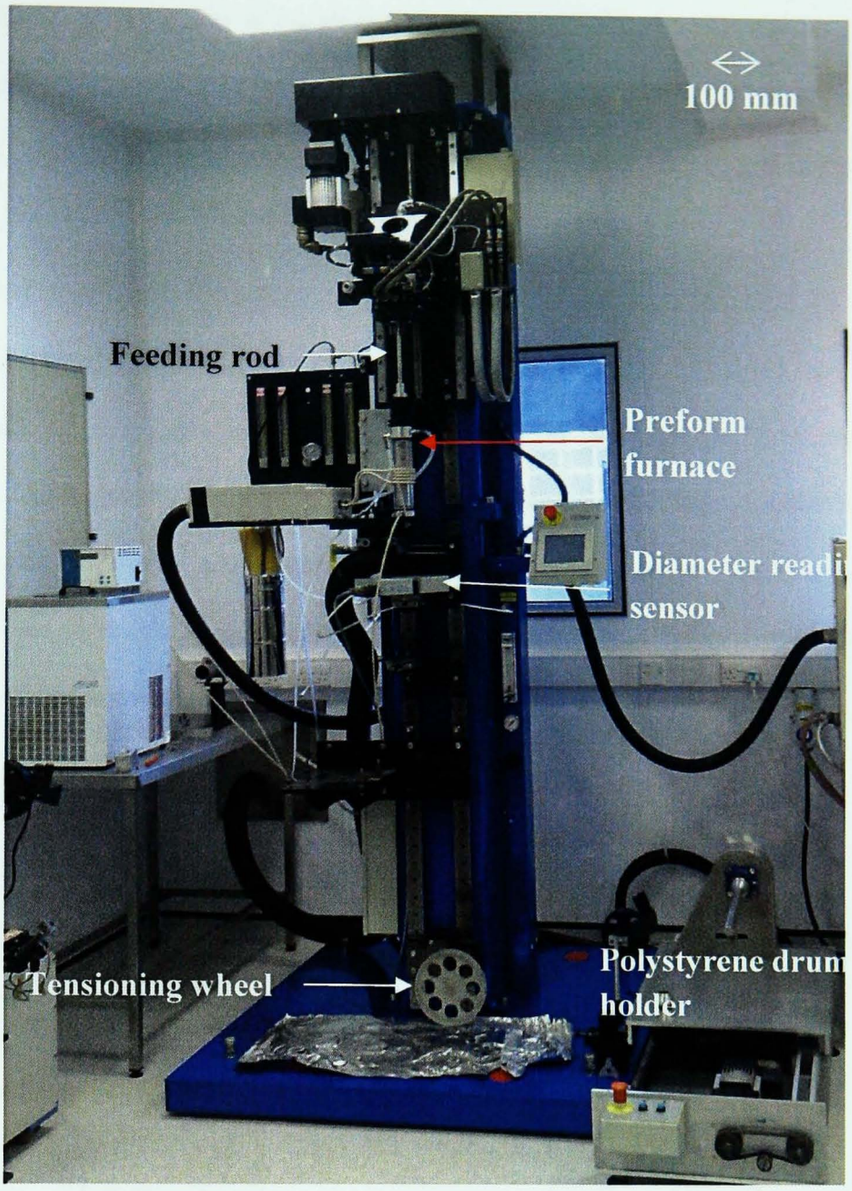

Figure 6.8: Fibre drawing tower situated in a clean environment (class 10,000 clean room) under controlled conditions of temperature (20 °C). The fibre tower was ~3 metres high, has a feeding rod, a sample supporter, a preform furnace, a diameter reading sensor, a tensioning wheel and a polystyrene drum.

Figure 6.9 is a schematic diagram shows that how the fibre preform was held by a clamp and suspended in the preform furnace which surrounded by the flowing cooling water (10°C) of the drawing tower. The bottom of the preform was positioned with approximately 5 mm below the graphite ring (susceptor) which supplies heat to the preform. The graphite ring was heated by radio frequency (RF) waves emitted from a copper coil. The exact temperature inside the furnace could not be measured, as a thermocouple would be heated independently by the radio frequency (RF). The power couple to the susceptor is not known because the size and the material of the susceptor changed the coupled power dramatically. The

RF unit used for applying power in the fibre-tower can supply about 4 kW of power, about 20% power setting is used for fibre drawing [178], so a perfect susceptor would get 800 W, in reality the susceptor get less power [178]. In the current project, the percentage power used by the copper coil was recorded [2].

The copper coil transferred RF energy to the graphite ring causing heating of the ring, and then the graphite ring heated the fibre preform. The heated point of the preform softened and narrowed down as shown in Figure 6.9 (b). Typically, it takes 5 minutes for the heated point of the preform to soften and narrow down. Due to gravity, the bottom part of the preform gradually drops down vertically. The thinner part which is the fibre was passed through a diameter reading sensor which indicates current fibre diameter and then passed through a tensioning wheel and finally reached the polystyrene drum. The fibre was sticked on the drum and pulled by a constant speed.

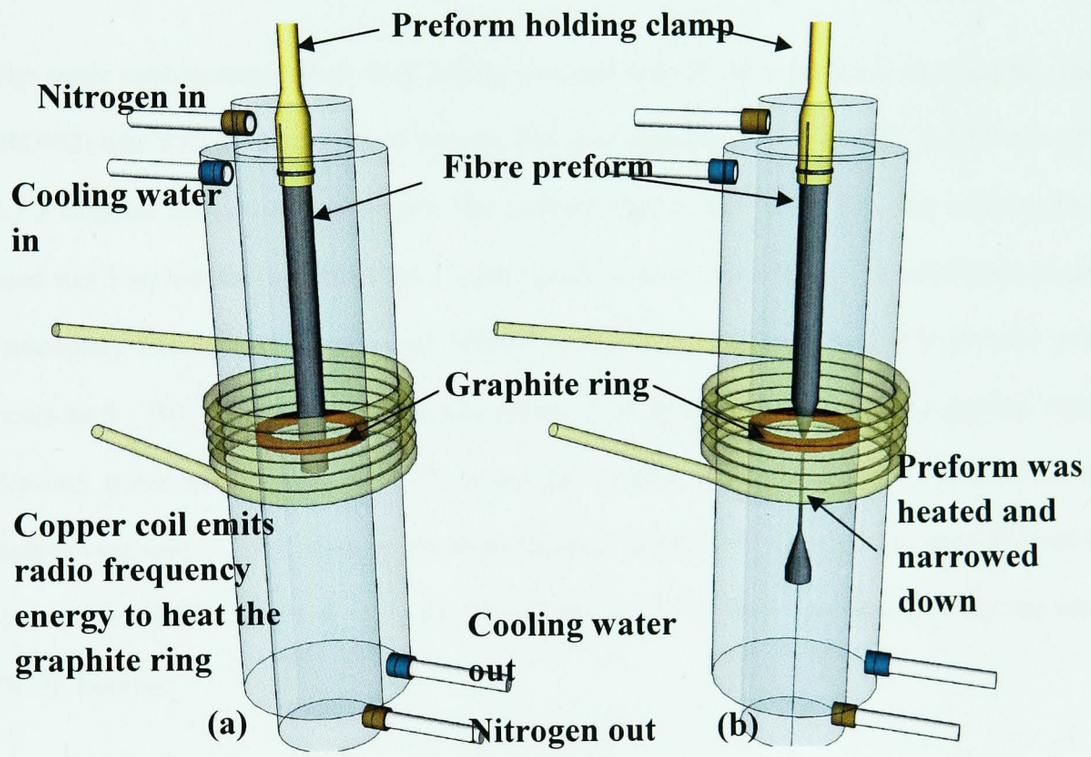

Figure 6.9: Schematic image of the fibre drawing procedure. (a) Here a fibre preform is held by a clamp and hung in the furnace of the tower. The copper coil emits RF to heat the graphite ring. (b) The graphite ring emits heat to the preform and narrow down the lower part.

(3) In a fibre drawing process, the volume fed in is always the same as the volume fed out. Therefore, the preform feed-in speed and the fibre-drawing speed depend on the diameter of the preform ($A_{preform}$) and

diameter of the fibre (A_{fibre}). Equation 6-3 shows the relationship between the feed in rate and the length of the fibre been drawn [2].

$$\frac{A_{fibre}}{A_{preform}} = \frac{L_{preform}}{L_{fibre}} \qquad 6\text{-}3$$

where, $L_{preform}$ is the length of the preform and L_{fibre} is the length of the fibre. Normally, the feed in speed is constant (e.g. 1.5 mm/minute), and change the feed out speed to control the fibre diameter. Therefore, having the diameters of the preform and the desired fibre, it is easy to calculate the feed out speed by giving a feed-in speed.

6.1.3.1 Cane drawing

The water cooling temperature used during cane-drawing of the rotationally cast $As_{40}Se_{60}$ tube preform (RC002) was 5°C; N_2 flowed at 10 ml/min. For cane drawing of tube RC002, the RF was 12% (section 6.1.3 explains the power percentage). The preform feed-in rate was 5 mm/min and the drawing speed used was 5 m/min. the bottom of the $As_{40}Se_{60}$ glass preform was located ~10 mm below the graphite ring (susceptor). The hollow core fibres of HFD001 were pulled down by hand slowly; then the power was cut down to 8 - 9%; then maintained at this power level throughout. There was a gradual increase in the drawing speed to 6.7 m/min to 7.5 m/min for producing thinner canes. As table 6.2 shows, two hollow-core canes (HFD) were drawn from $As_{40}Se_{60}$ RC002. HFD001 has 440 μm OD (wall thickness ~ 20 μm) and HFD002 has 1.0-1.2 mm OD (wall thickness ~50 μm). The cane-drawing was carried out by Dr. D. Furniss.

Environmental Scanning Electron Microscope (ESEM) was employed to image the quality of a typical tube cane (HFD001). Figure 6.10 (a) shows the end image of the HDF001 sample, the OD of the cane was ~440 μm and the outer and inner surfaces were smooth. The crack seen at the bottom was due to cleaving. Figure 6.10 (b) shows the cross-sectional view of the HDF001. The cane was unfortunately oval and the thickest part of the hollow fibre wall was measured to be 21.8 μm and the thinnest part of the wall was 16.6 μm. The canes will be later stacked inside of jacket tube to form preforms.

The elliptical shape of the hollow fibre was due to the ampoule containing the batch not being located in the centre of rotation during rotational casting. Thus the tube (RC002) had one side thicker than the other which can be observed from Figure 6.6 (b). During the fibre drawing process, the heat would not distribute uniformly, therefore, the elliptical shape was maintained and the fibre (HFD001) wall thickness was not redistributed. A good centralisation of the ampoule during rotational casting ensures the uniformity of tube wall thickness.

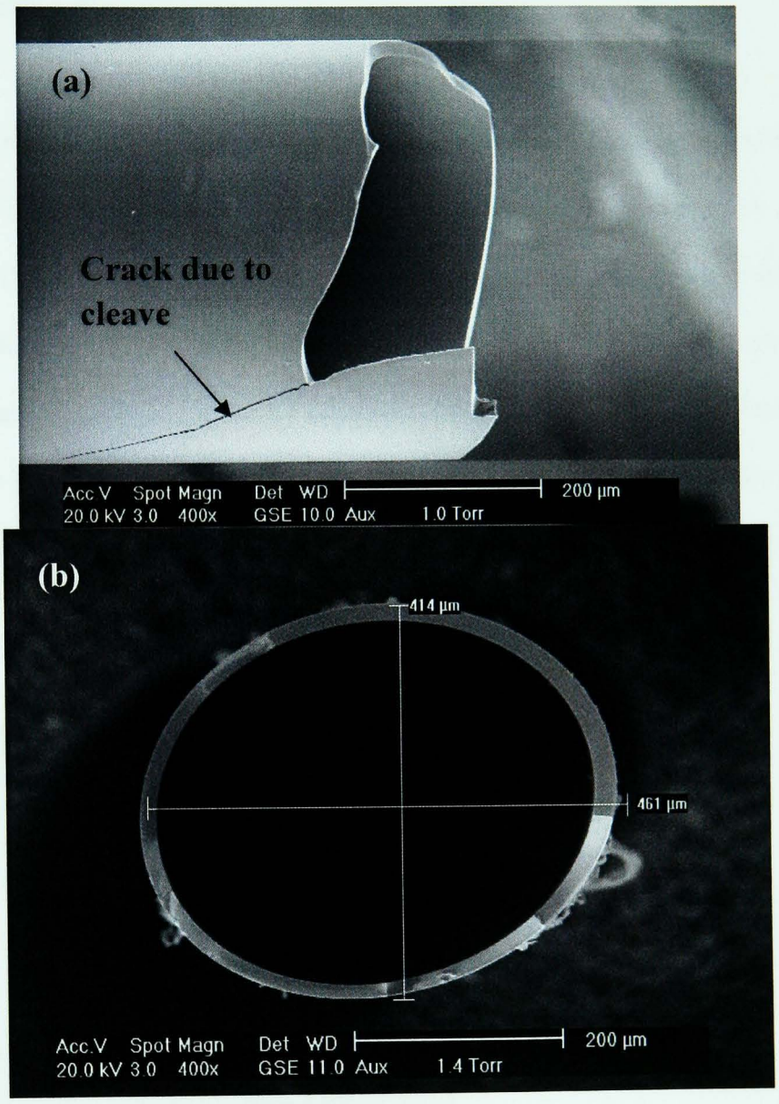

Figure 6.10: ESEM images of $As_{40}Se_{60}$ hollow fibre (HFD001, see Table 6.2). (a) One end of HFD001, the cleaving caused the cracks and (b) The cross - sectional shape of the fibre was oval; the wall thickness of the thinner part was 16.6 µm and thicker part was 21.8 µm.

6.1.3.2 Hollow core MOF drawing

(i) MOF001: The rotationally cast $As_{40}Se_{60}$ tube RC003 (5/10 mm ID/OD) was used as the jacket tube of the MOF001 preform. 18 $As_{40}Se_{60}$ tube canes HFD001 (~400 μm) were stacked as cladding surrounding one HFD002 (1.2 mm) core into the jacket tube to produce the MOF001 preform as shown in the schematic diagram in Figure 6.1 (a). The fibre drawing procedure was similar to that used for producing canes as described in section 6.1.2.

Several lengths of 20 mm fibre was cleaved from the drawn MOF001 fibre and viewed *via* reflection optical microscopy. Figure 6.11 shows a cross-sectional view of the hollow core $As_{40}Se_{60}$ MOF (MOF001). The MOF (RC003) was drawn to an outer diameter of ~ 300 μm. The outer jacket tube drawn was relatively round and solid. However the inner tubes (HFD001 and HFD002) were no longer stacked in the order the schematic diagram in Figure 6.1 (a) shows. Furthermore, all the inner fibres tended to fall apart and stick to the wall of the jacket tube. The reason that caused the inner structure to become disordered may be that the drawing RF power used was too high. Therefore, in the next experiment, the drawing power should be decreased.

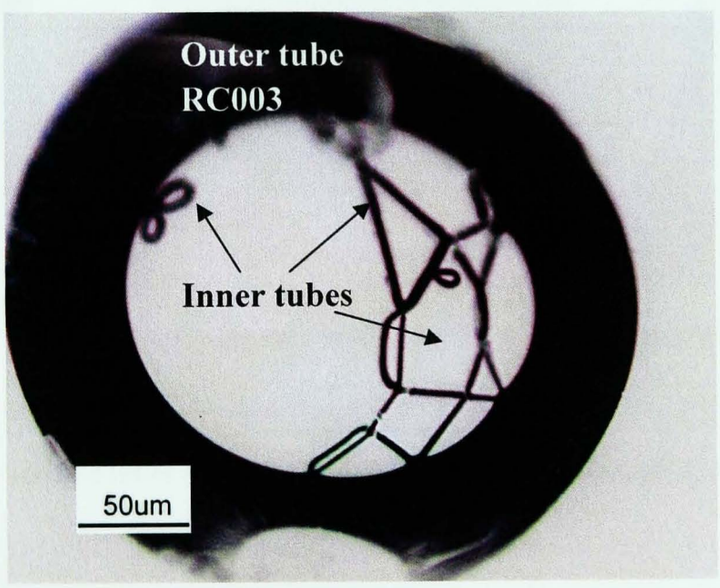

Figure 6.11: Cross-sectional view of a typical $As_{40}Se_{60}$ MOF (MOF001) *via* optical reflection microscopy. The outer $As_{40}Se_{60}$ tube (RC003) was drawn to ~ 300 μm. The inner stacked tubes (HFD001 and HFD002) tended to fall apart and stick to the wall of the jacket tube (see Table 6.2).

(ii) MOF002: The rotationally cast $As_{40}Se_{60}$ tube RC006 (5.6/10 mm ID/OD) was used for the jacket tube of MOF002 preform. Again 18 $As_{40}Se_{60}$ tube canes HFD004 having diameter 400 μm were stacked inside tube RC006 as in the schematic diagram shown in Figure 6.1(a) in section 6.1.

The MOF001 results showed that the drawing RF of 18% may be too high for hollow core MOF, therefore the initial RF used for MOF002 fibre drawing decreased to 12 % (typical RF for cane drawing). However, because the power was too low to draw the outer jacket tube, the RF then been increase to 17%. Around 100 meter fibre was drawn (MOF002). Several lengths of 20 mm fibres were cleaved from MOF002 and imaged *via* reflection optical microscopy. Figure 6.12 shows a cross-sectional view of the air / glass $As_{40}Se_{60}$ MOF002. The $As_{40}Se_{60}$ MOF (MOF002) was drawn to a diameter of ~ 280 μm. However the results were similar to MOF001. The inner tubes HFD004 were no longer stacked in order and all the inner fibres tended to fall apart and stick to the wall of the outer tube.

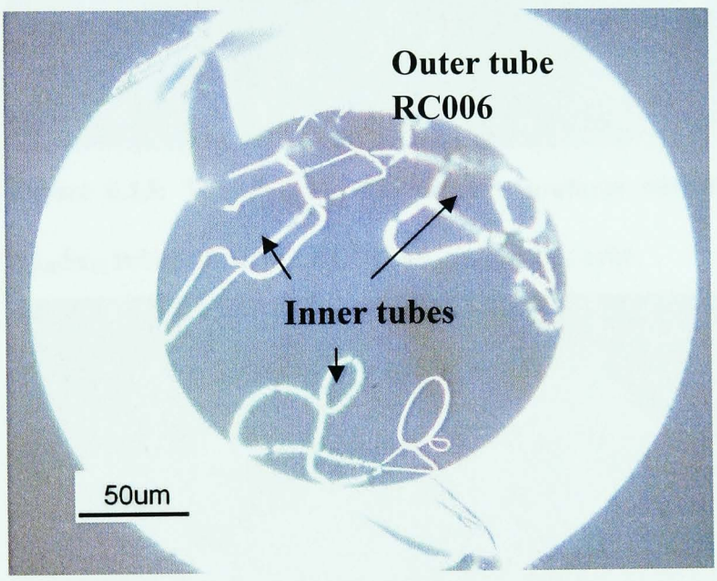

Figure 6.12: Cross-sectional view of a typical $As_{40}Se_{60}$ MOF (MOF002) *via* reflection optical microscopy. The $As_{40}Se_{60}$ jacket tube (RC006) was drawn to a radius of ~ 180 μm. The inner stacked tubes (HFD004) tended to fall apart and stick to the wall of the jacket tube (see Table 6.2).

Both MOF001 and MOF002 demonstrated that the jacket tubes could be successfully drawn to a standard optical fibre dimension (i.e. 125 μm), but that the inner structures can not be maintained. A possible reason could be that the large viscosity change during the fibre drawing process made the thin walled

(approximately 16-21 μm) $As_{40}Se_{60}$ tube canes lost their initial structure. The solution is to use relatively thicker wall tube canes which will be described in next trial of MOF003.

(iii) MOF003 preform was constructed from small tube canes which have thicker walls (ID/OD = 150/280 μm) and rotationally cast $As_{40}Se_{60}$ jacket tube RC007 as Figure 6.13 illustrates. The RF used was 18 %, and then the preform was drawn down to fibre MOF003 as Figure 6.13 shows. Hollow core MOF003 was formed, but the uniform size of the inner hollow core tubes was not maintained throughout. Some of the hollow core fibre tubes had even closed.

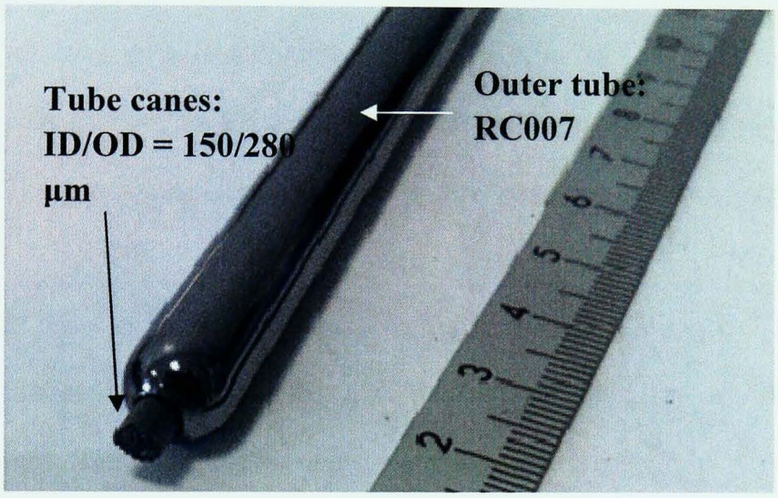

Figure 6.13: The $As_{40}Se_{60}$ hollow core preform MOF003, stacked from ID/OD = 150/280 μm $As_{40}Se_{60}$ tubes fibre into RC007$As_{40}Se_{60}$ jacket tube.

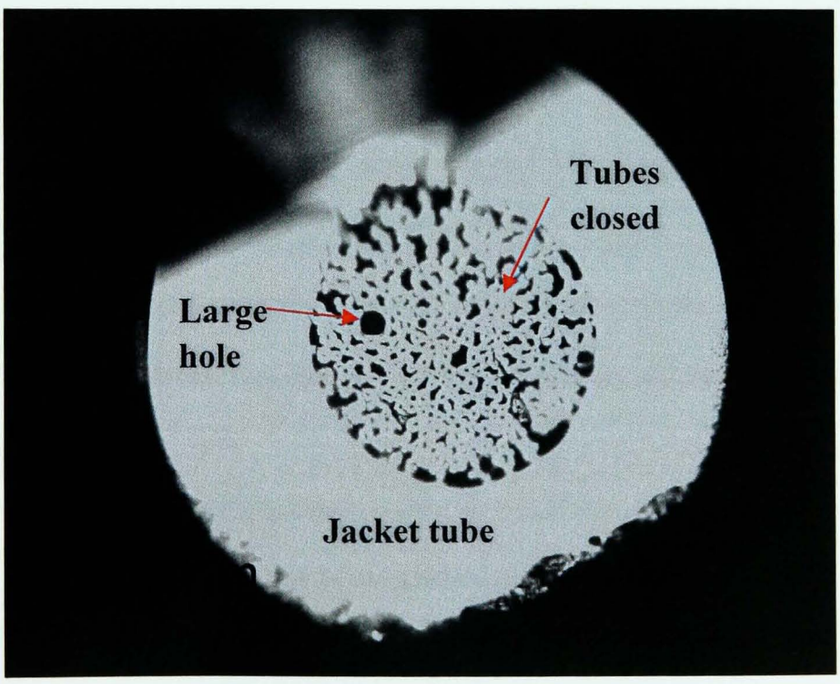

Figure 6.13: Cross-sectional view of the fibre drawn from the $As_{40}Se_{60}$ hollow core MOF (MOF003) preform. The size of the inner hollow core tubes was not maintained to be identical. Some of the hollow core fibres had even closed.

6.1.4 Discussion: work towards hollow core Microstructured Optical Fibre

Fabrication of single glass composition hollow core MOF was one of the objectives of this PhD project. Air core fibres are intriguing because light can be confined in an air (or liquid filled) core. Light is primarily in the air but not in solid materials, so potentially hollow core fibre could guide light at wavelengths for which transparent materials may not available. Compared with solid core fibres, air core fibres partially solve the problems caused by intrinsic and extrinsic absorption bands in the transmission windows, so hollow core fibre is more suitable for power delivery applications [2]. From a fabrication point of view, the advantage of air hole hollow core MOF is that only one glass composition is required. Thus, during the fabrication, there is no need to worry about any thermal expansion coefficient mismatch.

In this project, three attempts were reported to fabricate hollow core MOF in chalcogenide glasses. The preforms were successfully made but the desired hollow core MOFs were not successfully drawn from them. The reasons of the failures include:

(1) Failure to produce uniform chalcogenide glasses tubes. To make a MOF perform, several thin walled chalcogenide glass tubes were caned from a rotationally cast tube and stacked into a jacket tube. The wall thickness of the rotationally casted tube was not uniform due to the ampoule position not being central during the rotational casting process. As a result, an elliptical shape hollow cane was obtained. Later, the elliptical shape canes were stacked together into jacket tube. The non-uniform canes may distort the heat distribution during fibre drawing. The results of MOF001 and MOF002 fibres showed that all the inner canes were attached to the jacket tube and the shape was distorted.

The recommendation to overcome the wall thickness uniformity problem is to make a precisely designed ampoule alignment holder in the rotational casting rig.

(2) Failure to maintain the intended structure during fibre drawing. In experimental MOF003, the results showed the stacked canes had a large diameter variation after fibre drawing. This is partially because of the non-uniformity of the canes, but also there was no internal pressure applied to support each

individual cane. During the fibre drawing process, the heat applied to the fibre was high enough to soften the $As_{40}Se_{60}$ preform. Therefore, the surface tension of each cane will be high, yet the tube canes contract themselves. This situation causes some of the tubes to close during fibre drawing.

The recommendation is to apply an internal gas pressure (e.g. nitrogen or argon gas) into the MOF preform during fibre drawing. In this case, the air pressure could expand each individual cane to balance their surface tension. But because chalcogenide glasses are less robust than SiO_2 glass (section 2.5.3), a suitable gas flow rate needs to be determined experimentally and the power for fibre drawing may also need to be modified. As can be seen the production of the MOF preform is a costly and time consuming procedure.

Despite the big advantages of single composition hollow core MOF, the results of the fabrication trials demonstrated that achieving the desired air core chalcogenide glass MOF structure remains a challenging goal. The main difficulties of fabricating the desired structure using a stack-and-draw method is because the viscosity curves of non-silica glasses (lead silicate, telluride and chalcogenide glasses etc) are steep [179], therefore, it is hard to control the drawing conditions and speed to fabricate a holey cladding hollow core MOF that conforms to a specific design and meets the required tolerances. Consequently, the optical properties of many fabricated non-silica glass hollow core MOF show large deviation from the initial design target [179]. One way to overcome the fabrication problems that single glass composition hollow MOF faced is to use all solid two glass compositions with high refractive index contrast. This is described in detail the next section (section 6.2).

6.2 Solid core Microstructured Optical Fibres reslised using two glass compositions

For fabricating all solid MOFs, there will be no internal air pressure required. So this reduces the fabrication difficulty during fibre drawing. But in order to produce a refractive index contrast, two glass compositions with sufficient refractive index difference and matched thermal properties were required. After the study of the properties of some of the chalcogenide glasses in chapter 4, $As_{40}Se_{60}$ was chosen

for the core and $Ge_{10}As_{23.4}Se_{66.6}$ was carefully chosen as the cladding for solid core MOF (replacing the holes of the holey fibre). $Ge_{10}As_{23.4}Se_{66.6}$ is chosen because it has a Tg close to that of $As_{40}Se_{60}$, so co-extrusion and the stack and draw technique can be realised. Also, in order to confine light through the core, it requires that the core material has a refractive index (n) sufficiently larger that of the cladding material. The n of $As_{40}Se_{60}$ and $Ge_{10}As_{23.4}Se_{66.6}$ are 2.824 and 2.655 at wavelength of 1.55 μm, respectively and this refractive index difference is sufficiently large for optical guiding [155]. Calculations preformed by G. Athanasiou (PhD student) at the University of Nottingham that the refractive index contrast of $As_{40}Se_{60}$ and $Ge_{10}As_{23.4}Se_{66.6}$ is sufficient to permit periodic photonic crystal with bandgaps for an axial wavevesctor component consistent with propagation within a defect core [155]. This enabling multiple layers structures that exhibit large mode area and endless single mode behaviour. A one layer cladding MOF is proposed in this work to test the feasibility of fabricating all-solid multi-component chalcogenide glasses MOF. A one layer structure is studied because its fabrication is relatively simple. If a one layer cladding all-solid MOF could be fabricated using the multi-component chalcogenide glasses, in principle, complex structured MOF can also be fabricated, including multiple cladding layers and variable core diameter MOFs.

To prepare the preform of the two-glass-composition solid core MOF, several components were required: an $As_{40}Se_{60}$ core, $Ge_{10}As_{23.4}Se_{66.6}/As_{40}Se_{60}$ core/cladding canes and an $As_{40}Se_{60}$ jacket tube which is shown in the schematic diagram of Figure 6.14. The assembly required for stacking this preform include: (1) an $As_{40}Se_{60}$ glass jacket tube fabricated via rotational casting which was described in section 6.1.2; (2) one $As_{40}Se_{60}$ fibre which would locate centrally as the core and (3) Seven $Ge_{10}As_{23.4}Se_{66.6}$ /$As_{40}Se_{60}$ core-clad canes stacked around the core fibre. The core-clad canes were cane-drawn from core/cladding rod made via extrusion as described in the next sub-section (section 6.2.1).

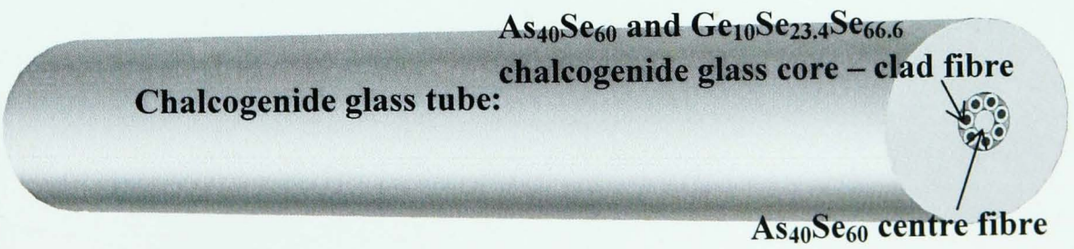

Figure 6.14: schematic diagram of an all-solid MOF preform. In the jacket tube, there are several canes including a core and cladding canes.

6.2.1 $Ge_{10}As_{23.4}Se_{66.6}$ and $As_{40}Se_{60}$ core/cladding extrusion and cane-drawing

The chalcogenide glass core/clad fibre preform was extruded using an extruder which had been in-house designed and built by Dr. D. Furniss [108]. A photograph of the extruder is provided in Figure 6.15 (a). The extruder was ~3 metres high and worked vertically with a nitrogen gas pipe connected. The load which the extruder could supply was up to ~2 kg. A thermocouple was embedded within the die. The extruder was linked to a computer which could record the load, die and furnace temperature using Pico Technology logging software. Figure 6.15 (b) shows the graphite-lined stainless steel die. The extrusion die used in the current work was designed with an orifice hole that allows the chalcogenide billet to extrude through at high temperature and shape the chalcogenide material to the desired shape. To produce a core/cladding rod of glass, the core and cladding glass pair were co-extruded [2] from solid glass boules. Figure 6.15 (c) shows a schematic diagram of the graphite lined stainless steel die and the bobbin was placed inside the barrel of the extruder with boule glasses. The barrel was located approximately in the middle of the extruder furnace [108, 112]. A detailed experimental process will be described in this section.

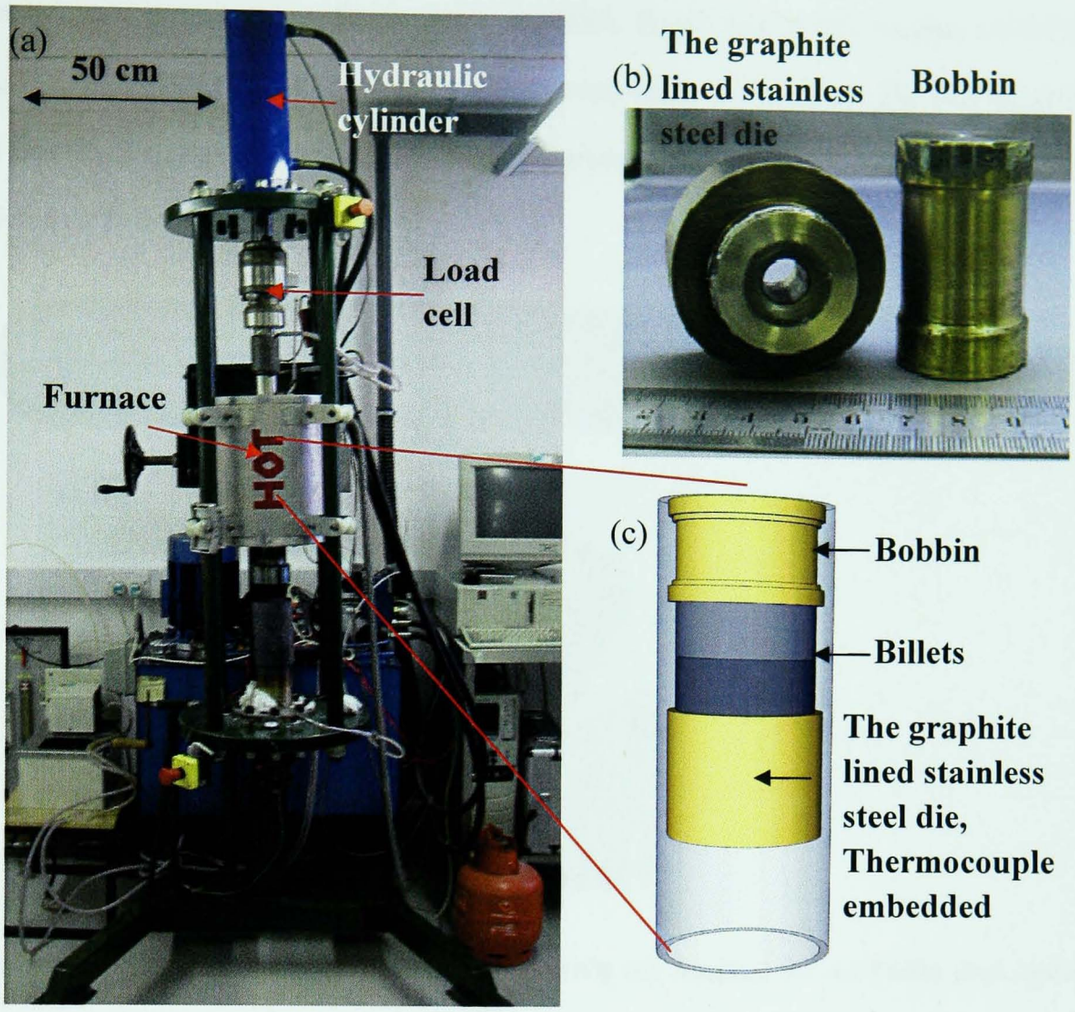

Figure 6.15: (a) The extruder, the hydraulic cylinder was located on the top which supply load to the load cell. (b) The graphite lined stainless steel die and bobbin. (c) Schematic diagram of the barrel which located in the middle of the furnace. The graphite lined stainless steel die and the bobbin were placed inside of the barrel of the extruder with glass billets in between.

1) Raw materials in the correct batch ratio for making the desired chalcogenide glass composition (e.g. purified As and Se) were batched inside of a 29 / 33 mm ID/OD silica glass ampoule that had been shown in Figure 6.16 (a) to produce chalcogenide glass billets. The silica ampoule (supplied by Multi-Lab Ltd) had OH level < 1ppm with one end sealed. The ampoule with the batched materials was sealed under vacuum (8×10^{-5} mbar) as described in section 3.1.2. Typically, to produce an $As_{40}Se_{60}$ boule, the batch weight was 90 g and resulted in a billet roughly 20 mm height. The batched chalcogenide glasses were melted in the rocking furnace as described in section 3.1.3.

95 g of $Ge_{10}As_{23.4}Se_{66.6}$ (ZGLCF034) and 97 g of $As_{40}Se_{60}$ (ZGLCF031) glasses were each melted and annealed. The two boules were cut to 15 mm height and the surfaces, which would later mate inside the

extruder, were ground then polished to a 1 μm finish. Figure 6.16 shows $As_{40}Se_{60}$ (ZGLCF031) and $Ge_{10}Se_{23.4}Se_{66.6}$ (ZGLCF034) boules of 29 mm diameter ready for extrusion. The $As_{40}Se_{60}$ (ZGLCF031) and $Ge_{10}Se_{23.4}Se_{66.6}$ (ZGLCF034) chalcogenide glass boules were then located on top of the die with the polished surfaces in contact.

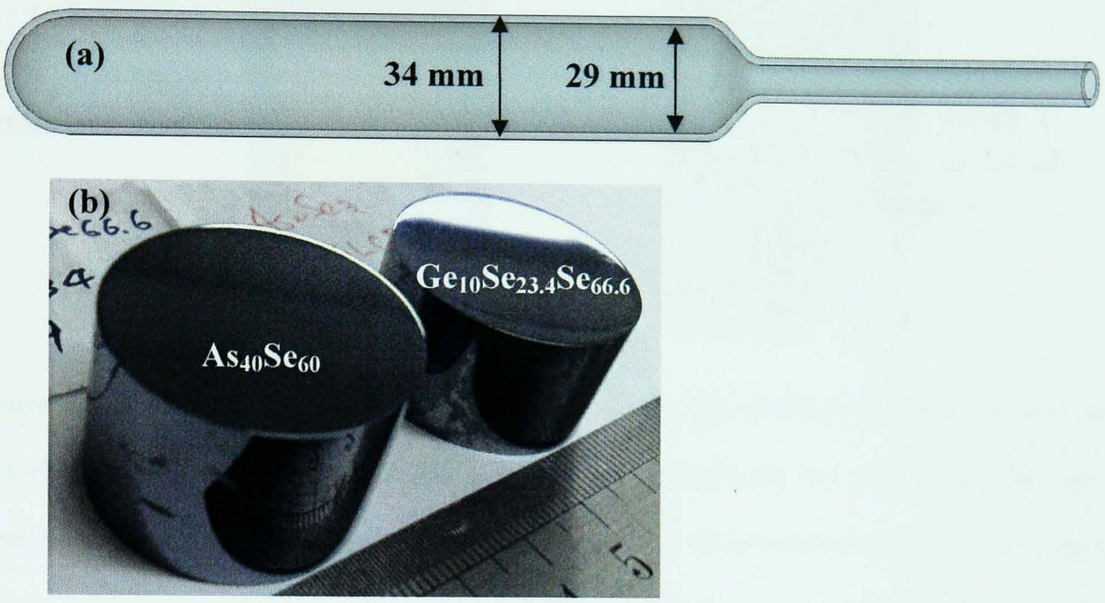

Figure 6.16: (a) Boule ampoules 29/34 mm ID/OD; (b) $As_{40}Se_{60}$ (ZGLCF031) chalcogenide glass boules of 29 mm diameter, 15 mm height and $Ge_{10}Se_{23.4}Se_{66.6}$ (ZGLCF034), chalcogenide glass boules of 29 mm diameter, 16 mm height. The end surfaces of both boules were polished to a 1 μm finish (see section 3.1.4). The vertical curved surfaces of each boule were glossy and "as - annealed".

2) The boule (or billets) were loaded into the extruder barrel and abutted such that, in the vertical position, the cladding glass was located underneath the core glass in the barrel and closer to the die [112]. In the current work, the $As_{40}Se_{60}$ was placed underneath as the cladding of the ultimate extruded preform and the $Ge_{10}Se_{23.4}Se_{66.6}$ was place on the top as the core. The bobbin was placed on top of the core glass boule (Figure 6.17). The size of the preform depends on the height and the diameter of the boules. The diameter of the boule is about 29 mm because the ampoule used has 29 mm ID. The thickness of the cladding of the core/clad preform is depends on the length of the boule located at the bottom. A longer boule resulted thicker cladding and vice versa. Prior to loading into the extruder, the mating surfaces of the glass boules were polished to a 1 μm finish.

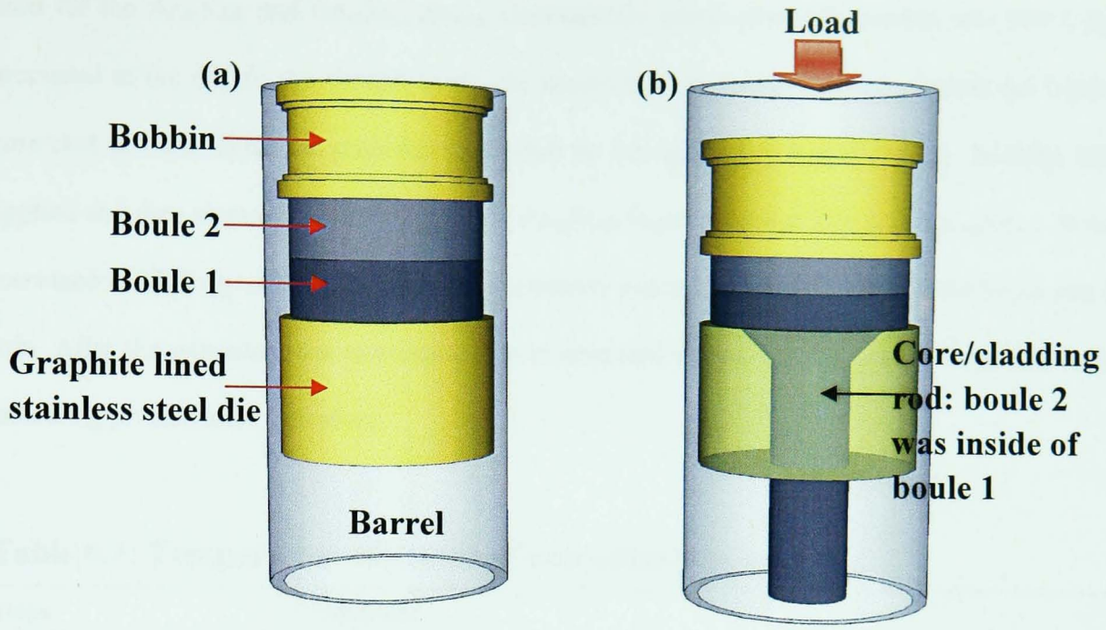

Figure 6.17: Schematic diagram of extruder barrel. (a) The cladding material boule 1 and core material boule 2 were located in the extruder barrel between the bobbin and graphite lined stainless steel die. (b) Heat and vertical load were applied downwards to boule 1 and boule 2. Boule 1 then became the cladding glass of the fibre optic preform and boule 2 was the core glass, therefore, core/clad structure was formed.

3) Nitrogen (supplier: BOC) atmosphere was applied to the barrel during the entire extrusion process to reduce the likelihood of oxidisation, e.g. when the furnace began to heat from RT to the extrusion temperature. To achieve this, above and below where the boules were located in the extruder barrel were purged with nitrogen (supplier: BOC; oxygen-free) at a flow rate ~500 ml/min surrounding the chalcogenide glass boules during the entire extrusion process. Typically, the furnace of the extruder was heated gradually at a rate ~200˚C/h to heat the entire assembly to 40-50 ˚C above Tg before the load was applied. The temperature of the furnace was controllable and the temperature of the chalcogenide supercooled melt was measured using a thermocouple embedded within the die; both temperatures were recorded using the Pico Technology logging software.

4) Figure 6.17 (b) shows schematically the application of load inside the extruder. During the temperature increases to the extrusion temperature, the viscosity of the boules decreases. The supercooled melt was pushed through the orifice of the die by the bobbin. The applied load and the position of the bobbin were detected and recorded by the Pico Technology logging software. Typically, the extrusion temperature

used for the $As_{40}Se_{60}$ and $Ge_{10}Se_{23.4}Se_{66.6}$ chalcogenide glass core-clad preform was 225°C which was measured at the die. In the current work, the application of the extrusion load used for fabricating the core/clad preform used the procedure provided by Savage [112] and Rowe [2]. Initially 500 kg was applied and then increased to 1000 kg as the $As_{40}Se_{60}$ began to merge into $Ge_{10}As_{23.4}Se_{66.6}$. It was further increased to 2000 kg towards the end of the extrusion process. The feed-in rate of the boule was 0.25 mm/ min. After the extrusion, the extruded rod was annealed at rate 100 °C / hour. Table 6.3 describes the annealing process after extrusion.

Table 6.3: Temperature schedule of extrusion process.

Steps	Schedule
1	RT → 220°C @ 300°C/60min
2	Dwell @ 220 °C during extrusion
3	220°C →RM @ 100°C/60min

The first part of the extrudate to emerge from the die was monolithic $As_{40}Se_{60}$ preform rod, this was followed by the second part of the extrudate which was a step index, core/cladding rod of $Ge_{10}As_{23.4}Se_{66.6}$ / $As_{40}Se_{60}$. Figure 6.19(a) shows a photograph of the extruded $Ge_{10}As_{23.4}Se_{66.6}$ core / $As_{40}Se_{60}$ cladding optical fibre preform (extrusion preform EP001), whose length was 300 mm and outside diameter was 9 ± 0.4 mm along the length, as estimated from previous work by Savage *et al.* [112]. The preform was straight (within ~1 mm) and its outer surface was smooth and glossy. Figure 6.18 (b) depicts a schematic diagram of the extruded preform rod showing the % total cross-sectional core area, with respect to the total, as estimated from Savage [112].

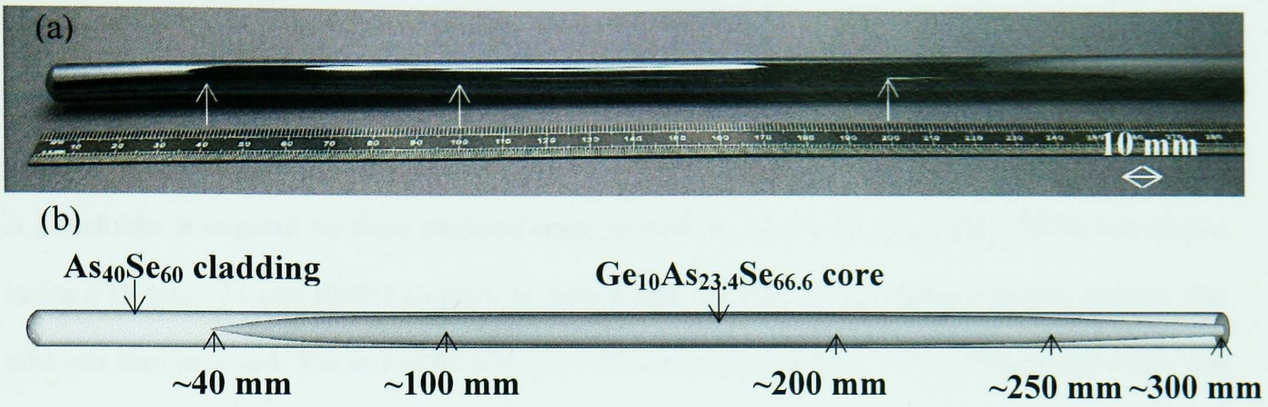

Figure 6.18: (a) Extruded $Ge_{10}As_{23.4}Se_{66.6}$ core / $As_{40}Se_{60}$ cladding optical fibre preform (EP001, extrusion preform); preform length was 300 mm and outside diameter was 9 ± 0.4 mm along the length. Note that the preform was straight (within ~1 mm) and its outer surface was smooth and glossy (the wide angle photograph is somewhat distorted, with spurious preform surface reflections). (b) Schematic diagram of the extruded preform rod shown in (a); % total cross-sectional core area, with respect to the total, was estimated from Savage *et al.* [112], to be slightly larger than 0 % (core started to appear) at ~ 40 mm along the preform rod and ~ 60% at 80 mm along the preform.

The extrudates are required to be cane-drawn to produce canes which later used for preform stacking. The dimensions of the canes stacked into the jacket tube should be slightly smaller than the required dimension to avoid fraction between the canes and the tube during stacking process. Therefore, the diameter of the $As_{40}Se_{60}$ core used 1.2 mm and the diameter of the core/cladding layer used 1.0 mm to fill the 3.8 mm diameter hollow core of the tube. As shown in Figure 6.18 (b), the first 40 mm of the extruded $As_{40}Se_{60}$/ $Ge_{10}As_{23.4}Se_{66.6}$ core/cladding rod was $As_{40}Se_{60}$, which was cane-drawn to obtain ~ 1.2 mm $As_{40}Se_{60}$ cane to stack in the preform as a core. The rest of the extruded core/cladding rod was then drawn into several ~1 mm diameter core-clad canes of length about 140 mm. The cane draw process was done by D. Furniss using the fibre tower as described in section 6.1. This cane drawing process is done by hand; therefore, the drawing rate was not accurately controlled and monitored. The diameters of the canes were not identical. This problem brings difficulties in stacking and may also affect final geometry of the MOF. In this PhD project, the way this problem was overcome was to draw a very long cane from one preform and chop the cane into short segments. Segments which have similar diameters (1.0 ± 0.1 mm) were then

chosen as shown in Figure 6.19. $As_{40}Se_{60}$ canes for the core of MOFs were produced in the same procedure as the first section of the extruded rod.

A jacket tube is required for these prepared canes to stack in. 34.7 g $As_{40}Se_{60}$ (ZGLCF036) was melted inside a 10 mm / 14 mm ID/OD ampoule to form a tube (RC008) using rotational casting method. The tube was then annealed. The size of RC008 was 140 mm length and 3.80 / 9.95 ± 0.01 mm ID / OD. The RC008 was then used as the jacket tube as shown in Figure 6.20. The MOF004 preform was assembled by stacking eight fibres into the RC008 $As_{40}Se_{60}$ tube: one $As_{40}Se_{60}$ fibre (1.2 mm) was stacked in the middle as a core; seven $Ge_{10}As_{23.4}Se_{66.6}$ (ZGLCF034) / $As_{40}Se_{60}$ (ZGLCF031) core-cladding fibres (1.0 mm diameter) were stacked to surround the core fibre as the schematic diagram of Figure 6.15 showed.

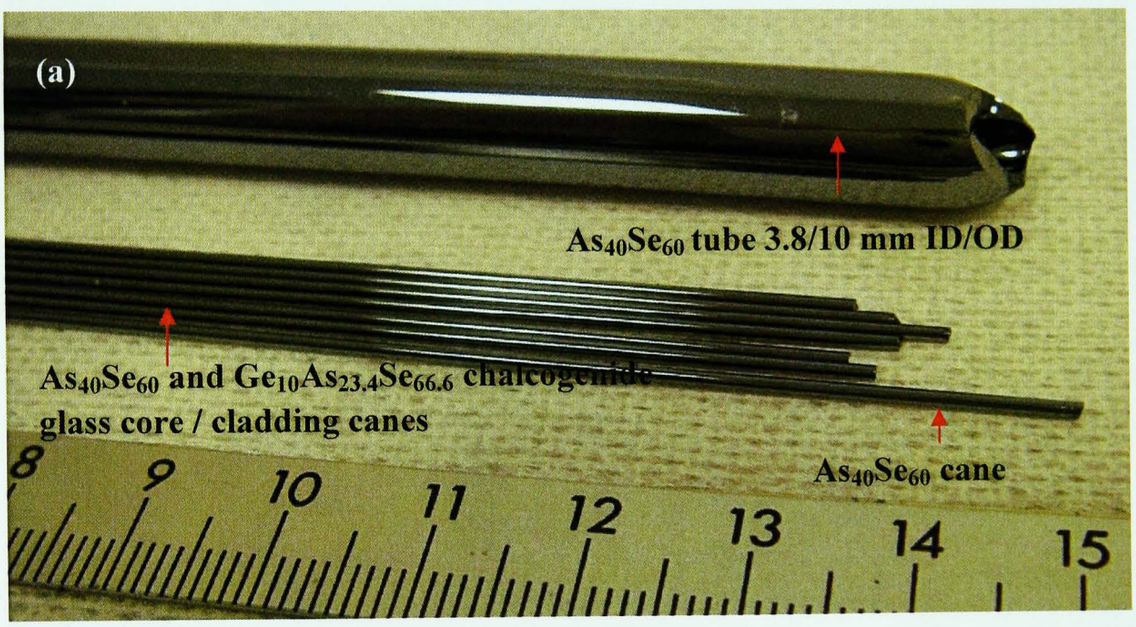

Figure 6.19: (a) The 1.2 mm diameter $As_{40}Se_{60}$ (EP001) chalcogenide central glass fibre and seven 1.0 mm diameter $Ge_{10}As_{23.4}Se_{66.6}$ (ZGLCF034) core / $As_{40}Se_{60}$ (ZGLCF031) cladding surrounding glass fibres (EP001) and a 3.8/10 mm ID/OD $As_{40}Se_{60}$ glass tube (RC008).

6.2.2 Fibre-drawing of the solid core MOF004 and results

The MOF004 fibre was drawn under control, to be of OD from 86 μm to 370 μm, and wound on a custom-built winder. The fibre drawing process was done by Dr. Furniss with assistance by the current

author. A cross-sectional view of a typical cross-section of the drawn fibre MOF004 was obtained by means of ESEM and optical microscopy. Figure 6.20 illustrates the ESEM image of the MOF004 core / cladding structure: the assembled preform had coalesced during the fibre drawing procedure and there was heptagonal packing of the fibres surrounding the central fibre. Figures 6.22 (a) and (b) show the optical microscope images of the structure: (a) 377 μm outer diameter MOF004 fibre which had a 52.6 μm core and (b) 86 μm outer diameter MOF004 fibre which had a 12.5 μm core. The optical micrograph images clearly show the micro-structuring of the seven circles ($Ge_{10}As_{23.4}Se_{66.6}$, ZGLCF034) formed a ring shape and surrounded a core ($As_{40}Se_{60}$, ZGLCF031).

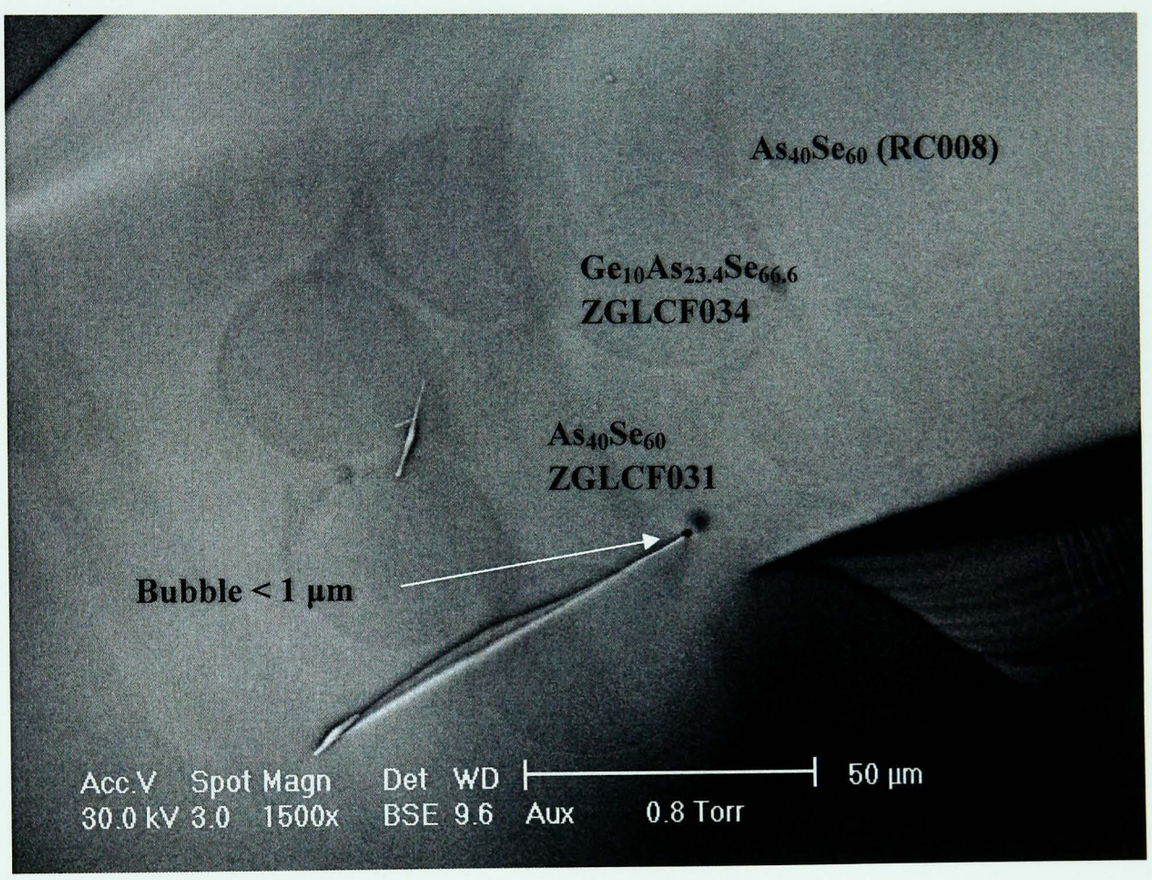

Fig. 6.20: ESEM image of a cross-section of MOF004 fibre which is seven $Ge_{10}As_{23.4}Se_{66.6}$ (ZGLCF034) fibres (EP001) surrounding a central $As_{40}Se_{60}$ (ZGLCF031) core. One bubble was found at the interface between the core and cladding in this particular cross-section.

Figure 6.21 (a) and (b) shows 377 μm and 86 μm OD solid MOF. The one layer cladding was clearly observed from these images. These images gave evidence that the geometrical proportions of the assembled MOF preform were largely maintained during the fibre drawing process. The all-solid chalcogenide glass MOF is much easier in fabrication compared to air/glass hollow core MOF

microstructuring. In general, all-solid chalcogenide glasses MOF seems a good way to overcome the fabrication difficulties that occurred in hollow chalcogenide MOF fabrications.

Measurements taken from the optical micrographs (Figure 6.21 (a) and (b)) indicated that the 377 μm and 85 μm OD MOF004 exhibited 52.6 μm and 12.5 μm diameter core regions, respectively. Therefore, the fabrication approach presented is scalable and adaptable to the future realisation of detailed MOF designs for diverse applications in terms of the core size, core materials, cladding size, cladding materials and layer numbers.

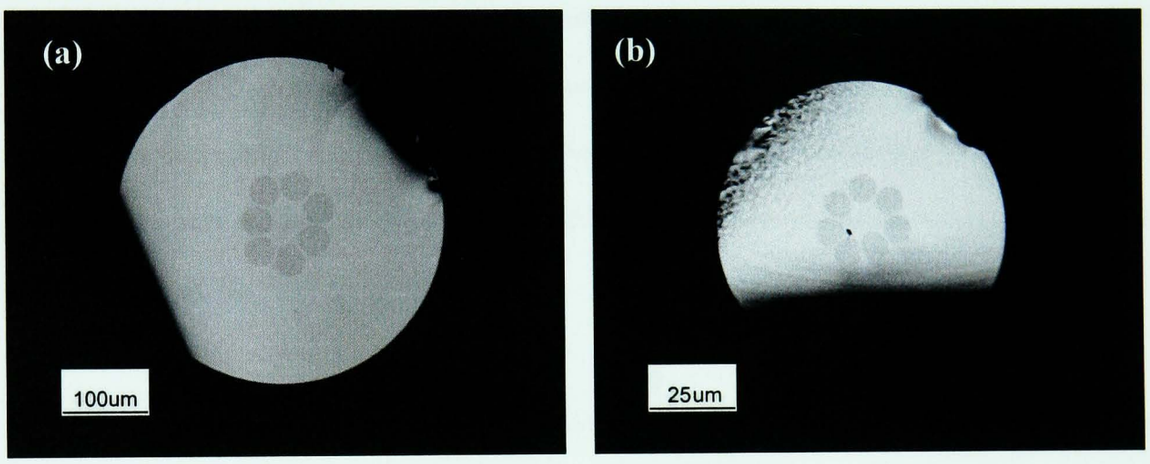

Figure 6.21: Optical reflection micrographs of the MOF004 of outer diameter and central region diameter: (a) 377 μm and 52.6 μm, respectively and (b) 86 μm and 12.5 μm, respectively [180].

Figure 6.22 shows compositional electron mapping of the MOF004 by means of backscattered electrons and electron dispersive spectroscopy (EDS) in a series: (a) arsenic mapping; (b) germanium mapping and (c) selenium mapping. It is evident that the central section of the MOF004 fibre and the outermost glass are As-Se as expected while the heptagonal ring of spots surrounding the central section have Ge-As-Se at their core as expected. The As content in the central core region and outer circumference are similar as expected and larger than that in the centre of each spot of the heptagonal ring, also as expected. Each of these spots in the heptagonal ring array has a border that does not contain Ge; this is again as expected because MOF preform was assembled using seven core/cladding fibres of $As_{40}Se_{60}$ / $Ge_{10}As_{23.4}Se_{66.6}$ glasses to surround the central core fibre.

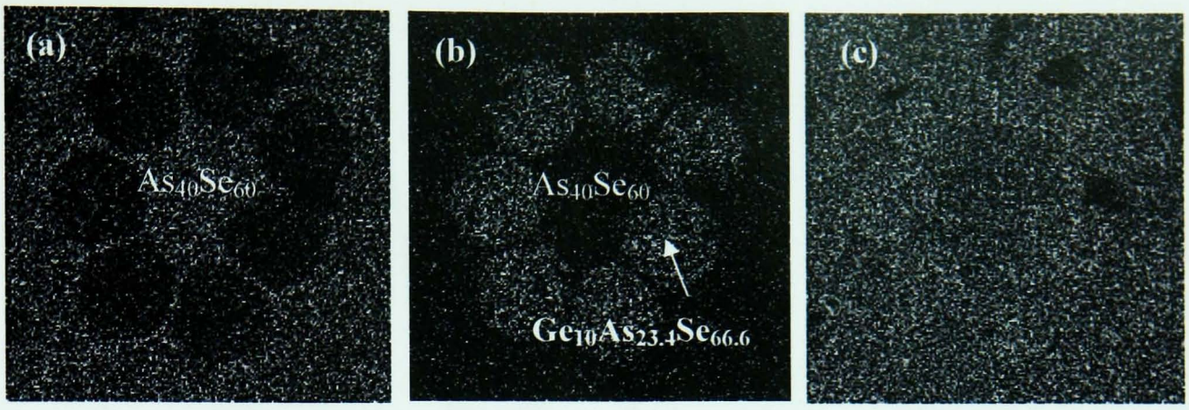

Figure 6.22: Elemental mapping of As, Ge and Se, respectively, in the MOF004. (a) As elemental mapping: the As content inside the spots arranged as a ring is lower than the As content in the central region of the MOF004 fibre, the As content between the spots in the ring and the As content in the peripheral glass as expected; (b) Ge elemental mapping: Ge only occurs in the spots arranged as a ring as expected and (c) the Se content shows up as apparently uniform across the whole fibre cross-section and indeed the expected atomic % of Se in the microstructured glass is between 60 at% and 66.6 at %.

The amorphous nature of both bulk $As_{40}Se_{60}$ and $Ge_{10}As_{23.4}Se_{66.6}$ was confirmed using XRD as discussed in section 4.2. After the multi-stage processing, amorphous nature of the solid core $As_{40}Se_{60}$ / $Ge_{10}As_{23.4}Se_{66.6}$ MOF needs to be re-checked. The lack of crystallisation was confirmed by crushing ~10 cm of the MOF004 and analyzing by means of powder XRD as shown in Figure 6.23. The fact that these glasses can be made through quite gentle quenching in air or liquid metal is further evidence of their resistance to devitrification on melt-cooling. XRD and ESEM imaging provides evidence for the stability against devitrification on repeatedly raising the temperature of the glasses above Tg for shaping followed by cooling to ambient.

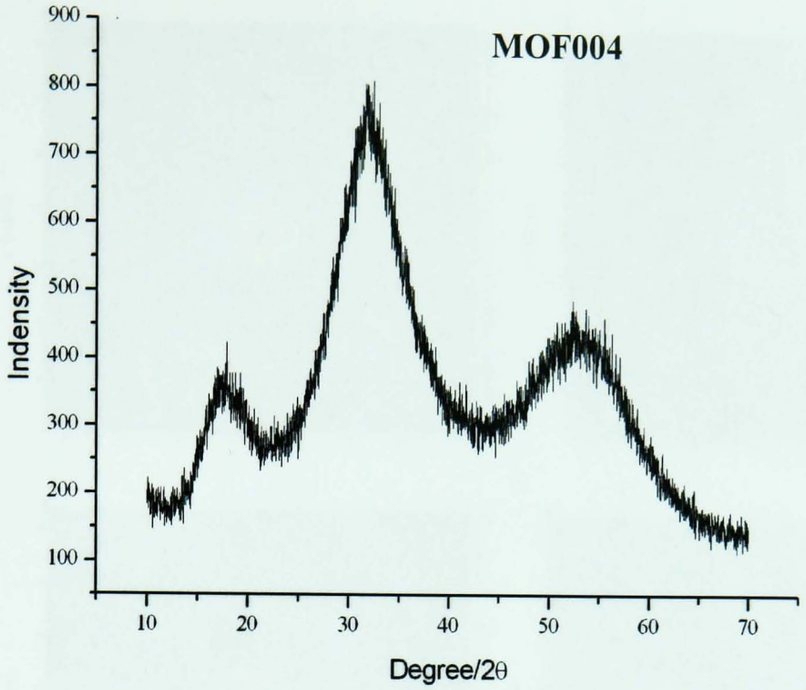

Figure 6.23: 10 cm of the MOF004 fibre sample was crushed to powder for XRD analysis. The XRD pattern confirmed amorphous nature of MOF004.

6.2.3 Optical assessment of solid core MOF004

A simulation of the one layer all-solid chalcogenide glasses MOF was carried out using a trial version of the commercial software Lumerical (Lumerical Solutions, Inc. Canada). PMLs (perfectly matched layers which simulated that no light is reflected from the boundary) were chosen as the problem boundary condition on all model boundaries. Multi-mode propagation was experimentally exhibited in this MOF structure. According to the simulation, there are more than 50 modes were supported by this one layer structure with a core diameter around 20 μm. Figure 6.24 (a) to (d) illustrate some of the modes at 1.55 μm. Optical assessments will be demonstrated later in this section to show wave guiding properties of the all-solid MOFs.

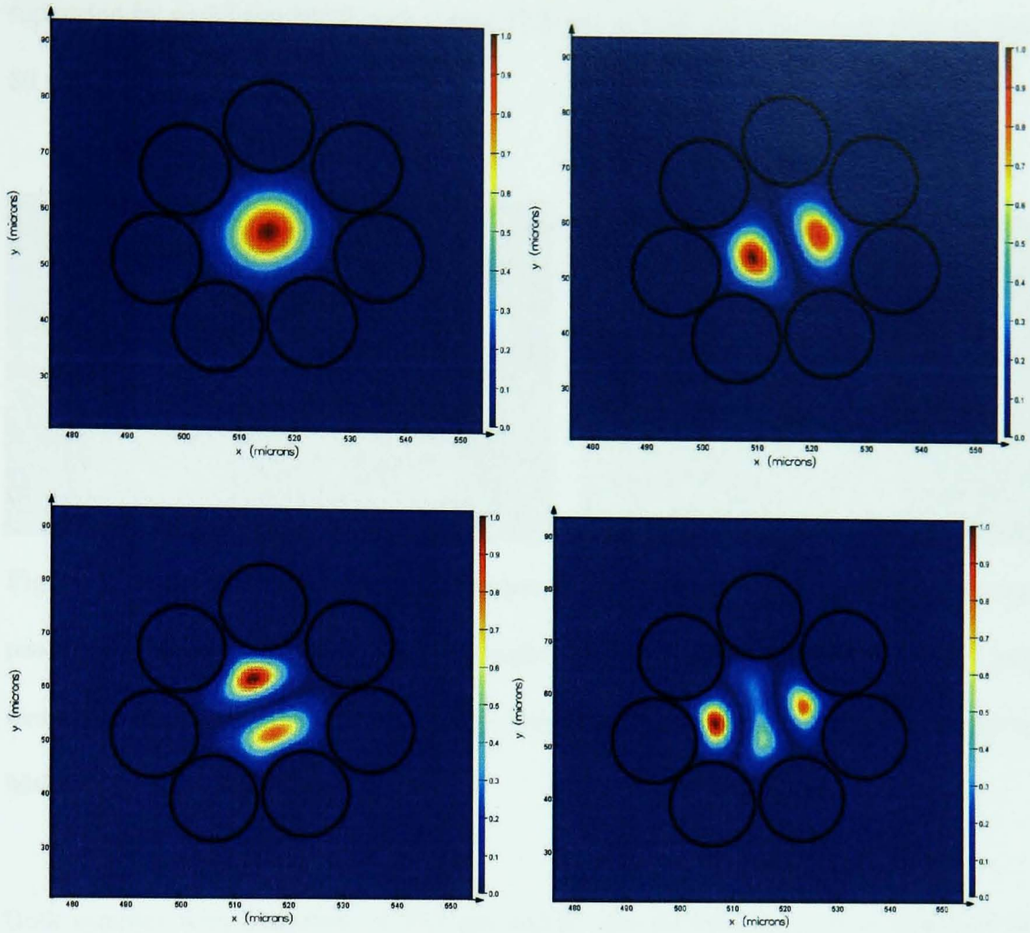

Figure 6.24: Simulation results, some of the modes of a 20 μm core diameter at the wavelength of 1.55 μm. The colour bar represent the intensity, red = 1.0 intensity and blue = 0.0 intensity. The position of the cladding layer is indicated as black circles.

An optical assessment of the all-solid MOF made will be described using samples approximately 80 mm long having outer diameters of 85 μm and 377 μm (cut from the MOF004 fibre). A tapered silica glass optical fibre was used to end-fire couple at 1.55 μm laser beam (supplied by Agilent, model 81980A) into one end of the MOF004 sample. The transmitted light from the MOF004 was collected from the opposite end-face of the waveguide using a ×10 microscope objective and focused onto an infrared sensitive camera (Siemens XQ1112). A television monitor and computer were connected to the infrared camera as a direct image output.

Both the 85 μm and 377 μm outer diameter samples of the MOF (MOF004) exhibited multi-mode propagation for 1.55 μm wavelength. Figure 6.25 (a) displays the near-field intensity profile of the multi - mode propagation supported by a 377 μm outer diameter sample of MOF004 with a core diameter 52.6 μm at 1.55 μm wavelength. Figure 6.25 (b) shows the near-field intensity profile of the multi - mode

supported by an 85 μm MOF with a core 12.5 μm at 1.55 μm wavelength after the light had propagated 80 mm.

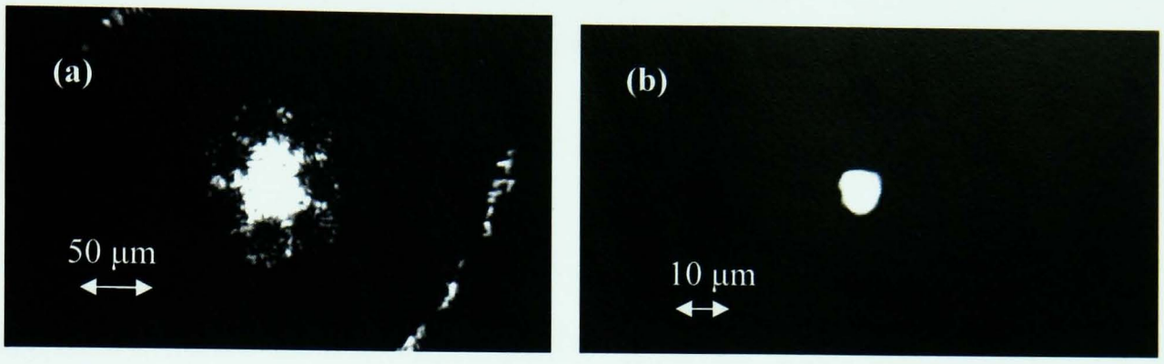

Figure 6.25: (a) The near-field intensity profile of the multi - mode propagation supported by a 52.6 μm core diameter, 80 mm length sample of MOF at 1.55 μm wavelength and (b) shows the near-field intensity profile of the multi - mode supported by a 12.5 μm core diameter, 80 mm length MOF at 1.55 μm wavelength.

Both samples with diameters of 377 μm and 85 μm guided light over a length of more than 80 mm. However, the optical loss of the one layer MOF was unfortunately not measured. The smallest optical loss of the one-layer all solid MOFs (12.5 μm core) was expected to be higher than 1 dB/m which was achieved by Helen [2] in a $As_{40}Se_{60}$ core conventional fibre (pre-distillation was done for $As_{40}Se_{60}$). The loss of the all-solid MOFs may due to the inherent intrinsic material loss of the core compared with hollow core fibre and material purification is suggested for further loss deduction [2]. For the MOF004 fibre, extrinsic loss was also expected to rise from the imperfect fabrication, for example the geometry of the structure was asymmetric and the canes used as cladding had variable diameters (non-uniform in diameters). The cane shape is considered to be a very important factor in preform stacking process as different canes shapes will result a non-uniform cladding layer. The cladding shape is uniform in length as several corss-sections from different segments of the MOF004 were measured to be identical. This suggests a symmetric cladding all solid MOF can be produced in a long distance fibre, if uniform diameter canes can be made.

Several cross-sections from MOF004 fibre were viewed using ESEM, one bubble defect was found in the fibre. The bubble was about 1 μm which was found between the core and the cladding as shown in the ESEM image in Figure 6.20. Such defects may be expected to introduce excess scattering loss; i.e. will

increase the total fibre loss. However, in general the bubble defects were seldom found in other part of the all solid MOFs. In addition, the bubble defects could be minimised by applying an internal vacuum during the fibre drawing process. In this case, when the drawing temperature increases, cladding and core materials soften and close the gaps between them. Again, uniform canes may also help to minimise the gaps between the core and cladding layers.

6.2.4 Discussion of all-solid MOFs

There are several disadvantages about the two glass compositions solid MOF compared with air/glass MOF:

(1) More than one glass compositions required. Two glass compositions were used as core and cladding of the MOF, therefore, it is required to measure some of the glass properties related to the fabrication process. These glass properties include: refractive index, viscosity and thermal expansion coefficient. In addition, more material purification will be needed to mitigate the effect of intrinsic material loss.

(2) More experimental steps involved. The idea of solid core MOF overcame some of the fabrication problems encountered in hollow core MOF manufacture in chalcogenide glasses. However, an extrusion technique was required to produce core/cladding preforms which caned for stacking of MOF preforms. This was not required in the hollow core MOF fabrication attempted in this project. To prepare the extruded canes, additional material purification, melting extrusion billets and polishing processes were required. In general, more experimental steps were involved for fabricating all solid MOFs.

All-solid MOFs were fabricated using two glass compositions; step index multi-mode guiding was demonstrated. In order to obtain a single mode guiding in all-solid MOFs use this fabrication approach, several factors need to be considered: the core size and the cladding layers. In theory, equation 6-4 [23] was used to estimate a core diameter for single mode guiding in step index guiding fibres.

$$0 < \frac{2\pi r}{\lambda}\sqrt{n_{core}^2 - n_{cladding}^2} < 2.405 \qquad 6\text{-}4$$

where r is the radius of the core, $\sqrt{n_{core}^2 - n_{cladding}^2}$ is the numerical aperture of the fibre. The refractive index of both core and cladding materials were taken from the experimental data which described in Chapter 4. The calculation shows that core diameter of 1.2 μm will be needed for single mode guiding in the all-solid chalcogenide glass MOF. The experimental results showed that the all-solid MOF fabrication approach is scalable, therefore, the core diameter could be modified to a desired dimension to realise single mode optical guiding. However, in current project, there was only one layer of cladding; therefore, the effective refractive index of the cladding may be different from the refractive index used in equation 6-4. Ideally, a thicker cladding (multi-layers in this case) will give a better step index from the core. Therefore, in order to fabricate a single mode guiding all-solid MOF, multiple cladding layers are required. This will be discussed in future work in Chapter 7.

Silica ampoule cracking problems

When producing $As_{40}Se_{60}$ tubes via rotational casting method, cracking problem was encountered. Typically, a batch of more than 20 g of $As_{40}Se_{60}$ in a standard silica melting ampoule (10 mm / 14 mm ID/OD, 400 mm length) was required in order to produce $As_{40}Se_{60}$ glass tubes. The silica ampoule containing the $As_{40}Se_{60}$ was place vertically in an annealing furnace for annealing. The bottom of the silica ampoules was sometimes cracked during annealing before ampoule re-seal as listed in Table 6.1, rotational casted sample RC009.

For more than a 20 g melt, it was found better to quench the melt into the 'homemade' sealed end of the melting ampoule rather than using the as-purchased rounded end of the melting ampoule. This action was found to reduce the probability of the melting ampoule cracking during glass annealing. The reason may due to the contraction of the melt during cooling. The as-purchased rounded end ampoule may have had a non-flat inner surface from manufacture. The contraction of a small melt was not significant, but the contraction of a large melt may have caused a serious stress build up between the melt and the ampoule and consequently caused the ampoule to crack. The sealing point of the ampoule was normally close to the middle of the standard ampoule, therefore the inner surface was relatively flat; the contraction of the large melt did not affect the ampoule seriously.

Also, hydrofluoric acid etching [2] of the ampoule before batching was found to be able to prevent the ampoule from cracking. The hydrofluoric acid etching of the ampoule was carried out under fume extraction by Dr. D. Furniss and T. Buss at the University of Nottingham. At room temperature, the ampoules were places in a plastic beaker and filled with 0.4 vol % hydrofluoric acid in distilled water. Etching took 30 minutes and the ampoules were then rinsed 3 times with distilled water. Subsequent to this project, further work has revealed that this problem may be related to the processing of the ampoules at the manufactures [126].

6.3 Summary

One of the objectives of this project is to fabricate a hollow core MOF in chalcogenide glasses. This chapter firstly presents the results of the investigation of fabricating single glass composition ($As_{40}Se_{60}$) hollow core MOFs. In section 6.1, three $As_{40}Se_{60}$ hollow core fibre fabrications using $As_{40}Se_{60}$ were reported. These fabrications were partially successful to the stage of preform stacking. However, the rotationally cast tubes were caned by hand; therefore, it is highly probably that the preforms may have been assembled using canes with slightly different diameters. As the MOF preform was located in the centre of the RF susceptor in the fibre tower, a non-uniform cladding could cause a non-uniform heat distribution during fibre drawing. The fibre drawing results showed it was hard to control the dimensions in the inner tube canes and hence to achieve the desired MOF structures. The single glass composition hollow core MOFs could not be successfully drawn from these performs due to fabrication difficulties. Some recommendations were discussed to improve the fabrication, including applying pressure to the preform to support the canes shapes and to produce more uniform wall thickness canes.

Alternatively, this chapter then shows two glass compositions all-solid MOFs were successfully drawn from $As_{40}Se_{60}$ and $Ge_{10}As_{23.4}Se_{66.6}$ chalcogenide glasses. The results demonstrated that a solid core MOF overcomes some of fabrication problems that hollow core MOFs suffer. The optical loss of all-solid MOFs fabricated was not measured but the results of the modelling using the Lumerical software to be above 1 dB/m. The optical loss can be attributed to the fact that there was only one layer cladding, the core shape was slightly asymmetric and materials were not purified in order to improve intrinsic losses.

The successful fabrication of all-solid MOF demonstrates that these two chalcogenide glass compositions are thermally, mechanically match and able to survive in a multiple process steps. The all solid MOF fabrication approach is scalable to future diverse applications. This fabrication success gives confidence that more complicated MOF structures such as multi-layer cladding in chalcogenide glasses can be successfully realised in the near future.

Chapter 7

Conclusions and Future work

The aim of this project was the development and fabrication of optical waveguide in the forms of planar rib waveguides and Microstructured Optical Fibres (MOFs) using chalcogenide glasses. The most significant contributions of the work undertaken can be categorised the following achievements:

(1) The properties of certain chalcogenide glasses are analysed and suitable glasses for rib waveguides and Microstructured Optical Fibres (MOFs) fabrications are suggested.

(2) Rib waveguides are formed directly in chalcogenide glass thin films using the hot embossing technique.

(3) Whilst attempts to fabricate of multi-layer hollow core chalcogenide glass MOF unfortunately failed, all-solid MOFs using a chalcogenide glass pair with sufficient index contrast are fabricated. It is suggested that the fabrications techniques can be extended to realise complex structures such as multi-layer cladding MOF in chalcogenide glasses in the near future.

The remainder of this chapter will summarise and present the conclusion drawn from the experimental work carried out for each of above categories. Also, it will make suggestions for future work where appropriate.

7.1 Suitable chalcogenide glasses

(1) $As_{40}Se_{60}$, $Ge_{17}As_{18}Se_{65}$ and $Ge_{10}As_{23.4}Se_{66.6}$ were analysed in terms of glass transition temperature, amorphous nature, thermal expansion coefficient (α), viscosity and refractive index (n). The Tg of $As_{40}Se_{60}$, $Ge_{17}As_{18}Se_{65}$ and $Ge_{10}As_{23.4}Se_{66.6}$ are 180 ± 5°C, 235 ± 5°C and 180 ± 5°C, respectively. The amorphous nature of these glasses was confirmed using XRD. The refractive index was measured by means of ellipsometry for wavelengths of 0.3 to 2.3 μm. According to the properties of these glasses, $As_{40}Se_{60}$ was chosen as the guiding material of rib waveguides and $Ge_{17}As_{18}Se_{65}$ was used as a lower

refractive index substrates (optical cladding); $As_{40}Se_{60}$ was chosen as the core in the all-solid MOF, and the cladding material was $Ge_{10}As_{23.4}Se_{66.6}$.

The refractive index of the thermally evaporated $As_{40}Se_{60}$ thin film samples increased after it was hot embossed. Enhanced understanding of this behaviour would benefit future design and fabrication of waveguides via the hot embossing technique. Therefore, further experiments to compare the as-evaporated and embossed samples should be continued:

- The density of the sputtered thin film may change during the embossing process. The flat-embossed thin film thickness is therefore expected to be thinner than that of the as-evaporated samples. The quantity of the thin film thickness change before and after hot embossing may be related to the refractive index change.

- The amorphous nature of thermally evaporated and sputtered thin films before and after embossing needs to be confirmed. The first sharp diffraction peak (FSDP) of XRD may potentially be used to estimate the atomic structure of materials. The thin film before and after embossing should therefore be analysed using this approach.

- The surface quality before and after flat-embossing may vary. This could affect the refractive index measurement since the ellipsometry measurement assumes the conditions of surface layers are identically smooth and flat. It will therefore be essential to check the surface quality of samples using a SEM before and after flat-embossing.

- The refractive indices of the thermally evaporated thin films before and after hot embossing are different. It will be interesting to investigate the refractive indices of thin films that are prepared using methods such as sputter coating. The process of hot embossing can potentially increase the refractive index of thin films to the value of the bulk material. An embossed sputter coated thin film is therefore expected to a have higher refractive index than that of the as-evaporated sample (densification).

7.2 Fabrication of Rib waveguides

Rib waveguides were successfully fabricated via a novel hot embossing technique, with waveguides directly formed in a thin film of chalcogenide glasses for the first time. Two key factors are required for this fabrication:

(a) The thermal expansion coefficient of the guiding material and the substrate material need to similar;
(b) In order to achieve full patterning, the glass thin films need to be flat and in good contact with the mould during embossing.

These factors were not achieved in the case of glass on semiconductor samples (GGS) and consequently some of these fabrication attempts failed. Replace the semiconductor substrate with a thicker chalcogenide glass substrate easily solved the problems, e.g. the thermal expansion coefficient of two chalcogenide glasses are similar; the thicker substrate acted as a levelling layer so the thin film was ensured to be flat and well contacted with the mould.

The rib waveguide loss was calculated using Febri-Perot method to be 2.9 dB/cm; this value may be overestimated since the waveguide facets were not perfectly cleaved. However, experiments are needed to further reduce the optical loss. (1) Materials purification may help to minimise intrinsic loss at some particular wavelengths as mentioned in section 3.3.2. Therefore, As and Se precursor purifications are recommended for all the glass melting in the future. (2) The wall smoothness of the wall of moulds needs to be improved. The nature of the hot embossing technique is to transfer the pattern of the mould onto the surface of the thin film. Any defects in the mould will be transferred onto the thin film and will result in optical devices with high optical loss. Intuitively, a high quality mould is a key requirement for the fabrication of good quality rib waveguides via hot embossing. The use of wet etching techniques to produce a high quality silicon mould was proposed and will be carried on by a PhD student, Nabil Abdel Moneim, in the Novel Photonic Glasses Research Group, University of Nottingham. (3) Also, a clean processing environment for all the fabrication processes developed during the course of this project would help to avoid dust contamination in the samples which can minimise the fabrication defects. It is recommended that the hot embossing rig should be moved from a normal laboratory to a clean room. (4)

A post-heat treatment of the ribs after-embossed will be a potential way to improve the surface quality even using a low quality mould.

In this PhD project, the ribs fabricated were typically 5 – 7 mm in length which is relatively short. If longer rib waveguides could be fabricated using hot embossing then the cut-back method [1, 2] could be used for optical loss measurement. The facility to make longer rib waveguides would also make it possible to attempt other optical structures such as optical couplers and splitters etc, also integrated components.

7.3 Fabrication of MOFs

The air core band gap MOF has advantages in applications such as laser power delivery, so it will be an interesting but challenging task to fabricate a multi-layer hollow core MOF in chalcogenide glass. As a stepping stone towards the fabrication of air core band-gap MOF, various wall thickness $As_{40}Se_{60}$ tubes were made via the rotational casting technique. The $As_{40}Se_{60}$ tubes were caned and stacked into a jacket $As_{40}Se_{60}$ tube to produce a multi-layer hollow core MOF preform. Several trials of fabricating multi-layer hollow core MOFs were made using the stack-and-draw method as described in Chapter 6. However, the aim of fabricating multi-layer hollow core MOFs in chalcogenide glasses was not achieved in this project. This was mainly because of difficulties in maintaining the internal structure during fibre drawing. Fibre preforms were successfully made but the inner stacked tube canes in the preform collapsed owing to lack of internal pressure during fibre drawing. These results showed that the hollow core multi-layer chalcogenide glass MOF remains a challenging task. Improvements are needed in the fabrication process such as increasing the pressure inside the preform during fibre drawing by introduce gas. Below are some suggestions for improvement to this technique and for future work.

- In this PhD project, tube canes for stacking the MOF preform were made by rotational casting followed by cane drawing. Rotational casting is a fast way to produce tubes, but can result in non-uniform wall thickness if the ampoule is not perfectly centred on its axis of rotation. Non-uniform wall thickness in the tube canes may result in asymmetry of the MOF structure. An

improvement of the ampoule alignment within the rotational casting rig may be needed in order to produce uniform wall thickness tubes.

- In the current project, the circular shaped canes were stacked inside a jacket tube to make the fibre preform. Intuitively, it would be easier and more stable to stack hexagonal shape tubes into the jacket tube. Extrusion is potentially able to fabricate tubes in a variety of shapes. A promising approach is therefore to produce hexagonal shape chalcogenide glass tubes via extrusion and then to stack them in either a circular or hexagonal jacket tube to make the preform.

- Instead of using the stack-and-draw method, the rod-in-tube method could be used to make the MOF preform. The extrusion method could be used to produce a multi-layer structure which then slots into a jacket tube to make a preform. The author suggests using a two layer cladding as an initial trial, since extrusion of two layers of hole has already been demonstrated by Feng *et al.* [91] in telluride glass. However, reports of the extrusion of chalcogenide glass MOF preforms are rare in the literature. Depending upon the application, the sizes of the core and the surrounding holes, the hole pitches and the layer numbers in the extrusion die could be varied. Using extrusion to produce MOF preform requires a good understanding of glass properties such as viscosity. The viscosity of chalcogenide glass changes very rapidly with the changing of processing temperature, so the extrusion temperature and load need to be carefully controlled.

According to Feng *et al.* [31], single material hollow core MOF has a disadvantage that it is not possible to maintain a uniform microstructure profile in a kilometre-scale length MOF even in silica because the pressure inside of the holes in the MOF accumulates during fibre drawing. One solution for making a robust MOF is to fabricate an index-contrast, all-solid MOF. In this case the dimensions of the core and cladding can be maintained without controlling pressure inside of holes. In this project, this task was achieved via a combination of several processes including: rotational casting tubes, extrusion, preform stacking and fibre drawing. In this way a one-layer solid core MOF was successfully drawn from $As_{40}Se_{60}$ and $Ge_{10}As_{23.4}Se_{66.6}$ glasses. Although the MOF structure was not perfectly symmetric, some defects were observed and the fibre was highly multi-mode, this approach presents a new and flexible route to

microstructuring chalcogenide glass fibres. Importantly, the glasses chosen in this project can withstand the multiple process steps, therefore, In the future, this fabrication approach could be extended to a range of further experiments, such as multi-layer cladding photonic bandgap all-solid MOFs and single mode all-solid MOF must be possible with 'usual' MOF designs.

The one layer all-solid MOF fabricated in the current project has relatively high loss. This was partially because there was only one layer and the material precursors were not purified. The As and Se purification technique and distillation technique [2] were introduced in earlier and current studies for making highly purified bulk chalcogenide glasses. To fabricate low loss MOF using the purified precursors will be next goal for the all-solid MOF.

The fabrication processes such as extrusion, rotational casting of tubes and fibre drawing of MOF were based on empirical estimation. Therefore, improper processing conditions may lead to distortion of tubes, surface oxidisation or crystallisation etc. Numerical modelling of the fabrication process could further our understanding of the pattern flow during extrusion and fibre drawing, and could help to modify a suitable process condition.

References

1. Pan, W.J., *Development of hot embossing for fabricating optical waveguides based on chalcogenide glasses*, in *Electrical and Electronic Engineering*. 2008, University of Nottingham: Thesis, Nottingham.
2. Rowe, H., *Development of low optical loss chalcogenide glass fibre for min-infrared transmission*. 2008, University of Nottingham: Thesis, Nottingham.
3. Hu, J., C.R. Menyuk, L.B. Shaw, J. Sanghera, and I. Aggarwal, *Maximazing the bandwidth of supercontinuum generation in As_2Se_3 chalcogenide fibers.* Optics Express, 2010. **18**(7): p. 6722-6739.
4. Zakery, A. and S.R. Elliott, *Optical properties and applications of chalcogenide glasses: a review.* Journal of Non-Crystalline solids, 2003. **330**(1-3): p. 1-12.
5. Sanghera, J.S., I.D. Aggarwal, S. L.B., C.M. Florea, and P.C. Pureza, *Nonlinear properties of chalcogenide glass fibers.* J.Optolelectron. Adv. Matt., 2006. **8**: p. 2148-2155.
6. Cardinal, T., K.A. Richardson, H. Shim, A. Schulte, R. Beatty, K.L. Foulgoc, C. Meneghini, J.F. Viens, and A. Villeneuve, *Non-linear optical properties of chalcogenide glasses in the system As-S-Se.* Journal of Non-Crystalline Solids, 1999. **256, 257**.
7. Smektala, F., C. Quemard, V. Couderc, and A. Barthelemy, *Non-linear optical properties of chalcogenide glasses measured by Z-scan.* Journal of Non-Crystalline Solids, 2000. **274**(1-3): p. 232-237.
8. Tanaka, K., *Photodarkening in amorphous As_2S_3 and Se under hydrostatic pressure.* Physical Review B, 1984. **30**(8): p. 4549 - 4554.
9. Zakery, A., P.J.S. Ewen, and A.E. Owen, *Photodarkening in As-S films and its application in grating fabrication.* Journal of Non-Crystalline solids, 1996. **198-200, part 2**: p. 769-773.
10. Petkov, K. and P.J.S. Ewen, *Photoinduced changes in the linear and nonlinear optical properties of chalcogenide glasses.* Journal of Non-Crystalline Solids, 1999. **249**(2-3): p. 150-159.
11. Popta, A.C.v., R.G. DeCorby, C.J. Haugen, T. Robinson, and J.N. McMullin, *Photoinduced refractive index change in As_2Se_3 by 633nm illumination.* Optic Express 2002. **10**(15): p. 639-644.
12. Galstyan, T.V., J.F. Viens, A. Villeneuve, K. Richardson, and M.A. Duguay, *Photoinduced self-developing relief gratings in thin film chalcogenide As_2S_3 glasses.* Journal of Lightwave Technology, 1997. **15**(8): p. 1343-1347.
13. Nagels, P., R. Mertens, and L. Tichý, *Reversible photodarkening in amorphous As_xS_{100-x} films prepared by thermal evaporation and plasma-enhanced chemical vapour deposition.* Material Letters, 2003. **57**(16-17): p. 2494-2500.
14. Kolobov, A.V., *Photo-induced metastablity in amorphous semiconductors*. Engineering glassy chalcogenide materials for integrated optical applications, ed. K. Richardson, T. Cardinal, M. Richardson, A. Schulte, and S. Seal. 2003: Wiley-VCH.
15. Meneghini, C. and A. Villeneuve, *As_2S_3 photosensitivity by two-photon absorptoon holographic gratings and self-written channel waveguides.* journal of optical Society of America, B, 1998. **15**(12): p. 1946-1950.

16. Seddon, A.B., *Chalcogenide glasses: A review of their preparation, properties and applications.* Journal of Non-cryst Solids, 1995. **184**: p. 44-50.
17. Viens, J.F., C. Meneghini, T.V. Galstian, K.A. Richardson, and T. Cardinal, *Fabrication and characterization of integrated optical waveguides in sulfide chalcogenide glasses.* Journal of Lightwave Technology, 1999. **17**(7): p. 1184-1191.
18. Zoubir, A., L. Shah, K. Richardon, and M. Richardon, *Technology developments towards the practical use of femtosecond laser micro-materials processing*, in *High power laser ablation IV*, C. Phipps, Editor. 2002. p. 406-414.
19. Suzuki, K. and K. Ogusu, *Single-mode Ag-As_2Se_3 strip-loaded waveguides for applications to all-optical devices.* Optics Express, 2005. **13**(21): p. 8634-8641.
20. Dale, G. and P.J.S. Ewen, *Photolithographic method for producing metal dissolved diffractive strucutres in As-S glasses.* IEE Proc.-Optoelectron, 1997. **144**(6): p. 426-432.
21. Ruan, Y., W. Li, R. Jarvis, N. Madsen, A. Rode., and B. Luther-Davies, *Fabrication and characterization of low loss rib chalcogenide waveguides made by dry etching.* Optic Express, 2004. **12**(21): p. 5140-5145.
22. Pan, W.J., H. Rowe, D. Zhang, Y. Zhang, A. Loni, D. Furniss, P. Sewell, T.M. Benson, and A.B. Seddon, *One-step hot embossing of optical rib waveguides in chalcogenide glasses.* Microwave and Optical Technology Letters, 2008. **50**(7): p. 1961-1963.
23. Snyder, A.W. and J.D. Love, *Optical Waveguide Theory*. 1983: Chapman and Hall.
24. Knight, J.C., *Photonic crystal fibres, Insight review articles.* Nature, 2003. **424**(14): p. 847-851.
25. Knight, J.C., T.A. Birks, P.S.J. Russell, and D.M. Atkin, *All-silica single-mode optical fiber with phtonic crystal cladding.* Optics Letters, 1996. **21**(19): p. 1547-1549.
26. Russell, P., *Photonic crystal fibre.* Science, 2003. **299**(5605): p. 358-362.
27. Monro, T.M., T.D. West, D.W. Hewak, N.G.R. Broderick, and D.J. Richardon, *Chalcogenide holey fibers.* Electronics Letters, 2000. **36**(24): p. 1998-2000.
28. Désévédavy, F., Renversez, G.L. Brilland, P. Houizot, J. Troles, Q. Coulombier, F. Smektala, N. Traynor, and J. Adam, *Small-core chalcogenide microstructured fibers for the infrared.* Applied Optics, 2008. **47**(32): p. 6014-6021.
29. Brilland, L., F. Smektala, G. Renversez, T. Chartier, J. Troles, T. Nguyen, N. Traynor, and A. Monteville, *Fabrication of complex structures of holey fibers in chalcogenide glass.* Optics Express, 2006. **14**(3): p. 1280-1285.
30. Sanghera, J., L. Shaw, B., C.M. Florea, V. Nguyen, D.J. Gibson, F. Kung, and I.D. Aggarwal, *Non-linearity in chalcogenide glasses and fibers, and their applications*, in *CLEO*. 2008: San Jose, CA. p. QTuL5.
31. Feng, X., T. Monro, P. Petropoulos, V. Finazzi, and D. Hewak, *Solid microstructured optical fiber.* Optic Express, 2003. **11**(18): p. 2225-2230.
32. Monro, T., D.J. Richardon, and N.G. Broderick, *Efficient modelling of holey fibers*, in *Optical Fibers Communication Conference*. 1999: San Diego, California.
33. Devyatykh, G.G., M.F. Churbanov, I.V. Scripachev, G.E. Snopatin, E.M. Dianov, and V.G. Plotnichenko, *Recent developments in As–S glass fibres.* Journal of Non-cryst Solids, 1999. **256-257**(2): p. 318-322.
34. Rawson, H., *Glass Science and Technology, Proterties and Applications of Glass 3*. 1980: Elsevier Scientific publishing company.
35. Tamulevich, T.W. and V.E. Moore, *The significance of glass transition temperature on epoxy resins for fiber optic applications*. 1980, Epoxy technology Inc.: Billerica.

36. Tikhomirov, V.K., D. Furniss, A.B. Seddon, J.A. Savage, P.D. Mason, D.A. Orchard, and K.L. Lewis, *Glass formation in the Te-enriched part of the quaternary Ge-As-Se-Te system and its implication for mid-infrared optical fibres.* Infrared Physics & Technology, 2004. **45**(2): p. 115-123.
37. Harbold, J.M., F.O. Ilday, F.W. Wise, J.S. Sanghera, V.Q. Nguyen, L.B. Shaw, and I.D. Aggarwal, *Highly nonlinear As-S-Se glasses for all-optical switching.* Optics Letters, 2002. **27**(2): p. 119-121.
38. Weber, M.J., *CRC Handbook of Laser Science and Technology* 1996, Roca Raton: Elsevier. 833.
39. Pope, A., A. Schulte, Y. Guo, L.K.Ono, B.R. Cuenya, C.Lopez, K. Richardson, K. Kitanovski, and T. Winningham, *Chalcogenide waveguide structures as substrates and guiding layers for evanescent wave Raman spectroscopy of bacteriorhodopsin'.* Vibrational Spectroscopy, 2006. **42**(2): p. 249-253.
40. Lezal, D., J. Pedlikova, and J. Zacalil, *Chalcogenide glass for optical and photonics applications.* Chalcogenide Letters 2004. **1**(1): p. 11-15.
41. Lenz, G., J. Zimmermann, T. Katsufuji, M.E. Lines, H.Y. Hwang, S. Spalter, R.E. Slusher, S.W. Cheong, J.S. Sanghera, and I.D. Aggarwal, *Large Kerr effect in bulk Se-based chalcogenide glasses.* Optics Letters, 2000. **25**(4): p. 254-256.
42. Popescu, M., *Non-crystalline chalcogenides*. 2000: Springer. 377.
43. Savage, J.A., *Infrared Optical Material and their Antireflection Coatings*. 1985, Bristol and Boston: Adam Hilger.
44. Ho, K.S., S.H. Liu, and G.S. He, *Physics of nonlinear optics*. 2000, London: World Scientific.
45. Jun, J.J.M., C.T. Moynihan, P.B. Macedo, and G.R. Srinivasan, *Microstructure and properties of an infra-red transmitting chalcogenide glass-ceramic* Journal of Materials Science, 1976. **11**(10): p. 1952-1960.
46. Requejo-Isidro, J., A.K. Mairaj, V. Pruneri, D.W. Hewak, M.C. Netti, and J.J. Baumberg, *Self refractive non-linearities in chalcogenide based glasses.* Journal of Non-Crystalline Solids, 2003. **317**(3): p. 241-246.
47. Fleming, J.W., *Material and mode dispersion in $GeO_2B_2O_3$-SiO_2 glasses.* Journal of American Ceramic Society, 1976. **59**: p. 503-507.
48. Kobayashi, S., S. Shibata, N. Shibata, and T. Izawa, *Refractive index dispersion of doped fused silica*, in *International conference on integrated optics and optical fibre communication 1977 Technical Digest*. 1977. p. 309-312.
49. Payne, D.N. and W.A. Gambling, *Zero material dispersion in optical fibres.* Electron Letters, 1975. **11**(8): p. 176-178.
50. Cohen, L.G. and C. Lin, *Transmission measurements of zero material dispersion in optical fibers.* Journal of Quantum Electron, 1977. **QE-13**(12): p. 91-92.
51. Fleming, J.W., *Material dispersion in lightguide glasses.* Electronic Letters, 1978. **14**(11): p. 326-328.
52. Cohen, L.G., C. Lin, and W.G. French, *Tailoring zero chromatic dispersion into the 1.5-1.6 um low-loss spectral region of single mode fibres.* Electronics Letters, 1979. **15**(12): p. 334-335.
53. Maiman, T.H., *Stimulated optical radiation in ruby.* Letters to Nature, 1960. **187**: p. 493-494.
54. Gopinath, J.T., M. Soljačić, E.P. Ippen, V.N. Fuflyigin, W.A.King, and M. Shurgalin, *Third order nonlinearities in Ge-As-Se-based glasses for telecommunications applications.* Journal of Applied Physics, 2004. **96**(11): p. 6931-6933.

55. Ta'eed, V., N.J. Baker, K. Finsterbusch, M. Lamont, D.J. Moss, H.C. Nguyen, B.J. Eggleton, D.Y. Choi, S. Madden, and B. Luther-Davies, *Ultrafast all-optical chalcogenide glass photonic circuits.* Optics Express, 2007. **15**(15): p. 9205-9221.

56. Nguyen, H.C., K. Finsterbusch, D.J. Moss, and B.J. Eggleton, *Dispersion in nonlinear figure of merit of As_2Se_3 chalcogenide fibre.* Electron Letters, 2006. **42**(10): p. 571-572.

57. Mizrahi, V., K.W. DeLong, G.I. Stegeman, M.A. Saifi, and M.J. Andrejco, *Two-photon absorption as a limitation to all-optical switching.* Optics Letters, 1989. **14**(20): p. 1140-1142.

58. Cable, M. and J.M. Parker, *High-performance glasses*. 1992, Glasgow and London: Blackie and Son Limited.

59. Zoubir, A., L. Shah, K.A. Richardon, and M.C. Richardon, *Technology developments towards the practical use of femtosecond laser micromaterials processing*, in *SPIE*. 2002: Taos, NM, USA. p. 406.

60. Efimov, O.M., L.B. Glebov, K.A. Richardson, E.V. Stryland, T. Cardinal, S.H. Park, M. Couzi, and J.L. Bruneel, *Waveguide writing in chalcogenide glasses by a train of femtosecond laser pulses.* Optical Materials, 2001. **17**(3): p. 379-386.

61. Balan, V., C. Vigreux, and A. Pradel, *Chalcogenide thin film deposited by radio frequency sputtering.* Journal of Optoelectronics and Advanced Materials, 2004. **6**(3): p. 875-882.

62. Ramachandran, S. and S.G.Bishop, *Excitation of Er^{3+} emission by host glass absorption in sputtered films of Er-doped $Ge_{10}As_{40}Se_{25}S_{25}$ glass.* Applied Physics Letters, 1998. **73**(22): p. 3196-3198.

63. Song, S. and S. Choi, *Spin coated Ge-Se-Te-Si_3N_4-CdS chalcogenide thin film* Journal of Non-Crystalline solids, 2001. **291**(1-2): p. 50-55.

64. Chern, G.C. and I. Lauks, *Spin-coated amorphous chalcogenide films.* Journal of Applied Physics, 1982. **53**(10): p. 6979-6982.

65. Kohoutek, T., T. Wagner, J. Orava, M. Frumar, V. Perina, A. Mackova, V. Hnatowitz, M. Vlcek, and S. Kasap, *Amorphous films of Ag-As-S system prepared by spin coating technique, preparation and films physico-chemical properties.* Vacuum, 2004. **76**(2-3): p. 191-194.

66. Rode, A.V., A. Zakery, M. Samoc, R.B. Charters, E.G. Gamaly, and L.-D. B, *Laser deposition As_2S_3 chalcogenide film for waveguide applications.* Applied Surface Science, 2002. **197-198**: p. 481-485.

67. Youden, K.E., T. Grevatt, R.W. Eason, H.N. Rutt, R.S. Deol, and G. Wylangowski, *Pulsed laser deposition of Ga-La-S chalcogenide glass thin film optical waveguides.* Applied Physics Letters, 1993. **63**(12): p. 1601-1603.

68. Fick, J., B. Nicolas, C. Rivero, K. Elshotb, R. Irwin, K.A. Richardson, M. Fischer, and R. Vallee, *Thermal activated silver diffusion in chalcogenide thin films.* Thin Solid Films, 2002. **418**(2): p. 215-221.

69. Huang, C.C., D.W. Hewak, and J.V. Badding, *Deposition and characterization of germanium sulphide glass planar waveguides.* Optic Express, 2004. **12**(11): p. 2501-2506.

70. Katsuyama, T., S. Satoh, and H. Matsumura, *Fabrication of high-purity chalcogenide glasses by chemical vapor deposition.* Journal of Applied Physics, 1986. **59**(5): p. 1446-1449.

71. Bao, Q., C. Chen, D. Wang, Q. Ji, and T. Lei, *Pulsed laser deposition and its current research status in preparing hydroxyapatite thin films.* Applied Surface Science, 2005. **252**(5): p. 1538-1544.

72. Richardson, K., T. Cardinal, M. Richardson, A. Schulte, and S. Seal, *Eneineering Glassy Chalcogenide Materials for Integrated Optics Applications*. Photoinduced Metastability in Amorphous semiconductors ed. A.V. Kolobov. 2003, Weinheim: Wiley VCH.
73. Hirao, K. and K. Miura, *Writing waveguides and gratings in silica and related materials by a femtosecond laser.* Journal of Non-Crystalline solids, 1998. **239**(1): p. 91-95.
74. Minoshima, K., A.M. Kowalevicz, I. Hartl, E.P. Ippen, and J.G. Fujimoto, *Photonic device fabrication in glass by use of nonlinear materials processing with a femtosecond laser oscillator.* Optics Letters, 2001. **26**(19): p. 1516-1518.
75. Spälter, S., H.Y. Hwang, J. Zimmermann, G. Lenz, T. Katsufuji, S.W. Cheong, and R.W. Slusher, *Strong self-phase modulation in planar chalcogenide glass waveguides.* Optics Letters, 2002. **27**(5): p. 363-365.
76. Zakery, A. and S.R. Elliott, *Optical nonlinearities in chalcogenide glasses and their applications*. 2007, Berlin: Springer. 199.
77. Belykh, A.V., O.M. Efimov, L.B. Glebov, Y.A. Matveev, A.M. Mekyukov, and K. Richardson, *Photo-structural transformation of chalcogenide glasses under nonlinear absorption of laser radiation.* Journal of Non-Crystalline solids, 1997. **213 and 214**: p. 330-335.
78. Cerqua-Richardson, K.A., J.M. McKinley, B. Lawrence, S. Joshi, and A. Villeneuve, *Comparison of nonlinear optical properties of sulfide glasses in bulk and thin film form* Optical Materials, 1998. **10**(2): p. 155-159.
79. Townsend, P.D., *Development of ion implantation for optical applications.* Vacuum, 1998. **51**(2): p. 301-304.
80. Bell, A.G., *Selenium and the photophone.* The Electrician, 1880: p. 214, 215, 220, 221.
81. Kaiser, P., E.A.J. Marcatili, and S.E. Miller, *A new optical fiber.* Bell System Technical Journal, 1973. **52**(2): p. 265-169.
82. Monro, T.M. and H. Ebendroff-Heidepriem, *Progress in microstructured optical fibre.* Annual Reviews 2006, 2006. **36**: p. 467-495.
83. Yablonovitch, E., *Inhibited spontaneous emission in solid state physics and electronics.* Physical Review Letters, 1987. **58**(20): p. 2059-2062.
84. Cregan, R.F., B.J. Mangan, J.C. Knight, T.A. Birks, S.S.J. Russell, R.J. Roberts, and D.C. Allan, *Single-mode photonic band gap guidance of light in air.* Science, 1999. **285**: p. 1537-1539.
85. Temelkuran, B., S.D. Hart, G. Benoit, J.D. Joannopoulos, and Y. Fink, *Wavelength-scalable hollow optical fibres with large photonic bandgaps for CO2 laser transmission.* Letters to Nature, 2002. **420**: p. 650-653.
86. Bayidir, M., O. Shapira, D. Saygin-Hinczewski, J. Viens, A.F. Abouraddy, J.D. Joannapoulos, and Y. Fink *Intergrated fibres for self-monitored optical transport.* Nature Materials, 2005. **4**: p. 820-825.
87. Bayidir, M., A.F. Abouraddy, J. Arnold, J.D. Joannapoulos, and Y. Fink, *Thermal-Sensing Fiber Devices by Multimaterial Codrawing.* Advanced Materials, 2006. **18**: p. 845-849.
88. Yeh, P., A. Yariv, and E. Marom, *Theory of Bragg fiber.* Journal of Optical Society of America, 1978. **68**(9): p. 1196-1201.
89. Brady, D.J., T. Schweizer, J. Wang, and D.W. Hewak, *Minimum loss predictions and measurements in gallium lanthanum sulphide based glasses and Fibre.* Journal of Non-Crystalline Solids, 1998. **242**(2-3): p. 92-98.

90. Feng, X., T.M. Monro, V. Finazzi, R.C. Moore, K. Frampton, P. Petropoulos, and D.J. Richardson, *Extruded singlemode, high nonlinearity tellurite glass holey fibre.* Electronic Letters, 2005. **41**(15): p. 835-837.

91. Feng, X., W.H. Loh, J.C. Flanagan, A. Camerlingo, S. Dasgupta, P. Petropoulos, P. Horak, K. Frampton, N. White, J.H.V. Price, H.N. Rutt, and D.J. Richardon, *Single-mode tellurite glass holey fiber with extremely large mode area for infrared nonlinear applications.* Optics Express, 2008. **16**(18): p. 13651-13656.

92. Ebendorff-Heidepriem, H., P. Petropoulos, S. Asimakis, V. Finazzi, R.C. Moore, K. Frampton, F. Koizumi, D.J. Richardson, and T.M. Monro, *Bismuth glass holey fibers with high nonlinearity.* Optics Express, 2004. **12**(21): p. 5082 - 5087.

93. Edendorff-Heidepriem, H. and T.M. Monro, *Extrusion of complex preforms for microstructured optical fibers.* Optics Express, 2007. **15**(23): p. 15086 - 15092.

94. Ebendorff-Heidepriem, H., Y. Li, and T. Monro, *Reduced loss in extruded soft glass microstructured fibre.* Electronics Letters, 2007. **43**(24): p. 1343-1345.

95. Edendorff-Heidepriem, H. and T. Monro, *Soft glass microstructured optical fibres: Recent progress in fabrication and opportunities for novel optical devices*, in *ICTON*. 2009, IEEE. p. Mo. A.3

96. Shaw, B., P. Thielen, F. Kung, V. Nguyen, J. Sanghera, and I. Aggarwal, *IR supercontinuum generatuon in As-Se photonic crystal fiber*, in *Advanced solid-state photonic*. 2005: Vienna, Austria. p. TuC5.

97. Large, M.C.J., S. Ponrathnam, A. Argyros, N.S. Pujari, and F. Cox, *Solution doping of microstructured polymer optical fibres.* Optic Express, 2004. **12**(9): p. 1966-1971.

98. Van Eijkelenborg, M.A., M.C.J. Large, A. Argyros, J. Zagari, S. Manos, N.A. Issa, I. Bassett, S. Fleming, R.C. McPhedran, C.M.d. Sterke, and N.A.P. Nicorovici, *Microstructured polymer optiacl fibre.* Optic Express, 2001. **9**(7): p. 319-327.

99. Vasil'ev, A.V., G.G. Devyatykh, E.M. Dianov, A.N. Gur'yanov, A.Y. Laptev, V.G. Plotnichenko, Y.N. Pyrkov, G.E. Snopatin, I.V. Skripachev, M. F. Churbanov, and V.A. Shipunov, *Two-layer chalcogenide-glass optical fibers with optical losses below 30 dB/km.* IEEE Quantum Electronics, 1993. **23**(2): p. 89.

100. Sanghera, J.S., I.D. Aggarwal, L.E. Busse, P.C. Pureza, V.Q. Nguyen, R.E. Miklos, F.H. Kung, and R. Mossadegh, *Development of low-loss IR transmitting chalcogenide glass fibers*, in *SPIE*, J.A. Harrington, D.M. Hrris, and A. Katzir, Editors. 1995. p. 71-77.

101. Kanamori, T., Y. Terunuma, S. Takahashi, and T. Miyashita, *Chalcogenide glass fibers for Mid infrared transmission.* Journal of Lightwave Technology, 1984. **2**(5): p. 607-613.

102. French, W.G., J.B. MacChesney, and A.D. Pearson, *Glass fibers for optical communications.* Annual Review of Materials Science 1975: p. 373-394.

103. Nishii, J., T. Yamashita, and T. Yamagishi, *Chalcogenide glass fiber with a core-cladding structure.* Applied Optics, 1989. **28**(23): p. 5122-5127.

104. Roeder, E., *Extrusion of glass.* Journal of Non-Crystalline solids, 1971. **5**(5): p. 377-388.

105. Roeder, E., *Flow behavious of glass during extrusion.* Journal of Non-Crystalline solids, 1972. **7**(2): p. 203-220.

106. Gibson, D.J. and J.A. Harrington, *Extrusion of hollow waveguide preforms witha one dimensional photonic bandgap strucutre.* Journal of Applied Physics, 2004. **95**(8): p. 3895-3900.

107. Sanghera, J.S. and I.D. Aggarwal, *Active and passive chalcogenide glass optical fibers for IR applications: A review.* Journal of Non-Crystalline Solids 1999. **256-257**: p. 6-16.

108. Furniss, D. and A.B. Seddon, *Towards monomode proportioned fibreoptic preforms by extrusion.* Journal of Non-Crystalline Solids 1999. **256-257**: p. 232-236.

109. Seddon, A.B., D. Furniss, and A. Motesharei, *Extrusion method for making fibreoptic preforms of special glasses*, in *SPIE*, M. Saad, Editor. 1998. p. 32-42.

110. Seddon, A.B., D. Furniss, and D. Simes, *Gallium-lanthanum-sulphide glasses: extrusion of fiber optic preforms and relevant physical properties*, in *SPIE*, M. Saad and J.A. Harrington, Editors. 1999. p. 160-168.

111. Furniss, D. and A.B. Seddon, *Extrusion of Gallium lanthanum sulfide glasses for fiber-optic preforms.* Journal of Materials Science Letters, 1998. **17**: p. 1541-1542.

112. Savage, S.D., C.A. Miller, D. Furniss, and A.B. Seddon, *Extrusion of chalcogenide glass preforms and drawing to multimode optical fibers.* Journal of Non-Crystalline Solids, 2008. **354**(29): p. 3418-3427.

113. Tran, D.C., C.F. Fisher, and G.H. Sigel, *Fluoride glass preforms prepared by a rotational casting process.* Electronics Letters, 1982. **18**(15): p. 657-658.

114. Sanghera, J.S. and I.D. Aggarwal, *Infrared fiber optics*. illustrated ed. 1998: CRC Press.

115. Vienne, G., Y. Xu, C. Jakobsen, H.J. Deyerl, T.P. Hansen, B.H. Larsen, J.B. Jensen, T.Serensen, M. Terrel, Y. Huang, R. Lee, N.A. Mortensen, J. Broeng, H. Simonsen, A. Bjarklev, and A. Yariv. *First demonstration of air-silica Bragg fiber.* in *Optical Fiber. Communication Conference (OFC)*. 2003.

116. Troles, J., F. Smektala, L. Brillant, P. Houizot, F. Desevedavy, G. Boudebs, T. Chartier, and N. Traynor, *Preparation of chalcogenide step index and micron structured fiber for telecommunications*, in *International Conference on Transparent Optical Networks* 2006: Nottingham. p. Tu.C2.4,112-115.

117. Shaw, L.B., P.A. Thielen, F.H. Kung, V.Q. Nguyen, J.S. Sanghera, and I.D. Aggarwal, *IR supercontinuum generation in As-Se photonic crystal fiber*, in *Proc of Advanced Solid State Physics (ASSP)*. 2005, Technical Digest Optical Society of America: Vienna, Austria. p. Waveguide Devices paper TuC5.

118. Fink, Y. *Applications of omnidirectional reflectivity. Communication and high power transmission through hollow Bragg (OmniGuide) fibers.* [cited 2008; Lecture presentation avaible online].

119. Bormashenko, E., R. Pogreb, Z. Pogreb, and S. Sutoski, *Development of new near-infrared filters based on the 'sandwich' polymer-chalcogenide glass-polymer compositions.* Optic Engineering, 2001. **40**(5): p. 661-662.

120. Inagawa, I., R. Lizuka, T. Yamagishi, and R. Yokota, *Optical and thermal properties of chalcogenide GeAsSeTe glasses for IR fibers.* Journal of Non-cryst Solids, 1987. **95-96**(Part 2): p. 801-808.

121. Sanghera, J. and I. Aggarwal, *Infrared Fiber Optics*. 1998, Washington D.C.: CRC Press LLC.

122. Moynihan, C.T., P.B. Macedo, M.S. Maklad, R.K. Mohr, and R.E. Howard, *Intrinsic and impurity infrared-absorption in As_2Se_3 glass.* Journal of Non-cryst Solids, 1975. **17**(3): p. 369-385.

123. Ma, D.S., P.S. Danielson, and C.T. Moynihan, *Bulk and impurity infrared-absorption in 0.5 As_2Se_3 - 0.5 $GeSe_2$ glass.* Journal of Non-cryst Solids, 1980. **37**(2): p. 181-190.

124. Reitter, A.M., A.N. Screeram, A.K.Varshneya, and D.R. Swiler, *Modified preparation procedure for laboratory melting of multicomponents chalcogenide glasses.* Journal of Non-cryst Solids, 1992. **139**: p. 121-128.

125. King, W.A., A.G. Clare, and W.C. Lacourse, *Laboratory preparaton of highly pure As_2Se_3 glass.* Journal of Non-cryst Solids, 1995. **181**(3): p. 231-237.
126. Seddon, A.B., *Personal communication.* 2009.
127. Atkins, P. and J. De Paula, *Atkins' Physical Chemistry.* 2006, Oxford.
128. Bragg, W.L. *The Diffraction of Short Electromagnetic Waves by a Crystal.* 1914: Proceedings of the Cambridge Philosophical Society.
129. Elliott, S.R., *Medium-range structural order in covalent amorphous solids.* Nature, 1991. **354**(12): p. 445-452.
130. Symon, K.R., *Mechanics (3rd Edition).* 1971, London, Amsterdam, Sydney: Addison-Wesley publishing company.
131. Webber, P.J. and J.A. Savage, *Measurement of the viscosity of chalcogenide glasses by a parallel plate technique.* Journal of Materials Science, 1981. **16**(3): p. 763-766.
132. Wang, J., *Glass viscosity and structural relaxation by parallel plate rheometry using a thermo-mechanical analyser.* Material Letters, 1996. **31**(1-2): p. 99-103.
133. Morse, P.M., *Diatomic molecules according to the wave mechanics. II. Vibrational levels.* Physical Review, 1929. **34**(1): p. 57-64.
134. Goodhew, P.J., *Specimen preparation in materials science.* 1972: Elsevier Science Ltd.
135. Jellison Jr, G.E. and F.A. Modine, *Parameterization of the optical functions of amorphous materials in the interband region.* Applied Physics Letters, 1996. **69**(3): p. 371-373.
136. Cauchy, L., *Sur La dispersion de la lumiere.* Bull. Des.Sc. math, 1830. **14**(9).
137. Wagner, T., *Personal communication.* 2008: Pardubice.
138. Orava, J., J. Sik, T. Wagner, and M. Frumar, *Optical properties of $As_{33}S_{67-x}Se_x$ bulk glasses studied by spectroscopic ellipsometry.* Journal of Applied Physics, 2008. **103**(8): p. 083512-083512-8.
139. Bruggeman, D.A.G., *Calculation of different physical constants of heterogeneous substances.* Annual Physics, 1935. **24**: p. 636-679.
140. Urbach, F., *The Long-Wavelength Edge of Photographic Sensitivity and of the Electronic Absorption of Solids.* Physical Review, 1953. **92**: p. 1324-1324.
141. Prasad, N., *Microwave assisted synthesis of chalcogenide glasses.* 2009, Unviersity of Nottingham: Thesis, Nottingham.
142. Glusker, J.P. and K.N. Trueblood, *Crystal structure analysis, A primer, Second edition.* 1985, New York, Oxford: Oxford University Press.
143. Kavetskyy, T., O. Shpotyuk, V. Boyko, J. Filipecki, and M. Popescu, *On the origion of nanovoids in binary chalcogenide glasses studies by FSDP-related XRD, PALS and Monte-Carlo simulation.* Ser.Physic, 2007. **40**: p. 153-158.
144. kavetskyy, T., I. Kaban, O. Shpotyuk, W. Hoyer, and J.T. Filipecki, V., *On the correlation between FSDP and PALS parameter in As-Se chalcogenide glasses.* Journal of Non-oxide and Photonic Glasses, 2009. **1**(1): p. 19-23.
145. Massobio, C. and A. Pasquarello, *Origin of the first sharp diffraction peak in the structure factor of disordered network-forming systems: layers or voids.* Journal of Chemical Physics, 2001. **114**(18): p. 7976-7979.
146. Elliott, S.R., *Origin of the First sharp Diffraction Peak in the structure factor of covalent glasses.* Physical Review Letters, 1991. **67**(6): p. 711-714.

147. Jing, C.B., X.J. Zhao, J.J. Han, H.Z. Tao, A.Y. Liu, and K. Zhu, *IR spectra analysis of SiO_2 - TiO_2 - GeO_2 gel glass of CO_2 laser transmitting hollow waveguide.* Journal of Wehan University of Technology - Mater. Sci. Ed, 2002. **17**(4): p. 54-57.

148. Orchard, D., *Refractive index measurement of chalcogenide glass:$As_{40}Se_{60}$* 2009, Unpublished work, QinetiQ, UK.

149. John, S.M., *Optical fiber communications: Principles and practice.* Prentice Hall International Series in Optoelectronics. 1985, New York, London, Toronto, Sydney, Tokyo and Singapore: Prentice Hall International (UK) Ltd.

150. Ohmachi, Y., *Refractive index of vitreous As_2Se_3.* Journal of the optical Society of America, 1973. **63**(5): p. 630-631.

151. Bruhat, G. in *Cours de Physique Generale, Optique, sixth.* 1965. Masson, Paris.

152. Sutton, L.E. and O.N. Stavroudis, *Fitting refractive index data by least squares.* Journal of Optical Society of America, 1961. **51**(8): p. 901-905.

153. Ditchburn, R.W., *Light.* 1991: Courier Dover Publications.

154. Tatian, B., *Fitting refractive index data with Sellmeier dispersion formula.* Applied Optics, 1984. **23**(24): p. 4477-4485.

155. Athanasiou, G., *Personal communication.* 2009.

156. Jellison, G.E. and F.A. Modine, *Parameterization of optical functions of amorphous materials in the interband region.* Applied Physics Letters, 1996. **69**(3): p. 371 - 373.

157. Sakka, S. and J.D. Mackenzie, *Relation between apparent glass transition temperature and liquids temperature for inorgnic glasses.* Journal of Non-cryst Solids, 1971. **6**(2): p. 145-162.

158. Laniel, J.M., J.-M. Menard, K. Turcotte, A. Villeneuve, R. Vallee, C. Lopez, and K.A. Richardson, *Refractive index measurements of planar chalcogenide thin film.* Journal of Non-cryst Solids, 2003. **328**: p. 183-191.

159. Wu, W.-L., W.E. Wallace, and J.V. Zanten, *Glass transition temperature of ultrathin polymer films on silicon,* in *Mat. Res.Soc.Symp.* 1995, Material Research Society: Gaithersburg. p. 147-151.

160. Lucas, P., A.A. Wilhelm, M. Videa, C. Boussard-Pledel, and B. Bureau, *Chemical stability of chalcogenide infrared glass fibers.* Corrosion Science, 2008. **50**(7): p. 2047-2052.

161. Chou, S.Y., P.R. Krauss, and P.J. Renstrom, *Nano-imprint lithography.* Journal of Vacuum Science and Technology B, 1996. **14**(6): p. 4129-4133.

162. Chou, S.Y., P.R. Krauss, and P.J. Renstrom, *Imprint of sub-25 nm vias and treches in polymers.* Applied Physics Letters, 1995. **67**(21): p. 3114-4116.

163. Huang, X.D., L.R. Bao, X. Cheng, L.J. Guo, S.W. Pang, and A.F. Yee, *Reversal imprinting by transferring polymer from mold to substrate.* Journal of Vacuum Science and Technology B, 2002. **20**(6): p. 2872-2876.

164. Kim, J.T., K.B. Yoom, and C.G. Choi, *Passive alignment method of polymer PLC devices by using a hot embossing technique.* IEEE Photonics Technology Letters, 2004. **16**(7): p. 1664-1666.

165. Mizuno, H., S. Jordan, O. Sugihara, T. Kaino, N. Okamoto, and M. Ohama, *Polymer optical waveguide with plastic optical fiber guides for passive alignment fabricated by hot embossing.* Japanese Journal of Applied Physics Part 2-Letters and Express Letters, 2004. **43**: p. L1496-1498.

166. Choi, C.G., *Fabrication of optical waveguides in thermosetting polymers using hot embossing.* Journal of Micromechanics and Microengineering, 2004. **14**: p. 945-949.

167. Soref, R.A., J. Schmidtchen, and K. Petermann, *Large single-mode rib waveguides in GeSi-Si and Si-on-SiO2.* IEEE Journal of Quantum Electronics, 1991. **27**(9): p. 1971-1974.

168. Pan, W.J., D. Furniss, H. Rowe, C.A. Miller, A. Loni, P. Sewell, T.M. Benson, and A.B. Seddon, *Fine embossing of chalcogenide glasses: First time submicron definition of surface embossed features.* Journal of Non-Crystalline Solids, 2007. **353**(13-15): p. 1302-1306.

169. Seddon, A.B., W.J. Pan, D. Furniss, C.A. Miller, H. Rowe, D.M. Zhang, E.M. Mcbrearty, Y. Zhang, A. Loni, P. Sewell, and T.B. Benson, *Fine embossing of chalcogenide glasses – A new fabrication route for photonic integrated circuits.* Journal of Non-Crystalline Solids 2006. **352**(23-25): p. 2515-2520.

170. Seddon, A.B., D. Furniss, W.J. Pan, P. Sewell, A. Loni, Y. Zhang, and T.M. Benson, *Review: Fine embossing of novel glasses for photonic integrated circuits*. 2007, Proc. 9th Int. Conf. on Transparent Optical Networks. p. 280-283.

171. Stern, M.S., P.C. Kendall, R.C. Hewson-Browne, and P.N. Bobson, *Scattering loss from rough sidewalls in semiconductor rib waveguides.* Electron Letters, 1989. **25**(18): p. 1231-1232.

172. Lian, Z.G., W.J. Pan, D. Furniss, T.M. Benson, A.B. Seddon, T. Kohoutek, J. Orava, and T. Wagner, *Embossing of chalcogenide glass: monomode rib optical waveguides in ecaporated thin films.* Optics Letters, 2009. **34**(8): p. 1234-1236.

173. Adachi, S., *GaAs, AlAs and $Al_xGa_{1-x}As$: Material parameters for use in research and device applications.* Journal of Applied Physics, 1985. **58**(3): p. R1-R29.

174. Walker, R.G., *Simple and accurate loss measurement technique for semiconductor optical waveguides.* Electronics Letters, 1985. **21**(13): p. 581-583.

175. Sewell, P., *Personal communication.* 2009.

176. Barwicz, T. and H.A. haus, *Three-dimensional analysis of scattering losses due to sidewall roughness in microphotonic waveguides.* Journal of Lightwave Technology, 2005. **23**(9): p. 2719-2732.

177. Feng, X., A.K. Mariraj, D. Hewak, and T. Monro, *Towards high-index-glass based monomode holey fibre with large-mode-area.* Electron Letters, 2004. **40**(3): p. 167-169.

178. Furniss, D., *Personal communication.* 2009.

179. Feng, X., F. Poletti, A. Carmerlingo, F. Parmigiani, P. Horak, P. Petropoulos, W.H. Loh, and D.J. Richardon, *Dispersion-shift all solid high index-contrast microstructured optical fiber for nonlinear application at 1.55 um.* Optics Express, 2009. **17**(22): p. 20249-20255.

180. Lian, Z.G., Q.Q. Li, D. Furniss, T.M. Benson, and A.B. Seddon, *Solid micro-structured chalcogenide glass optical fibers for the near- and mid-infrared spectral regions.* Photonics Technology Letters, IEEE, 2009. **21**(24): p. 1804-1806.

Appendix A: Refractive index of $As_{40}Se_{60}$ samples prepared by University of Nottingham and University of Pardubice								
Wavelength / nm	uofn01(i)/n	uofn01(i)/k	uofn01(ii)/n	uofn01(ii)/k	uofp01(i)/n	uofp01(i)/k	uofp01(ii)/n	uofp01(ii)/k
260	2.4499	1.7689	2.6402	1.6179	2.6391	1.6515	2.9112	1.5261
280	2.6509	1.7142	2.8054	1.5366	2.8181	1.5647	3.0688	1.3862
300	2.8308	1.6355	2.9471	1.4416	2.9696	1.4609	3.1858	1.2398
320	2.9874	1.5385	3.0661	1.3378	3.0943	1.3468	3.268	1.0958
340	3.12	1.4287	3.1637	1.2291	3.1938	1.2277	3.3221	0.95951
360	3.2289	1.3109	3.2416	1.1189	3.2705	1.1081	3.3543	0.83381
380	3.3155	1.1896	3.3019	1.0096	3.3271	0.99091	3.3696	0.71978
400	3.3815	1.068	3.3464	0.90305	3.3665	0.87843	3.3723	0.61745
420	3.429	0.9489	3.377	0.80069	3.3912	0.77206	3.3655	0.52628
440	3.4602	0.83431	3.3958	0.70347	3.4036	0.67267	3.3518	0.44548
460	3.4774	0.72564	3.4041	0.61205	3.4059	0.58069	3.333	0.37415
480	3.4824	0.62385	3.4036	0.52683	3.3998	0.49629	3.3106	0.31141
500	3.4771	0.52956	3.3955	0.44807	3.3868	0.41943	3.2856	0.25644
520	3.4634	0.4431	3.3811	0.37588	3.3683	0.34996	3.2589	0.20848
540	3.4425	0.36462	3.3614	0.31028	3.3454	0.28764	3.2312	0.16686
560	3.4159	0.29414	3.3374	0.25124	3.3191	0.23223	3.203	0.131
580	3.3846	0.23161	3.3098	0.1987	3.2901	0.18343	3.1746	0.10038
600	3.3499	0.17689	3.2795	0.15256	3.2593	0.14097	3.1464	0.07455
620	3.3126	0.12986	3.2471	0.11273	3.2272	0.10458	3.1188	0.05312
640	3.2735	0.09034	3.2134	0.07909	3.1944	0.074	3.0919	0.03573
660	3.2337	0.05818	3.1791	0.05154	3.1616	0.04901	3.0661	0.02209
680	3.1939	0.03323	3.1447	0.02998	3.1291	0.02938	3.0415	0.01193

700	3.155	0.01533	3.1112	0.0143	3.0977	0.0149	3.0185	0.005
720	3.1183	0.00433	3.0794	0.0044	3.068	0.00538	2.9975	0.0011
740	3.0854	6.86E-05	3.0505	1.83E-04	3.0408	6.40E-04	2.9791	0
760	3.0596	0	3.0274	0	3.0181	0	2.9643	0
780	3.0386	0	3.0088	0	3	0	2.9517	0
800	3.0207	0	2.993	0	2.9845	0	2.9408	0
820	3.0051	0	2.9791	0	2.9711	0	2.931	0
840	2.9913	0	2.9669	0	2.9593	0	2.9223	0
860	2.9791	0	2.956	0	2.9487	0	2.9145	0
880	2.9681	0	2.9462	0	2.9391	0	2.9074	0
900	2.9581	0	2.9373	0	2.9305	0	2.9009	0
920	2.949	0	2.9293	0	2.9227	0	2.895	0
940	2.9408	0	2.9219	0	2.9155	0	2.8896	0
960	2.9332	0	2.9151	0	2.9089	0	2.8846	0
980	2.9262	0	2.9089	0	2.9029	0	2.8799	0
1000	2.9198	0	2.9032	0	2.8973	0	2.8756	0
1020	2.9138	0	2.8978	0	2.8921	0	2.8717	0
1040	2.9083	0	2.8929	0	2.8873	0	2.8679	0
1060	2.9032	0	2.8883	0	2.8828	0	2.8645	0
1080	2.8984	0	2.884	0	2.8786	0	2.8613	0
1100	2.8939	0	2.88	0	2.8747	0	2.8582	0
1120	2.8897	0	2.8763	0	2.8711	0	2.8554	0
1140	2.8858	0	2.8728	0	2.8676	0	2.8527	0
1160	2.8821	0	2.8694	0	2.8644	0	2.8502	0

1180	2.8787	0	2.8663	0	2.8614	0	2.8478	0
1200	2.8754	0	2.8634	0	2.8585	0	2.8456	0
1220	2.8723	0	2.8607	0	2.8558	0	2.8435	0
1240	2.8694	0	2.858	0	2.8533	0	2.8415	0
1260	2.8667	0	2.8556	0	2.8509	0	2.8396	0
1280	2.8641	0	2.8532	0	2.8486	0	2.8378	0
1300	2.8616	0	2.851	0	2.8464	0	2.8361	0
1320	2.8593	0	2.8489	0	2.8444	0	2.8345	0
1340	2.857	0	2.8469	0	2.8424	0	2.833	0
1360	2.8549	0	2.845	0	2.8406	0	2.8315	0
1380	2.8529	0	2.8432	0	2.8388	0	2.8301	0
1400	2.851	0	2.8415	0	2.8371	0	2.8288	0
1420	2.8492	0	2.8399	0	2.8355	0	2.8275	0
1440	2.8474	0	2.8383	0	2.834	0	2.8263	0
1460	2.8458	0	2.8368	0	2.8325	0	2.8251	0
1480	2.8442	0	2.8354	0	2.8311	0	2.824	0
1500	2.8427	0	2.834	0	2.8298	0	2.823	0
1520	2.8412	0	2.8327	0	2.8285	0	2.8219	0
1540	2.8398	0	2.8314	0	2.8273	0	2.821	0
1560	2.8385	0	2.8302	0	2.8261	0	2.82	0
1580	2.8372	0	2.8291	0	2.825	0	2.8191	0
1600	2.836	0	2.828	0	2.8239	0	2.8183	0
1620	2.8348	0	2.8269	0	2.8229	0	2.8175	0
1640	2.8337	0	2.8259	0	2.8219	0	2.8167	0

1660	2.8326	0	2.8249	0	2.8209	0	2.8159	0
1680	2.8315	0	2.8239	0	2.82	0	2.8152	0
1700	2.8305	0	2.823	0	2.8191	0	2.8144	0
1720	2.8295	0	2.8222	0	2.8182	0	2.8138	0
1740	2.8286	0	2.8213	0	2.8174	0	2.8131	0
1760	2.8277	0	2.8205	0	2.8166	0	2.8125	0
1780	2.8268	0	2.8197	0	2.8159	0	2.8119	0
1800	2.826	0	2.819	0	2.8151	0	2.8113	0
1820	2.8252	0	2.8182	0	2.8144	0	2.8107	0
1840	2.8244	0	2.8175	0	2.8137	0	2.8102	0
1860	2.8236	0	2.8168	0	2.813	0	2.8096	0
1880	2.8229	0	2.8162	0	2.8124	0	2.8091	0
1900	2.8222	0	2.8155	0	2.8118	0	2.8086	0
1920	2.8215	0	2.8149	0	2.8112	0	2.8081	0
1940	2.8209	0	2.8143	0	2.8106	0	2.8077	0
1960	2.8202	0	2.8137	0	2.81	0	2.8072	0
1980	2.8196	0	2.8132	0	2.8095	0	2.8068	0
2000	2.819	0	2.8126	0	2.809	0	2.8063	0
2020	2.8184	0	2.8121	0	2.8084	0	2.8059	0
2040	2.8178	0	2.8116	0	2.8079	0	2.8055	0
2060	2.8173	0	2.8111	0	2.8075	0	2.8052	0
2080	2.8168	0	2.8106	0	2.807	0	2.8048	0
2100	2.8163	0	2.8102	0	2.8065	0	2.8044	0
2120	2.8158	0	2.8097	0	2.8061	0	2.8041	0

2140	2.8153	0	2.8093	0	2.8057	0	2.8037	0
2160	2.8148	0	2.8089	0	2.8053	0	2.8034	0
2180	2.8143	0	2.8084	0	2.8049	0	2.8031	0
2200	2.8139	0	2.808	0	2.8045	0	2.8028	0
2220	2.8135	0	2.8077	0	2.8041	0	2.8024	0
2240	2.813	0	2.8073	0	2.8037	0	2.8021	0
2260	2.8126	0	2.8069	0	2.8033	0	2.8019	0
2280	2.8122	0	2.8066	0	2.803	0	2.8016	0
2300	2.8119	0	2.8062	0	2.8027	0	2.8013	0

Appendix B: Refractive index of bulk $As_{40}Se_{60}$ and flat-embossed bulk $As_{40}Se_{60}$; thin film $As_{40}Se_{60}$ and flat-embossed thin film $As_{40}Se_{60}$											
Wavelength	Bulk ZGLCF009		Wavelength	Flat-embossed bulk ZGLCF007		Wavelength	Thin film GG20080223		Wavelength	Flat-embossed thin film GG20080223_f	
/ nm	n	k	/ nm	n	k	/ nm	n	k	/ nm	n	k
300	2.7634	1.8025	300	2.9869	1.7176	300	2.4525	1.7244	300	2.4254	1.7331
325	2.9908	1.6876	320	3.1481	1.5958	305	2.5002	1.7122	305	2.4924	1.732
350	3.1823	1.5439	340	3.2812	1.4617	310	2.5469	1.6984	310	2.5591	1.7269
375	3.3353	1.3809	360	3.387	1.3209	315	2.5926	1.683	315	2.625	1.7181
400	3.45	1.2077	380	3.4672	1.1782	320	2.6371	1.6662	320	2.69	1.7055
425	3.5283	1.0324	400	3.5241	1.0374	325	2.6805	1.648	325	2.7536	1.6892
450	3.5737	0.86142	420	3.5602	0.90156	330	2.7228	1.6284	330	2.8157	1.6694
475	3.5902	0.69973	440	3.5783	0.77273	335	2.7637	1.6077	335	2.8758	1.6463
500	3.5822	0.55092	460	3.5809	0.65242	340	2.8034	1.5857	340	2.9339	1.6199
525	3.554	0.4175	480	3.5706	0.54161	345	2.8418	1.5626	345	2.9895	1.5906
550	3.5096	0.30111	500	3.5494	0.44087	350	2.8789	1.5385	350	3.0426	1.5586
575	3.453	0.20284	520	3.5194	0.35052	355	2.9145	1.5135	355	3.0929	1.5242
600	3.3876	0.12341	540	3.4824	0.27069	360	2.9488	1.4876	360	3.1403	1.4875
625	3.3172	0.063316	560	3.4399	0.20136	365	2.9817	1.4609	365	3.1848	1.449
650	3.2457	0.022952	580	3.3935	0.14248	370	3.0132	1.4335	370	3.2261	1.4089
675	3.1781	0.002611	600	3.3445	0.093938	375	3.0433	1.4054	375	3.2644	1.3675
700	3.1243	0	620	3.2943	0.055611	380	3.0719	1.3768	380	3.2995	1.325
725	3.0858	0	640	3.2443	0.027377	385	3.0992	1.3476	385	3.3316	1.2818
750	3.0551	0	660	3.1962	0.0091089	390	3.125	1.3181	390	3.3606	1.238
775	3.0296	0	680	3.1522	0.00066761	395	3.1495	1.2881	395	3.3866	1.194

800	3.008	0	700	3.117	0	400	3.1725	1.2579	400	3.4097	1.15
825	2.9894	0	720	3.0897	0	405	3.1942	1.2274	405	3.4301	1.1061
850	2.9732	0	740	3.0669	0	410	3.2146	1.1968	410	3.4478	1.0625
875	2.959	0	760	3.0472	0	415	3.2336	1.1661	415	3.463	1.0194
900	2.9463	0	780	3.0301	0	420	3.2514	1.1352	420	3.4758	0.977
925	2.935	0	800	3.015	0	425	3.2678	1.1044	425	3.4864	0.93532
950	2.9249	0	820	3.0015	0	430	3.283	1.0736	430	3.4948	0.8945
975	2.9157	0	840	2.9894	0	435	3.2971	1.0429	435	3.5014	0.85462
1000	2.9074	0	860	2.9784	0	440	3.3099	1.0123	440	3.5061	0.81575
1025	2.8999	0	880	2.9685	0	445	3.3215	0.98189	445	3.5091	0.77794
1050	2.893	0	900	2.9595	0	450	3.3321	0.95168	450	3.5106	0.74124
1075	2.8867	0	920	2.9512	0	455	3.3415	0.92171	455	3.5107	0.70566
1100	2.8809	0	940	2.9436	0	460	3.3499	0.89201	460	3.5095	0.67123
1125	2.8755	0	960	2.9367	0	465	3.3573	0.86262	465	3.5071	0.63796
1150	2.8706	0	980	2.9302	0	470	3.3637	0.83356	470	3.5036	0.60584
1175	2.866	0	1000	2.9242	0	475	3.3692	0.80485	475	3.4992	0.57488
1200	2.8617	0	1020	2.9187	0	480	3.3737	0.77653	480	3.4938	0.54507
1225	2.8578	0	1040	2.9135	0	485	3.3773	0.74861	485	3.4877	0.51638
1250	2.8541	0	1060	2.9087	0	490	3.3801	0.72111	490	3.4809	0.4888
1275	2.8506	0	1080	2.9042	0	495	3.3821	0.69405	495	3.4735	0.46231
1300	2.8474	0	1100	2.8999	0	500	3.3833	0.66745	500	3.4655	0.43689
1325	2.8444	0	1120	2.896	0	505	3.3837	0.64131	505	3.4569	0.4125
1350	2.8415	0	1140	2.8923	0	510	3.3835	0.61566	510	3.448	0.38912
1375	2.8389	0	1160	2.8888	0	515	3.3825	0.5905	515	3.4386	0.36672

1400	2.8364	0	1180	2.8855	0	520	3.3808	0.56585	520	3.429	0.34528
1425	2.834	0	1200	2.8824	0	525	3.3786	0.5417	525	3.419	0.32476
1450	2.8318	0	1220	2.8794	0	530	3.3757	0.51807	530	3.4088	0.30514
1475	2.8297	0	1240	2.8767	0	535	3.3722	0.49497	535	3.3983	0.28638
1500	2.8277	0	1260	2.874	0	540	3.3682	0.4724	540	3.3877	0.26847
1525	2.8258	0	1280	2.8716	0	545	3.3637	0.45036	545	3.377	0.25136
1550	2.824	0	1300	2.8692	0	550	3.3587	0.42886	550	3.3661	0.23504
1575	2.8223	0	1320	2.867	0	555	3.3532	0.40791	555	3.3551	0.21947
1600	2.8207	0	1340	2.8648	0	560	3.3473	0.38749	560	3.3441	0.20463
1625	2.8191	0	1360	2.8628	0	565	3.3409	0.36762	565	3.333	0.1905
1650	2.8177	0	1380	2.8609	0	570	3.3342	0.34829	570	3.3219	0.17705
1675	2.8163	0	1400	2.859	0	575	3.327	0.32951	575	3.3108	0.16426
1700	2.8149	0	1420	2.8573	0	580	3.3196	0.31128	580	3.2996	0.1521
1725	2.8137	0	1440	2.8556	0	585	3.3117	0.29359	585	3.2886	0.14056
1750	2.8125	0	1460	2.854	0	590	3.3036	0.27644	590	3.2775	0.1296
1775	2.8113	0	1480	2.8524	0	595	3.2952	0.25984	595	3.2665	0.11922
1800	2.8102	0	1500	2.851	0	600	3.2865	0.24377	600	3.2556	0.10939
1825	2.8092	0	1520	2.8496	0	605	3.2775	0.22825	605	3.2447	0.1001
1850	2.8081	0	1540	2.8482	0	610	3.2683	0.21326	610	3.2339	0.091315
1875	2.8072	0	1560	2.8469	0	615	3.2589	0.19881	615	3.2233	0.083035
1900	2.8062	0	1580	2.8457	0	620	3.2493	0.18489	620	3.2127	0.075236
1925	2.8054	0	1600	2.8445	0	625	3.2395	0.1715	625	3.2022	0.067905
1950	2.8045	0	1620	2.8434	0	630	3.2295	0.15864	630	3.1918	0.061025
1975	2.8037	0	1640	2.8423	0	635	3.2194	0.14631	635	3.1816	0.054583

2000	2.8029	0	1660	2.8412	0	640	3.2091	0.13449	640	3.1715	0.048565
2025	2.8021	0	1680	2.8402	0	645	3.1988	0.1232	645	3.1615	0.042957
2050	2.8014	0	1700	2.8392	0	650	3.1883	0.11242	650	3.1517	0.037747
2075	2.8007	0	1720	2.8383	0	655	3.1777	0.10215	655	3.1421	0.032923
2100	2.8	0	1740	2.8374	0	660	3.1671	0.092396	660	3.1325	0.028474
2125	2.7994	0	1760	2.8365	0	665	3.1564	0.083149	665	3.1232	0.024387
2150	2.7987	0	1780	2.8356	0	670	3.1457	0.074407	670	3.114	0.020654
2175	2.7981	0	1800	2.8348	0	675	3.1349	0.066166	675	3.105	0.017263
2200	2.7975	0	1820	2.834	0	680	3.1242	0.058424	680	3.0962	0.014204
2225	2.797	0	1840	2.8333	0	685	3.1134	0.051178	685	3.0875	0.011469
2250	2.7964	0	1860	2.8325	0	690	3.1027	0.044425	690	3.0791	0.0090477
2275	2.7959	0	1880	2.8318	0	695	3.092	0.038162	695	3.0709	0.0069321
2300	2.7954	0	1900	2.8311	0	700	3.0814	0.032386	700	3.0628	0.0051137
			1920	2.8305	0	705	3.0708	0.027094	705	3.055	0.0035843
			1940	2.8298	0	710	3.0603	0.022284	710	3.0474	0.0023363
			1960	2.8292	0	715	3.05	0.017953	715	3.0401	0.001362
			1980	2.8286	0	720	3.0398	0.014097	720	3.0331	0.00065431
			2000	2.828	0	725	3.0297	0.010713	725	3.0263	0.00020606
			2020	2.8275	0	730	3.0198	0.0077996	730	3.0198	1.04E-05
			2040	2.8269	0	735	3.0101	0.0053526	735	3.0138	0
			2060	2.8264	0	740	3.0007	0.0033691	740	3.0082	0
			2080	2.8259	0	745	2.9915	0.001846	745	3.0029	0
			2100	2.8254	0	750	2.9827	0.00077984	750	2.9978	0
			2120	2.8249	0	755	2.9742	0.00016712	755	2.9929	0

			2140	2.8244	0	760	2.9663	0	760	2.9883	0
			2160	2.8239	0	765	2.959	0	765	2.9838	0
			2180	2.8235	0	770	2.9522	0	770	2.9795	0
			2200	2.8231	0	775	2.9458	0	775	2.9753	0
			2220	2.8226	0	780	2.9397	0	780	2.9713	0
			2240	2.8222	0	785	2.9339	0	785	2.9674	0
			2260	2.8218	0	790	2.9283	0	790	2.9637	0
			2280	2.8215	0	795	2.923	0	795	2.96	0
			2300	2.8211	0	800	2.9178	0	800	2.9565	0
						805	2.9129	0	805	2.9531	0
						810	2.9082	0	810	2.9498	0
						815	2.9036	0	815	2.9466	0
						820	2.8991	0	820	2.9435	0
						825	2.8949	0	825	2.9405	0
						830	2.8907	0	830	2.9376	0
						835	2.8867	0	835	2.9347	0
						840	2.8828	0	840	2.932	0
						845	2.879	0	845	2.9293	0
						850	2.8754	0	850	2.9266	0
						855	2.8718	0	855	2.9241	0
						860	2.8684	0	860	2.9216	0
						865	2.865	0	865	2.9192	0
						870	2.8618	0	870	2.9168	0
						875	2.8586	0	875	2.9145	0

						880	2.8555	0	880	2.9122	0
						885	2.8525	0	885	2.91	0
						890	2.8496	0	890	2.9079	0
						895	2.8467	0	895	2.9058	0
						900	2.8439	0	900	2.9037	0
						905	2.8412	0	905	2.9017	0
						910	2.8385	0	910	2.8998	0
						915	2.836	0	915	2.8979	0
						920	2.8334	0	920	2.896	0
						925	2.831	0	925	2.8942	0
						930	2.8286	0	930	2.8924	0
						935	2.8262	0	935	2.8906	0
						940	2.8239	0	940	2.8889	0
						945	2.8217	0	945	2.8872	0
						950	2.8195	0	950	2.8856	0
						955	2.8173	0	955	2.884	0
						960	2.8152	0	960	2.8824	0
						965	2.8132	0	965	2.8809	0
						970	2.8111	0	970	2.8794	0
						975	2.8092	0	975	2.8779	0
						980	2.8072	0	980	2.8764	0
						985	2.8053	0	985	2.875	0
						990	2.8035	0	990	2.8736	0
						995	2.8017	0	995	2.8722	0

						1000	2.7999	0	1000	2.8709	0
						1005	2.7981	0	1005	2.8696	0
						1010	2.7964	0	1010	2.8683	0
						1015	2.7948	0	1015	2.867	0
						1020	2.7931	0	1020	2.8658	0
						1025	2.7915	0	1025	2.8645	0
						1030	2.7899	0	1030	2.8633	0
						1035	2.7884	0	1035	2.8622	0
						1040	2.7868	0	1040	2.861	0
						1045	2.7853	0	1045	2.8599	0
						1050	2.7839	0	1050	2.8587	0
						1055	2.7824	0	1055	2.8576	0
						1060	2.781	0	1060	2.8566	0
						1065	2.7796	0	1065	2.8555	0
						1070	2.7782	0	1070	2.8545	0
						1075	2.7769	0	1075	2.8534	0
						1080	2.7756	0	1080	2.8524	0
						1085	2.7743	0	1085	2.8514	0
						1090	2.773	0	1090	2.8505	0
						1095	2.7718	0	1095	2.8495	0
						1100	2.7705	0	1100	2.8486	0
						1105	2.7693	0	1105	2.8477	0
						1110	2.7681	0	1110	2.8467	0
						1115	2.767	0	1115	2.8458	0

						1120	2.7658	0	1120	2.845	0
						1125	2.7647	0	1125	2.8441	0
						1130	2.7636	0	1130	2.8432	0
						1135	2.7625	0	1135	2.8424	0
						1140	2.7614	0	1140	2.8416	0
						1145	2.7603	0	1145	2.8408	0
						1150	2.7593	0	1150	2.84	0
						1155	2.7583	0	1155	2.8392	0
						1160	2.7572	0	1160	2.8384	0
						1165	2.7562	0	1165	2.8376	0
						1170	2.7553	0	1170	2.8369	0
						1175	2.7543	0	1175	2.8361	0
						1180	2.7533	0	1180	2.8354	0
						1185	2.7524	0	1185	2.8347	0
						1190	2.7515	0	1190	2.834	0
						1195	2.7506	0	1195	2.8333	0
						1200	2.7497	0	1200	2.8326	0
						1205	2.7488	0	1205	2.8319	0
						1210	2.7479	0	1210	2.8312	0
						1215	2.7471	0	1215	2.8306	0
						1220	2.7462	0	1220	2.8299	0
						1225	2.7454	0	1225	2.8293	0
						1230	2.7446	0	1230	2.8286	0
						1235	2.7438	0	1235	2.828	0

						1240	2.743	0	1240	2.8274	0
						1245	2.7422	0	1245	2.8268	0
						1250	2.7414	0	1250	2.8262	0
						1255	2.7406	0	1255	2.8256	0
						1260	2.7399	0	1260	2.825	0
						1265	2.7391	0	1265	2.8244	0
						1270	2.7384	0	1270	2.8239	0
						1275	2.7377	0	1275	2.8233	0
						1280	2.737	0	1280	2.8228	0
						1285	2.7363	0	1285	2.8222	0
						1290	2.7356	0	1290	2.8217	0
						1295	2.7349	0	1295	2.8211	0
						1300	2.7342	0	1300	2.8206	0
						1305	2.7336	0	1305	2.8201	0
						1310	2.7329	0	1310	2.8196	0
						1315	2.7322	0	1315	2.8191	0
						1320	2.7316	0	1320	2.8186	0
						1325	2.731	0	1325	2.8181	0
						1330	2.7303	0	1330	2.8176	0
						1335	2.7297	0	1335	2.8171	0
						1340	2.7291	0	1340	2.8167	0
						1345	2.7285	0	1345	2.8162	0
						1350	2.7279	0	1350	2.8157	0
						1355	2.7273	0	1355	2.8153	0

						1360	2.7268	0	1360	2.8148	0
						1365	2.7262	0	1365	2.8144	0
						1370	2.7256	0	1370	2.814	0
						1375	2.7251	0	1375	2.8135	0
						1380	2.7245	0	1380	2.8131	0
						1385	2.724	0	1385	2.8127	0
						1390	2.7234	0	1390	2.8123	0
						1395	2.7229	0	1395	2.8118	0
						1400	2.7224	0	1400	2.8114	0
						1405	2.7219	0	1405	2.811	0
						1410	2.7214	0	1410	2.8106	0
						1415	2.7209	0	1415	2.8102	0
						1420	2.7204	0	1420	2.8098	0
						1425	2.7199	0	1425	2.8095	0
						1430	2.7194	0	1430	2.8091	0
						1435	2.7189	0	1435	2.8087	0
						1440	2.7184	0	1440	2.8083	0
						1445	2.7179	0	1445	2.808	0
						1450	2.7175	0	1450	2.8076	0
						1455	2.717	0	1455	2.8073	0
						1460	2.7166	0	1460	2.8069	0
						1465	2.7161	0	1465	2.8065	0
						1470	2.7157	0	1470	2.8062	0
						1475	2.7152	0	1475	2.8059	0

						1480	2.7148	0	1480	2.8055	0
						1485	2.7144	0	1485	2.8052	0
						1490	2.7139	0	1490	2.8049	0
						1495	2.7135	0	1495	2.8045	0
						1500	2.7131	0	1500	2.8042	0
						1505	2.7127	0	1505	2.8039	0
						1510	2.7123	0	1510	2.8036	0
						1515	2.7119	0	1515	2.8032	0
						1520	2.7115	0	1520	2.8029	0
						1525	2.7111	0	1525	2.8026	0
						1530	2.7107	0	1530	2.8023	0
						1535	2.7103	0	1535	2.802	0
						1540	2.7099	0	1540	2.8017	0
						1545	2.7096	0	1545	2.8014	0
						1550	2.7092	0	1550	2.8011	0
						1555	2.7088	0	1555	2.8009	0
						1560	2.7085	0	1560	2.8006	0
						1565	2.7081	0	1565	2.8003	0
						1570	2.7077	0	1570	2.8	0
						1575	2.7074	0	1575	2.7997	0
						1580	2.707	0	1580	2.7995	0
						1585	2.7067	0	1585	2.7992	0
						1590	2.7063	0	1590	2.7989	0
						1595	2.706	0	1595	2.7987	0

						1600	2.7057	0	1600	2.7984	0
						1605	2.7053	0	1605	2.7981	0
						1610	2.705	0	1610	2.7979	0
						1615	2.7047	0	1615	2.7976	0
						1620	2.7044	0	1620	2.7974	0
						1625	2.704	0	1625	2.7971	0
						1630	2.7037	0	1630	2.7969	0
						1635	2.7034	0	1635	2.7966	0
						1640	2.7031	0	1640	2.7964	0
						1645	2.7028	0	1645	2.7961	0
						1650	2.7025	0	1650	2.7959	0
						1655	2.7022	0	1655	2.7957	0
						1660	2.7019	0	1660	2.7954	0
						1665	2.7016	0	1665	2.7952	0
						1670	2.7013	0	1670	2.795	0
						1675	2.701	0	1675	2.7948	0
						1680	2.7007	0	1680	2.7945	0
						1685	2.7004	0	1685	2.7943	0
						1690	2.7002	0	1690	2.7941	0
						1695	2.6999	0	1695	2.7939	0
						1700	2.6996	0	1700	2.7937	0
						1705	2.6993	0	1705	2.7934	0
						1710	2.6991	0	1710	2.7932	0
						1715	2.6988	0	1715	2.793	0

						1720	2.6985	0	1720	2.7928	0
						1725	2.6983	0	1725	2.7926	0
						1730	2.698	0	1730	2.7924	0
						1735	2.6977	0	1735	2.7922	0
						1740	2.6975	0	1740	2.792	0
						1745	2.6972	0	1745	2.7918	0
						1750	2.697	0	1750	2.7916	0
						1755	2.6967	0	1755	2.7914	0
						1760	2.6965	0	1760	2.7912	0
						1765	2.6963	0	1765	2.791	0
						1770	2.696	0	1770	2.7908	0
						1775	2.6958	0	1775	2.7907	0
						1780	2.6955	0	1780	2.7905	0
						1785	2.6953	0	1785	2.7903	0
						1790	2.6951	0	1790	2.7901	0
						1795	2.6948	0	1795	2.7899	0
						1800	2.6946	0	1800	2.7897	0
						1805	2.6944	0	1805	2.7896	0
						1810	2.6942	0	1810	2.7894	0
						1815	2.6939	0	1815	2.7892	0
						1820	2.6937	0	1820	2.789	0
						1825	2.6935	0	1825	2.7889	0
						1830	2.6933	0	1830	2.7887	0
						1835	2.6931	0	1835	2.7885	0

						1840	2.6928	0	1840	2.7884	0
						1845	2.6926	0	1845	2.7882	0
						1850	2.6924	0	1850	2.788	0
						1855	2.6922	0	1855	2.7879	0
						1860	2.692	0	1860	2.7877	0
						1865	2.6918	0	1865	2.7875	0
						1870	2.6916	0	1870	2.7874	0
						1875	2.6914	0	1875	2.7872	0
						1880	2.6912	0	1880	2.7871	0
						1885	2.691	0	1885	2.7869	0
						1890	2.6908	0	1890	2.7868	0
						1895	2.6906	0	1895	2.7866	0
						1900	2.6904	0	1900	2.7865	0
						1905	2.6902	0	1905	2.7863	0
						1910	2.69	0	1910	2.7862	0
						1915	2.6898	0	1915	2.786	0
						1920	2.6897	0	1920	2.7859	0
						1925	2.6895	0	1925	2.7857	0
						1930	2.6893	0	1930	2.7856	0
						1935	2.6891	0	1935	2.7854	0
						1940	2.6889	0	1940	2.7853	0
						1945	2.6888	0	1945	2.7851	0
						1950	2.6886	0	1950	2.785	0
						1955	2.6884	0	1955	2.7849	0

						1960	2.6882	0	1960	2.7847	0
						1965	2.6881	0	1965	2.7846	0
						1970	2.6879	0	1970	2.7845	0
						1975	2.6877	0	1975	2.7843	0
						1980	2.6875	0	1980	2.7842	0
						1985	2.6874	0	1985	2.7841	0
						1990	2.6872	0	1990	2.7839	0
						1995	2.687	0	1995	2.7838	0
						2000	2.6869	0	2000	2.7837	0
						2005	2.6867	0	2005	2.7836	0
						2010	2.6866	0	2010	2.7834	0
						2015	2.6864	0	2015	2.7833	0
						2020	2.6862	0	2020	2.7832	0
						2025	2.6861	0	2025	2.7831	0
						2030	2.6859	0	2030	2.7829	0
						2035	2.6858	0	2035	2.7828	0
						2040	2.6856	0	2040	2.7827	0
						2045	2.6855	0	2045	2.7826	0
						2050	2.6853	0	2050	2.7824	0
						2055	2.6852	0	2055	2.7823	0
						2060	2.685	0	2060	2.7822	0
						2065	2.6849	0	2065	2.7821	0
						2070	2.6847	0	2070	2.782	0
						2075	2.6846	0	2075	2.7819	0

						2080	2.6844	0	2080	2.7818	0
						2085	2.6843	0	2085	2.7816	0
						2090	2.6841	0	2090	2.7815	0
						2095	2.684	0	2095	2.7814	0
						2100	2.6839	0	2100	2.7813	0
						2105	2.6837	0	2105	2.7812	0
						2110	2.6836	0	2110	2.7811	0
						2115	2.6834	0	2115	2.781	0
						2120	2.6833	0	2120	2.7809	0
						2125	2.6832	0	2125	2.7808	0
						2130	2.683	0	2130	2.7807	0
						2135	2.6829	0	2135	2.7806	0
						2140	2.6828	0	2140	2.7805	0
						2145	2.6826	0	2145	2.7804	0
						2150	2.6825	0	2150	2.7802	0
						2155	2.6824	0	2155	2.7801	0
						2160	2.6823	0	2160	2.78	0
						2165	2.6821	0	2165	2.7799	0
						2170	2.682	0	2170	2.7798	0
						2175	2.6819	0	2175	2.7797	0
						2180	2.6818	0	2180	2.7796	0
						2185	2.6816	0	2185	2.7796	0
						2190	2.6815	0	2190	2.7795	0
						2195	2.6814	0	2195	2.7794	0

						2200	2.6813	0	2200	2.7793	0
						2205	2.6811	0	2205	2.7792	0
						2210	2.681	0	2210	2.7791	0
						2215	2.6809	0	2215	2.779	0
						2220	2.6808	0	2220	2.7789	0
						2225	2.6807	0	2225	2.7788	0
						2230	2.6806	0	2230	2.7787	0
						2235	2.6804	0	2235	2.7786	0
						2240	2.6803	0	2240	2.7785	0
						2245	2.6802	0	2245	2.7784	0
						2250	2.6801	0	2250	2.7783	0
						2255	2.68	0	2255	2.7783	0
						2260	2.6799	0	2260	2.7782	0
						2265	2.6798	0	2265	2.7781	0
						2270	2.6797	0	2270	2.778	0
						2275	2.6795	0	2275	2.7779	0
						2280	2.6794	0	2280	2.7778	0
						2285	2.6793	0	2285	2.7777	0
						2290	2.6792	0	2290	2.7777	0
						2295	2.6791	0	2295	2.7776	0
						2300	2.679	0	2300	2.7775	0

Appendix C: Refractive index of three chalcogenide glasses, i.e. $As_{40}Se_{60}$, $Ge_{17}As_{18}Se_{65}$ and $Ge_{10}As_{23.4}Se_{66.6}$ prepared in the University of Nottingham

Wavelength	As40Se60		Wavelength	Ge17As18Se65		Wavelength	Ge10As23.4Se66.6	
	ZGLCF009			ZGLCF010			ZGLCF038	
/ nm	n	k	/ nm	n	k	/ nm	n	k
300	2.7634	1.8025	300	2.7778	1.3249	260	2.4557	1.4565
325	2.9908	1.6876	320	2.8946	1.2246	280	2.6088	1.3922
350	3.1823	1.5439	340	2.9918	1.117	300	2.7437	1.3138
375	3.3353	1.3809	360	3.0699	1.005	320	2.8602	1.2248
400	3.45	1.2077	380	3.1298	0.89117	340	2.9586	1.1284
425	3.5283	1.0324	400	3.1726	0.77776	360	3.0396	1.0273
450	3.5737	0.86142	420	3.1993	0.66674	380	3.1039	0.92389
475	3.5902	0.69973	440	3.2112	0.55983	400	3.1526	0.82014
500	3.5822	0.55092	460	3.2094	0.45855	420	3.1867	0.71782
525	3.554	0.4175	480	3.1954	0.36427	440	3.2074	0.61842
550	3.5096	0.30111	500	3.1705	0.27824	460	3.2157	0.52322
575	3.453	0.20284	520	3.1361	0.20164	480	3.2129	0.43333
600	3.3876	0.12341	540	3.0937	0.13561	500	3.2	0.34971
625	3.3172	0.063316	560	3.0451	0.081305	520	3.1783	0.27322
650	3.2457	0.022952	580	2.9924	0.039879	540	3.1489	0.20466
675	3.1781	0.0026111	600	2.9384	0.012538	560	3.113	0.14477
700	3.1243	0	620	2.8875	0.00048848	580	3.072	0.094255
725	3.0858	0	640	2.8491	0	600	3.0273	0.053822
750	3.0551	0	660	2.8203	0	620	2.9808	0.024175

775	3.0296	0	680	2.7969	0	640	2.9349	0.006014
800	3.008	0	700	2.7771	0	660	2.8936	0
825	2.9894	0	720	2.7601	0	680	2.8634	0
850	2.9732	0	740	2.7453	0	700	2.8396	0
875	2.959	0	760	2.7322	0	720	2.8198	0
900	2.9463	0	780	2.7206	0	740	2.8028	0
925	2.935	0	800	2.7102	0	760	2.7881	0
950	2.9249	0	820	2.7009	0	780	2.7752	0
975	2.9157	0	840	2.6925	0	800	2.7637	0
1000	2.9074	0	860	2.6848	0	820	2.7534	0
1025	2.8999	0	880	2.6778	0	840	2.7442	0
1050	2.893	0	900	2.6714	0	860	2.7358	0
1075	2.8867	0	920	2.6655	0	880	2.7282	0
1100	2.8809	0	940	2.66	0	900	2.7213	0
1125	2.8755	0	960	2.655	0	920	2.7149	0
1150	2.8706	0	980	2.6504	0	940	2.7091	0
1175	2.866	0	1000	2.6461	0	960	2.7037	0
1200	2.8617	0	1020	2.642	0	980	2.6987	0
1225	2.8578	0	1040	2.6383	0	1000	2.6941	0
1250	2.8541	0	1060	2.6348	0	1020	2.6898	0
1275	2.8506	0	1080	2.6315	0	1040	2.6858	0
1300	2.8474	0	1100	2.6284	0	1060	2.6821	0
1325	2.8444	0	1120	2.6255	0	1080	2.6786	0
1350	2.8415	0	1140	2.6228	0	1100	2.6754	0

1375	2.8389	0	1160	2.6203	0	1120	2.6723	0
1400	2.8364	0	1180	2.6179	0	1140	2.6694	0
1425	2.834	0	1200	2.6156	0	1160	2.6667	0
1450	2.8318	0	1220	2.6134	0	1180	2.6642	0
1475	2.8297	0	1240	2.6114	0	1200	2.6618	0
1500	2.8277	0	1260	2.6095	0	1220	2.6595	0
1525	2.8258	0	1280	2.6076	0	1240	2.6574	0
1550	2.824	0	1300	2.6059	0	1260	2.6553	0
1575	2.8223	0	1320	2.6043	0	1280	2.6534	0
1600	2.8207	0	1340	2.6027	0	1300	2.6516	0
1625	2.8191	0	1360	2.6012	0	1320	2.6498	0
1650	2.8177	0	1380	2.5998	0	1340	2.6482	0
1675	2.8163	0	1400	2.5984	0	1360	2.6466	0
1700	2.8149	0	1420	2.5971	0	1380	2.6451	0
1725	2.8137	0	1440	2.5959	0	1400	2.6437	0
1750	2.8125	0	1460	2.5947	0	1420	2.6423	0
1775	2.8113	0	1480	2.5935	0	1440	2.641	0
1800	2.8102	0	1500	2.5925	0	1460	2.6398	0
1825	2.8092	0	1520	2.5914	0	1480	2.6386	0
1850	2.8081	0	1540	2.5904	0	1500	2.6375	0
1875	2.8072	0	1560	2.5895	0	1520	2.6364	0
1900	2.8062	0	1580	2.5885	0	1540	2.6353	0
1925	2.8054	0	1600	2.5877	0	1560	2.6343	0
1950	2.8045	0	1620	2.5868	0	1580	2.6334	0

1975	2.8037	0	1640	2.586	0	1600	2.6324	0
2000	2.8029	0	1660	2.5852	0	1620	2.6315	0
2025	2.8021	0	1680	2.5845	0	1640	2.6307	0
2050	2.8014	0	1700	2.5837	0	1660	2.6299	0
2075	2.8007	0	1720	2.583	0	1680	2.6291	0
2100	2.8	0	1740	2.5824	0	1700	2.6283	0
2125	2.7994	0	1760	2.5817	0	1720	2.6276	0
2150	2.7987	0	1780	2.5811	0	1740	2.6269	0
2175	2.7981	0	1800	2.5805	0	1760	2.6262	0
2200	2.7975	0	1820	2.5799	0	1780	2.6256	0
2225	2.797	0	1840	2.5793	0	1800	2.6249	0
2250	2.7964	0	1860	2.5788	0	1820	2.6243	0
2275	2.7959	0	1880	2.5783	0	1840	2.6237	0
2300	2.7954	0	1900	2.5777	0	1860	2.6232	0
			1920	2.5773	0	1880	2.6226	0
			1940	2.5768	0	1900	2.6221	0
			1960	2.5763	0	1920	2.6216	0
			1980	2.5759	0	1940	2.6211	0
			2000	2.5754	0	1960	2.6206	0
			2020	2.575	0	1980	2.6201	0
			2040	2.5746	0	2000	2.6197	0
			2060	2.5742	0	2020	2.6192	0
			2080	2.5738	0	2040	2.6188	0
			2100	2.5734	0	2060	2.6184	0

			2120	2.5731	0	2080	2.618	0
			2140	2.5727	0	2100	2.6176	0
			2160	2.5724	0	2120	2.6172	0
			2180	2.5721	0	2140	2.6168	0
			2200	2.5717	0	2160	2.6165	0
			2220	2.5714	0	2180	2.6161	0
			2240	2.5711	0	2200	2.6158	0
			2260	2.5708	0	2220	2.6155	0
			2280	2.5705	0	2240	2.6152	0
			2300	2.5702	0	2260	2.6148	0
						2280	2.6145	0
						2300	2.6143	0

Appendix D: Refractive index of $Ge_{17}As_{18}Se_{65}$ uofngas_01 (i),(ii),(iii) and (iv)								
Wavelength	uofngas_01(i)		uofngas_01(i)		uofngas_01(i)		uofngas_01(i)	
/ nm	n	k	n	k	n	k	n	k
300	2.7455	1.443	2.8054	1.3687	2.8077	1.3424	2.7788	1.398
320	2.8879	1.3336	2.9268	1.256	2.9266	1.2316	2.9066	1.2883
340	3.006	1.2115	3.0258	1.1357	3.0239	1.1134	3.0123	1.1694
360	3.0995	1.0815	3.1029	1.0114	3.1001	0.99086	3.0961	1.0449
380	3.169	0.94789	3.1595	0.88624	3.1562	0.86708	3.1588	0.91818
400	3.2158	0.8145	3.1969	0.76291	3.1934	0.74462	3.2016	0.792
420	3.2416	0.68463	3.2166	0.64369	3.2129	0.62576	3.2258	0.66892
440	3.2484	0.56102	3.2204	0.53051	3.2162	0.5125	3.2328	0.55117
460	3.2383	0.4459	3.2098	0.42501	3.2048	0.40663	3.2242	0.44068
480	3.2136	0.34114	3.1867	0.32857	3.1802	0.30976	3.2018	0.33916
500	3.1765	0.24824	3.1528	0.24245	3.1442	0.2234	3.1673	0.24817
520	3.1294	0.16848	3.1099	0.16773	3.0986	0.14899	3.1225	0.16918
540	3.0748	0.10297	3.0599	0.10546	3.0455	0.08797	3.0696	0.10359
560	3.0153	0.05273	3.0051	0.05666	2.9874	0.04181	3.0112	0.05281
580	2.9541	0.01871	2.9481	0.02234	2.9277	0.01203	2.9503	0.01828
600	2.8958	0.00181	2.8927	0.0035	2.8721	1.52E-04	2.8918	0.00146
620	2.8496	0	2.8463	0	2.8316	0	2.8461	0
640	2.8161	0	2.8131	0	2.801	0	2.8129	0
660	2.7891	0	2.7866	0	2.7761	0	2.7861	0
680	2.7666	0	2.7645	0	2.7552	0	2.7638	0
700	2.7473	0	2.7456	0	2.7372	0	2.7447	0
720	2.7306	0	2.7293	0	2.7215	0	2.7281	0
740	2.716	0	2.715	0	2.7078	0	2.7135	0
760	2.703	0	2.7023	0	2.6956	0	2.7007	0
780	2.6915	0	2.691	0	2.6847	0	2.6892	0
800	2.6811	0	2.6808	0	2.6749	0	2.6789	0
820	2.6718	0	2.6717	0	2.6661	0	2.6696	0
840	2.6633	0	2.6634	0	2.6581	0	2.6612	0
860	2.6556	0	2.6558	0	2.6508	0	2.6535	0
880	2.6486	0	2.6489	0	2.6441	0	2.6465	0
900	2.6421	0	2.6426	0	2.638	0	2.6401	0
920	2.6362	0	2.6368	0	2.6324	0	2.6341	0
940	2.6307	0	2.6314	0	2.6272	0	2.6287	0
960	2.6256	0	2.6264	0	2.6224	0	2.6236	0
980	2.6209	0	2.6218	0	2.6179	0	2.619	0
1000	2.6166	0	2.6176	0	2.6137	0	2.6146	0
1020	2.6125	0	2.6136	0	2.6099	0	2.6106	0
1040	2.6087	0	2.6099	0	2.6063	0	2.6068	0
1060	2.6052	0	2.6064	0	2.6029	0	2.6032	0

1080	2.6018	0	2.6031	0	2.5997	0	2.5999	0
1100	2.5987	0	2.6001	0	2.5968	0	2.5968	0
1120	2.5958	0	2.5972	0	2.594	0	2.5939	0
1140	2.593	0	2.5945	0	2.5913	0	2.5912	0
1160	2.5905	0	2.5919	0	2.5889	0	2.5886	0
1180	2.588	0	2.5895	0	2.5865	0	2.5862	0
1200	2.5857	0	2.5873	0	2.5843	0	2.5839	0
1220	2.5835	0	2.5851	0	2.5823	0	2.5817	0
1240	2.5815	0	2.5831	0	2.5803	0	2.5796	0
1260	2.5795	0	2.5812	0	2.5784	0	2.5777	0
1280	2.5776	0	2.5793	0	2.5766	0	2.5758	0
1300	2.5759	0	2.5776	0	2.575	0	2.5741	0
1320	2.5742	0	2.576	0	2.5733	0	2.5724	0
1340	2.5726	0	2.5744	0	2.5718	0	2.5708	0
1360	2.5711	0	2.5729	0	2.5704	0	2.5693	0
1380	2.5696	0	2.5715	0	2.569	0	2.5678	0
1400	2.5682	0	2.5701	0	2.5677	0	2.5664	0
1420	2.5669	0	2.5688	0	2.5664	0	2.5651	0
1440	2.5657	0	2.5676	0	2.5652	0	2.5639	0
1460	2.5645	0	2.5664	0	2.564	0	2.5627	0
1480	2.5633	0	2.5653	0	2.5629	0	2.5615	0
1500	2.5622	0	2.5642	0	2.5619	0	2.5604	0
1520	2.5611	0	2.5631	0	2.5609	0	2.5594	0
1540	2.5601	0	2.5621	0	2.5599	0	2.5583	0
1560	2.5592	0	2.5612	0	2.559	0	2.5574	0
1580	2.5582	0	2.5603	0	2.5581	0	2.5564	0
1600	2.5573	0	2.5594	0	2.5572	0	2.5555	0
1620	2.5565	0	2.5585	0	2.5564	0	2.5547	0
1640	2.5556	0	2.5577	0	2.5556	0	2.5539	0
1660	2.5548	0	2.5569	0	2.5548	0	2.5531	0
1680	2.5541	0	2.5562	0	2.5541	0	2.5523	0
1700	2.5533	0	2.5554	0	2.5534	0	2.5516	0
1720	2.5526	0	2.5547	0	2.5527	0	2.5508	0
1740	2.5519	0	2.5541	0	2.5521	0	2.5502	0
1760	2.5513	0	2.5534	0	2.5514	0	2.5495	0
1780	2.5506	0	2.5528	0	2.5508	0	2.5489	0
1800	2.55	0	2.5522	0	2.5502	0	2.5482	0
1820	2.5494	0	2.5516	0	2.5496	0	2.5477	0
1840	2.5488	0	2.551	0	2.5491	0	2.5471	0
1860	2.5483	0	2.5505	0	2.5486	0	2.5465	0
1880	2.5478	0	2.55	0	2.548	0	2.546	0
1900	2.5472	0	2.5494	0	2.5475	0	2.5455	0

1920	2.5467	0	2.5489	0	2.5471	0	2.545	0
1940	2.5462	0	2.5485	0	2.5466	0	2.5445	0
1960	2.5458	0	2.548	0	2.5461	0	2.544	0
1980	2.5453	0	2.5476	0	2.5457	0	2.5435	0
2000	2.5449	0	2.5471	0	2.5453	0	2.5431	0
2020	2.5444	0	2.5467	0	2.5449	0	2.5427	0
2040	2.544	0	2.5463	0	2.5445	0	2.5423	0
2060	2.5436	0	2.5459	0	2.5441	0	2.5419	0
2080	2.5432	0	2.5455	0	2.5437	0	2.5415	0
2100	2.5429	0	2.5451	0	2.5433	0	2.5411	0
2120	2.5425	0	2.5448	0	2.543	0	2.5407	0
2140	2.5421	0	2.5444	0	2.5427	0	2.5404	0
2160	2.5418	0	2.5441	0	2.5423	0	2.54	0
2180	2.5414	0	2.5437	0	2.542	0	2.5397	0
2200	2.5411	0	2.5434	0	2.5417	0	2.5393	0
2220	2.5408	0	2.5431	0	2.5414	0	2.539	0
2240	2.5405	0	2.5428	0	2.5411	0	2.5387	0
2260	2.5402	0	2.5425	0	2.5408	0	2.5384	0
2280	2.5399	0	2.5422	0	2.5405	0	2.5381	0
2300	2.5396	0	2.5419	0	2.5402	0	2.5378	0